

**PALEOSEISMOLOGICAL STUDIES ON DÜZCE  
FAULT AND GEOLOGICAL DATA ON THE  
SEISMOGENIC SOURCES IN THE VICINITY OF  
DÜZCE AREA**

Tolga KOMUT

Boğaziçi University

October 2005

**PALEOSEISMOLOGICAL STUDIES ON DÜZCE  
FAULT AND GEOLOGICAL DATA ON THE  
SEISMOGENIC SOURCES IN THE VICINITY OF  
DÜZCE AREA**

by

TOLGA KOMUT

B. Sc. in İstanbul Technical University, 1994

M.S. in Department of Geophysics, Boğaziçi University, 1998

Submitted to the Kandilli Observatory and Earthquake Research Institute  
in partial fulfillment of the requirements for the degree of

Doctor  
of  
Philosophy

Boğaziçi University

October 2005

Bogazici University Library



39001102825596

14

The appropriate evaluation of them is more important than the amount of data.

## PREFACE

People are increasingly experiencing strong ground shakings during the earthquakes in the world. Before high population and urban expansion, the earthquake threat had been widely ignored in general. Rapid population growth in Turkey and urban expansion are placing pressure on the local authorities to allow the development in areas that are previously considered unsuitable because of their exposure to hazards such as earthquake, flooding or landslides. Strong ground shaking is one of the threats that the people face today and will be in the future. In spite of the fact that every individual will never be ready enough for disasters, there are many lessons to be learned from the earthquakes to prevent and mitigate the lasting and future disasters and minimize the risk. For this reason, we should evaluate all opportunities such as experienced earthquakes like occurred in Turkey in 1999. In addition, for the future planning and decision-making processes to work effectively, hazard information must be captured systematically. Düzce city experienced two major earthquakes on August 17 and November 12, 1999. Active tectonics has been and will continue to be of great interest to me. The primary purpose of this PhD study is to understand and to learn scientific techniques for studying earthquakes and to provide people geological information about earthquake hazards. Most of the paleoseismological results are being published by TURQUA organization (Turkish Quaternary Symposium V, 2-5 June 2005 in İstanbul). Paleoseismological investigations provide the direct evidence about the surface deformations. However, these are providing indirect evidence about crustal deformations. In addition, deformation along the faults associated with displacements is known to be chaotic and thus, exhibits a statistical process. So, most of the parameters are derived using some approximations. The following contribution might be serve as a general idea about the seismotectonics of the Düzce area and recurrence period of large earthquakes along the Düzce fault.

# LIST OF FIGURES

**Figure 1.** Location of the study area. A: Seismicity and active fault map of Turkey and surrounding area. Black dots are all the earthquakes taken from USGS catalogue. Red lines are active faults (Şaroğlu et al., 1992). B: The study area is shaded from southwest on the relief map. It is shown with a rectangle in A. Red lines are surface breaks of earthquakes since 1944. P: 2.

**Figure 2.** The surface breaks of 1999 Kocaeli (yellow line) and 1999 Düzce (red line) earthquakes on topographic map. White line shows other active faults and dashed line is probable active faults. P: 3.

**Figure 3.** Locations of trench sites that age results were got from excavations along the Düzce fault on relief map below that shaded from southwest. The map area is shown with a rectangle in the map above. There is one trench site in Kaledibi, one site in Bend and two sites in Töngelli location. Map location is shown with a rectangle in Fig. 1B. The red line represents the surface breaks of the 1999 Düzce earthquake. P: 4.

**Figure 4.** Active subparallel strands of the western part of the NAF (WNAF) zone in the Marmara region (west of about 31°30' longitude); yellow line: Northern Armutlu strand (NArS), green line: Southern Armutlu Strand (SArS), Blue line: Southern Almacık Strand (SAIS), Red Line Northern Almacık Strand (NAIS). White line: Single strand part of the NAF. Orange line: Bursa strand. Dashed lines: probably active faults. The fault locations have been compiled from Arpat et al. (2001), Ambraseys and Zatopek (1969), Öcal (1959), Taşman (1944) and this study. P: 6.

**Figure 5.** Surface rupture of the 1999 Kocaeli (yellow line), 1999 Düzce (red line), 1967 Mudurnu (white line), 1957 Abant (black line) and 1944 Bolu (light green line) earthquakes on the relief map shaded from southwest. The dark green line between the 1999 Düzce and Kocaeli surface ruptures represents a part that was ruptured by both of the earthquakes. The rupture locations of Mudurnu, Abant and Bolu earthquakes have been compiled from Ambraseys and Zatopek (1969), Öcal (1959) and Taşman (1944), respectively. The other rupture locations are drawn according to this study. P: 10.

**Figure 6.** Geomorphological map of the Düzce area (After Pekcan, 2000). 1: New alluvium. 2: Post Pliocene erosional surfaces. 3: Dissected and deformed Pliocene erosional surface. 4: High mountaneous area. 5: Dissected pediment. 6: Stream terraces. 7: Incised channel. 8: River. 9: Fault. Arrows show direction of down tilting.

**Figure 7.** Topographic contour map of the study area on southwest shaded relief map. Yellow lines are active faults. Circles are centers of settlements. P: 14.

**Figure 8.** Incised meandering of Büyükmelen stream in mountain area on LANSAT TM image. Location of the image map is shown above on relief map with a rectangle. See figure 9 for detail. The arrow on the LANDSAT image shows shoot direction of the picture in figure 13. P: 15.

**Figure 9.** Meandering and incised meandering parts of the Küçükmenen and Büyükmelen streams. The locations of maps below are shown on topographic map above. Meandering in the mountain area and in the Düzce plain seems to be similar, implying that those in the mountainous area are incised equivalent of those seen on the actual Düzce plain. P: 16.

**Figure 10.** Abandoned terraces and flat-lying eroded surfaces. Locations of the pictures B and C are shown on LANDSAT image (A) including shooting points and approximate ranges of the picture area with ellipses. Observation points 34 and 04 correspond shoot points of pictures B and C, respectively. The arrow in B shows an abandoned terrace of the Büyükmelen stream. P: 17.

**Figure 11.** The lineaments along the borders of the Düzce basin and surrounding area on topographic contour map. The first contour level is limited at 200 m to represent linear nature of the borders. P: 19.

**Figure 12.** Geology map of the Düzce area (After MTA, 2000). 1: Quaternary alluvium. 2: Pliocene continental deposits. 3: Lower Miocene volcanic rocks. 4: Lower, Middle Eocene sediments. 5: Paleocene – Lower Eocene volcanic rocks. 6: Upper Cretaceous – Lower Eocene continental shelf deposits. 7: Turonian – Campanian slope deposits. 8: Upper Cretaceous – Lower Eocene olistostromal deposits. 9: Upper Cretaceous – Paleocene shelf

deposits. 10: Ophiolitic assemblage. 11: Lower Cretaceous – Paleocene deep sea sediments. 12: Jurassic – Lower Cretaceous sediments. 13: Paleozoic and Early Mesozoic sedimentary rocks. 14: Granitoids of Precambrian. 15: Thrust. 16: Over thrust. P: 21.

**Figure 13.** Picture of the southern coast of Hasanlar Dam. Looking from west (see the arrow in Figure 8 for the shooting direction of the picture). ENE-WSW lineations are remarkable on morphology because of the general trend and dips of sedimentary layers. The flat surface in the figure represents bedding plain of limestones. Primary (sedimentary) relationship exists between limestones which is resistant to erosion and clays along this lineation. The lineation is related to material difference between the resistant limestones and weak clayey layers. P: 23.

**Figure 14.** The location of observation points of young tectonic features on pseudo topographic map layer that is draped on LANSAT-PAN image with topographic contours. Color scale shows altitude in meter. Intensity layer of topographic map is shaded from north as natural shading of LANDSAT image. The A and B: Alluvium (Fig. 15-1,2,3). C and A: Young flatness on eroded basement rocks (Fig. 15-4,5) and eroded young alluvium (Fig. 15-4). D and E young faults (Fig. 16-1,2). Light green line: 1999 Kocaeli surface rupture along the Aksu fault. Red line: 1999 Düzce surface rupture along the Düzce fault. Dark green line: the surface ruptures of both 1999 Düzce and Kocaeli earthquakes. P: 24.

**Figure 15.** Observations on young sedimentary and erosional features. 1, 2, 3 and 4: stream alluvium. 5: erosional surface on basement rocks. 4: angular unconformity between basement and young alluvium and younger flat-lying erosional surface developed both on the alluvium and the basement rock. See figure 14 for the location points of observations. Observation locations of 1 and 4 are shown as point A; 2 and 3 are point B; 5 point is C in figure 14. Shooting directions of 1, 2, 3, 4 and 5 are about east, west, west, east and east, respectively. P: 26.

**Figure 16.** Observations on young faults. The observation locations of 1 are shown as point D; 2 as point E in figure 14. 1: The picture was taken towards east. A young fault juxtaposes Lower-Middle Eocene bedrocks (left) with unconsolidated clays (right). The contact is vertical, so the possibility of the strike-slip faulting is higher. 2: The picture was taken towards west. Gravels in the young unconsolidated alluvium are showing vertical lineations in a narrow zone. Considering vertical lineations, the fault is probably strike-slip.

**Figure 17.** Young fault in northwest of the Bolu basin along Elmalık fault. Light blue line: surface breaks of the 1999 Kocaeli earthquake; red line: 1999 Düzce rupture. Yellow line; 1967 Mudurnu rupture; black line: 1957 Abant rupture; white line: 1944 Bolu rupture; dark blue line: Bakacak and Elmalık faults (suggested by Hitchcock et al., 2003). Relief map shaded from south. Outcrop in the picture shows a young fault that displaced unconsolidated alluvium. On the right in picture above much older bedrocks (Cretaceous melange) are seen at the same level with the young alluvium (Pliocene ?) to the left. Younger erosional surface that is cutting the fault suggests inactive nature for the fault. P: 28.

**Figure 18.** Locations of the boreholes in the Düzce basin. Topographic relief map shaded from south. Black and yellow points are the basement-reaching and hanging boreholes in alluvium, respectively. See table 1 for information about the boreholes. P: 30.

**Figure 19.** Sediment thickness map of the Düzce basin deduced from borehole data. Color scale shows thicknesses. See figure 21 to see the map area and information about boreholes. P: 30.

**Figure 20.** Basement topography of the Düzce basin is deduced from borehole data (Table 1). Basement topography (BT) grid (rectangle) is draped on contoured surface topography map (STM). Both are shaded from south. First contour level of the STM is taken 300 m to avoid overlapping between colored area of the BT and the STM contours. Along the southern and western boundary of the basin, two lows are noticed on the STM. They are located around south and west of the basin on the STM (See fig. 19 or 14). The other low is at the southwestern corner of the basin coinciding to the right stepping between the Aksu and Düzce faults (see fig. 14). P: 31.

**Figure 21.** The borehole data and dummy points to produce sediment thickness model on surface topography map (STM) shaded from south. Rectangle shows map area of figure 19. Black and red points are the basement-reaching and hanging boreholes in alluvium, respectively. Green points are dummy data that are produced by using surface topography map to constrain the model better. P: 33.

**Figure 22.** The final basement topography model (shaded from south), location of the boreholes and surface topographic data points around basement area are surrounding the basin that is having zero sediment thickness. See the figure 20 for interpretative explanation. Black and red points are the basement-reaching and hanging boreholes in alluvium, respectively. Green points are the surface topographic data points on bed rock. These are used to constrain a better model. P:34.

**Figure 23.** A basement topography model of the Düzce basin that is deduced from borehole data those reach to the basement (Table 1). Black points are the basement-reaching boreholes in alluvium. Green points: surface topographic data points that are used to constrain the model better. P:34.

**Figure 24.** Slip distribution and surface rupture of the 1999 Kocaeli earthquake on the contoured and shaded (from south) topographic relief map (After Komut and Ikeda, 2000). The chart above is proportional to the map below. The ruptured fault is colored with blue, yellow and red lines representing probable seismic segments on the map. Red line: Aksu segment; Yellow line: Gölcük segment; Blue line: Çınarcık segment that was probably ruptured during the earthquake. White lines are other active faults in the map area. Dashed white lines are showing probably active faults. Red and yellow filled circles are representing dextral offset along the Aksu and Gölcük segments, respectively. P: 44.

**Figure 25.** Efteni Lake basin, a local depression in southwest of the Düzce basin above. The vertical slip distribution of the 1999 earthquake below. To see the location of the Efteni Lake basin area as a local depression according to the Düzce basin see the topographic relief and blue colored altitudes in figures 14 or 18. The color scale shows altitude between 115 and 125 meters in this figure. First contour level is 130 m. Contour interval is 100 m. The local high in the western Efteni Lake basin is the alluvium cone of the Aksu stream (Fig. 34). Yellow line: Surface rupture of the 1999 Kocaeli earthquake. Red line: 1999 Düzce rupture. The green line between the 1999 Düzce and Kocaeli surface ruptures represents a part that was ruptured by both of the earthquakes. The map above is proportional to the vertical slip distribution below. “-” displacement represents north side down in the slip distribution chart along the Y-axis. X-axis: the distance along the surface rupture according to zero point at the 40:46:20.74N; 31:10:42.04E coordinates south of the Beyköy (See appendix 1). The only systematic vertical (upside south) deformation occurred within the 5 km right stepping area between Düzce and Kocaeli rupture. The 1999 Kocaeli rupture is reaching up to the Büyükmelen and Küçükmelen streams (Fig. 35). P: 45.

**Figure 26.** Slip distribution of the 1999 Düzce earthquake. Yellow line: Surface rupture of the 1999 Kocaeli earthquake. Red line: 1999 Düzce rupture. The green line between the 1999 Düzce and Kocaeli surface ruptures represents a part that was ruptured by both of the earthquakes. On the other hand, some of the observers suggest that the 1999 Kocaeli rupture extends trough 10 km south of Düzce, about 31:10E latitude (See Gökten et al., 1999). The map above is proportional to the slip distribution chart below. Red “x” represents dextral and blue points vertical offsets. “-” displacement represents north side up in the chart along the Y-axis. X-axis: the distance along the surface rupture according to zero point at the 40:46:20.74N; 31:10:42.04E coordinates south of the Beyköy (See appendix 1). The only systematic vertical (upside south) deformation occurred within the 5 km right stepping area between Düzce and Kocaeli rupture. 2 period moving average regression applied to draw the trend lines. Blue and black lines are the trend of vertical and dextral offsets, respectively. P: 48.

**Figure 27.** The surface breaks of 1999 earthquakes on relief map (shaded form NNE) and probable seismic segments of the Düzce fault. Segments are bounded by three left stepover areas within the Düzce fault (Fig. 30, 31 and 33). The segments are represented by different colors. Yellow lines show the surface breaks of the 1999 Kocaeli rupture in the area. Eastern extending part of the rupture has small en-echelon fractures. This is represented by dashed lines. P: 49.

**Figure 28.** Eastern termination area of the 1999 Düzce surface rupture. See the easternmost observation point (D0001) in the appendix 1 for location. Picture was taken by looking from west. En-echelon fractures are reflecting right-lateral movement. They have been developed in the Asar valley followed by the highway, which is under construction. Four to five of these en-echelon fractures form groups that repeat in every few hundreds meters, fading eastward. Arrow is showing compass in 10x6x2 cm dimensions. P: 51.

**Figure 29.** Location of the small ridges along the Düzce fault on relief map shaded from north. P: 53.

**Figure 30.** Şabakay left stepover area. White lines: the surface breaks of the 1999 Düzce rupture. Black dots show downthrown block of reverse faults. Vertical displacement is about 50 cm. The color scale shows altitude

that is also shown by contours. Colored altitude layer is draped on the south shaded relief map. See figure 29 and 27 for the location of the Şabakay ridge and stepover. P: 55.

**Figure 31.** Boncuk left stepover area. White lines: the surface breaks of the 1999 Düzce rupture. Black dots show downthrown block of reverse faults. Vertical displacement is about 30 cm. Local left lateral offsets occurred because of the resistance of Boncuk ridge to the right movement. The resistance leads in tear along the eastern boundary of the ridge. Between the southern dextral zone having 150 cm slip and reverse zone around N40°46'45" latitude the area is moving to the east having slip value more than reverse zone. Thus, the northern boundary of the area is having left lateral component. A picture from the 45 cm left lateral offset rupture is shown in figure 32. The color scale shows altitude that is also shown by contours. Colored altitude layer is draped on south shaded relief map. See figures 29 and 27 for the location of the Şabakay ridge and stepover. P: 56.

**Figure 32.** Left lateral movement having reverse component along the southwestern boundary of the Boncuk ridge along the Düzce fault. Picture is clearly showing left offset along the fences (looking from south). See figure 31 for the location of the picture. P: 57.

**Figure 33.** Değirmen left stepover area. Black lines: the surface breaks of the 1999 Düzce rupture. Black and white dots show downthrown block of reverse and normal faults, respectively. Vertical and dextral displacements are shown by white and black colored texts, respectively. The color scale shows altitude that is also shown by contours. Colored altitude layer is draped on south shaded relief map. See figures 29 and 27 for the location of the Şabakay ridge and stepover. The dextral offset difference is obvious between east and west of 31°5'30" longitude. Efteni segment that is mostly characterized by normal faulting ends between 31°4'30" and 31°5' longitudes. See figure 25 to locate the map area taking reference longitude 31°5'. P: 58.

**Figure 34.** Splay of the 1999 Kocaeli rupture around western part of the Efteni Lake basin (Fig. 25) on the alluvial fan of the Aksu stream. Yellow short lines are showing exact locations of the cracks that have systematic strike. Yellow filled radar chart box upper left corner is showing general strike of the cracks. The strike is measured mostly (more than 20 cracks) about N113°E that is evident from the yellow filled radar. Average interval is at least one crack about every 100 m at the mouth of the Aksu valley. The color scale shows altitude between 155 and 180 meters in this figure. Contour interval is 20 m. The relief is shaded from northwest to show the details of the fan. Dark blue short lines are showing the location of cracks that mm to cm scale deformation occurred during both 1999 Kocaeli and Düzce earthquakes and western terminus point of the 1999 Düzce rupture. P: 62.

**Figure 35.** Right-lateral displacements of the 1999 Kocaeli rupture near Küçükmelen stream. See figure 25 for the location of the intersection point between the stream and rupture. Picture below and above were taken from southwest and north, respectively. The offset is a couple of centimeters in the location that is shown in the picture above. The offset that is deduced from en-echelon structures (see picture below) is more than 20 cm in the area. P: 63.

**Figure 36.** Reconstruction by left-lateral displacement of the shutter ridges to the probable original locations according to the morphological signs. The match of the valleys suggest at this reconstruction is a possible one. The map above is current relief. White line is the surface breaks of the 1999 Düzce rupture on this map. See figure 29 to see the location of the series of the shutter ridges. The relief is shaded from south. The figure below shows left lateral reconstruction of northern block with respect to southern about 1 km along the Düzce fault (red line). Blue lines are stream valleys. Take ridge and hill names and stream valleys as references to notice the cumulated displacement. P: 65.

**Figure 37.** The 1999 Düzce rupture and Mezarlık shutter ridge. Looking from the east on Şabakay hill. Shutter ridges exhibit typical strike-slip fault morphology lining up along the fault. See figures 29 and 36 for the location of the ridge, the rupture and the Düzce fault. P: 66.

**Figure 38.** Linearity along the northern slope of the shutter ridges (dashed black line). This linearity suggests the existence of an abandoned rupture zone of the Düzce fault and probable southern migration of the fault zone because of the counterclockwise rotation of the Almacık block (See text in section 3.1.3). Topographic relief map is shaded from south. Color scale is showing altitude. See figure 29 for the location of the ridges and northern linearity. Same linearity also exists along the northern border of the Tilkili, Meşelik, Yakup and Mezarlık shutter ridge series (Fig. 36). P: 67.

**Figure 39.** Deflected alluvial fan of the Uğursuyu stream. Altitude colored between 210 and 450 meters (see color scale bar) to identify relief along the fault zone. Relief layers are draped on aerial photo. Yellow dotted line is showing the borders of the current fan. White dotted line borders an observation area that includes deflected remnants of the older fan (Fig. 40). Numbered (1, 2 and 3) stream channels had been probably belonging to the Uğursuyu stream. According to the horizontal length scale, the channel 1 on the older fan has been dragged up to about 3 km to the east according to the main hill slope and Uğursuyu valley. The older fan area including Şabakay ridge on the left stepping area of the 1999 rupture (Fig. 30) made up with alluvial deposits. P: 68.

**Figure 40.** The Şabakay ridge (Fig. 39) is made up with alluvial deposits that consist of granitoid and sedimentary gravels and blocks which are transported by Uğursuyu stream from the main slope. P: 69.

**Figure 41.** Surface rupture of the 1944 Bolu earthquake (After Ketin, 1969). Black line: the 1944 rupture. P: 72.

**Figure 42.** The surface rupture locations of 1957 Abant (black line, after Öcal, 1959) and 1967 Mudurnu (yellow line, after Ambraseys and Zatopek, 1969) earthquakes. Blue, red and white lines show the 1999 Kocaeli, Düzce and 1944 Bolu ruptures, respectively in the map area. Color scale shows altitude. Relief is shaded from south. P: 72.

**Figure 43.** Damage distribution map. White dots: observation points. Black line: the 1967 Mudurnu rupture. Ratio of houses 'destroyed or damaged' to 'total number of houses' in villages based on Ambraseys and Zatopek (1969) grided and contoured. Color scale shows the ratio. 1: no damage; 2: 10%>; 3: 10%-25%; 4: 25% – 50%; 5: 50% – 75%; 6: 75% - 100%. The ratio is draped on topographic relief map that is shaded from south. Damage in the south of the rupture was pronounced more than north. P: 74.

**Figure 44.** Location of the Kaledibi-1 trench in Kaledibi site. The location of the site map below is shown by a black box in the map above (See fig. 3 for the location of the map above). Black rectangle in the map below represents the trench. The other trenches that are shown with gray rectangles are exploratory. Air is photo draped on colored and contoured relief map shaded from south. Red line represents the 1999 Düzce rupture. P: 80.

**Figure 45.** Locations of excavations are shown on topographic map along the Mengencik segment. The rectangle to the left and right shows the Bend and Töngelli sites, respectively. See figures 46 and 47 for large-scale maps of the rectangle areas. Trenches at the Çayır site in the location of right rectangle do not have visible stratigraphy. Yellow and orange areas are Quaternary alluvium and alluvial cones of streams, respectively. Short black lines: excavations, red line: surface breaks of the 1999 Düzce earthquake. Trenches that their names are collared with red, contain dated events. Trenches that their names are colored with yellow contain events but do not have dating. Trenches that their names are colored with black do not have visible stratigraphy. White squares are observation points of the 1999 surface rupture. P: 81.

**Figure 46.** Töngelli and Çayır paleoseismological sites. The color scale shows altitude. Topographic data are draped on aerial photo. Relief is shaded from south. Contour interval is one m. Trenches that names are colored with red contain dated events. Trenches that names are colored with yellow contain events but do not have dating. Trenches that their names are colored with black do not have visible stratigraphy. Dotted lines are representing boundaries of the alluvial fans and dashed lines streams. See figure 45 for the location of the map area in small scale. P: 82.

**Figure 47.** Locations of Bend 1, 2, 3 trenches in the alluvial cone of Bend stream. A: topographic relief map of the Bend site. Altitude is represented by color scale and relief is shaded from southwest. Rectangles are trench locations. No event was recognised in a trench that has black font trench name. Events were recognised and dated in the trenches that have red label. B is showing Quaternary development of Bend stream fan in the same area on contoured (1 m interval) topographic map. Both A and B have identical scale. Trapped alluvial cone of the Bend stream is shaded by dark yellow color drape on aerial photo. Light yellow is showing current bed of the stream. The fan had been propagated back in to the valley filling it towards uphill direction because it has been blocked from north by the Kahveci shutter ridge. See figure 45 for smaller scale topographic map of the area. Convex fan geometry on the topography does not exist here. This rather abnormal 3-D geometry is probably related to the erosion and faulting. P: 84.

**Figure 48.** The picture of the Çayır trench site looking from north and the excavator that was used for trenching. See figure 46 for the location of the site. P: 86.

**Figure 49.** Gasoline powered water pump engine was used for dewatering operations. P: 87.

**Figure 50.** Trenches were shored by building a wooden frame in order to prevent collapse of the trench walls in the unconsolidated sediments. Screw jacks were used for executing shoring. P: 88.

**Figure 51.**  $^{14}\text{C}$  decay curve. Decrease in radiocarbon with time according to radioactive decay (From Trumbore, 2000). Carbon content was expressed as the ratio of  $^{14}\text{C}$  to  $^{12}\text{C}$ . Half-life of  $\beta$ -decaying of  $^{14}\text{C}$  to  $^{14}\text{N}$  is 5730 years. P: 93.

**Figure 52.** Radiocarbon calibration curve for recent years (Stuiver et al., 1998). Dilution of amount of  $^{14}\text{C}$  in the atmosphere by releasing large amounts of  $^{12}\text{C}$  after about 1950. Over 400 years correspond to a plateau in time range 1650-1950 A.D. P: 94.

**Figure 53.** Radiocarbon calibration curve from studies of tree-rings of the ancient trees (Stuiver et al., 1998). It goes back nearly 11,000 years. P: 95.

**Figure 54.** Example of a wide time range radiocarbon calibration (R26946/5 sample, Table 2). Conventional radiocarbon age of the sample is  $266 \pm 50$  years BP. Calibration curve of Stuiver et al. (1998) is shown as blue line. Error curve of the conventional date is shown by red line. Probability curves of calibrated data are shown by black filled curves.  $\sigma_1$  (68.2% probability) ranges below the probability curves,  $\sigma_2$  (95.4% probability) ranges below  $\sigma_1$  ranges and 99.7% probability range below  $\sigma_2$  ranges. The conventional date corresponds to more than one (three) corrected date ranges for this sample according to  $\sigma_2$  and  $\sigma_1$  threshold levels. This wide time range is the result of plateau in time range 1650-1950 A.D. of the calibration curve (See also fig. 52). P: 96.

**Figure 55.** The picture of the Töngelli-1 trench (looking from north). Alluvial cone of the Töngelli stream was excavated perpendicular to the surface rupture of the 1999 Düzce earthquake. See figure 46 for the location of the trench. P: 99.

**Figure 56.** Log of the west wall of trench Töngelli-1. Carbon sample location is outlined in black rectangles.  $^{14}\text{C}$  ages is given in the rectangles. See figure 46 for the trench site. More detail drawing is available in appendix 4. There are two structural blocks left and right of the 6<sup>th</sup> meter (See the section 4.3.1.1). The 1999 rupture not visible in the exposure because of the chaotic nature of the fault material. The rupture clearly observed on the surface. The surface break location outlined in the figure. Event A was recognized as a normal faulting between 8<sup>th</sup> and 10<sup>th</sup> meters and event F as a compressional feature related to a push up. The local depression between 0<sup>th</sup> and 4<sup>th</sup> meters occurred between the push-up and slope of the fan. Unit A is the fill deposited in the depression. P: 100.

**Figure 57.** There is depression area between the slope of the hill and push-ups of the surface break. Northside up vertical displacements on the 1999 Düzce rupture, a couple of meters east of the Töngelli 1 trench. Pictures above and below were taken by looking from eastsoutheast and westnorthwest, respectively. P: 101.

**Figure 58.** Log of the west wall of trench Töngelli-3. Carbon sample location is outlined in black square (R28325/10).  $^{14}\text{C}$  age is given in the rectangles. Shaded area in Unit A is a wedge fill that contains gravelly sand deposit (Unit C). Uniform deposition of the unit A around 2 m depth and around 2<sup>nd</sup> meter from sotuh was probably interrupted (locally) by the deformation related to event E and unit C fill the fissure that was occurred on the event horizon like the fissure of the 1999 event. The other fissure fill (Unit D) represents another event. However it is not dated in this study. All of the events including the 1999 rupture have similar deformation as a normal faulting in the site. Both the sizes and shapes of the fissures are similar to each other. The typical trough morphology related to rupture clearly observed from the surface rupture of the 1999 earthquake in the site (See fig. 59). See figure 46 for the trench site. The part between 8<sup>th</sup> and 13<sup>th</sup> meters of the rech log is imported from the parallel trench (Töngelli-2). P: 104.

**Figure 59.** Surface deformation of the 1999 rupture near Töngelli-3 trench location. Trough morphology is clear along much of the valley from the trench location to the east (See fig. 46). P: 105.

**Figure 60.** Normal faulting in clayey units (unit 2) cannot be seen because of their fine-grained nature. The faulting can be recognized by the existence of three evidence at the same time. One is offset of the unit boundaries (the boundary between units 1 and 2) below this kind of material. The other is existence of a cavity in

the material. The cavity in the figure A related to occurrence of trough along the fault. The third, position of the cavity that has similar geometry to the normal faulting should be just on the normal faulting that is directly detectable along the boundary. P: 106.

**Figure 61.** Exposure of the Bend-1 trench. Carbon sample location is outlined in black square (R28325/9, Table 2).  $^{14}\text{C}$  age is given in the rectangle. Unit D is shown with a rectified picture (Fig. 62) on log with radial transparency. It is a wedge fill that contains gravel deposit. The surface rupture of the 1999 event is 1 m north of the left boundary of the log and perpendicular to the trench. See figure 47 for the trench site. P: 107.

**Figure 62.** The picture of the eastern wall of the Bend-1 trench. A wedge fill contains gravel deposit (See fig. 61). P: 107.

**Figure 63.** The log of the east wall of trench Bend-3. Location of the 1999 rupture not clearly detectable do to the fine nature of the material. Unit D is a wedge fill that contains gravelly silt deposit. Gravels are shaded by gray and brick pieces with orange in this unit. Carbon sample location is outlined in black square at 0.5 meter north of the station 2<sup>nd</sup> and at the bottom tip of the wedge (R28325/3).  $^{14}\text{C}$  age is given in the rectangle. The sample represents the starting time of the deposition of the fill material just after the earthquake. Unit A and B: flood deposits. See figure 47 for the trench site. P: 109.

**Figure 64.** Kaledibi-1 trench exposure. Carbon sample location is outlined in black square (R28325/5).  $^{14}\text{C}$  age is given in the rectangle. The deeper half of the trench are divided into four structural blocks according to faults a, b and c. The faulting b is buried by unit C and dated by the sample. See figure 44 for the trench location. P: 110.

**Figure 65.** Collapsed trench (Kaledibi-1). Some of the trenches have high collapse risk. P: 111.

**Figure 66.** Western wall of the Töngelli-1 trench. All the units bend towards the surface along the fault zone related to compressional component. Black arrow represents the fault zone including the 1999 rupture. White lines indicate unit boundaries. See figure 56 for the complete log of this exposure. P: 118.

**Figure 67.** Serial-A least square fit of maximum limits of the maximum constraining event dates (See table 2). The November 12, 1999 (1999,9) event (0<sup>th</sup> rupture) is set as intercept in regressions. Equations of the trends are shown in boxes colored according to pattern and the color of the trend lines. The four events including 1999 event in the serial are designed using data from this study. The serial seem to be sequential. P: 121.

**Figure 68.** Serial-B least square fit of maximum and minimum limits of the maximum and minimum constraining event dates (See table 2). The November 12, 1999 (1999,9) event (0<sup>th</sup> rupture) is set as intercept in regressions. Equations of the trends are shown in boxes colored according to pattern and color of the trend lines. The earthquake recurrence interval value changes between 350 and 405 years according to  $\sigma 1$  interval. The last seven events including 1999 event in the serial are designed using data both from this study and from Hitchcock et al. (2003). The serial seem to be sequential. This serial is extended version of the serial-A including data from the previous study (Fig. 67). The data fills the gaps in my data and extends the serial back in time. P: 123.

**Figure 69.** Least square fit of the minimum limits of the minimum constraining event dates assigning the event B to the 7<sup>th</sup> rupture (See table 2). RMS values related to this design worse values than the fit that modeled considering the event as the 6<sup>th</sup> rupture. The November 12, 1999 (1999,9) event (0<sup>th</sup> rupture) is set as intercept in regressions. Equations of the trends are shown in boxes colored according to pattern and color of the trend lines. P: 126.

**Figure 70.** Probability distribution for the 1999 rupture (0<sup>th</sup> rupture) according to distribution for each probability of the constraints. This best estimation of the rupture is made by using the design of the final event serial that is shown in figure 72. P: 128.

**Figure 71.** Probability distribution of the future rupture (-1<sup>st</sup>) according to distribution for each probability of the constraints. This distribution calculated using the model that best estimates the 1999 (0<sup>th</sup>) rupture (Fig. 70). P: 129.

**Figure 72.** Final serial least square fit of maximum and minimum limits of the maximum and minimum constraining event dates (See table 2). The November 12, 1999 (1999,9) event (0<sup>th</sup>) is set as intercept in regressions. Equations of the trends are shown in boxes colored according to pattern and the color of the trend

lines. The earthquake recurrence interval value changes between 350 and 394 years according to  $\sigma_1$  interval. The last twelve events including 1999 event in the final serial are designed using data both from this study and from Hitchcock et al. (2003). The oldest two events result in irregularities in the periodical model. Probably unrecognized two events between 6<sup>th</sup> and 9<sup>th</sup> ruptures and one event between 9<sup>th</sup> and 11<sup>th</sup> ruptures in the sequence erase the irregularities. This model is best estimates the 1999 event (See fig. 72) according to distribution for each probability method (See section 4.4.1.4). P: 130.

# LIST OF TABLES

**Table 1.** Selected borehole data that are used for basement topography and sediment thickness models (see section 2.2) was taken from DSI. First 8 are the basement reaching and the others are hanging boreholes in alluvium. Some of the hanging boreholes are eliminated (see section 2.2). Locations are shown on figure 18. P: 32.

**Table 2.** Radiocarbon dates from trenches across the November 12, 1999 Düzce rupture. P: 98.

## ABBREVIATIONS

|        |  |
|--------|--|
| AD:    | CAL (calendar) years or absolute years |
| AES:   | Aegean Extensional System              |
| AMS:   | Accelerator mass spectrometry          |
| BP:    | Before present (1950)                  |
| BT:    | Basement topography                    |
| GMT:   | Greenwich Mean Time                    |
| GPS:   | Global Positioning System              |
| HL:    | Half-life                              |
| IDT:   | Initial dextral transtensional         |
| LSQ:   | Least Squares method                   |
| NAF:   | North Anatolian Fault                  |
| NAFZ:  | North Anatolian Fault Zone             |
| NAIS:  | Northern Almacık Strand                |
| NArS:  | Northern Armutlu Strand                |
| NSC:   | N-S compression                        |
| RMS:   | Root mean square                       |
| SAIS:  | Southern Almacık Strand                |
| SAR:   | Synthetic Aperture Radar               |
| SArS:  | Southern Armutlu Strand                |
| SASS:  | South Aegean Subduction System         |
| SLR:   | Satellite Laser Ranging                |
| STM:   | Surface topography map                 |
| WNAF:  | Western North Anatolian Fault          |
| WNAFS: | Western North Anatolian Fault System   |

## Abstract

In 1999, two earthquakes ruptured the Northern Almacık strand (NAIS) of the North Anatolian Fault that includes the Düzce and Aksu faults, producing surface rupture along the northern border of the Almacık block. Paleoseismological trenching is performed at four sites along the Aydınpınar and Mengencik segments of four-structural-segmented Düzce fault. Six dated-events from eleven trenches that cross cuts the fault zone provided insights on its seismogenic behavior. The excavations from five trenches at three sites expose evidence for six earthquakes that occurred since B. C. 1740. A shallow of watertable, unfavorable trench materials and lack of financial support to perform 3-D trenching made the identification and characterization of individual paleoearthquakes difficult. However, by integrating date constrains of events from the trenches that were performed along the Düzce fault including previous studies along the easternmost segment, a periodical recurrence model seems to be concordant with the radiocarbon age data. Seven serial surface-rupturing earthquakes including the 1999 Düzce event along the Düzce fault are defined. The model suggests that the Düzce fault is behaving as a single seismic segment at least for the last serial rupture in Holocene time. The additional two older events are showing an irregularity in the serial. Hitherto unrecognized earthquakes probably would eliminate this irregularity. A recurrence interval is estimated by also considering the two older earthquakes. This final sequential model suggests that 1999-type earthquakes repeat each  $355\pm 35$  year (% 70 probability). The slip rate that was calculated from 350 cm average slip of the 1999 event and the recurrence period is about  $9.5\pm 1$  mm/yr having % 70 probability. This value is in agreement with geodetic measurements (10 mm/yr) from independent studies. Because short time has elapsed since the 1999 earthquake that occurred along the Düzce fault, the Düzce fault does not appear to have an important seismogenic potential in near future. The Düzce plain is one of the major basins of the Marmara region. There is no active faulting excluding Düzce and Aksu faults that is detected in the basin and surrounding borders according to this study. In addition to this pull-apart and then continuing active formation of the Düzce basin hypothesis is not validated by rigorous data. Therefore, considering these data, it may be suggested that Düzce area is not under a severe seismogenic threat for very near future.

## Özet

1999 yılında iki deprem Düzce ve Aksu faylarının yer aldığı Kuzey Anadolu fayına ait Kuzey Almacık kolunun kırılmaya uğramasına sebep olup, Düzce havzasının güney sınırı boyunca yüzey kırığı oluşturmuştur. Dört yapısal parçaya ayrılan Düzce fayının Aydınpınar ve Mengencik parçalarındaki dört yerde paleosismolojik hendek kazısı yapılmıştır. Fay zonunu dikine kesecek şekilde açılan onbir hendekten elde edilen altı adet tarihlendirilmiş deprem olayı fayın sismojenik davranışı hakkındaki ilksel düşüncelerin gelişmesine hizmet etmiştir. Üç yerde açılan beş hendekten M. Ö. 1740'tan itibaren oluşmuş altı depreme ait kanıtlar ortaya çıkartılmıştır. Yüksek yeraltı suyu seviyesi, istenmeyen hendek malzemeleri ve finansal desteğin yetersizliği nedeniyle 3 boyutlu hendek açamama sebeplerinden ötürü eski depremlerin karakteristik özellikleri ve ayırt edilmelerinde güçlüklerle karşılaşmıştır. Ancak Düzce fayı boyunca açılmış hendekler ve en doğu parçada açılan önceki çalışmalara ait hendeklerden ortaya çıkartılan olaylara ait zaman sınırların bütünleştirilmesi ile yaş verisi ile ters düşmeyen uygun bir periyodik deprem tekrarlama modeli bulunmuştur. 1999 Düzce depremi de dahil olmak üzere yedi yüzey kırığı oluşturan bir seri deprem tanımlanmıştır. Model Düzce fayının en azından bu son seri için Holosen'de yalnız bir sismik fay parçası olarak davrandığına işaret etmektedir. Daha yaşlı olan diğer iki olay ise seride uyumsuzluk göstermektedir. Ancak henüz rastlanmamış olan depremler bu uyumsuzluğu muhtemelen ortadan kaldırabilir. Bu iki deprem de işin içine katılarak bir tekrarlanma aralığı hesaplanmıştır. Tekrarlamalı son modele göre 1999 benzeri depremler  $355 \pm 30$  (% 70 olasılıkla) yılda bir tekrar etmektedir. Kayma hızı miktarı ise 1999 depremine ait 350 cm ortalama atım ve bu tekrarlama aralığı göz önüne alınarak % 70 olasılıkla yaklaşık  $9.5 \pm 1$  mm/yıl olarak hesap edilmiştir. Bu değer jeodetik ölçümlerle ortaya konulan 10 mm/yıl kayma hızı miktarı ile uyum içerisindedir. Düzce fayında meydana gelen 1999 depreminden bu yana az bir zaman geçtiğinden dolayı yakın bir gelecek için Düzce fayı önemli bir sismojenik potansiyel teşkil etmemektedir. Düzce ovası Marmara bölgesindeki önemli havzalardan birisini temsil etmektedir. Bu çalışma çerçevesinde yapılan araştırmalarda Düzce havzası yakınları veya sınırlarında, 1999 depremlerinde etkinlik göstermiş olan Düzce ve Aksu faylarının dışında bir diri faya rastlanmamıştır. Ayrıca, Düzce ovasının bir çek-ayır havza niteliğinde ve aktif olduğu savı yeterli ayrıntıda verilerle kanıtlanamamış bulunmaktadır. Bu nedenlerle, bu verilerden hareketle Düzce bölgesinin yakın gelecekte önemli sismik kökenli bir tehdit altında olmadığı görüşü ağırlık kazanmaktadır.

# TABLE OF CONTENTS

|   |           |
|---|-----------|
| Preface.....  | i         |
| List of Figures.....  | ii        |
| List of Tables.....   | x         |
| Abbreviations.....  | xi        |
| Abstract.....   | xii       |
| Özet.....   | xiii      |
| Table of Contents.....  | xiv       |
| <br>  |           |
| <b>1. INTRODUCTION.....</b>   | <b>1</b>  |
| 1.1. HISTORICAL ACCOUNTS FOR EARTHQUAKES.....                         | 7         |
| <b>2. GENERAL TECTONIC REGIME.....</b>                                | <b>10</b> |
| 2.1. GEOMORPHOLOGY.....   | 12        |
| 2.2. GENERAL GEOLOGY.....   | 20        |
| 2.3. SEISMICITY.....  | 36        |
| 2.4. GEODETIC MEASUREMENTS.....                                       | 37        |
| 2.5. SUMMARY AND DISCUSSION.....                                      | 39        |
| <b>3. THE MAJOR ACTIVE FAULTS.....</b>                                | <b>42</b> |
| 3.1. NORTHERN ALMACIK STRAND OF THE NAF.....                          | 43        |
| 3.1.1. <i>DÜZCE FAULT</i> .....                                       | 47        |
| 3.1.1.1. Geometry.....  | 52        |
| 3.1.1.2. Rupture Slip.....  | 55        |
| 3.1.1.3. Discussions.....   | 58        |
| 3.1.2. <i>AKSU FAULT</i> .....  | 60        |
| 3.1.3. <i>QUATERNARY OFFSET</i> .....                                 | 64        |
| 3.1.4. <i>SEGMENTATION</i> .....                                      | 69        |
| 3.1.5. <i>SLIP RATE</i> .....   | 70        |
| 3.2. SOUTHERN ALMACIK STRAND OF THE NAF.....                          | 70        |
| 3.2.1. <i>1944 BOLU RUPTURE</i> .....                                 | 71        |
| 3.2.2. <i>1957 ABANT RUPTURE</i> .....                                | 73        |
| 3.2.3. <i>1967 MUDURNU RUPTURE</i> .....                              | 73        |
| 3.2.4. <i>SEGMENTATION</i> .....                                      | 75        |
| <b>4. PALEOSEISMOLOGICAL INVESTIGATIONS:<br/>THE DÜZCE FAULT.....</b> | <b>78</b> |
| 4.1. SITE DESCRIPTION AND TRENCH LOCATION.....                        | 79        |
| 4.2. METHODS.....   | 85        |
| 4.2.1. <i>TRENCH LOCATING AND EXCAVATION STRATEGIES</i> .....         | 85        |
| 4.2.2. <i>IDENTIFICATION OF EARTHQUAKE HORIZONS</i> .....             | 90        |
| 4.2.3. <i>RADIOCARBON DATING ISSUES</i> .....                         | 92        |
| 4.3. ANALYSIS OF THE EXPOSURES.....                                   | 99        |
| 4.3.1. <i>THE EXCAVATIONS</i> .....                                   | 99        |
| 4.3.1.1. Töngelli-1 (T1).....   | 99        |
| 4.3.1.2. Töngelli-3 (T3).....   | 103       |
| 4.3.1.3. Bend-1 (B1).....   | 106       |
| 4.3.1.4. Bend-3 (B3).....   | 108       |
| 4.3.1.5. Kaledibi-1 (K1).....   | 109       |
| 4.3.2. <i>EVIDENCE FOR PALEOSEISMIC EVENTS</i> .....                  | 113       |
| 4.3.2.1. Event A.....   | 113       |

|   |            |
|---|------------|
| 4.3.2.2. Event B.....                                 | 114        |
| 4.3.2.3. Event C.....                                 | 114        |
| 4.3.2.4. Event D.....                                 | 115        |
| 4.3.2.5. Event E.....                                 | 116        |
| 4.3.2.6. Event F.....                                 | 117        |
| 4.4. TIMING THE EARTHQUAKES.....                      | 119        |
| 4.4.1. SEQUENTIAL MODEL.....                          | 119        |
| 4.4.1.1. Data-set Quality.....                        | 119        |
| 4.4.1.2. Serial-A Model.....                          | 120        |
| 4.4.1.2.1. Event Identification and Model Design..... | 120        |
| 4.4.1.3. Serial-B Model.....                          | 123        |
| 4.4.1.3.1. Event Identification and Model Design..... | 124        |
| 4.4.1.4. Final Serial Model.....                      | 127        |
| 4.4.1.4.1. Distribution for Each Probability.....     | 127        |
| 4.4.1.4.2. Model.....                                 | 128        |
| 4.4.2. ASSIGNING HISTORICAL DATA.....                 | 131        |
| <b>5. SUMMARY AND DISCUSSION ON TECTONICS.....</b>    | <b>134</b> |
| <b>6. CONCLUSION.....</b>                             | <b>136</b> |
| <b>ACKNOWLEDGEMENTS.....</b>                          | <b>141</b> |
| <b>REFERENCES.....</b>                                | <b>142</b> |
| <b>APPENDIX 1.....</b>                                | <b>154</b> |
| <b>APPENDIX 2.....</b>                                | <b>154</b> |
| <b>APPENDIX 3.....</b>                                | <b>154</b> |
| <b>APPENDIX 4.....</b>                                | <b>154</b> |

# 1. INTRODUCTION

On 17<sup>th</sup> August 1999, a destructive Kocaeli earthquake struck the city of İzmit and surrounding area including the high-populated town of Düzce. The earthquake was followed by a second destructive earthquake (1999 Düzce earthquake) to the east about 3 months later. The November 12, 1999 Düzce earthquake ( $M_w=7.2$ ) occurred on the Western North Anatolian Fault System (WNAFS) near the town of Düzce (today, it is a city) that takes part in the middle of Düzce basin. The 1999 Düzce earthquake was strongly felt in eastern Marmara region including the city of Bolu. It resulted in tragic deaths and considerable structural damage to buildings in Düzce city. In this study, basic geological data of the seismogenic sources that are threatening urbanization in the Düzce plain is provided. This site and its broad vicinity are studied to identify potentially active faults behaving as a seismic source (Fig. 1). Behaviors of the identified faults are described using earthquake-geology techniques as well as existing literature. The 1999 Düzce and Kocaeli earthquakes served great opportunity to make detailed investigations (Fig. 2). To utilize this opportunity and to increase detailed information about the parameters of these faults, paleoseismological techniques were used along the 1999 Düzce rupture zone (Fig. 3).

A critical issue facing seismic hazard analysis is; whether the fault catalogue which serves as knowledge base for fault parameters is complete or not. The main parameters are (1) slip per event, (2) slip rate, (3) recurrence time and (4) elapsed time. Starting from geological data, the main parameters that describe the characteristics of the Düzce fault that were ruptured by the 1999 Düzce earthquake (Fig. 2) are calculated. These parameters are all referred to the occurrence of repeated surface faulting (large) earthquakes on the fault. Evidence and reported dates are described for six large earthquakes in 3540 years before 1800 A.D. which occurred before the 12<sup>th</sup> November 1999 Düzce earthquake. These events were revealed in excavations across the middle part of the Düzce fault at four sites in three locations (Fig. 3). Using several radiocarbon ( $^{14}\text{C}$ ) age determinations for various faulted late Holocene layers including paleoseismological results of Hitchcock et al. (2003) from the eastern part of the fault, a recurrence interval is suggested between the events in section 5.

In the section 4, the identified major active faults are described near the Düzce city using the

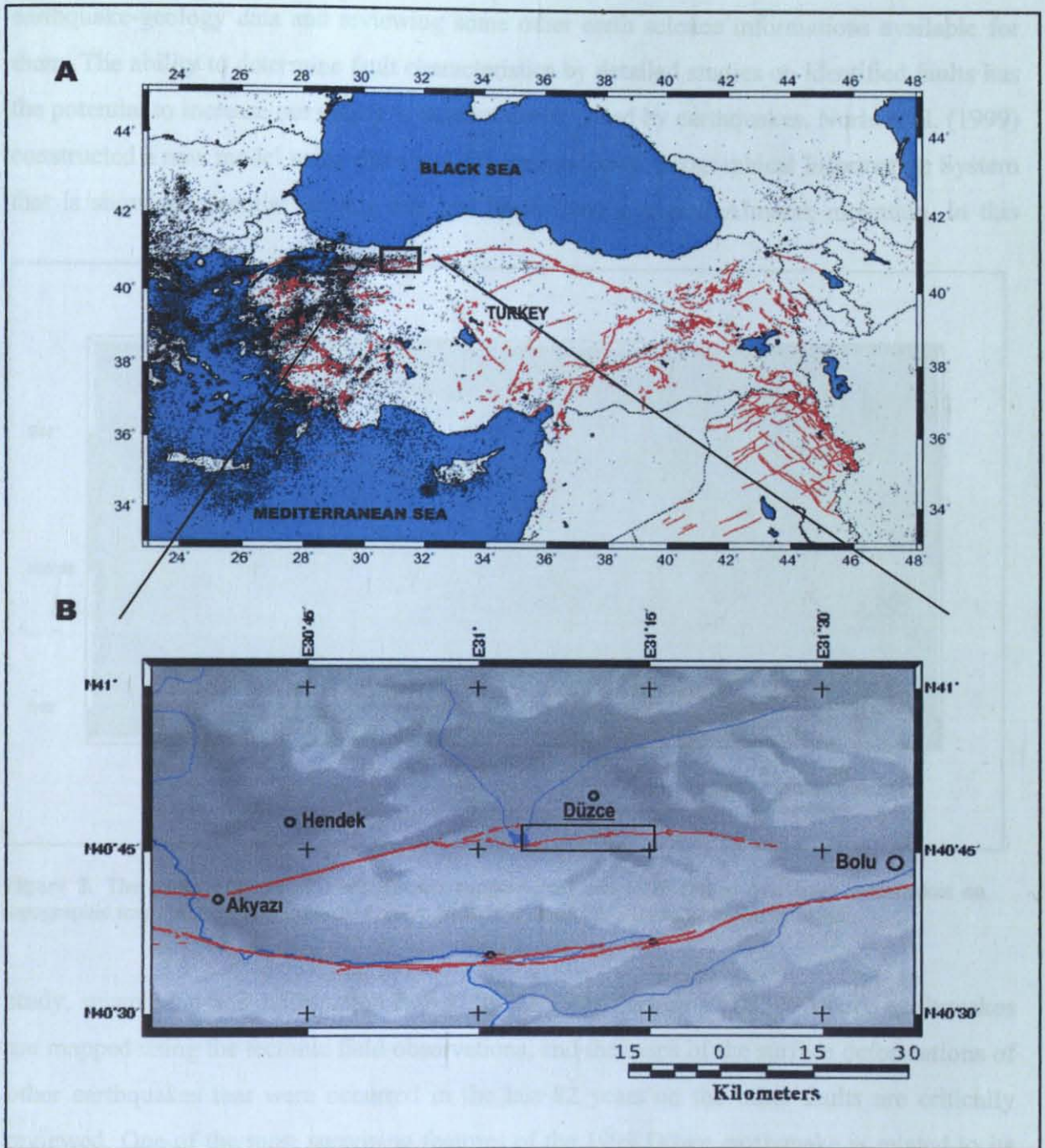


**Figure 1.** Location of the study area. A: Seismicity and active fault map of Turkey and surrounding area. Black dots are all the earthquakes taken from USGS catalogue. Red lines are active faults (Şaroğlu et al., 1992). B: The study area is shaded from southwest on the relief map. It is shown with a rectangle in A. Red lines are surface breaks of earthquakes since 1944.

earthquake-geology data and reviewing some other earth science informations available for them. The ability to determine fault characteristics by detailed studies on identified faults has the potential to increase our ability to assess the risk posed by earthquakes. Nurlu et al. (1999) constructed a new model using them and site parameters in Geographical Information System that is showing potential seismic risk and hazard zones around Almacik mountain. In this

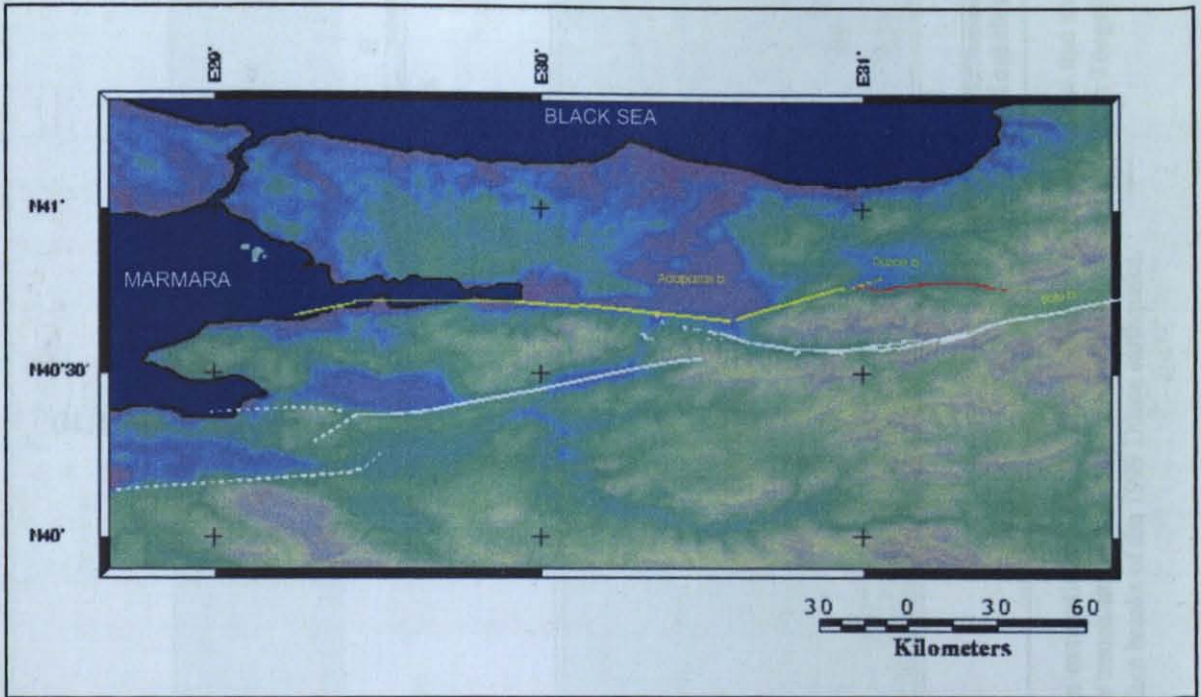


**Figure 2.** The surface breaks of 1999 Kocaeli (yellow line) and 1999 Düzce (red line) earthquakes on topographic map. White line shows other active faults and dashed line is probable active faults.

study, seismic surface deformation caused by the 1999 Kocaeli and 1999 Düzce earthquakes are mapped using the tectonic field observations, and the maps of the surface deformations of other earthquakes that were occurred in the last 82 years on the other faults are critically reviewed. One of the most surprising features of the 1999 Düzce earthquake is related to its rupture geometry which appears to contradict what is commonly observed in strike-slip earthquakes. Its fault plane dips to the north at a very low ( $\sim 65^\circ$ ) angle which is inconsistent with its rake. This angle was gathered by evaluating seismological data that were collected from local stations by Milkereit et al. (2000). The other studies that depend on the modeling of geodetic and seismic data show similar north directed dip angle ranging between  $53^\circ$  and  $65^\circ$  (E.g., Harvard, web; Yagi and Kikuchi, web; Özalaybey et al., 2000; Bock et al., 2000;

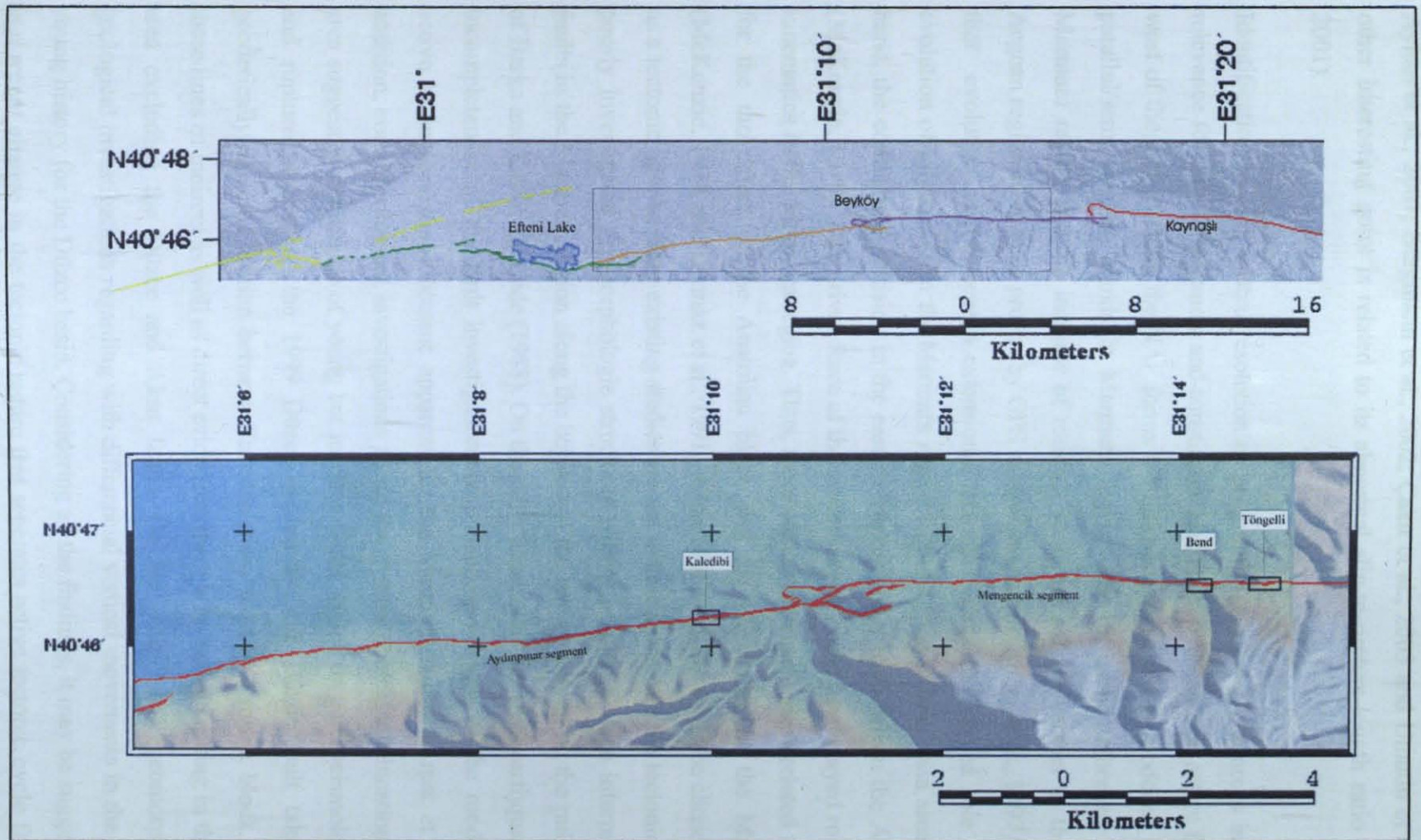


**Figure 3.** Locations of trench sites that age results were got from excavations along the Düzce fault on relief map below that shaded from southwest. The map area is shown with a rectangle in the map above. There is one trench site in Kaledibi, one site in Bend and two sites in Töngelli location. Map location is shown with a rectangle in Fig. 1B. The red line represents the surface breaks of the 1999 Düzce earthquake.

Ayhan et al., 2001; Bürgmann et al., 2002; Çakır et al., 2003 and Umutlu et al., 2004). The other interesting point is related to its abnormal slip-to-rupture-length ratio (Ayhan et al., 2001).

Identification at high spatial resolution of potentially seismogenic sources is of significant relevance for risk management and constitutes the first step to describe active faulting. To the west of the city of Bolu, the NAF forms a diffuse boundary that is produced by a couple of parallel/semi-parallel strands in Marmara region. The diffusely deforming nature of the Marmara region and the increase of residual velocities of slip vectors to the south in the Aegean region have been proven by GPS measurements (Reilinger et al., 1997). It is probable that evolution of the Aegean extensional tectonic regime has played role in changes or evolution of kinematics in the Marmara region including the Düzce basin area. On the other hand, the continental collision in the eastern Turkey could have driven the Anatolian block (McKenzie, 1978). This driven force of the tectonic event could have played role about recent kinematics in the Marmara region. Thus, there are controversial ideas related to driven force for the movement of the Anatolian block and the kinematics of the Marmara region (McKenzie, 1978 and Taymaz et al., 1991). None of the models could be chosen in this study as a tectonic base because existing studies are not mature to explain the tectonic nature. Some poorly investigated geomorphologic structures within the NAFZ were interpreted as active faults in the Marmara region along the borders of the basins leaning on the pull-apart models of Barka and Kadinsky-Cade (1988). On the other hand, after the 1999 earthquakes in Turkey, incompleteness of the fault investigations and inappropriateness of the models to explain active basin formations became apparent for the Marmara region (Arpat et al., 2001). In addition, some geological investigations along the geomorphological lineations in the study area suggest the existence of young but inactive faults. Based on paleoseismological findings and rupture process of the 1999 Düzce earthquake, the Düzce fault takes up all the geodetically detected motion between Eurasian plate and the Almacık block. According to these lines of indirect as well as direct evidences, there is no active faulting in the Düzce basin area excluding the Düzce and Aksu faults. On the other hand, geomorphological and geological investigations regarding with differential vertical movements in the area suggest a young history for the Düzce basin. Considering all the findings, it may be suggested that there is a recent change in the tectonic nature that separates active tectonic cycle from the young basin formation cycle. The recent variations in the tectonic regimes that consist of the study area should be considered for active fault identification studies. Some of the young faults

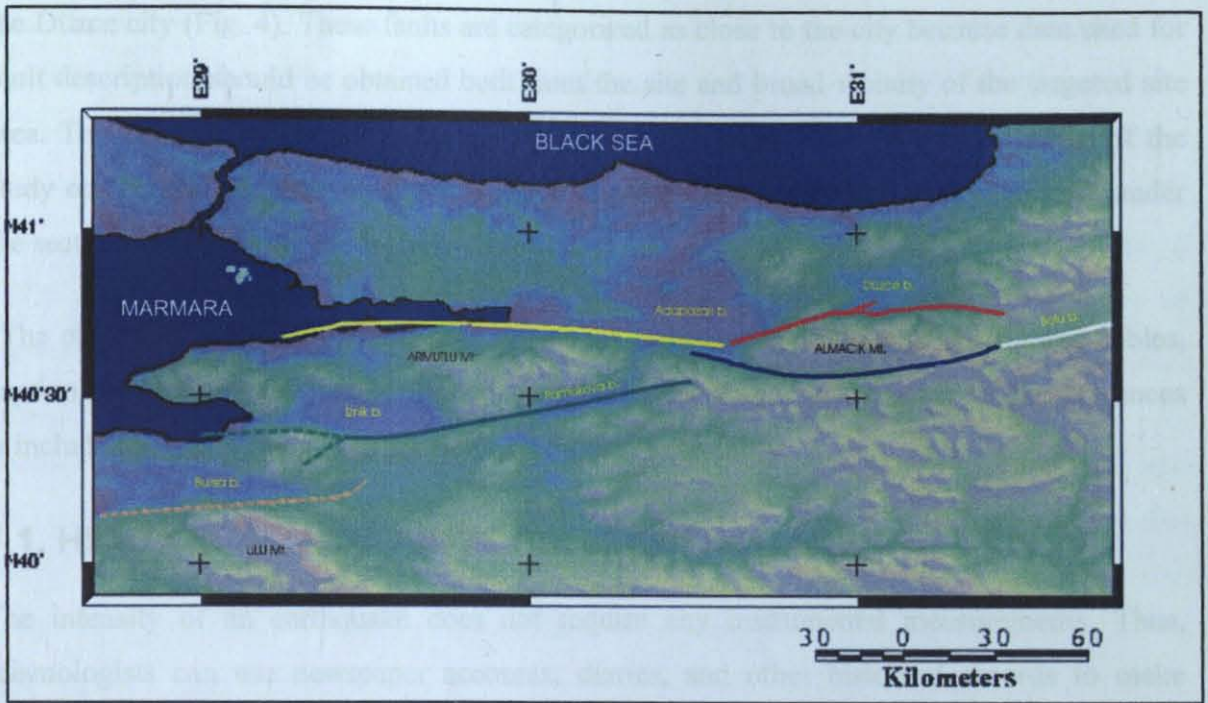


**Figure 4.** Active subparallel strands of the western part of the NAF (WNAF) zone in the Marmara region (west of about  $31^{\circ}30'$  longitude); yellow line: Northern Armutlu strand (NArS), green line: Southern Armutlu Strand (SArS), Blue line: Southern Almacık Strand (SAIS), Red Line Northern Almacık Strand (NAIS). White line: Single strand part of the NAF. Orange line: Bursa strand. Dashed lines: probably active faults. The fault locations have been compiled from Arpat et al. (2001), Ambraseys and Zatopek (1969), Öcal (1959), Taşman (1944) and this study.

probably became inactive during the younger variations in the tectonic regimes as well as during the evolutionary history of the fault zones. Regarding with the relation between the Aegean extensional system and kinematics of the Marmara region (McKenzie, 1978), some of the young features in my study area that is situated in the eastern Marmara region shouldn't be concerned as active, because the recent collision (Early Pleistocene) along the South Aegean Subduction Boundary might have altered the tectonic regime in the Aegean region as well as the Marmara region including Düzce basin. Thus, this alteration might be resulted in the inactivation of some faults that are young in the study area. For this reason, most of the lineations that are detectable on morphology were revised in this study. To the near west of Bolu, the NAF system has two apparent strands bounding the Almacık Mountain from north and south. The northern branch is firstly called Northern Almacık strand (NAIS) and the southern branch is the Southern Almacık Strand (SAIS) in this study. The strands in the eastern Marmara region are distinguished each other according to their different slip rates and locations. The right-lateral motion of the NAF seems to be shared by these two strands along the longitude range from eastern and western margin of the Almacık Mountain (Ayhan et al., 2001). These active strands and eastern extension of the NAF in the Bolu basin are close to

the Düzce city (Fig. 4). These faults are categorized as close to the city because data used for fault description should be obtained both from the site and broad vicinity of the targeted site area. The effort is expended to identify possible active faults close to the city. Most of the study on the identification of active faulting in and around Düzce city is documented under the section 3 considering the regional tectonics.

“The electronic version” of the whole document including hyperlinks to the figures, tables, captions of sections, references, appendixes and the documents of the some of the references is included in the CD media to provide readers easy accesibility.

## **1.1. HISTORICAL ACCOUNTS FOR EARTHQUAKES**

The intensity of an earthquake does not require any instrumental measurements. Thus, seismologists can use newspaper accounts, diaries, and other historical records to make intensity ratings of past earthquakes for which there are no instrumental recordings. As radiocarbon analyses constrain the fault ruptures which have been identified in my excavations to the historical period, it may be possible to assign specific dates to these events (see section 4.4). Such research helps to promote our understanding of the earthquake history of a region and estimates future hazards better.

Instrumental monitoring of seismicity is marking the beginning of modern record. Thus, earthquakes prior to instrumental monitoring are considered as a part of the historical record. The available historical record is too short, sparse, and uneven quality in Düzce region. The last rupture of the Düzce fault occurred in 1999 and we have detailed information about this rupture. However, the historical records of major earthquakes affecting Düzce area before the 1999 event are missing. According to the reviews of historical records (Konukçu, 1984), even before the first Turks (Ottomans) arrived, it is probable that Düzce basin and surrounding area were one of the most populated regions in northwestern Anatolia, particularly around northern part of the Düzce plain especially around Üskübü (Konuralp) that is a settlement in north of the Düzce plain. Üskübü never lost its status. Düzce became a town in 1870 and a city in 2000 (Konukçu, 1984).

Centuries-long historical record is available for large earthquakes which affected İstanbul. This is because İstanbul (formerly Constantinople) has long been a centre of trade and political activity. Several earthquake catalogues have been compiled using this historical record. Ambraseys and Finkel (1995), Ambraseys (2002) and Sakin (2002) have provided the

most recent review of historical records for especially Ottoman period. But, there is no specific information about any Düzce earthquakes in these reviews. However, some obscure information of historical record during Ottoman period regarding two earthquakes around Bolu and Düzce have been reported in Ambraseys and Finkel (1995). These 1719 and 1509 events occurred in Ottoman period. Bakır (2002) made a systematic study concerning earthquakes felt in the city of Constantinople (İstanbul) and its vicinity in Byzantine period by reviewing historical records. Results show that there is no specific information on probable Düzce earthquake. However, some information regarding an earthquake (September 2, 967 earthquake) felt in Bolu and İstanbul is given by Bakır (2002) (See also Ambraseys and Jackson, 1998). During the 967 earthquake, there was no any damage in İstanbul, on the other hand, in Bolu (Claudiopolis) the damage was substantial (Bakır, 2002). At this time, there was a small town in Düzce on the contrary, Bolu is an important city (E.g., Konukçu, 1984). For this reason, it could be recorded just for damage of Bolu area but not for the region of Düzce. However, it could be still a Bolu fault earthquake as suggested by Ambraseys and Jackson (1998).

During the 1509 İstanbul earthquake, walls and towers collapsed. The only available information for Bolu region is very brief and, although it implies heavy damage, there is no mentioning for the loss of life (Ambraseys and Finkel, 1995). “This was one of the largest and most destructive earthquakes of the last five centuries in the Eastern Mediterranean; it occurred in the Sea of Marmara, and was felt over a very large area, causing damage from Bolu to Edirne.” wrote N.N. Ambraseys and C.F. Finkel (1995). Aftershocks had continued to be felt intermittently for over a month in İstanbul and for eighteen days in Bolu. Since there are no reports about the rupture, the location of the rupture is largely a matter of speculation (Klinger et al., 2003). According to the reports (Ambraseys and Finkel, 1995), İstanbul and İzmit were severely damaged. The date of earthquake is also controversial (Sakin, 2002). There are three dates designated to 1509 earthquake: 11 August 1509, 21 August 1509, and 10 September 1509. This discrepancy could be the result of a triggering phenomena like the one which occurred in 1999.

The earthquake of 25 May 1719 destroyed most of the towns on the coasts of the Bay of İzmit, and was effective from Yalova to Düzce like 17 August 1999 Kocaeli earthquake. It has remarkable similarity with 1999 Kocaeli earthquake according to historical records (Sakin, 2002). In concordance with this idea, Ambraseys and Jackson (2000) have estimated a

magnitude of  $M_s$  7.4 for this event, identical to the magnitude of the 1999 Kocaeli earthquake.

## 2. GENERAL TECTONIC REGIME

The Düzce plain lies within the diffusely active part of the dextral tectonic boundary between the Anatolian block and the Eurasian plate, which passes through south of the Black Sea mountains along the northern Turkey. It is within the area of high seismicity and occupies one of the highest earthquake activity regions of Turkey (Fig. 1A).

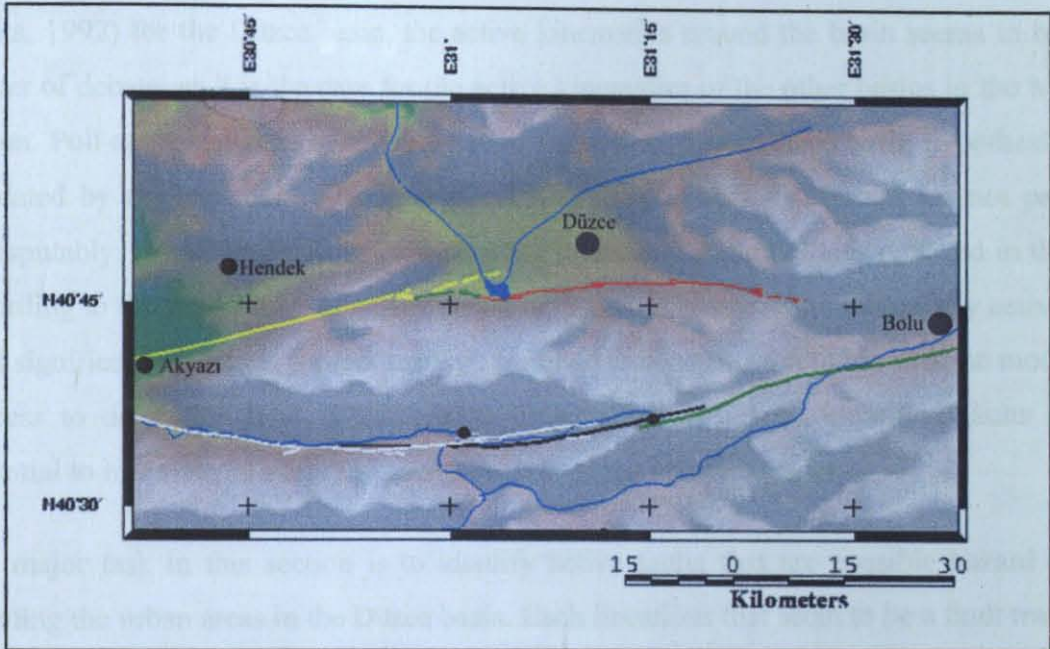


**Figure 5.** Surface rupture of the 1999 Kocaeli (yellow line), 1999 Düzce (red line), 1967 Mudurnu (white line), 1957 Abant (black line) and 1944 Bolu (light green line) earthquakes on the relief map shaded from southwest. The dark green line between the 1999 Düzce and Kocaeli surface ruptures represents a part that was ruptured by both of the earthquakes. The rupture locations of Mudurnu, Abant and Bolu earthquakes have been compiled from Ambraseys and Zatopek (1969), Öcal (1959) and Taşman (1944), respectively. The other rupture locations are drawn according to this study.

The tectonic boundary between the northern margin of the Anatolian block and southern margin of Eurasian plate in Turkey has been called as North Anatolian Fault (NAF) since 1948 (Ketin, 1948). The NAF is a right-lateral tectonic system in an arcuate shape. Along its eastern 1000 km, the structure primarily consists of a single fault. On the other hand, in the west of Bolu it forms a diffuse boundary that is produced by a couple of parallel/semi-parallel strands in the Marmara region (Fig. 4). Near to the west of Bolu, the NAF system has two apparent strands bounding the Almacık Mountain from the north and the south both of which have been ruptured by large earthquakes since 1944 (Fig. 5). The northern branch that is

called as Northern Almacık strand (NAIS), was ruptured in 1999 by two large earthquakes: 1999 Kocaeli and Düzce earthquakes. The eastern part of the NAIS was ruptured during the 1999 Düzce earthquake and the western part during the 1999 Kocaeli earthquake that has additional ruptured strands, further to the west, through Yalova (Fig. 2). The southern branch which is called as Southern Almacık strand (SAIS), has been ruptured by 1944 Bolu, 1957 Abant and 1967 Mudurnu earthquakes (Fig. 5). The right-lateral motion of the NAF is shared by at least these two strands along the longitude range from eastern and western margin of the Almacık Mountain. In spite of the widely accepted suggestions of pull-apart model (e.g., Barka, 1992) for the Düzce basin, the active kinematics around the basin seems to be still a matter of debate, as it is the case for the active kinematics of the other basins in the Marmara region. Pull-apart and then continuing active formation of the Düzce basin hypothesis is not validated by rigorous data. Elements of active pull-apart tectonic system are not presented undisputably. No active faulting excluding the Düzce and Aksu faults is detected in the basin according to the field study. Identification at high spatial resolution of potentially active faults is of significant relevance for risk management and to construct a reliable tectonic model. The success to determine fault characteristics by detailed studies on identified faults has the potential to increase our ability to assess the risk posed by earthquakes.

The major task in this section is to identify active faults that are possible hazard sources threatening the urban areas in the Düzce basin. Each lineations that seem to be a fault trace were studied. Some of them are faults and the others are not. Some of the faults are active and the others inactive. Description of the term “active” could be discussionable as far as the practical puposes are concerned. In this study the term active fault was used as a fault active in the current kinematic pattern. The current and previous regimes that have shaped the study area are discussed in the following sections. According to geological and geomorphological observations, Düzce and Aksu faults are the active faults that are the elements of the current kinematics in the Düzce basin. Some of the active faults in the Düzce basin are so close to the city and some of them are outside of the basin but still close enough to affect it. For this reason the study area, involve close vicinity of the Düzce basin. In the summary of this section, a fault set is prepared that certainly threats the urbanization in the Düzce plain. The proximity to the several tectonic regimes of episodes and overprinted pre-existing many tectonic structures complicate the tectonics of the region. These structures orientate the local active tectonic processes considerably. The presence of several parallel active dextral faults in the region rather than of a single fault may be related to these structures. The consistent active

tectonics is discussed at the summary of this section and the study on the prepared set of fault is presented in the section 3.

As a practical matter, fault investigation should be directed at the problem of locating existing faults and then attempting to evaluate the recency of their activity. The most useful and direct method of evaluating recency is to observe the youngest geological unit faulted. However, in most it is impossible or difficult to find valuable observation site (trench or outcrop) to apply a direct method. For this reason, hardly applicable methods should be considered as a subsequent stage after applying relatively more easily applicable methods. Therefore, fault investigations need to be conducted in conjunction with various methods (McCalpin, 1996). Recently active faults may be identified by the direct examination of young, fault-related geomorphic features that have been recognized on aerial images. Geomorphology gives first and very realistic information about faults. On the other hand, sometimes geomorphological findings could not be enough and many times, they need to be verified by other disciplines. Geophysical investigations are indirect methods that require the knowledge of specific geologic conditions for final stage reliable interpretations. Therefore, neither geophysical methods and aerial images are sufficient to prove the absence of a fault nor they identify the recency of activity. Earthquake surface breaks give important information about fault mechanisms. However, they provide direct information just about surface deformation but not about source fault. Most of the maps and cross sections based on instrumental seismicity, like geological cross sections, are interpretive. In summary, all the disciplines are questionable and are in need of verification. For this reason, a comprehensive study is tried to make and any other methods are used to understand the tectonic phenomenon in both this section and the following. Direct, indirect, and more interpretive methods are applied and related studies are reviewed and criticized for the Düzce and surrounding area in this section.

## 2.1. GEOMORPHOLOGY

Differential vertical motions which characterize the evolution of the Düzce basin between the plain and surrounding mountains are due to the active- and neo-tectonics. To investigate through morphotectonic, geomorphology that has a relationship between topography and active tectonics in the vicinity of Düzce plain was used. Morphotectonic was studied using remote sensing (Landsat Thematic Mapper images, radar mosaics, 1:250,000), digital topographic maps (1:25:000) and stereoscopic aerial photographs (1:8000 and 1:30000) of

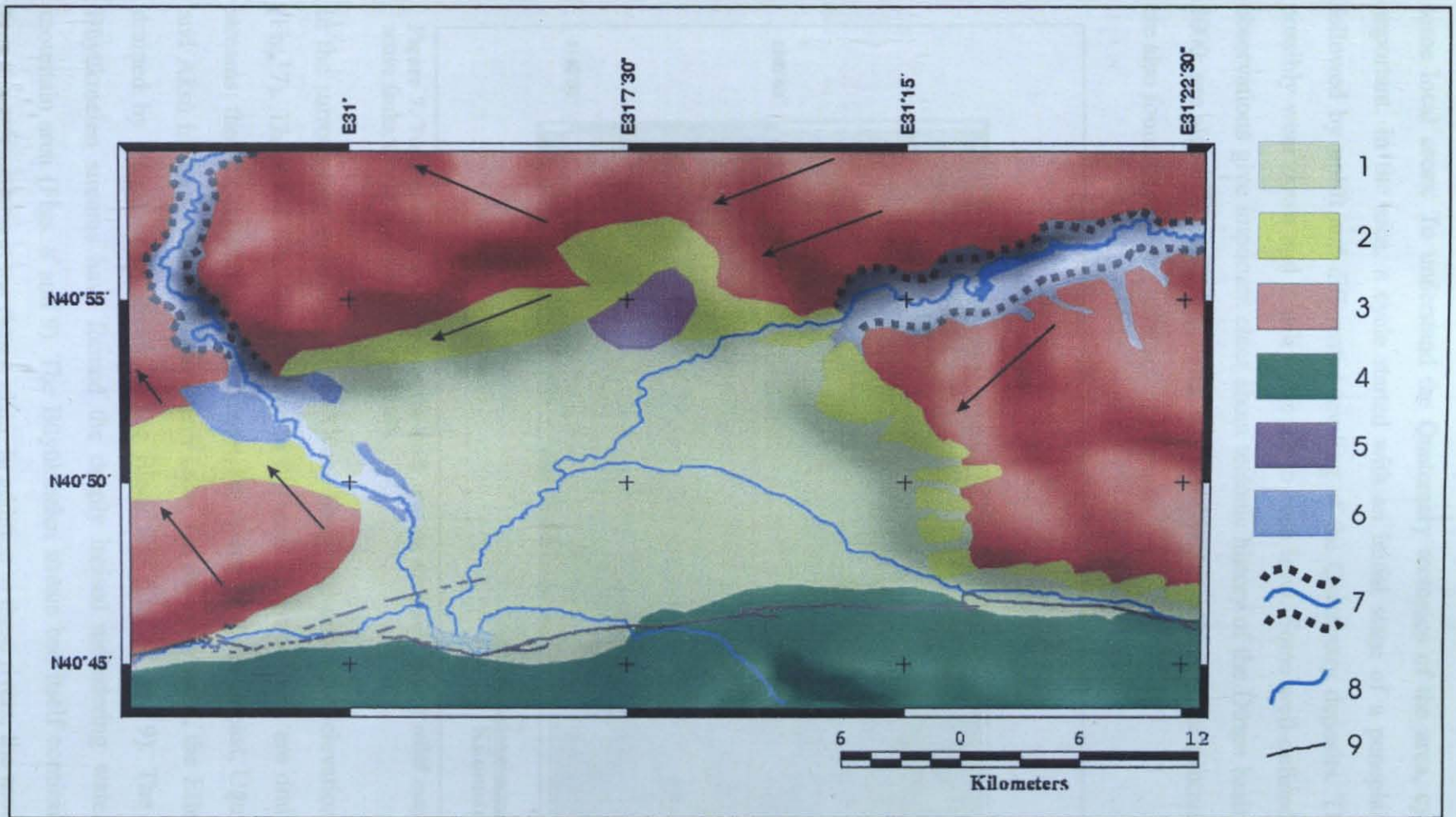


**Figure 6.** Geomorphological map of the Düzce area (After Pekcan, 2000). 1: New alluvium. 2: Post Pliocene erosional surfaces. 3: Dissected and deformed Pliocene erosional surface. 4: High mountainous area. 5: Dissected pediment. 6: Stream terraces. 7: Incised channel. 8: River. 9: Fault. Arrows show direction of down tilting.

some local areas. To understand the Quaternary tectonics of the area, cycle of erosion is important. In the area, a cycle started with an initial stage of a peneplanation. This was followed by uplift and differential leveling of the Quaternary deposits. The landscape will possibly wear down and it will approach to base level. Some well-defined geomorphologic observations give important clues about tectonic history of the Düzce basin (Fig. 6; Pekcan, 2000; see also Erinç et al., 1961 and Ardel, 1964). In addition, some geomorphic fingerprints are also found concerning local active tectonics.

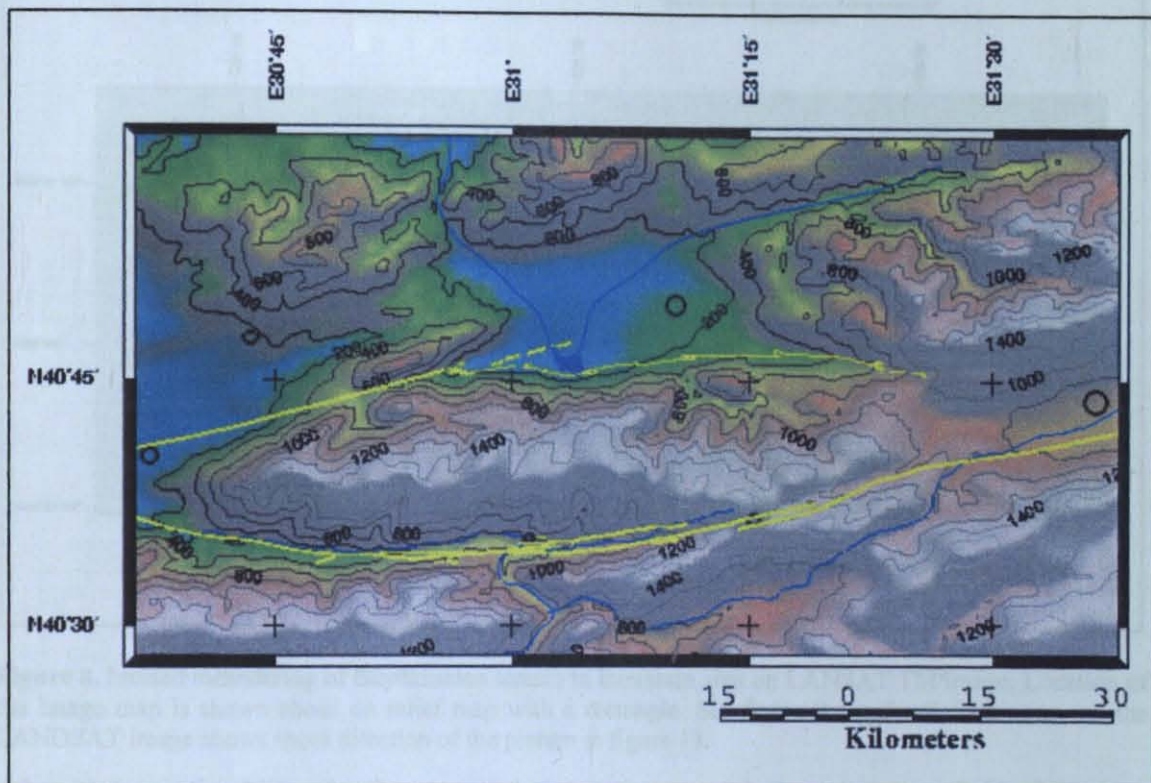


**Figure 7.** Topographic contour map of the study area on southwest shaded relief map. Yellow lines are active faults. Circles are centers of settlements.

In the surrounding mountains of the Düzce basin, the maximum elevation exceeds 1000 m (Fig. 7). There are five main streams in the area. The mountains are drained by four main streams; the Küçükmeden in the northeast, the Asarsu in the southeast, Uğursuyu in the south and Aksu in the southwest to the Efteni Lake. On the other hand, the Efteni Lake has been drained by Büyükmelen stream to the Black Sea (Figs. 8 and 9). The Küçükmeden and Büyükmelen streams have formed the deeply incised meandering water channels in the mountain area (Figs. 8 and 9). The Büyükmelen stream bed itself continues meandering on both mountainside and the Düzce plain. In addition to these rivers, the mountains at east and north of the basin are characterized by a prominent set of small-incised meandering channels.

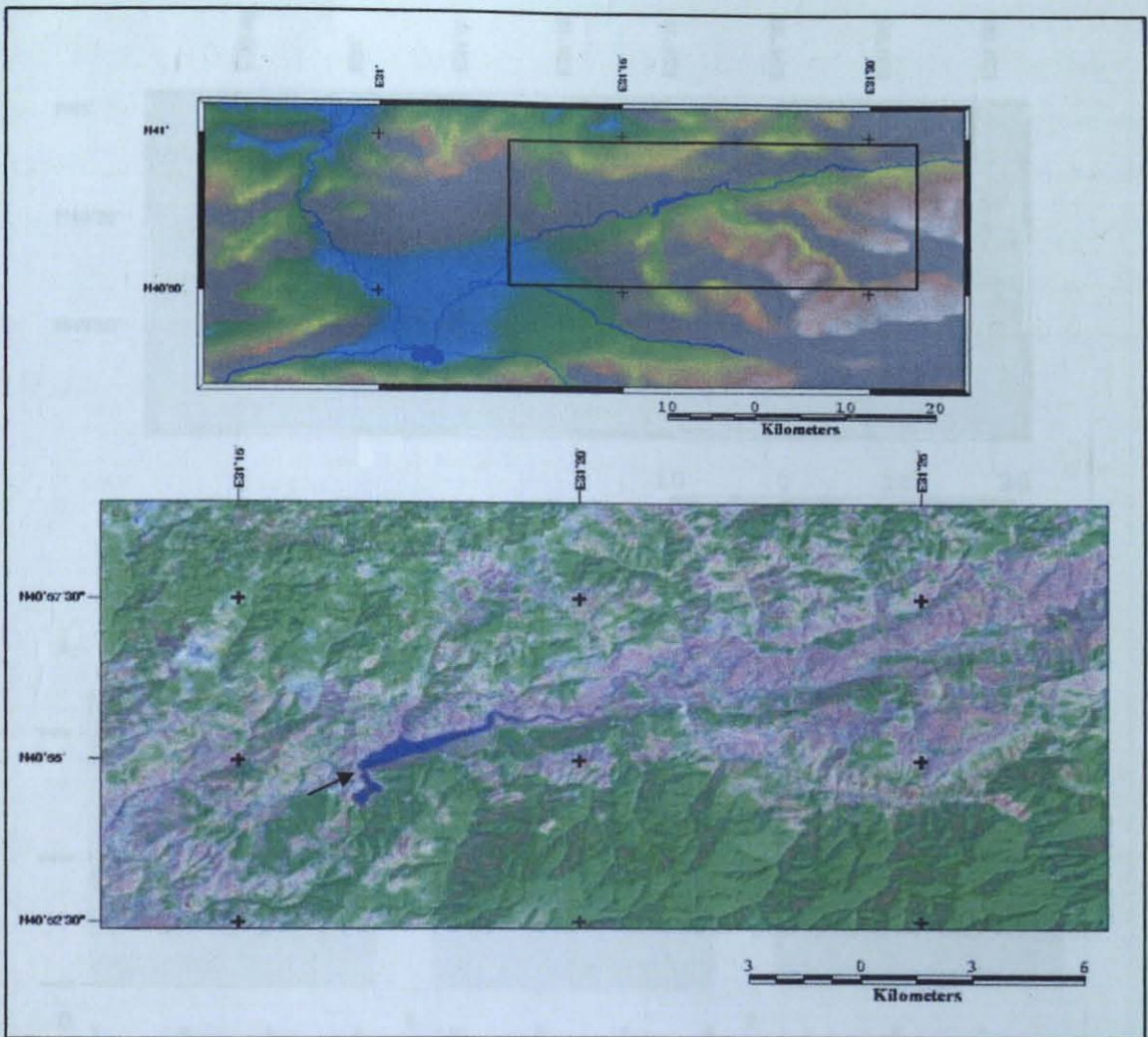


**Figure 8.** Incised meandering of Büyükmelen stream in mountain area on LANSAT TM image. Location of the image map is shown above on relief map with a rectangle. See figure 9 for detail. The arrow on the LANDSAT image shows shoot direction of the picture in figure 13.

It should be noticed that in the mountain area the meandering pattern of the Büyük and Küçük melen streams were originated in a tectonic phase (Phase-A) when the rivers must have been flowing over a relatively flat area of their flood plain (Erinç et al., 1961 and Pekcan, 2000). Then at some time, a relatively rapid lowering of base level occurs due to either the uplift of the land or a lowering of the regional outlet level. The rivers no longer could meander and just cut downward and incise into the surface of the peneplain that was formed during phase-A. This marks the end of the initial tectonic phase (phase-A). The morphologic anomaly which represents the Düzce plain must be related to tectonic forces that appear after the formation of the peneplain. The flat plane (peneplain) subsequently elevated, the rivers rapidly cut down (vertically) into their own meandering bed (existing meander) as they follow the course of the original meanders to reach the level where the water likes to rest at the water

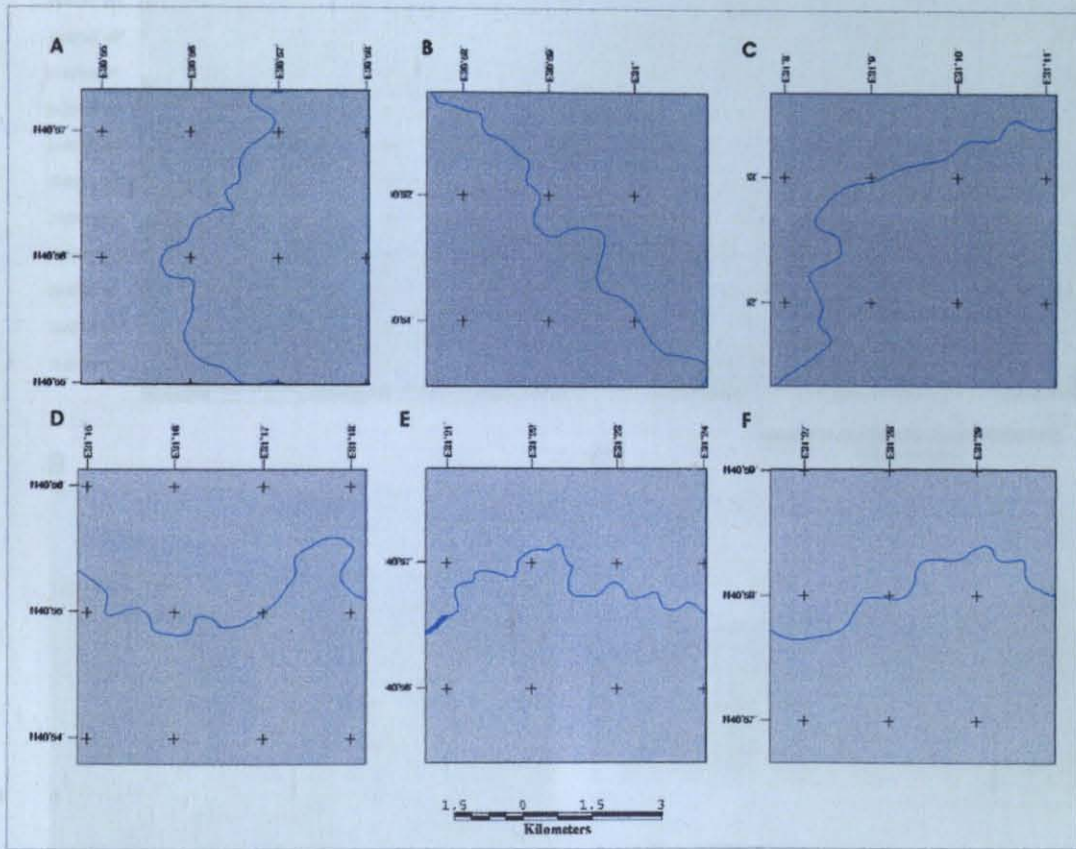
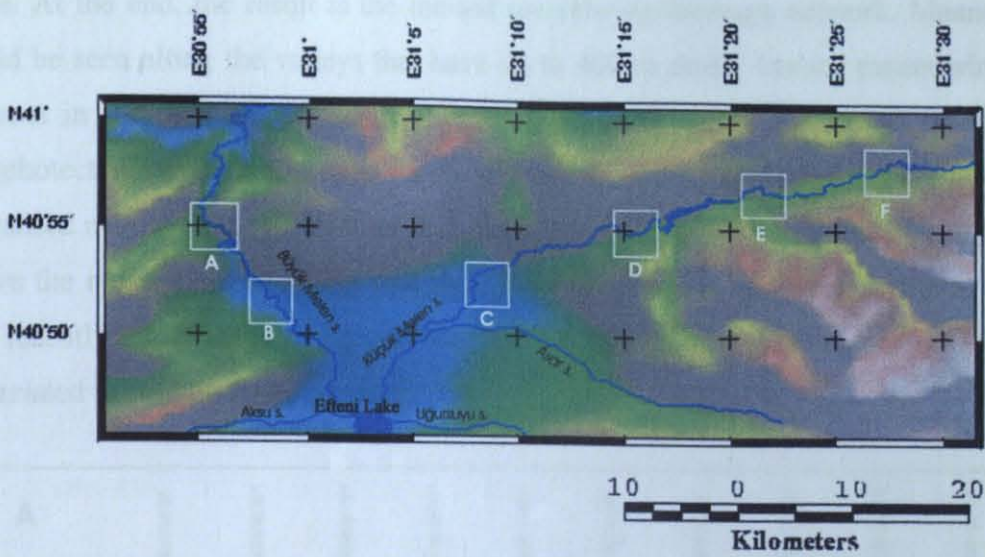


**Figure 9.** Meandering and incised meandering parts of the Küçük and Büyük Melen streams. The locations of maps below are shown on topographic map above. Meandering in the mountain area and in the Düzce plain seems to be similar, implying that those in the mountainous area are incised equivalent of those seen on the actual Düzce plain.

table. At the end, the result is the incised meandering drainage network. Meanderin pattern could be seen along the valleys that have up to 400-m depth. Incised meandering rivers and streams in the area are still cutting down through the rocks today and marking a recent morphotectonic evolution printed on the valleys. How did the change occur from meandering to incised meandering system form and when did it all begin? The answers of these questions prove the morphotectonic history of the Düzce basin which is very valuable to locate active and recently inactivated (young but inactive) features in the tectonic regime and old faults that are related to paleotectonic regimes.

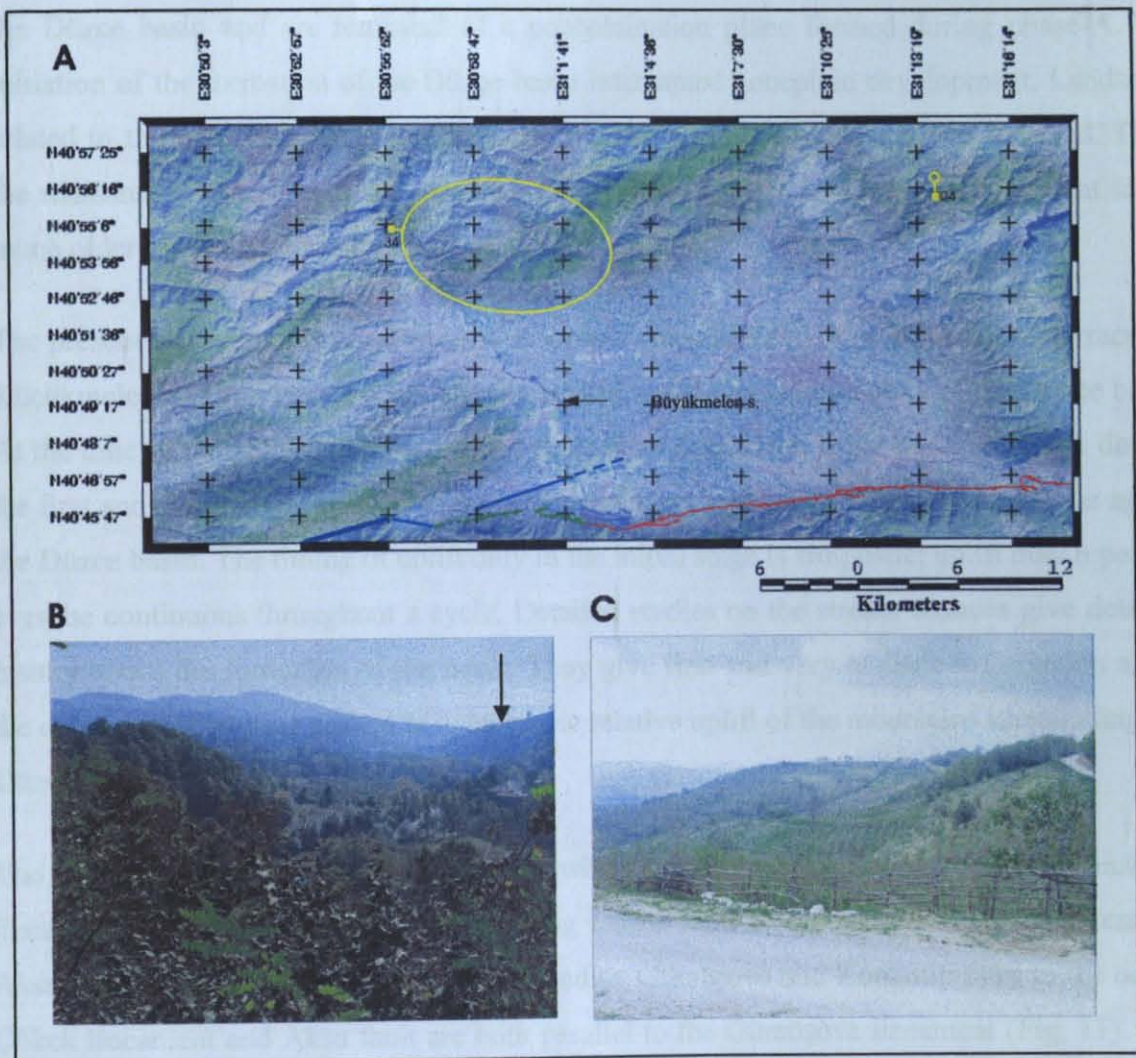


**Figure 10.** Abandoned terraces and flat-lying eroded surfaces. Locations of the pictures B and C are shown on LANDSAT image (A) including shooting points and approximate ranges of the picture area with ellipses. Observation points 34 and 04 correspond shoot points of pictures B and C, respectively. The arrow in B shows an abandoned terrace of the Büyükmelen stream.

Features such as abandoned terraces along rivers are also related to the tectonic uplift in the area (Fig. 10). Abandoned stream terraces that are sitting unconcordantly on the folded old bedrock in mountain area represent graded period of the streams that were in equilibrium

condition before perturbation. They are preserved and observable on both sides of the valleys of the Küçükmenen and Büyükmenen streams (Erinç et al., 1961; Pekcan, 2000; see also, Emre et al, 1999). They can be dated in the future studies to lighten the tectonic history of the area.

There are flat-lying surfaces on the top of the hills in the mountain area (Pekcan, 2000). This observation is also in concordance with the geomorphologic data that were mentioned in the paragraphs above. Flat-lying surfaces are the indicators of sudden uplift of mountain areas according to neighboring depression, as they form isolated land forms separated from younger erosional areas. They are concentrated in a very wide zone on mountainous area surrounding the Düzce basin and are remnants of a peneplanation plane formed during phase-A. The initiation of the formation of the Düzce basin interrupted peneplain development. Landscape related to the peneplain stage started to worn down and erosional stage was initiated. Then, the remnants of the peneplain formed the top of the hills with angularly unconcordant to the much older basement rocks.

The presence of remnants of peneplains of incised meanders and of uplifted stream terraces of Küçükmenen and Büyükmenen are directly related to the formation history of the Düzce basin. At the time of the peneplanation period/s there is no depression at the basin area. The date of the first and main peneplanation event is the minimum limiting date that constrains the age of the Düzce basin. The timing of uplift only in the initial stage is simplistic; uplift may repeat or even be continuous throughout a cycle. Detailed studies on the stream terraces give detailed history about the formation of the basin. They give first and very realistic information about the existence of faulting related to neotectonic relative uplift of the mountains surrounding the Düzce basin.

The Düzce plain depicts a topographic low which is surrounded by faults. The main tectonic lineaments in the area are the E-W trending Düzce fault to the south the NE-SW trending Aksu fault to the southwest and the E-W trending Gümüşova and Konuralp lines to the north. Çökek lineament and Aksu fault are both parallel to the Gümüşova lineament (Fig. 11). The eastern and western borders of the plain also give a linearity impression (Karakuz and Sultaniye lineaments). They seem to be trending NW-SE and are parallel to the each other (Fig. 11). Both the Düzce and Aksu faults represent active dextral shear zones characterized by the 1999 Kocaeli and Düzce earthquakes, respectively. Some slices of basement were thrust in the area and rapid change in lithology common along linear contacts. One of these structures corresponds to the Küçükmenen lineament (see section 2.2).

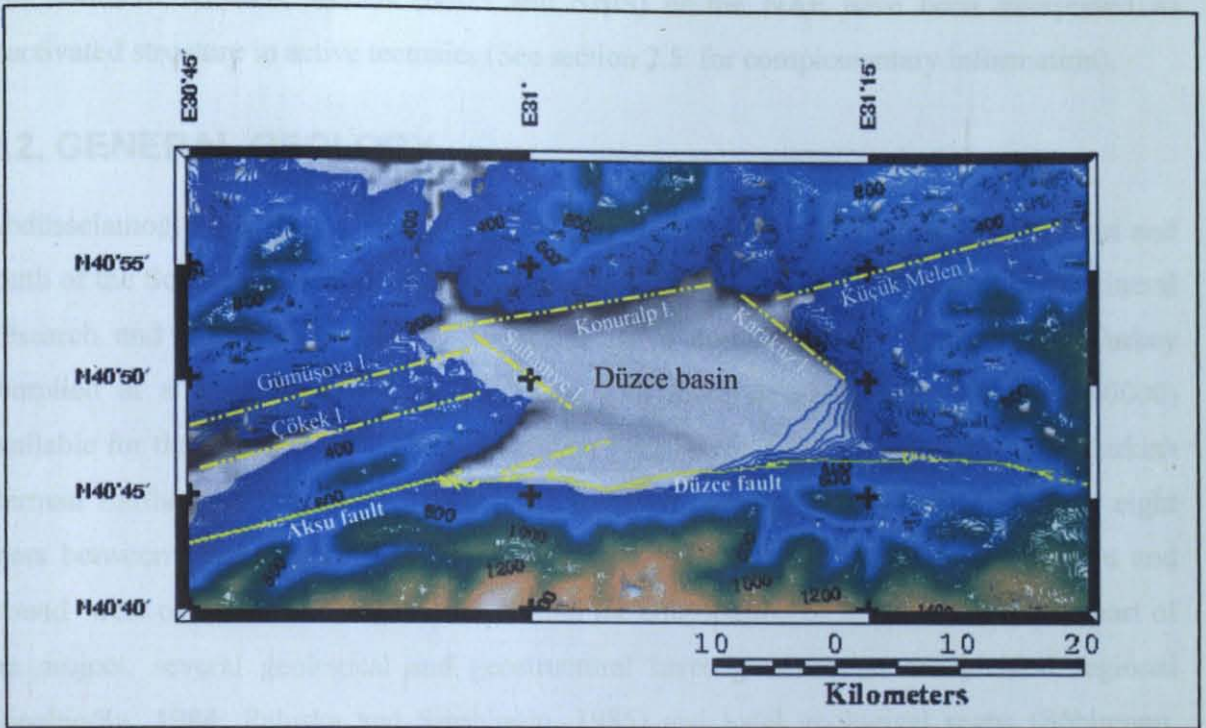


**Figure 11.** The lineaments along the borders of the Düzce basin and surrounding area on topographic contour map. The first contour level is limited at 200 m to represent linear nature of the borders.

Morphological texture of the current topography reveals a dissection pattern in western Turkey. NE-SW and NW-SE morphotectonic lines related to a N-S compressional phase are remarkable in the morphology (Arpat and Şentürk, 2000). In addition to these, E-W trending thrust zones which may belong to the same N-S compressive tectonic phase display a paleotectonic/paleogeomorphologic evolution (see section 2.2). Most of the fault structures may have been reactivated at different times and may have canalized deformations along these structures that offer weak zones. Thus, the compressive tectonic regimes take important role to shape the background landscape of the Marmara region. On the other hand, neotectonics in this area is dominated by E-W shearing and N-S extension. Geometries of the most of active faults within the current stress field have varying orientations in the Marmara region (Fig. 4). However, the current stress field isn't known directly. Because in situ stress measurements have not been made in the area surrounding the NAF. On the other hand, varying orientations of the faults could be indication of incompatibility of geometrical positions of some of the young faults with current stress field. Optimally-oriented structures of the tectonic lines that are constituting weakness zones could have been reactivated in a coeval E-W shearing and/or N-S extensional Neogene tectonics. The abnormal dip angle of the Düzce strike slip fault plane and its optimally-oriented geometrical positions in the current tectonic regime can be explained in this way (See section 3). Within the context, the Northern

and Southern Almacık strands (NAIS and SAIS) of the NAF have been interpreted as reactivated structure in active tectonics (See section 2.5. for complementary information).

## **2.2. GENERAL GEOLOGY**

Abdüsselamoğlu (1959) has mapped the geology of the most of the Almacık Mountain and south of the Southern Almacık Strand (SAIS). The Institute of General Directorate of Mineral Research and Exploration (MTA), Ankara, holds a digital geology database for Turkey compiled at a scale of 1:500000 (Fig. 12), with more detailed compilation (1:100000) available for the area along the North Anatolian Fault (Herece and Akay, 2003). The Turkish German Earthquake Prediction Research Project was established and built up during eight years between 1984 and 1992, incorporation with more than 20 institutes to study in and around west of the Almacık mountain. Within the contribution of Michel (1994) as a part of the project, several geological and geostructural investigations that are yielded regional (Sipahioğlu, 1984; Paluska and Sipahioğlu, 1985) and local geological maps (Söhlmann, 1989; Vogelmann, 1989; Michel, 1990; Stablein, 1991; Gaiser, 1991; Herford, 1991; Maiwaldt, 1991; Huss, 1992) were reviewed. Herford (1991), Gaiser (1991), Huss (1992) and Michel (1994) investigated the area for the changing states of deformation or the subrecent kinematic field (see Michel, 1994). The study of Şimşek and Dalgıç (1997) and contributonal study of Ankara University and MTA (Emre et al., 1999) on the geotechnical characteristics of the alluvium of the Düzce plain are also an important contribution related to the formation of the Düzce basin. These sources of geological data provide an important support for searching active faults and characteristics of them.

The tectonics that shaped the Anatolia has undergone a significant and complex evolution. The surrounding mountains of the Düzce plain were formed by two groups of rocks; the İstanbul tectonic unit in the north and the Sakarya Continent in the south (Şengör and Yılmaz, 1980) from north to south. According to the detailed field geological studies (Yılmaz et al., 1982), the basement rocks that belong to the İstanbul tectonic unit to the north are marked by the thrusts and associated imbricate zones. This unit is structurally complex. It consists of the Paleozoic sedimentary sequence and the cover rocks (Yılmaz et al., 1982). According to 1:25000 scale geological mapping (Yılmaz et al., 1982), the basement rocks that belong to the Sakarya Continent consist of continues sedimetary sequence that is indicating the formation

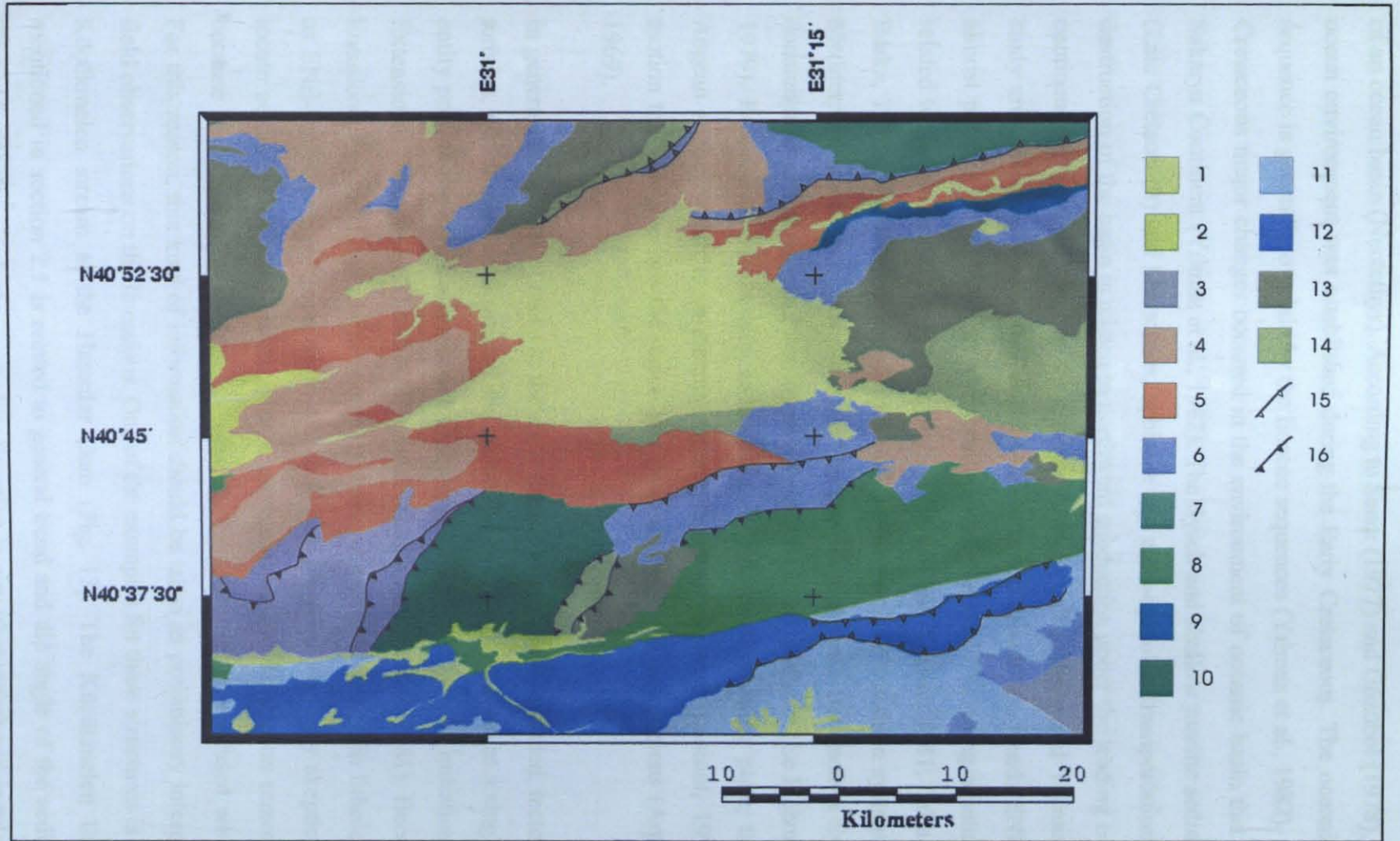


**Figure 12.** Geology map of the Düzce area (After MTA, 2000). 1: Quaternary alluvium. 2: Pliocene continental deposits. 3: Lower Miocene volcanic rocks. 4: Lower, Middle Eocene sediments. 5: Paleocene – Lower Eocene volcanic rocks. 6: Upper Cretaceous – Lower Eocene continental shelf deposits. 7: Turronian – Campanian slope deposits. 8: Upper Cretaceous – Lower Eocene olistostromal deposits. 9: Upper Cretaceous – Paleocene shelf deposits. 10: Ophiolitic assemblage. 11: Lower Cretaceous – Paleocene deep sea sediments. 12: Jurassic – Lower Cretaceous sediments. 13: Paleozoic and Early Mesozoic sedimentary rocks. 14: Granitoids of Precambrian. 15: Thrust. 16: Over thrust.

of an ocean basin (Neotethys). According to Saner (1977) and Gözübol (1978), the deep water ocean environment was established during the Early Cretaceous. The oceanic basin related sequence is generally overlain by the Eocene sequences (Yılmaz et al., 1982). After the Early Cretaceous major changes occurred in the environment of oceanic basin that belongs to the Sakarya Continent (Yılmaz et al., 1982). The flysch and shallow marine sediment deposition (Late Cretaceous) and blueschists, ophiolite and meta-ophiolite transportation occurred. The destruction of the basin is related to northward subduction under the leading edge of northern continent that is represented by the İstanbul tectonic unit (Şengör and Yılmaz, 1981). In the study area, the suture zone that was formed after the destruction trends ENE-WSW and is almost parallel to the NAF. In a general opinion, the NAFZ is using a suture zone that is related to the closure of the Neotethys (E.g., Şengör and Yılmaz, 1981; Yılmaz et al., 1982; Barka, 1992). The latest closure which may be the part of Neotethian system in the Eastern Mediterranean area has been dominated by the South Aegean Subduction System which is consumption of the African Plate towards the north or/and northeast (Le Pichon and Angelier, 1979). Because of the ongoing extension (AES) on the overriding plate, the crust of the Aegean region which is continental, was considerably thinned (Komut, 1998). Stretching motion that characterizes the region has taken up by horsts and grabens (Arpat and Bingöl, 1969).

In general, the basement rocks in the study area consist of fault-bounded, tectonostratigraphic terrains, which were amalgamated and assembled to the present form as a single geographical entity prior to the Late Eocene Epoch (Yılmaz et al., 1982) before the initiation of the Aegean Extensional System (AES) and NAF system (Şengör and Yılmaz, 1981). Because of general lineation of tectonic and environmental features, abrupt N-S change in lithology is observed as ENE-WSW or E-W lineation on morphology. One should be very skeptic and careful to locate active faults based on the interpretative information leaning on remote sensing data because these linearities observed on morphology can easily be confused with active faults. For this reason, this kind of information should be taken as preliminary interpretation before field observations on the lineations. One of the examples for these structures is lying along the Küçükmenen stream at the Hasanlar Dam (Fig. 13). The Küçükmenen lineation that is mentioned in section 2.1 is related to general trend and dip angle of the sedimentary layers (Figs. 11, 13). Even it is the most clear lineation in airy photographs it is related to material difference between the resistant limestones and weak clayey layers but not a fault. In other words, the limestones are more resistant to erosion than the overlying clayey sequence.

Primary (sedimentary) relationship exists between limestones and clays along this lineation. This relationship is clearly observable near the dam.

About E-W trending thrusts and set of NE-SW/NW-SE trending faults are the large scale structural products of the collisions. These are one of the important characteristics of the N-S compression (NSC) in the northwestern Turkey and postdate the closures of the oceanic basins according to basaltic andesite volcanism in Eocene (Yılmaz et al., 1982). In the area, the thrust zones created weaknesses (inhomogeneity) in the crust juxtaposing different blocks with different lithology and ages and they preceded the recent ones (Yılmaz et al., 1982; Şengör et al., 1985; Huss, 1992). The active faults in the study area commonly use these weakness zones. The other product of the NSC is the set of NW-SE/NE-SW trending faults (set of conjugate faults) that gives its special geomorphologic character to the topographic relief of whole northwestern Turkey (Arpat and Şentürk, 2000). Same texture also exists in active compressional domain in the eastern Anatolia (Şengör et al., 1985). Some of the weakness zones of these faults are also used by faults of following tectonic regimes depending on their orientation and locations in the general stress domain (see also Arpat and

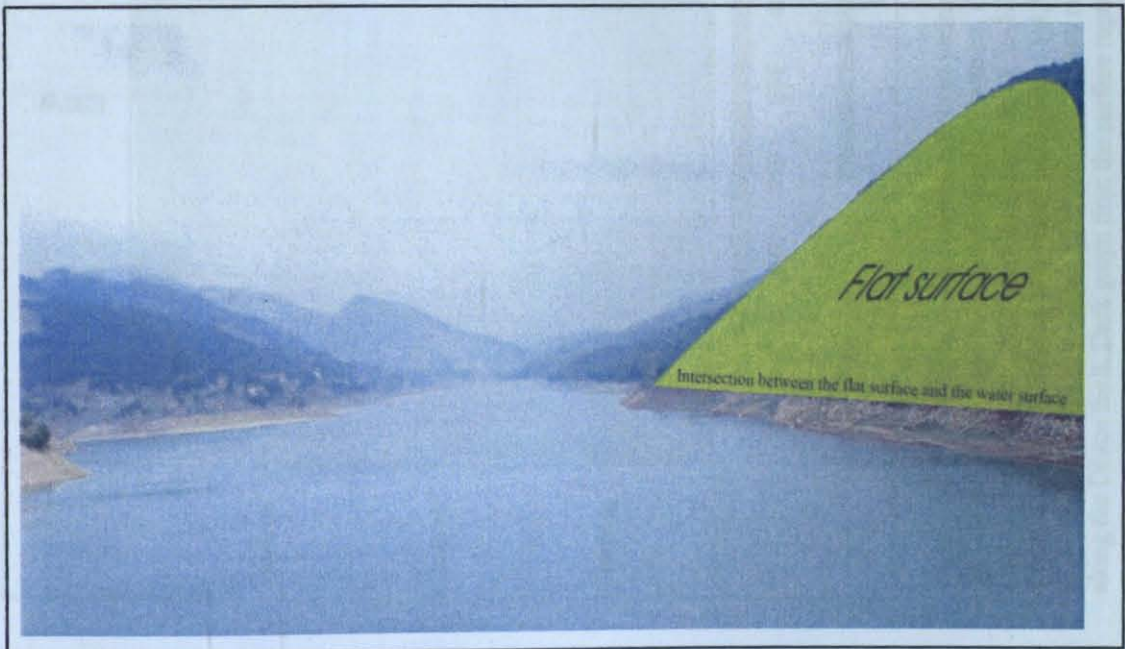


**Figure 13.** Picture of the southern coast of Hasanlar Dam. Looking from west (see the arrow in Figure 8 for the shooting direction of the picture). ENE-WSW lineations are remarkable on morphology because of the general trend and dips of sedimentary layers. The flat surface in the figure represents bedding plain of limestones. Primary (sedimentary) relationship exists between limestones which is resistant to erosion and clays along this lineation. The lineation is related to material difference between the resistant limestones and weak clayey layers.

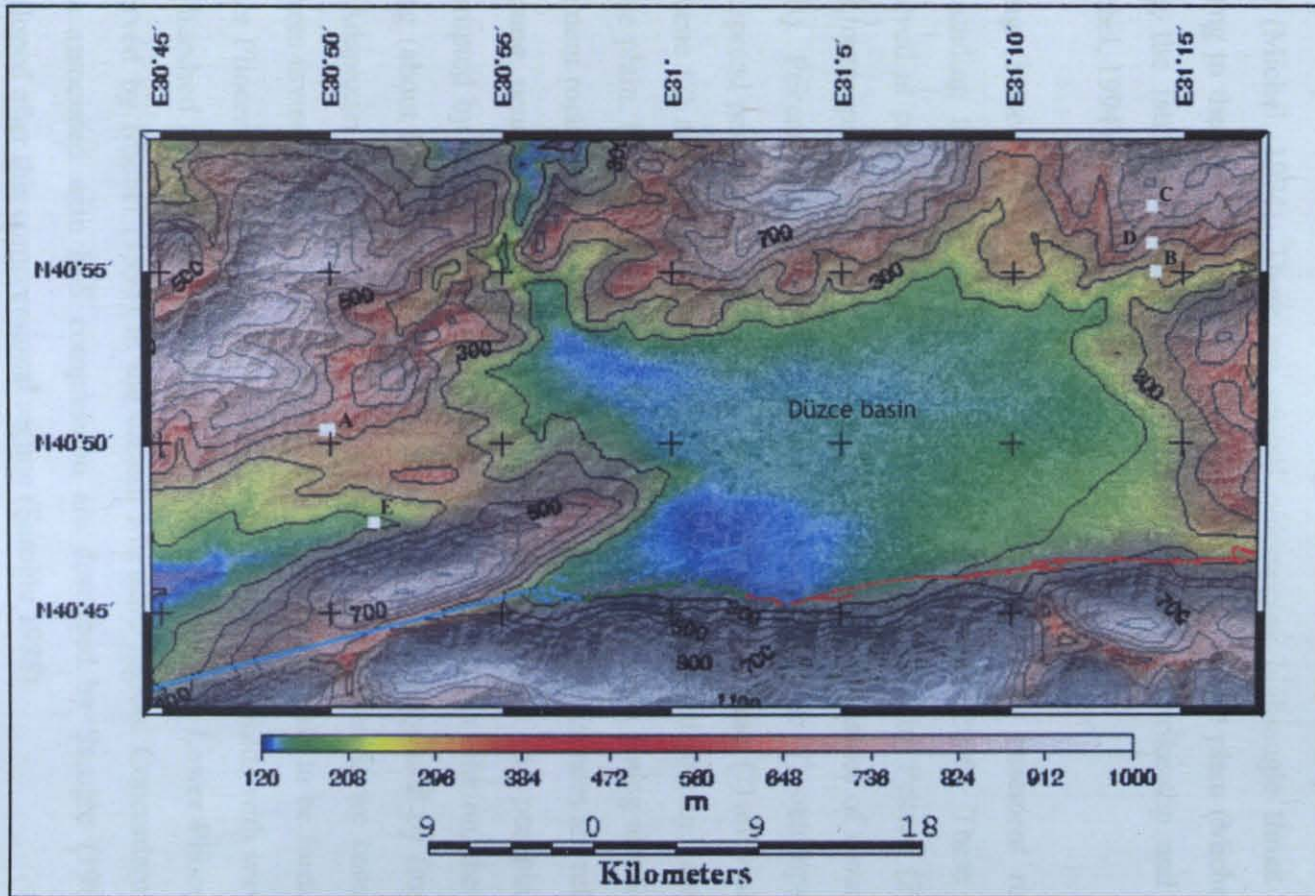


**Figure 14.** The location of observation points of young tectonic features on pseudo topographic map layer that is draped on LANSAT-PAN image with topographic contours. Color scale shows altitude in meter. Intensity layer of topographic map is shaded from north as natural shading of LANDSAT image. The A and B: Alluvium (Fig. 15-1,2,3). C and A: Young flatness on eroded basement rocks (Fig. 15-4,5) and eroded young alluvium (Fig. 15-4). D and E young faults (Fig. 16-1,2). Light green line: 1999 Kocaeli surface rupture along the Aksu fault. Red line: 1999 Düzce surface rupture along the Düzce fault. Dark green line: the surface ruptures of both 1999 Düzce and Kocaeli earthquakes.

Bingöl, 1969; Arpat and Şentürk, 2000). These structures are marked by trends of outcrops of Neogene sediments and Neogene volcanism on surface geology in western Turkey (E.g., Arpat and Bingöl, 1969). The high angle deviation between the principal axes derived by Michel (1994) for some active faults (such as Mudurnu fault) and remaining axes (general trend) interpreted as reuse of pre-existing thrust faults oriented prior to the NAF kinematic field (Michel, 1994). There are several outcropping high-angle thrust planes dominantly dipping to the north along the southern border of the Düzce plain (Michel, 1994). Striations along the faults indicate that they were reactivated as strike-slip and oblique-slip faults (Michel, 1994).

Young (Pliocene ?) alluvial beds unconformably overlies basement rocks on mountains surrounding the Düzce plain (Akartuna, 1968; Pekcan, 2000). These sediments are not observed at peaks of some high hills that were described by Pekcan (2000). On the other hand, outcrops of young alluviums are widespread over hillsides of mountains (e.g., Fig. 11 A, B). Pekcan (2000) interpreted these young (Pliocene ?) outcrops as remains of a widespread peneplain. According to Pekcan (2000) Pleistocene (?) alluvial beds are overlying Pliocene (?) alluvial beds in Gümüşova lineation and infill lowland areas surrounding the Düzce plain. Flat-lying erosional surfaces were observed on young alluvial beds and also on basement rocks (see Fig. 14-A,C and Fig. 15-4,5). These evidences are related to remnants of a young peneplain. Thus, Düzce basin is younger than the peneplain because it was interrupted by the formation of the basin. According to this relation, the age of the basin is young (about Pliocene-Pleistocene ?). Similar date was suggested by Emre et al. (1998) for the Adapazarı basin according to dating of micromammals. If we consider compressional features investigated by Şaroğlu (1988), the basins were likely to be formed in the Middle or Upper Pliocene-Pleistocene (See also Michel, 1994). Open folds with wavelengths of up to a few hundred meters that are abundant in the Miocene and Lower Pliocene sediments were observed by Michel (1994) in the eastern Marmara region. Concordantly, Lower Pliocene folds associated with N-S compression are described by Şaroğlu (1988). The NAF was developed after this compressional regime (Şaroğlu 1988).

Geological and geomorphologic field investigations are conducted along the Gümüşova valley (lineament) and the Northern border of the plain (Konuralp lineament) that faulting was expected along them according to their lineational nature in geomorphology. However, any data that are related to active faults and active fault morphology do not exist. Even the

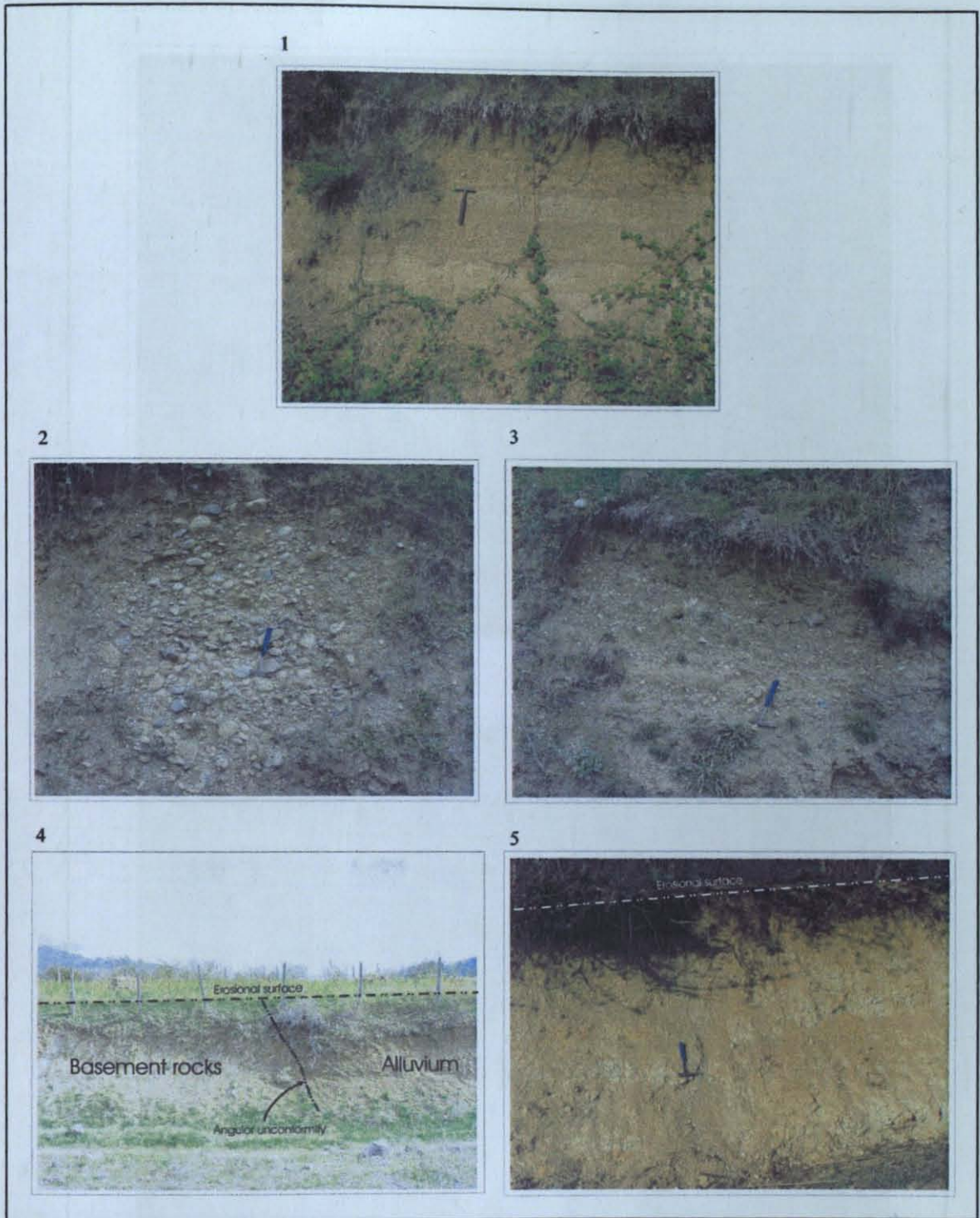


**Figure 15.** Observations on young sedimentary and erosional features. 1, 2, 3 and 4: stream alluvium. 5: erosional surface on basement rocks. 4: angular unconformity between basement and young alluvium and younger flat-lying erosional surface developed both on the alluvium and the basement rock. See figure 14 for the location points of observations. Observation locations of 1 and 4 are shown as point A; 2 and 3 are point B; 5 point is C in figure 14. Shooting directions of 1, 2, 3, 4 and 5 are about east, west, west, east and east, respectively.

1



2



**Figure 16.** Observations on young faults. The observation locations of 1 are shown as point D; 2 as point E in figure 14. 1: The picture was taken towards east. A young fault juxtaposes Lower-Middle Eocene bedrocks (left) with unconsolidated clays (right). The contact is vertical, so the possibility of the strike-slip faulting is higher. 2: The picture was taken towards west. Gravels in the young unconsolidated alluvium are showing vertical lineations in a narrow zone. Considering vertical lineations, the fault is probably strike-slip.

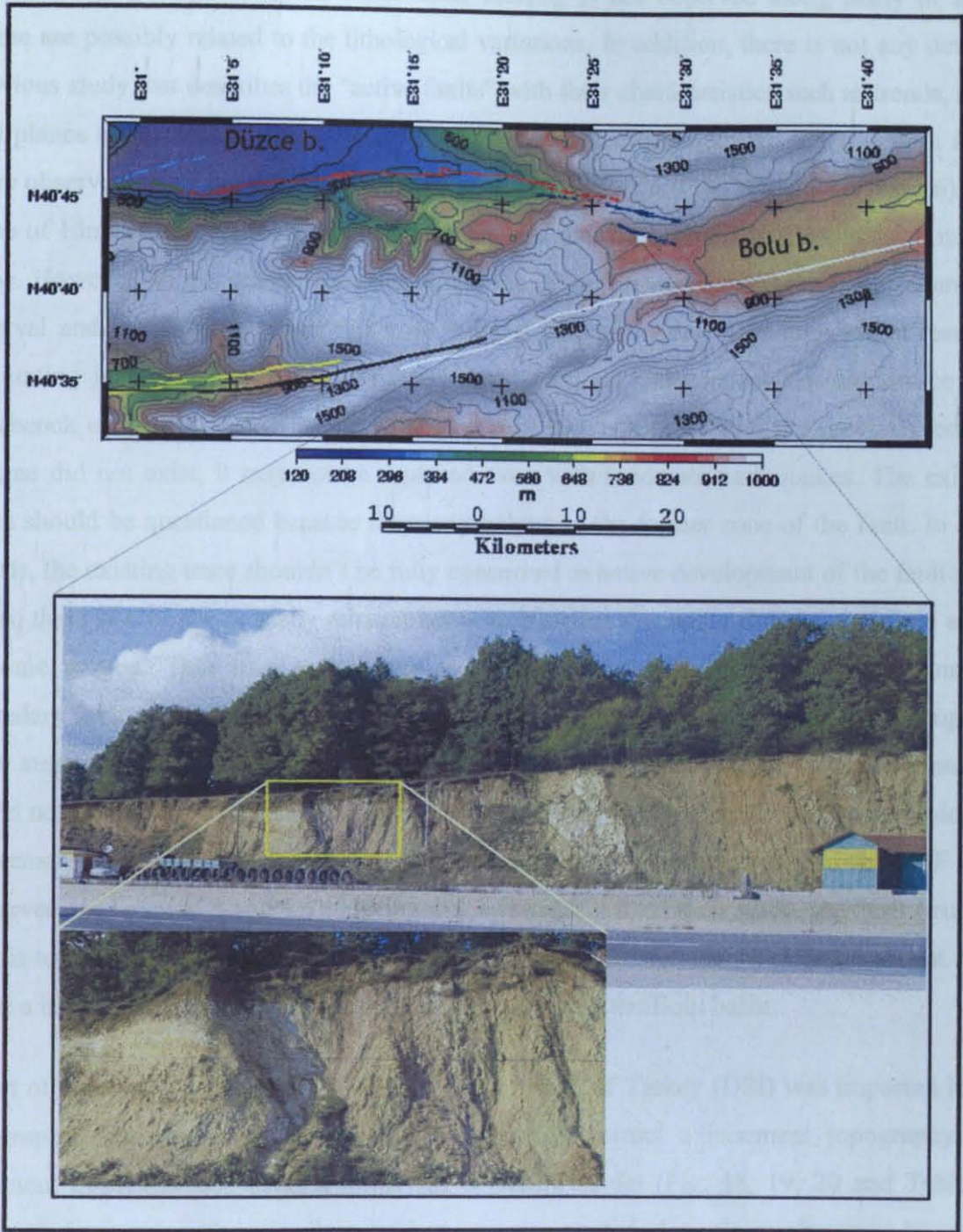


**Figure 17.** Young fault in northwest of the Bolu basin along Elmalık fault. Light blue line: surface breaks of the 1999 Kocaeli earthquake; red line: 1999 Düzce rupture. Yellow line; 1967 Mudurnu rupture; black line: 1957 Abant rupture; white line: 1944 Bolu rupture; dark blue line: Bakacak and Elmalık faults (suggested by Hitchcock et al., 2003). Relief map shaded from south. Outcrop in the picture shows a young fault that displaced unconsolidated alluvium. On the right in picture above much older bedrocks (Cretaceous melange) are seen at the same level with the young alluvium (Pliocene ?) to the left. Younger erosional surface that is cutting the fault suggests inactive nature for the fault.

existence of outcrops along the lineaments, faulting is not observed along many of them. These are possibly related to the lithological variations. In addition, there is not any detailed previous study that describes the “active faults” with their characteristics such as trends, types and planes of them along the lineaments. On the other hand, young but inactive fault zones were observed along the Çökek line and northeast of the basin (Fig. 11, 14-E, D and 16). The zone of Elmalık and Bakacak faults are young and had been probably constituted a mature zone. However, in the active tectonic regime, the discontinuous nature, the large recurrence interval and the short length of this zone suggest immaturity and dependency that result in generating just moderate to small size of earthquakes as a dependent seismic source (See Hitchcock et al., 2003). If a young weakness zone that is representing the previous tectonic regime did not exist, it may not be ruptured even with moderate earthquakes. The existing trace should be questioned because they may belong to the former zone of the fault. In other words, the existing trace shouldn't be fully concerned as active development of the fault zone. Thus, there is probably a tricky relation between Holocen secondary deformations and active tectonic system. This zone is trending as eastern expected continuation of the southern boundary fault zone of the Düzce basin in the northern part of the Bolu plain after a couple of right steppings (Fig. 17) (See also Herece, 2003). On the other hand, its eastern continuation could not be found. According to the trench results of Hitchcock et al. (2003), some Holocene movements that have very long time span with respect to the Düzce fault and the NAF were observed (see section 3 and 4.4). Having this information from their study, the fault structure seems to be unable to transfer the slip of the Düzce fault through the NAF and does not seem to be a major active structural element that is constructing the Bolu basin.

A set of borehole data from the state of hydrolic works of Turkey (DSİ) was imported into a geographic information system (GIS) in order to construct a basement topography and sediment thickness map using a minimum curvature model (Fig. 18, 19, 20 and Table 1). Dummy data points of zero sediment thickness were created along the surface map boundary between soft and stiff materials of the alluvial and surrounding basement, respectively to constrain the sediment thickness model better (Fig. 21). The analysis showed that the thickness of the Quaternary alluvium of the Düzce plain ranges 0 to over 200 km thick (Fig. 19) (See also Emre et al., 1999). Topographic codes of zero sediment thickness areas surrounding the alluviums of the Düzce basin and further heights were created from surface

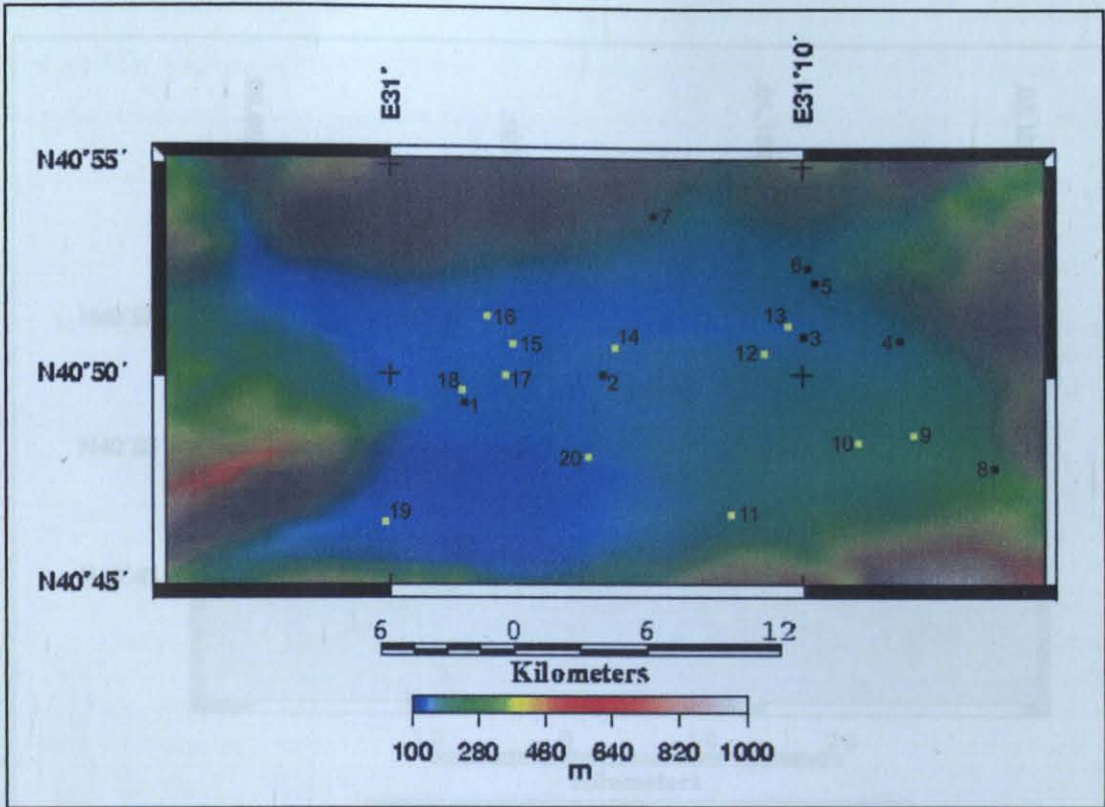


**Figure 18.** Locations of the boreholes in the Düzce basin. Topographic relief map shaded from south. Black and yellow points are the basement-reaching and hanging boreholes in alluvium, respectively. See table 1 for information about the boreholes.

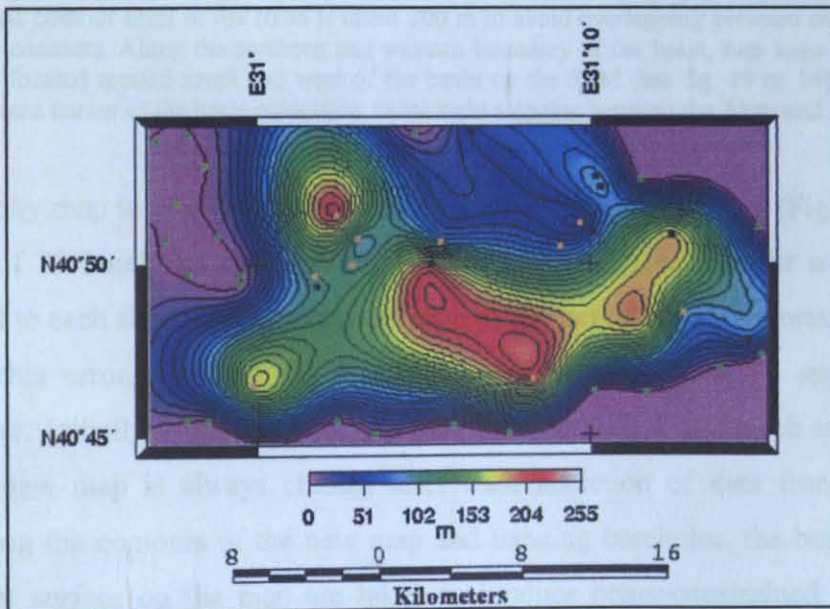


**Figure 19.** Sediment thickness map of the Düzce basin deduced from borehole data. Color scale shows thicknesses. See figure 21 to see the map area and information about boreholes.

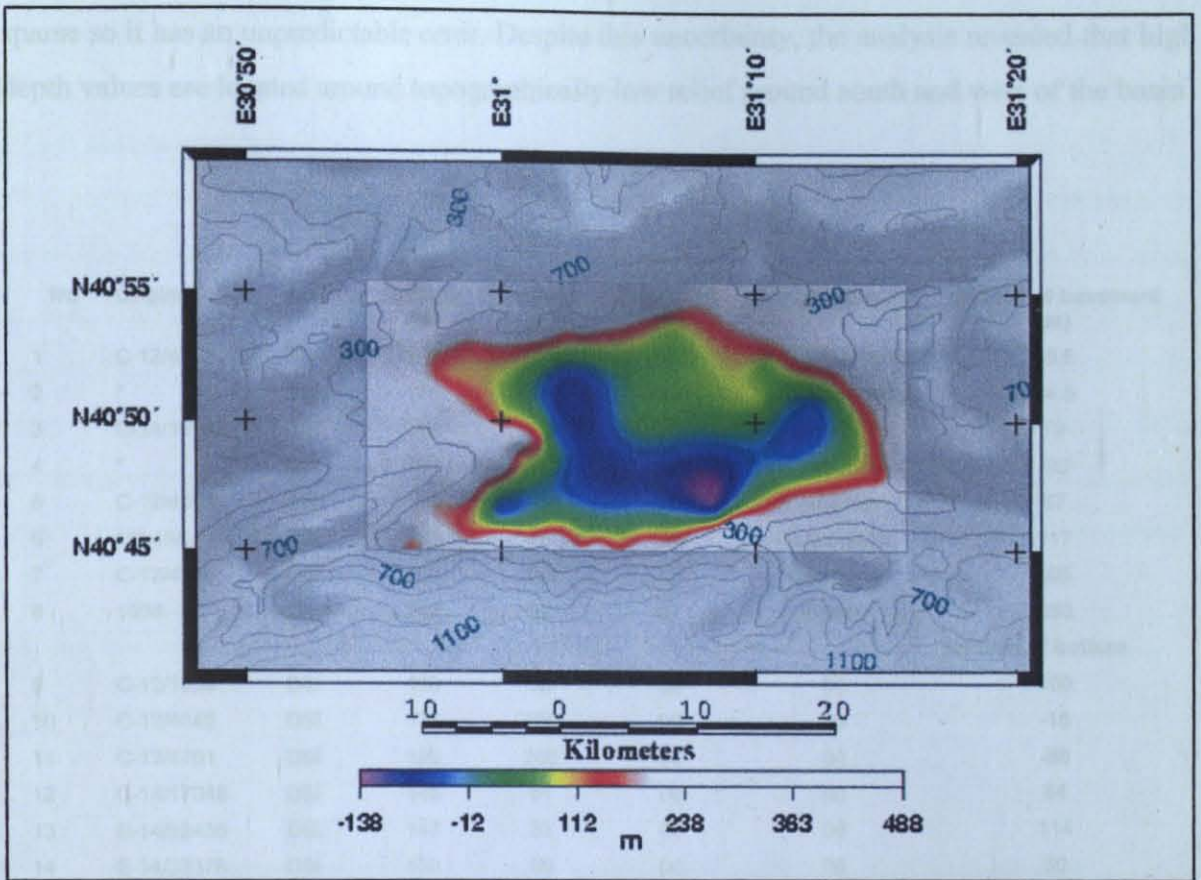


**Figure 20.** Basement topography of the Düzce basin is deduced from borehole data (Table 1). Basement topography (BT) grid (rectangle) is draped on contoured surface topography map (STM). Both are shaded from south. First contour level of the STM is taken 300 m to avoid overlapping between colored area of the BT and the STM contours. Along the southern and western boundary of the basin, two lows are noticed on the STM. They are located around south and west of the basin on the STM (see fig. 19 or 14). The other low is at the southwestern corner of the basin coinciding to the right stepping between the Aksu and Düzce faults (see fig.14).

topography map to constrain the basement topography model better (Fig. 22). Unfortunately, only 8 of 20 boreholes reach to the basement (Fig. 18), so that for many thickness value assigned to each site from the basement topography may have an important error (Fig. 23). To reduce this error, some of the hanging boreholes were used by applying a systematic procedure. Initially a map was created using the boreholes that reach to the basement (Fig. 23). A new map is always created after each addition of data from a borehole. Then, comparing the contours of the new map and hanging boreholes, the boreholes that pass the basement surface on the map are taken to produce better-constrained model (Fig. 23 and Table 1). These boreholes are used in an order considering the passing distances. The boreholes that have longer passing distance are priorly added to the model one by one. After each usage of a borehole, the contour map was re-generated up to passing holes end. Applying this method 6-borehole data were added to the data set. Totally 14 borehole data were used in

the final model (Fig. 22 and 20). Even some of the errors are reduced ; the used data are very sparse so it has an unpredictable error. Despite this uncertainty, the analysis revealed that high depth values are located around topographically low relief around south and west of the basin

| No                        | Original code | Source | Altitude (m) | Bottom (m) | Basement (m) | Basement rocks    | Altitude of basement (m) |
|---------------------------|---------------|--------|--------------|------------|--------------|-------------------|--------------------------|
| 1                         | C-12/4358     | DSİ    | 125          | 135.85     | 105.5        | Cretaceous flysch | 19.5                     |
| 2                         | *             | DSİ    | 130          | 197.15     | 105.5        | Cretaceous flysch | 24.5                     |
| 3                         | C-14/19992    | DSİ    | 149          | 74         | 70           | Serpentinite      | 79                       |
| 4                         | *             | DSİ    | 160          |            | 180          | Sandstone         | -20                      |
| 5                         | C-12/4354     | DSİ    | 153          | 104        | 86           | Peridotite        | 67                       |
| 6                         | 16348A        | DSİ    | 153          | 70         | 36           | Serpantinite      | 117                      |
| 7                         | C-12/4356     | DSİ    | 150          | 117        | 45           | Claystone         | 105                      |
| 8                         | 1038          | DSİ    | 217          | 92         | 67           | Schist            | 150                      |
| <b>Altitude of bottom</b> |               |        |              |            |              |                   |                          |
| 9                         | C-12/1039     | DSİ    | 190          | 90         | (x)          | (x)               | 100                      |
| 10                        | C-12/4845     | DSİ    | 175          | 190        | (x)          | (x)               | -15                      |
| 11                        | C-12/4701     | DSİ    | 120          | 206        | (x)          | (x)               | -86                      |
| 12                        | C-14/17048    | DSİ    | 145          | 61         | (x)          | (x)               | 84                       |
| 13                        | E-14/32436    | DSİ    | 147          | 33         | (x)          | (x)               | 114                      |
| 14                        | E-14/33378    | DSİ    | 130          | 80         | (x)          | (x)               | 50                       |
| 15                        | C-12/1035     | DSİ    | 127          | 100        | (x)          | (x)               | 27                       |
| 16                        | C-12/4704     | DSİ    | 125          | 210        | (x)          | (x)               | -85                      |
| 17                        | C-12/1034     | DSİ    | 130          | 107        | (x)          | (x)               | 23                       |
| 18                        | C-12/1033     | DSİ    | 125          | 110        | (x)          | (x)               | 15                       |
| 19                        | C-12/4846     | DSİ    | 127          | 168.5      | (x)          | (x)               | -41                      |
| 20                        | C12/4702      | DSİ    | 125          | 196        | (x)          | (x)               | -71                      |

**Table 1.** Selected borehole data that is used for basement topography and sediment thickness models (see section 2.2) taken form DSİ. First 8 are the basement reaching and the others are hanging boreholes in alluvium. Some of the hanging boreholes are eliminated (see section 2.2). Locations are shown on figure 18.

\* The data from Pekcan (2000).

(Fig. 18 and 20). On the other hand, a low relief area is at the southwestern corner of the basin coinciding to the right stepping between the Aksu and Düzce faults (see fig. 14). The sediment thickness map was also created by using the final data set of 14 borehole (Fig. 19). This map and basement topography map seems to be similar each other (Fig. 19 and 20). This is because modelled basement topographic anomaly is more dominant than the modelled surface topographic anomaly. In conclusion, two interpretation can be made; (1) sedimentation rate is high enough at least for the recent to compensate the basement topographic anomaly that occurred with ongoing cumulative vertical movements or (2) these anomalies are related

to a former tectonic regime that was responsible to the formation of the basin. Considering the second case, even with low rates, sedimentation process has enough time to infill low areas and to bury the basement topographic anomaly. The resultant landscape is a nearly planar surface that is representing the actual Düzce plain. Nonexistence of seismic signature and active normal fault morphology along the borders of the basin, except the southwesternmost part of the basin, suggest the invalidity of the first case. It is fact that, existing borehole data are not convenient to make valid interpretations as mentioned previously. However, considering the whole available information based on geomorphological and geological field observations, GPS measurements and paleoseismological findings, including borehole data the basin seems to be an inactive structure (Section 2.5). The tectonically active local small basin (Efteni basin) in the southwestern corner of the Düzce basin is out of this discussion

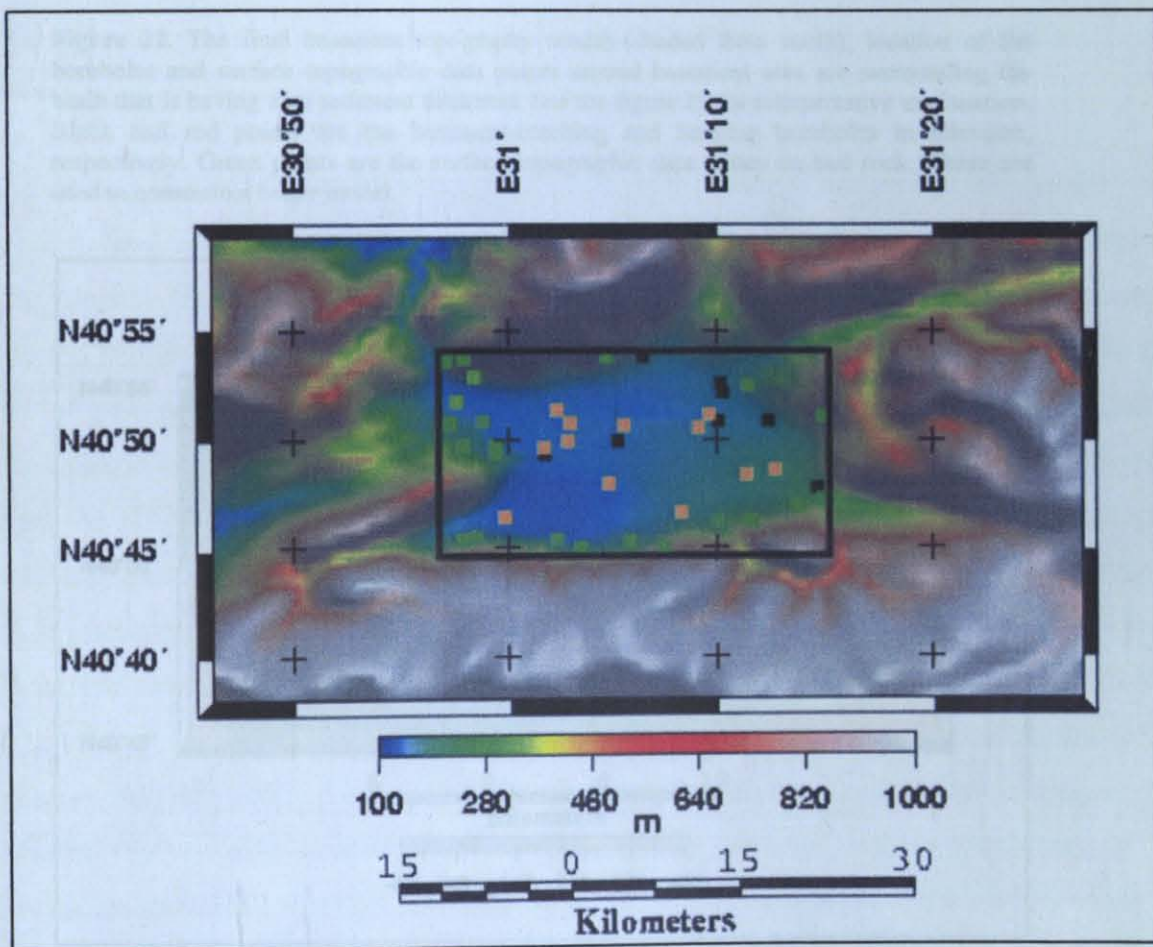


**Figure 21.** The borehole data and dummy points to produce sediment thickness model on surface topography map (STM) shaded from south. Rectangle shows map area of figure 19. Black and red points are the basement-reaching and hanging boreholes in alluvium, respectively. Green points are dummy data that are produced by using surface topography map to constrain the model better.

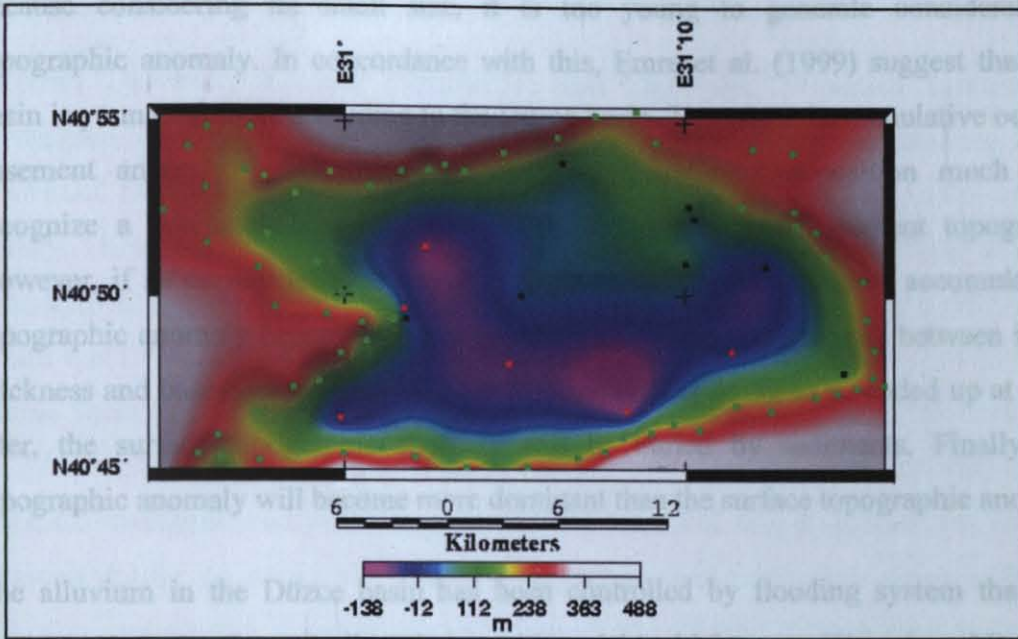


**Figure 22.** The final basement topography model (shaded from south), location of the boreholes and surface topographic data points around basement area are surrounding the basin that is having zero sediment thickness. See the figure 20 for interpretative explanation. Black and red points are the basement-reaching and hanging boreholes in alluvium, respectively. Green points are the surface topographic data points on bed rock. These are used to constrain a better model.

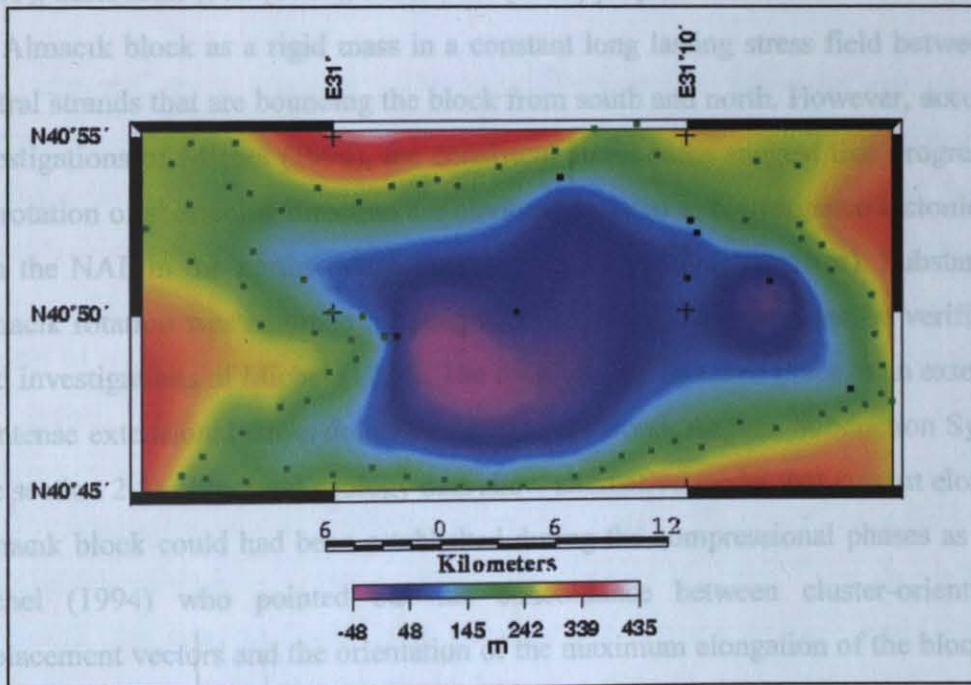


**Figure 23.** A basement topography model of the Düzce basin that is deduced from borehole data those reach to the basement (Table 1). Black points are the basement-reaching boreholes in alluvium. Green points: surface topographic data points that are used to constrain the model better.

because considering its small size, it is too young to generate considerable surface topographic anomaly. In concordance with this, Emre et al. (1999) suggest that the Efteni basin is younger feature according to the Düzce basin. Therefore, its cumulative occurrence of basement anomaly is not exceeding cumulative sediment deposition much enough to recognize a mismatch between sediment thickness map and basement topography map. However, if its current tectonic activity continues to a critical time, its accumulated surface topographic anomaly becomes clearly apparent and a mismatch occurs between its sediment thickness and basement topography map. If its activity is going to be ended up at this time or later, the surface topographic anomaly will be buried by sediments. Finally, basement topographic anomaly will become more dominant than the surface topographic anomaly.

The alluvium in the Düzce basin has been controlled by flooding system that comprises interfingering gravel, sand, silt and clay with variable thicknesses (Şimşek and Dalgıç, 1997). The episodic gravel sedimentation around the middle of the plain could be related to episodic lowering of the basement level of the plain with tectonic movements.

According to tectonic model assumptions and paleomagnetic measurements, Şengör et al. (1985), Saribudak et al. (1990), Tatar et al. (1995) proposed a clockwise  $120^{\circ}$ - $212^{\circ}$  rotation of the Almacık block as a rigid mass in a constant long lasting stress field between interacting dextral strands that are bounding the block from south and north. However, according to field investigations of Michel (1994), the consistent strain-paths suggest that progressive steps in the rotation of shortening direction are obviously related to convergence-tectonics much older than the NAF in the northwestern Turkey (see the paragraphs above). Substantial Neogene Almacık rotation was assumed by Şengör et al. (1985), but could not be verified during the field investigations of Michel (1994). The rotation may be taken place in an extensional phase in intense extensional stress domain related to the South Aegean Subduction System (SASS) (see section 2.5). Structural geology data show alternative model that current elongation of the Almacık block could had been established during the compressional phases as suggested by Michel (1994) who pointed out the concordance between cluster-orientation of the displacement vectors and the orientation of the maximum elongation of the blocks. Along the southern border of the Düzce basin, there are sub-parallel abandoned fault traces in the north of the active fault trace. The sub-parallel abandoned fault traces may give a key clue about the possible motion of the Almacık block (See sections 3.1.1.1 and 3.1.1.2).

## 2.3. SEISMICITY

Boğaziçi University Kandilli Observatory and Earthquake Research Institute National Earthquake Monitoring Centre and the Ministry of Settlement and Construction Department of General Directory of Disaster Management networks obtain raw earthquake catalogues in Turkey. These networks are not designed to monitor small earthquakes related to background seismicity of specific active faults such as faults in the Düzce area. The seismicity distribution before the 1999 Kocaeli and Düzce shocks could not define fault activities in and around Düzce. Saraç (1995) identified the concentration of a seismic activity to the northern part of the Almacık Mountain along the longitudes of Northern Almacık Strand (NAIS) according to statistical earthquake analysis. However, small earthquakes with good locations could only be observed during the aftershock period of the earthquakes with local networks in the study area. The source mechanisms of some of the moderate aftershocks were analyzed by using the regional moment tensor inversion method using data from near-regional broadband stations (Örgülü and Aktar, 2001). Recent seismicity that could be determined in this period is very useful to understand some parameters of the faults and kinematics in the study area. The results of seismicity studies and discussions are related to the 1999 Kocaeli and Düzce ruptures given in section 3.1.

Permanent and three temporary networks determine the aftershock period of the 1999 earthquakes. (1) A semi-permanent seismic network was installed between the Sapanca Lake and Bolu in 1985 within the frame of the Turkish-German Joint Project for Earthquake Research (Neugebauer et al., 1997). This network was transformed into a permanent seismic network called SABOnet in 1996 within the frame of the same project (Milkereit et al., 2000). In order to increase coverage and facilitate source mechanism studies, additional stations of the German Task Force for Earthquakes were installed immediately after the 1999 earthquakes (Milkereit et al., 2000). After 1999 Kocaeli earthquake, the majority of stations were installed in the west of Adapazarı in order to monitor the aftershock activity in epicentral region of this earthquake. It was operated until October 21, 1999. Three days after the Düzce earthquake, the German Task Force extended the network towards east. This temporary “Düzce” net was operated until December 13, 1999. (2) In addition, Marmara Research Centre (MRC) of The Scientific and Technical Research Council of Turkey (TÜBİTAK) installed a temporal network in the area to monitor aftershock activity (Özalaybey et al., 2002). (3) Another temporal seismic network was installed in the eastern part of the

aftershock region of the 1999 Kocaeli earthquake by Iio et al. (2002). After the occurrence of the 1999 Düzce earthquake, the network was rearranged to cover its aftershock activity area.

## **2.4. GEODETIC MEASUREMENTS**

Although the GPS data are giving the information about short-term (existing) deformations, it also measures very accurate and detailed lateral movements on the earth surface. Since 1988, GPS experiments have been conducted simultaneously with the SLR observations in Turkey (Oral et al., 1993, 1995). Since 1990, GPS campaigns have been carried out across a dense network in northwestern Turkey (see Straub and Kahle, 1994, 1997). The results from this network are summarized by Straub and Kahle (1997). The network includes continuously recording stations. In response to the occurrence of the 1999 Kocaeli and Düzce earthquakes, a large GPS data set was collected by continuous GPS stations installed by the Scientific and Technical Research Council of Turkey (TÜBİTAK) and Earth and Marine Sciences Research Institute (EMSRI) including contributions from the Marmara Continuous Global Positioning System Network (MAGNET) and repeated GPS surveys of many bench marks in the area (Ergintav et al., 2002). The General Command of Mapping was conducted regional and local surveys to establish additional geodetic control points. After the 1999 Düzce earthquake, GPS campaigns that were conducted after 1999 Kocaeli earthquake were extended to Düzce area (Ayhan, et al., 2001). On the other hand, the SAR data were used to map the co-seismic surface deformation caused by 1999 Kocaeli and Düzce earthquakes by Bürgmann et al. (2002) and Çakır et al. (2003).

From GPS and SLR data Oral et al. (1995) modeled the velocity field of the Anatolia as a counter-clockwise rigid rotation about an Euler pole located in northern Egypt (near the Sinai Peninsula) relative to Eurasia (see also Oral et al., 1993; Noomen et al., 1993; Oral, 1994; Le Pichon et al., 1995; Cianetti et al., 1997; Reilinger et al., 1997). At least 90 per cent of the motion of the Anatolia can be accounted by such rotation (see Reilinger et al., 1997). Along the North Anatolia, GPS data give clear evidence that most of the deformation occurs along a single fault trace of the NAF and its western section along the Marmara region (Kahle et al., 2000). The sites in the west of the Karlıova have a tendency to a more westerly directed motion which becomes progressively more pronounced as the WSW with stations in southwestern Turkey indicating SW oriented rates (Reilinger et al., 1997; Mueller, Kahle and Barka, 1997). However, the magnitudes of the vectors are not all the same. Residual velocities appear to increase regularly toward the Southern Aegean Subduction system (SASS) (Oral et

al., 1995; Reilinger et al., 1997). A 2 mm/yr internal deformation is observed on the Anatolian block based on the residual velocities. On the other hand, on the basis of the GPS and SLR velocities Reilinger et al. (1997) suggests that the motion of the Anatolian-Aegean region may be best described in terms of a single plate (Anatolian Plate) in those western part (the Aegean region) gradual deformation is taking place internally (N-S extension increasing to the South). Even within the Marmara region, the highest south directed rates are found in the South relative to Eurasia (Straub and Kahle, 1995 see also Mueller, Kahle and Barka, 1997). On the other hand, the west directed velocity component increases along the northern part of the Marmara region. This velocity field concentrates along the Northern Armutlu strand (Fig. 4) of the western NAF (WNAF) (Kahle et al., 2000) which is trending nearly in E-W direction.

Most recently integrated data from a number of campaigns suggest that the WNAF zone accommodates ~25 mm/yr of right-lateral motion between Anatolia and Eurasia (McClusky et al., 2000). The strain rate calculations based on this updated version of the velocity field indicate that the NAF is characterized by compressional strain rate components between 34°E and 31.5°E while from 31° E to 30°E, extensional strain rate components predominate (Fig. 1 and 4) (Kahle et al., 2000). The localized deformation along the NAF appears to broaden and extensional along the Marmara region. This diffusion of deformation is corresponding to the sub-parallel fault structure in the Marmara region (Fig. 4) (See also Meade et al., 2002). The slip rates associated with the model of Meade et al. (2002) based on the updated GPS data suggest that deformation is localized on specific faults even in the Marmara region which is deforming diffusely. According to the results of Meade et al. (2002) Northern Armutlu Strand (NArS) that is extending from Kuzuluk to Marmara Sea in E-W direction carries more dextral motion than the Southern Armutlu Strand (SArS) which is extending from Kuzuluk to İznik. Analysis of local GPS data on sub-parallel strands in the WNAF zone suggest that up to 10 mm/yr slip is accommodated on the NAIS (Northern Almacık Strand) that is extending from Kuzuluk to Kaynaşlı, and 15 mm/yr on the SAIS (Southern Almacık Strand) which is extending from Kuzuluk to Bolu (Ayhan et al., 1999). Thus, total amount of motion is 25 mm/yr that is equal to directly measured amount of motion between the Anatolia and Eurasia. Straub, Kahle and Schindler (1997) surmised that additional important fault traces between the SAIS and the NAIS might exist. These fault traces may be trending parallel to the main faults (NAIS and SAIS). To make a conclusive result concerning research on the active fault locations, critical measurement points between the NAIS and the Black Sea coast including the area between the NAIS and the SAIS will be very useful. However, the distance between

them may be too short (changing between 5 and 22 km) to distinguish other probable deformation zones between these strands. In other words, elastic deformation zones of these sub-parallel strands could be intersecting in that range.

Straub et al. (1997) calculated the strain rate field based on the displacement rates and then projected onto the tectonic structures. According to the results, western part of the NAIS from Akyazı to the Düzce plain (Aksu fault) is associated with the thrust components and an extensional component exists at the western tip area of the Almacık block (Fig. 4). It is already clear from the geometries of the faults (See section 3.1). Nothing is known about the velocity field in the east and northeast of the Almacık block by the means of geodetic data.

## **2.5. SUMMARY AND DISCUSSION**

In the Düzce area, a tectonic cycle ended and a new regime started with an initial stage of a peneplanation according to the geological and geomorphological findings related to the morphology and the deposits of the peneplain. The presence of remnants of the peneplain, incised meanders and uplifted stream terraces are directly related to the formation of the Düzce basin following the peneplanation. The existence of alluvial materials over hill sides (Fig. 11; Pekcan, 2000) their unconsolidated nature, existence of their uneroded remnants and the uplifted terraces along the valleys of the present drainage system suggest a young age for the formation of the Düzce basin. On the other hand, the structural geological field investigations of Michel (1994) show that onset of the young dextral shear in the Marmara region starts within Pliocene (see also Şaroğlu, 1988). If the basin formation is directly related to the dextral shear, the model should be a pull-apart system.

Several lines of evidence suggest that the faults of the study area are not a part of an active pull-apart system that has been forming the Düzce plain. (1) The 1999 earthquake ruptures and field investigations show that the Düzce fault is not connecting an active normal fault system bounding the Düzce basin from west but (2) connecting another dextral fault that is the part of the 1999 Kocaeli rupture (Fig. 2). According to the field observations during this study along the northern, eastern and western borders of the basin, no active fault morphology and no geological evidence related to the active faulting is detected. (3) Finding out the nature of the eastern connection system of the Düzce fault in the NAF system may be the key concept to solve the basin formation problem in the region. Contrary to strike-slip faults of a dextral pull-apart basin model, no significantly recognized connection that was detected during our

field investigation between the Düzce fault and an active right-lateral fault system that can transfer most of the motion to the east, to form the Düzce basin (See also Hitchcock et al., 2003). (4) Furthermore, no basin-bounding active normal faults are detected along the eastern boundary of the Düzce depression and (5) no active dextral fault is detected along its northern boundary. (6) As mentioned in the previous paragraph, the Düzce basin is quite young as the Marmara sea basins (Arpat and Şentürk, 2000). Current tectonic regime across the Marmara region may be younger than the basins, because the east-west dextral shearing system is cross cutting the plains and some of their boundaries that are represented by diagonal submarine hills in the Marmara Sea (Arpat and Şentürk, 2000; Le Pichon et al., 2001 and 2003). According to the borehole data, an area of local sediment thickening was identified southwest of the Düzce basin beneath Efteni Lake area, where a well known right stepping occurred between the 1999 Kocaeli and Düzce ruptures (Figs. 2 and 20). Any active basin forming extensional feature along none of the borders of the basin could have been observed during the present study, except this local Efteni subsiding system.

It is a fact that the occurrence of the Marmara basin system is young as mentioned in previous paragraphs. However, the active faults in the area are right lateral and active boundary faults that bounding the basins do not probably exist any more (Arpat and Şentürk, 2000 and Le Pichon et al., 2001, 2003). In this case, the occurrence of the basins is very young at most Pliocene (E.g., Emre et al. 1998) but surprisingly inactive. Michel (1994) suggests that onset of a right-lateral shearing in the Marmara region starts within the Pliocene (See also, Şaroğlu, 1988). Following the end of basin formation stage, probably in Quaternary (?), currently active dextral fault system was initiated in the Marmara (Arpat and Şentürk, 2000). Similar differentiation of stages of the North Anatolian dextral shearing system was made by Şaroğlu (1988). Eastern continuation strand of Düzce fault could have been one of the major dextral fault zones that were forming the southern boundary of the pull-apart system that is responsible for the formation of the Düzce basin. At the same time, this former dextral shear zone could have been responsible for the formation of the northern border fault of the Bolu basin (See Gökten, 2004). As already mentioned, some of the NW-SE zones of the set of old conjugate faults had probably been reused as normal faults in the Düzce basin. The other, young but probably inactive, strand is trending along the northern boundary of the Düzce basin through Çökek valley and far west. The reason of the recent ending of the basin formation stage (See also, Şaroğlu, 1988) is a good subject of a further study.

There are two principle well-known hypothesis related to the movement of the Anatolian block. One is continent-continent collision (tectonic escape) in eastern Turkey and the other is the South Aegean Subduction (SAS)-based driving force (McKenzie, 1978). Recent ending of the basin formation stage could be related to a young alteration of the tectonic regime that is responsible for kinematics in the Marmara region. The only known recent alteration in the proposed tectonic systems occurs in the SAS system. In the south of the South Aegean Arc, a recent collision was suggested by Piper and Perissoratis (2003) according to the new seismic profiling performed in this area. If the Marmara region had been under dominant influence of the Aegean Extensional system before the collision than following the collision, the deformation of the Marmara region might have been restricted to a narrow zone rather than its former diffuse and basin forming nature. Similar stress regime alteration was described by Şaroğlu (1988). On the other hand, the recent inactivation of the basin formation process could also be associated with the normal evolution of fault systems following a trend of progressively toward a more strait and higher dipping fault planes. If it is the case, none of the driving forces could be preferred to explain the variations in the tectonic history of the fault zone. However, it is very difficult to explain diagonal structures (basin boundaries) cutting by active faults. This may require a nonprogressive tectonic development. Therefore, it seems unlikely to associate the ending of the basin formation process with the common evalutional history of the fault system.

### 3. THE MAJOR ACTIVE FAULTS

Along the eastern ~1000 km of the NAF system, faults lie within a narrow zone along the broad convex-to-the-south arc (Barka, 1992). Farther west, the fault system consists of a diffuse deformation zone (Western NAF). E-W-trending right-lateral strike-slip sub-parallel faults accommodate the plate boundary strain in the Western NAF (WNAF) system (Fig. 4). See section 2 and 2.5. for the location of active, inactive and recently inactivated faults in the region. According to GPS measurements, most of the motion was taken up along the Southern Almacık strand (SAIS) and Northern Armutlu strand (NArS) of the NAF zone that has about 24-25 mm/yr dextral slip rate (McClusky et al., 2000; Ayhan et al., 1999). A slip rate of about 17 mm/yr derived for the NArS, combined rate of about 7 mm/yr for the Southern Armutlu (SArS) and the Bursa strands; about 15 mm/yr for the SAIS and about 10 mm/yr for the Northern Almacık strand (Section 2.4). The geometrical positions of the faults in the WNAF zone may result from the previous pattern of the overall transtensional (IDT) system of the Marmara region, or from the older pre-existing structural pattern or both of them (See section 2.5). In this section, each active seismogenic fault in the WNAF zone is studied with a closer look to understand the behaviors of the faults.

To understand fault behavior, main parameters characterizing a seismogenic fault must be explained. These are (1) the geometry of the rupture and the distribution of slip during an individual earthquake, (2) the time elapsed since the last earthquake, (3) the recurrence intervals and variations in the recurrence intervals and earthquake size and (4) the slip rate of the fault. Earthquake ruptures bring us an important information related to the main parameters about a fault. For this reason, the study of fault ruptures after the large earthquakes is one of the most valuable afford of the scientists. In the study area, five large earthquakes occurred in the last 100 years (Fig. 5). The last two of them were studied in detail. However, the details of the studies decrease gradually for older earthquakes. The August, 17 1999 Kocaeli and the November, 12 1999 Düzce earthquakes occurred on the NAIS and NArS; the May, 26 1957 Almacık and the July, 22 1967 Mudurnu earthquakes occurred on the SAIS; the February, 1 1944 Bolu earthquake rupture extended from the eastern part of the SAIS to the single strand part of the NAF leaving WNAF zone to the east (Fig. 4 and 5). Fault scarp and surface breaks can reflect the seismogenic fault planes; consequently, its characteristics are an expression of the main parameters of the fault plane that was ruptured at depth. For this

reason the field investigation of the surface rupture is one of the most important and useful method for understanding the fault behaviors. In this study, the main parameters of the faults are studied by critically reviewing the previous studies of all disciplines. And also concerning them, earthquake-geology tool is used for investigating the 1999 Kocaeli and Düzce earthquake ruptures. General characteristics of the surface breaks of the 1999 Kocaeli and Düzce earthquakes were observed in the field in the following hours after the occurrence time of them (Komut and Ikeda, 2000 and Arpat et al., 2001). Very detailed observations are made on the surface breaks of the 1999 Düzce earthquake all the way along the rupture (Appendix 1) and the eastern part of the surface breaks of the 1999 Kocaeli earthquake along the Aksu fault (Section 3.1.2). Active fault morphology is identified very clearly and examined from the stereoscopic 1:8000 scale aerial photos which their positions were designated after preliminary field observations of the surface rupture (Komut and Ikeda, 2000; Arpat et al., 2001). Aerial photos were taken by General Command of Mapping (HGK). Scanned and rectified images were geocoded using the ground control points by taking WGS84 geodetic datum and GEODETIC projection and using ErMapper 6.1 software. Rather detailed observations are also available for the surface breaks of the July 22 1967 Mudurnu earthquake from the study of Ambraseys and Zatopek (1969). However, only general characteristics of the surface breaks of the May 26 1957 Abant (Öcal, 1959) and the February 1 1944 Bolu (Ketin, 1969) earthquakes are available. The surface rupture maps of these studies were scanned and rectified using the same procedure described above to get digital data that are used in the figures.

### **3.1. NORTHERN ALMACIK STRAND OF THE NAF**

This strand lies along the northern border of the Almacık block and seems to be forming northernmost margin of the WNAF zone along the block (Fig. 4). It is a dextral zone that is formed as a single fault trace. The easternmost segment of the 1999 Kocaeli rupture is represented as Aksu segment or fault that is forming the western part of the NAIS (Section 3.1.2). On the other hand, the 1999 Düzce rupture is forming the eastern part of the NAIS (Section 3.1.1) (Fig. 24). At a glance, the NAIS consists of at least two segments. One is Aksu fault and the other is Düzce fault. A major right stepping in the Northern Almacık Strand (NAIS) at about 31°E longitude has formed a local depression (Efteni Lake basin) at the southwestern tip of the Düzce basin (Fig. 4 and 25). This structure appeared as a segment

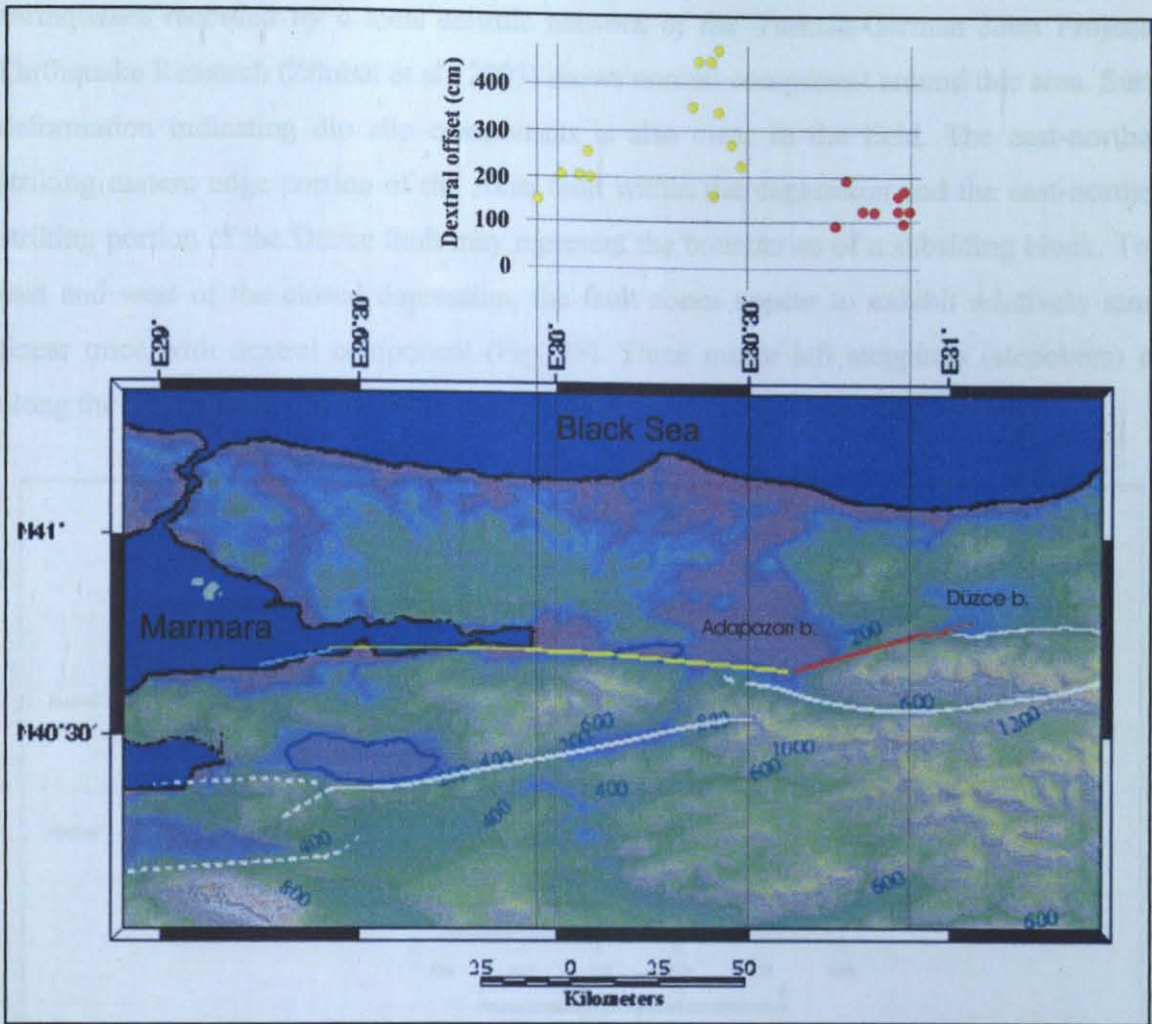


**Figure 24.** Slip distribution and surface rupture of the 1999 Kocaeli earthquake on the contoured and shaded (from south) topographic relief map (After Komut and Ikeda, 2000). The chart above is proportional to the map below. The ruptured fault is colored with blue, yellow and red lines representing probable seismic segments on the map. Red line: Aksu segment; Yellow line: Gölcük segment; Blue line: Çınarcık segment that was probably ruptured during the earthquake. White lines are other active faults in the map area. Dashed white lines are showing probably active faults. Red and yellow filled circles are representing dextral offset along the Aksu and Gölcük segments, respectively.

junction after the 1999 Kocaeli and Düzce Earthquakes. According to the field observations in this study, in the east, the 1999 Kocaeli rupture was terminated about 7 km east of Gölyaka (Fig. 25). On the other hand, according to Gökten et al. (1999) the 1999 Kocaeli rupture extends through 10 km south of Düzce. The easternmost segment of the 1999 Kocaeli earthquake rupture is striking NE-SW on the other hand the 1999 Düzce rupture is striking E-W. Because of this difference in the fault geometry, the faults are forming right stepping at Gölyaka area (Fig. 25). This geometry of the faults suggests that the Efteni Lake basin has been formed largely as a pull-apart basin or rhomboid graben within the right stepover.

Supporting this idea, composite focal mechanism solution of the aftershocks of the 1999 earthquakes recorded by a local seismic network of the Turkish-German Joint Project for Earthquake Research (Zünbül et al., 2003) shows normal component around this area. Surface deformation indicating dip slip components is also clear in the field. The east-northeast-striking eastern edge portion of the Aksu fault within the depression and the east-northeast-striking portion of the Düzce fault may represent the boundaries of a subsiding block. To the east and west of the closed depression, the fault zones appear to exhibit relatively simple, linear trace with dextral component (Fig. 25). Three minor left-steppings (stepovers) exist along the Düzce fault. On the other hand, there is no stepping along the Aksu fault.

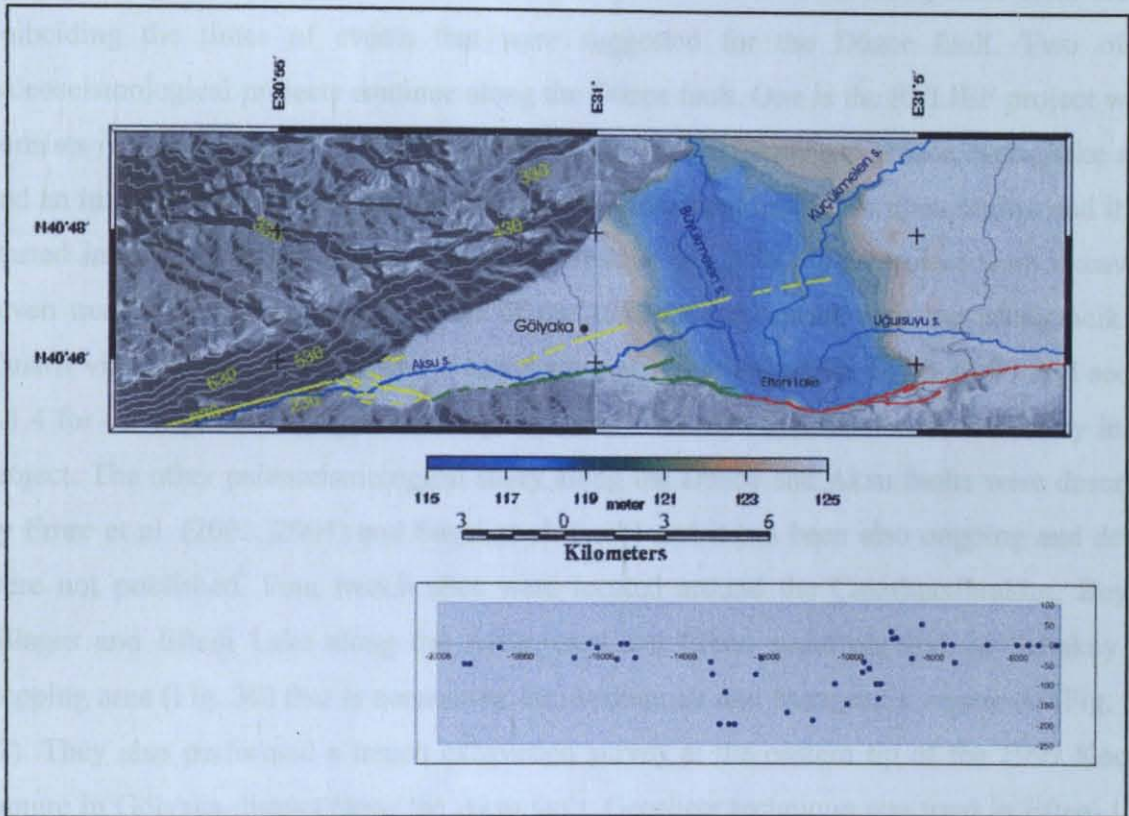


**Figure 25.** Efteni Lake basin, a local depression in southwest of the Düzce basin above. The vertical slip distribution of the 1999 earthquake below. To see the location of the Efteni Lake basin area as a local depression according to the Düzce basin see the topographic relief and blue colored altitudes in figures 14 or 18. The color scale shows altitude between 115 and 125 meters in this figure. First contour level is 130 m. Contour interval is 100 m. The local high in the western Efteni Lake basin is the alluvium cone of the Aksu stream (Fig. 34). Yellow line: Surface rupture of the 1999 Kocaeli earthquake. Red line: 1999 Düzce rupture. The green line between the 1999 Düzce and Kocaeli surface ruptures represents a part that was ruptured by both of the earthquakes. The map above is proportional to the vertical slip distribution below. “-” displacement represents north side down in the slip distribution chart along the Y-axis. X-axis: the distance along the surface rupture according to zero point at the 40:46:20.74N; 31:10:42.04E coordinates south of the Beyköy (See appendix 1). The only systematic vertical (upside south) deformation occurred within the 5 km right stepping area between Düzce and Kocaeli rupture. The 1999 Kocaeli rupture is reaching up to the Büyükmelen and Küçükkmelen streams (Fig. 35).

Including this study, four paleoseismological studies were conducted along the NAIS after the 1999 earthquakes. One of the paleoseismic studies along the Kaynaşlı segment of the Düzce fault was performed and published by Hitchcock et al. (2003). Three paleoseismic trenches were excavated. According to the results, pre-1999 surface-faulting events were comparable in size to the 1999 earthquake and in some cases, may have been larger. Penultimate event occurred about 300 years ago and the recurrence time is in the range of between 300 and 800 years. They suggested 300 years minimum recurrence interval. Some of the sample dates of the events are used in my study combining with mines to calculate probability distribution of the future earthquake (Section 4.4). In addition, they performed paleoseismological trenching on the Bakacak and Elmalık faults (Section 2.2). The event times from these sites are not coinciding the times of events that were suggested for the Düzce fault. Two of the paleoseismological projects continue along the Düzce fault. One is the RELIEF project which consists of data collection and the analysis of the 1999 Kocaeli and Düzce earthquake areas and an integrated analysis of the seismic hazard assessment in the Marmara region and it was started in 2002 (Meghraoui et al., 2004; Pantosti et al., 2004). The project team excavated seven trenches around the central part of the 1999 Düzce rupture near the Mengencik and Çınarlı villages along the Mengecik and Aydınpınar segments (See fig. 3 or 27 and section 3.1.4 for the location strategy about segmentation). The dating procedure is underway in this project. The other paleoseismological study along the Düzce and Aksu faults were described by Emre et al. (2002, 2004) and Sugai et al. (web) and it has been also ongoing and details were not published. Four trench sites were located around the Çakırhacıbrahim, Beyköy villages and Efteni Lake along the Aydınpınar and Efteni segments and on Şabakay left stepping area (Fig. 30) that is connecting the Aydınpınar and Mengencik segments (Fig. 3 or 27). They also performed a trench excavation survey at the eastern tip of the 1999 Kocaeli rupture in Gölyaka district along the Aksu fault. Geoslicer technique was used in Efteni Lake site to obtain exposures from sites that contain too much water to excavate trenches (Sugai et al., web). According to their preliminary results, three faulting earthquakes occurred in the last millennium. Aksu (Karadere) fault does not have regular recurrence interval. However, Aksu fault exhibits synchronous earthquakes with the Düzce fault (Emre et al., 2004). The penultimate earthquake occurred between A.D. 1650 and 1750 having a magnitude probably larger than the 1999 earthquake. They correlated this event with historically recorded 1719 earthquake (Section 1.1). Average recurrence interval of the surface rupturing earthquakes were calculated around 400 to 500 from Efteni Lake site (Sugai et al., web). The 3<sup>rd</sup> event back occurred between A.D. 665 and 1050 according to Emre et al. (2004) and Sugai et al.

(web). See section 4 for paleoseismic performances within my study and evaluation of paleoseismological results of previous and ongoing studies and historical records concerning segmentation.

### **3.1.1. DÜZCE FAULT**

The fault was previously mapped by Orkan et al. (1977), Şaroğlu et al. (1992) and Barka (1996). A major earthquake has occurred along the eastern part of the Northern Almacık Strand (NAIS) of the NAFZ on November 12, 1999 (Figs. 2 and 4). The fault zone which the rupture occurred on during the earthquake, has been called as Düzce fault. The rupture produced about 42 km long surface rupture all the way along the southern boundary of the Düzce plain having average 350 cm and maximum 500 cm dextral offset (Fig. 26). Average 150, 350, 450 and 300 cm dextral and about 350, 450, 500 and 350 cm maximum offsets were measured along the Efteni, Aydınpınar, Mengencik and Kaynaşlı segments, respectively (See fig. 27 for the segment locations and section 3.1.4 for the strategy about segmentation). The surface ruptures are distributed in a zone with width ranging from a few meters to 1 km, but generally from 1 to 5 m. The width up to 300, 100, 150 and 150 m was measured on Efteni, Aydınpınar, Mengencik and Kaynaşlı segments, respectively. About 500 m wide deformation zones appeared at the stepover areas and about 1 km zone representing easternmost section of the faults. There is not clear information about the eastern extension of the rupture line within the Bolu Mountain. On the other hand, its western end is rather clear. The sense of the deformation is generally pure dextral strike slip except its western end. At the western end, there is a systematic vertical component with dextral strike slip component connecting the Düzce fault with the Aksu fault to the west (Fig. 25).

Rupture parameters of the Düzce earthquake have been measured and modeled using teleseismic, strong motion, geodetic, geologic and seismic data by scientists since 1999. Three detailed surface break studies were made along the 1999 rupture of the Düzce earthquake. One of them was published in detail by Akyüz et al. (2002), the other one was published in some details by Emre et al., (2000). The third is published in this study with all details (see appendix 1 and following paragraphs). General strike is measured about  $270^\circ$  from the surface break data (See appendix 1; Emre et al., 2000 and Akyüz et al., 2002). It is also modeled from teleseismic, GPS and strong ground motion data within the range of  $258^\circ - 275^\circ$  (USGS, web; Harvard, web; Yagi and Kikuchi, web; Irmak, 2000; Ayhan et al., 2001 and Umutlu et al.,

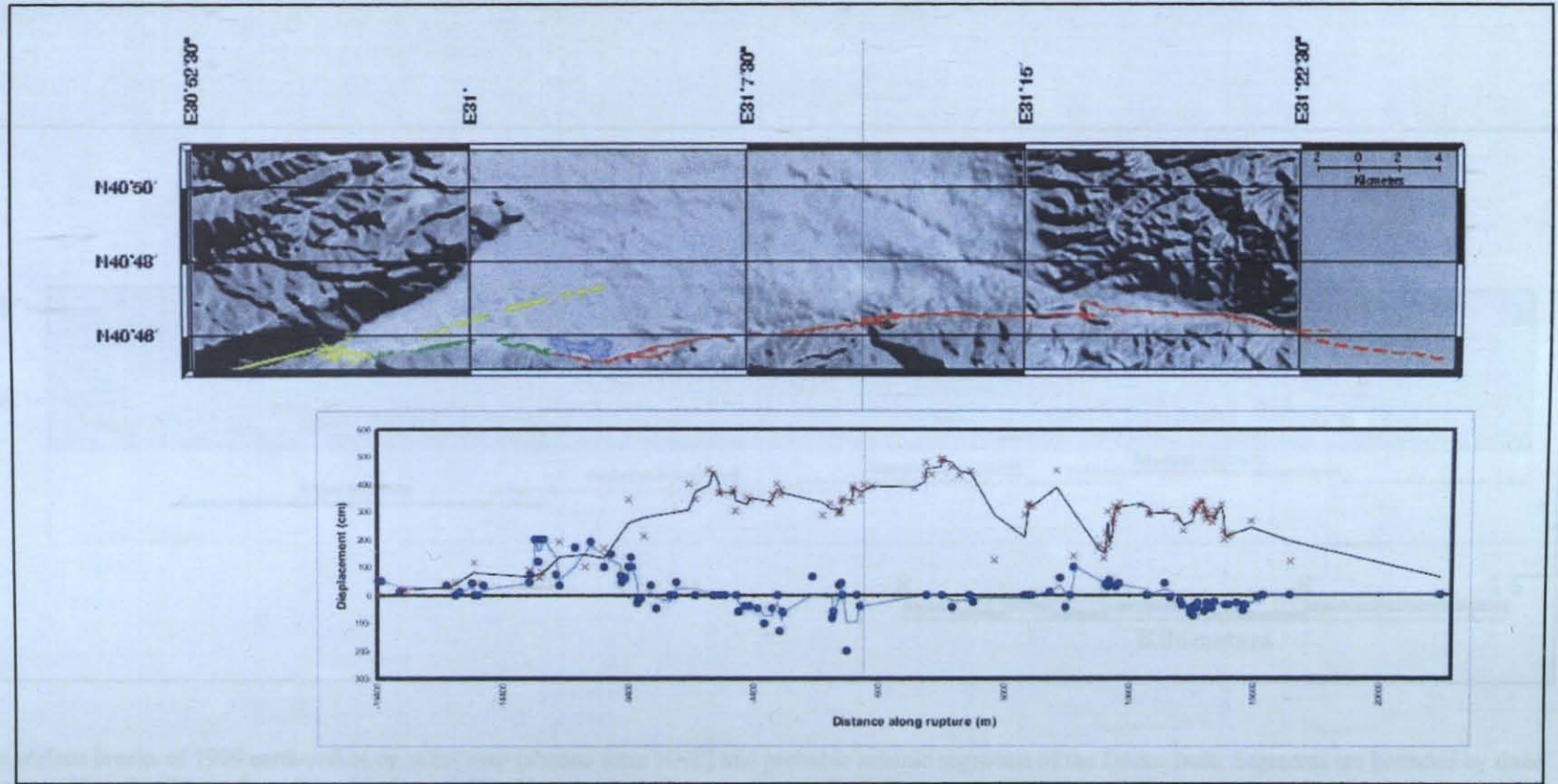


**Figure 26.** Slip distribution of the 1999 Düzce earthquake. Yellow line: Surface rupture of the 1999 Kocaeli earthquake. Red line: 1999 Düzce rupture. The green line between the 1999 Düzce and Kocaeli surface ruptures represents a part that was ruptured by both of the earthquakes. On the other hand, some of the observers suggest that the 1999 Kocaeli rupture extends trough 10 km south of Düzce, about 31:10E latitude (See Gökten et al., 1999). The map above is proportional to the slip distribution chart below. Red "x" represents dextral and blue points vertical offsets. "-" displacement represents north side up in the chart along the Y-axis. X-axis: the distance along the surface rupture according to zero point at the 40:46:20.74N; 31:10:42.04E coordinates south of the Beyköy (See appendix 1). The only systematic vertical (upside south) deformation occurred within the 5 km right stepping area between Düzce and Kocaeli rupture. 2 period moving average regression applied to draw the trend lines. Blue and black lines are the trend of vertical and dextral offsets, respectively.

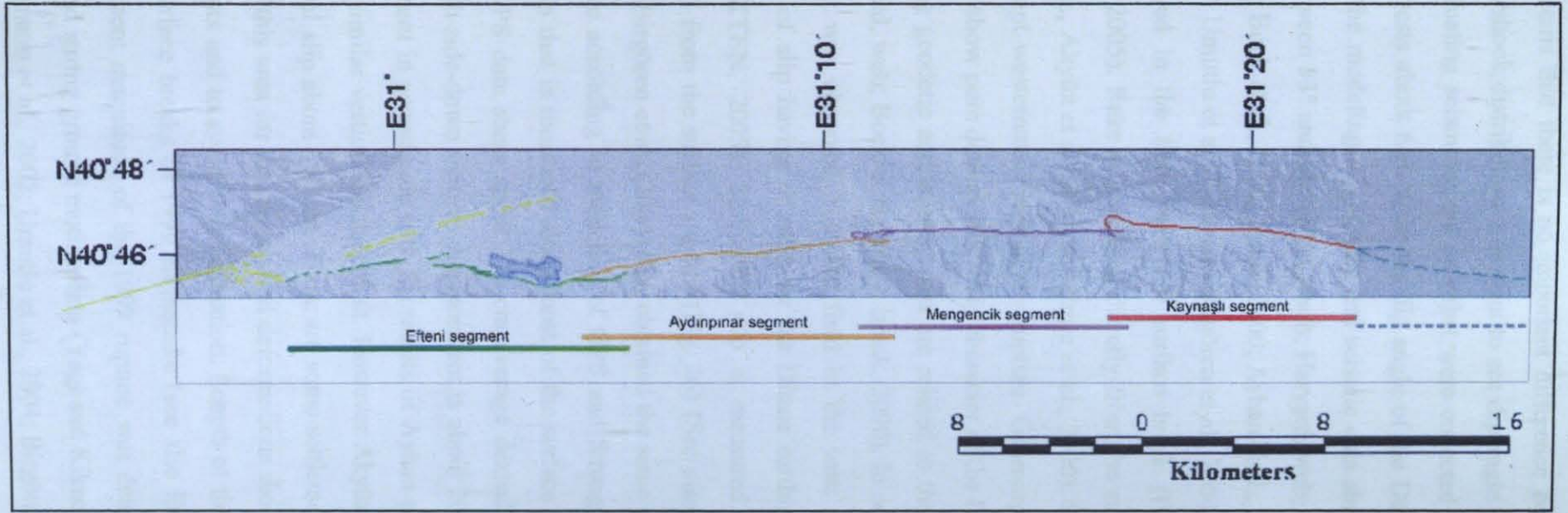


**Figure 27.** The surface breaks of 1999 earthquakes on relief map (shaded form NNE) and probable seismic segments of the Düzce fault. Segments are bounded by three left stepover areas within the Düzce fault (Fig. 30, 31 and 33). The segments are represented by different colors. Yellow lines show the surface breaks of the 1999 Kocaeli rupture in the area. Eastern extending part of the rupture has small en-echelon fractures. This is represented by dashed lines.

2004). It seems that there is no important difference between the modeled and measured strike. Aftershock distribution is evident to see dip angle of the Düzce fault (Milkereit et al., 2000). Evaluating seismological data that were collected from local stations Milkereit et al. (2000) suggests about  $66^\circ$  N for the dip angle of the Düzce rupture. The other studies that depend on the modeling of geodetic and seismic data show similar north directed dip angle ranging between  $53^\circ$  and  $65^\circ$  (NEIC, web; Harvard, web; Yagi and Kikuchi, web; Özalaybey et al., 2000; Bock et al., 2000; Irmak, 2000; Ayhan et al., 2001; Bürgmann et al., 2002; Çakır et al., 2003; Umutlu et al., 2004 and Birgören et al., 2004). On the other hand, vertical plane was observed in the field from the surface break (Personel communication with Ergun GÖKTEN, 2005). Rake is measured directly from the surface ruptures (See section 3.1.1.1 and also e.g., Akyüz et al. 2002 and Emre et al., 2000). Sense of deformation is nearly pure dextral except westernmost part of the rupture. Geomorphological and geological evidence also clearly show pure dextral strike slip character of the Düzce fault. Similar results obtained by modeling geodetic and seismic data are related to the 1999 Düzce rupture (e.g., USGS, web; Harvard, web; Bock et al., 2000; Irmak, 2000). In addition, vertical plane related to the rupture that was observed from the field in the west of Kaynaşlı suggests pure dextral component of slip having  $0^\circ$  rake for the Düzce earthquake (Personel communication with Ergun GÖKTEN, 2005). Maximum slip is measured about 500 cm at  $40:46:35.67\text{N}$ ;  $31:12:49.6\text{E}$  from the surface rupture (Fig. 26) (See also Akyüz et al., 2002). Ayhan et al. (2001) and Birgören et al. (2004) also obtained the same results for the maximum slip of the 1999 rupture according to modeling of GPS and Strong ground motion data, respectively. Average slip that is measured along most of the surface rupture is about 350 cm (Fig. 26). Similarly GPS data show about 376 cm average dextral slip of the rupture (Ayhan et al., 2001). North-side-down vertical displacement is about 200 cm that was measured along the Efteni segment in accordance with the results of Ayhan et al. (2001). Emre et al. (2000) are suggesting similar vertical displacement. However Akyüz et al. (2002) are suggesting much more vertical slip about 350 cm. There are some settlement related (secondary) deformation occurred in this area for this reason soil deformations should be eliminated to obtain tectonic displacements and to avoid over estimation. Length of the rupture is measured about 42 km from the surface breaks of 1999 earthquake (see also Emre et al., 2000 and Akyüz et al., 2002). Moment magnitude of the 1999 rupture was determined 7.1 ( $M_w$ ) from waveform solutions and strong ground motion data (Yagi and Kikuchi, web; Irmak, 2000; Woith et al., 2000; Bürgmann et al., 2002; Umutlu et al., 2004; Birgören et al., 2004). Ayhan et al. (2001) also determined similar moment magnitude using slip data from GPS measurements. Depth of

the hypocenter is not clear. It ranges between 10 to 20 km from one study to another (USGS, web; Harvard, web; Irmak, 2000; Milkereit et al., 2000; Zünbül et al., 2001; Woith et al., 2000; Tibi et al., 2001; Birgören et al., 2004). GMT of the earthquake is 16:57:20,8 and the location of the hypocenter is 40:818 N; 31.198 E according to local network that is nearly covering the hypocenter (Milkereit et al., 2000). All the wave form modeling studies using teleseismic and strong ground motion data have similar conclusion about bilateral rupture process (Yagi and Kikuchi, web; Irmak, 2000; Buchon et al., 2001; Tibi et al., 2001; Umutlu

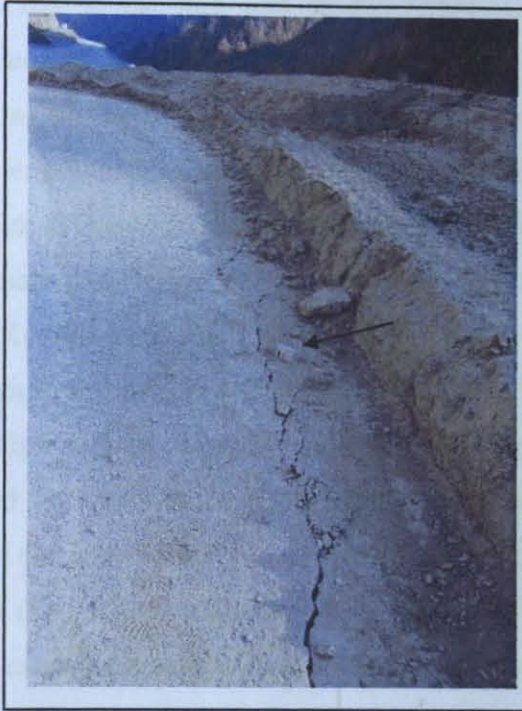


**Figure 28.** Eastern termination area of the 1999 Düzce surface rupture. See the easternmost observation point (D0001) in the appendix 1 for location. Picture was taken by looking from west. En-echelon fractures are reflecting right-lateral movement. They have been developed in the Asar valley followed by the highway, which is under construction. Four to five of these en-echelon fractures form groups that repeat in every few hundreds meters, fading eastward. Arrow is showing compass in 10x6x2 cm dimensions.

et al., 2004). Slip measured from surface breaks also decreases to the edges (Fig. 26). The same result was founded from GPS modeling and analysis of strong ground motion data (Ayhan et al., 2001; Buchon et al., 2001 and Birgören et al., 2004). According to these studies, the rupture nucleated near the bottom center of the rupture and propagated bilaterally. Direct evidence of strong ground motion data show that the Düzce rupture propagated at a

super-shear speed (4.3 km/sc) exceeding the Rayleigh wave velocity along the eastern part Buchon et al. (2001) (see also Birgören et al., 2004).

### 3.1.1.1. Geometry

According to detailed field investigations on the surface breaks of the 1999 Düzce earthquake the rupture produced 42.429 km long surface rupture along the Düzce fault (Fig. 26; Appendix 1; see also Emre et al., 2000 and Akyüz et al., 2002). Its extremities are located at 40:45:26.91N/30:57:20.76E in the west and 40:45:17.99N/31:29:33.96E in the east. GPS coverage is partly inadequate to determine exact length of the rupture (Ayhan et al., 2001). The linear distance along the fault is 40 km so the sinuosity is calculated 0,95 dividing the linear distance by the length of the surface rupture. It has generally E-W direction having a slight bow shape convex to the north (See also Emre et al., 2000). About 2.4 km difference between the linear distance and rupture length along the fault is related to this bow geometry. The August 17, 1999 Kocaeli earthquake was followed by the 1999 Düzce earthquake. The following rupture began in the west at the southwestern corner of the Düzce plain. About 9 km overlapping part exists between these two surface rupture along the boundary of the basin on the same trace and 12 km overlapping occurred between the Düzce rupture and the northern bifurcation of the easternmost Kocaeli rupture having about 4 km N-S maximum distance between them (Fig. 25). On the other hand, Gökten et al. (1999) suggested that the 1999 Kocaeli rupture extends through 10 km south of Düzce. The location of the western termination of the rupture is clear (Section 3.1.2) but there are controversial ideas about the eastern location of the termination and existence of unbroken seismic segment to the east. According to field observations here, the surface breaks of the 1999 Düzce earthquake disappear after small en-echelons (Fig. 28). Along the Düzce fault three left stepping appeared during 1999 rupture having similar distance between them (about 10,5 km) and similar stepping amount (about 300-500 m) (Fig. 27-33). These left stepping areas coincide with the geomorphologically observed small ridges. These are the Boncuk, Şabakay and Değirmen ridges from east to west (Fig. 29). The stepovers are named according to these ridges as Boncuk, Şabakay and Değirmen stepovers (Fig. 29 and 27). Possible seismic segmentation is configured considering these stepover structures along the Düzce fault (Fig. 27; see section 3.1.4). However, aftershock distribution of the 1999 Düzce earthquake seems to be uniform not to concentrate at specific locations (Tibi et al., 2001 and Zünbül at al., 2003). According to this nature, the 1999 Düzce earthquake seems to be ruptured as a single event (Zünbül et

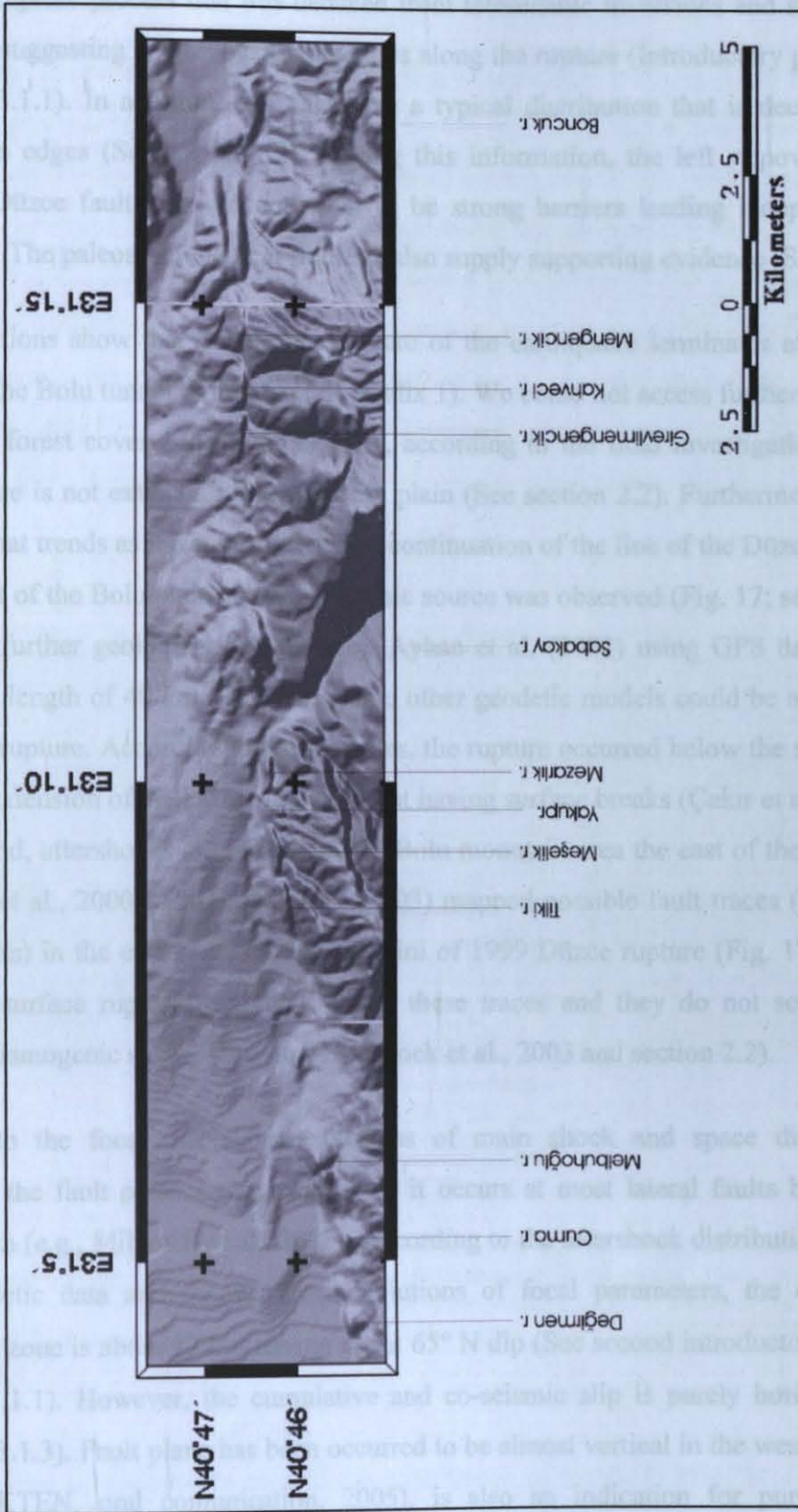


Figure 29. Location of the small ridges along the Düzce fault on relief map shaded from north.

al., 2003). Rupture process that was deduced from teleseismic inversions and strong motion data are not suggesting any segment boundaries along the rupture (Introductory paragraphs of the section 3.1.1). In addition, slip data have a typical distribution that is decreasing from center to the edges (Section 3.1.1.2). Having this information, the left stepover structures within the Düzce fault zone do not seem to be strong barriers leading independent large earthquakes. The paleoseismological findings also supply supporting evidence (Section 4.4).

The observations show that the surface rupture of the earthquake terminates at the western entrance of the Bolu tunnel to the east (Appendix 1). We could not access further east because of its dense forest cover. On the other hand, according to the field investigations the 1999 Düzce rupture is not extending into the Bolu plain (See section 2.2). Furthermore, no active fault scarp that trends as the eastern expected continuation of the line of the Düzce fault in the northern part of the Bolu plain as a seismogenic source was observed (Fig. 17; see section 2.2 and 2.5 for further geological information). Ayhan et al. (2001) using GPS data suggested similar fault length of 40 km. However, some other geodetic models could be appropriate to longer fault rupture. According to these studies, the rupture occurred below the surface along the eastern extension of the Düzce fault without having surface breaks (Çakır et al., 2003). On the other hand, aftershocks are remarkable in Bolu mountain area the east of the Düzce plain (Özalaybey et al., 2000). Hitchcock et al. (2003) mapped possible fault traces (Bakacak and Elmalık faults) in the east of the eastern termini of 1999 Düzce rupture (Fig. 17). However, there is no surface rupture that occurred on these traces and they do not seem to be an important seismogenic source (See also Hitchcock et al., 2003 and section 2.2).

According to the focal mechanism solutions of main shock and space distribution of aftershocks, the fault plane is not vertical as it occurs at most lateral faults but has a dip towards north (e.g., Milkereit et al., 2000). According to the aftershock distribution, modeling of the geodetic data and the waveform solutions of focal parameters, the depth of the seismogenic zone is about 15 km having about 65° N dip (See second introductory paragraph of section 3.1.1). However, the cumulative and co-seismic slip is purely horizontal (Next section and 3.1.3). Fault plane has been occurred to be almost vertical in the west of Kaynaşlı (Ergun GÖKTEN, oral communication, 2005), is also an indication for pure strike slip displacement as expected for the surface deformation of the strike-slip faults. Thus, the active faulting is not normal or reverse here but its fault plane has an abnormal dip angle.

### 3.1.1.2. Rupture Slip

Slip per event is one of the main parameters that characterize a seismogenic fault. It is the amount of rupture or co-seismic slip produced by a single event and it is representative of the energy released during an earthquake. Right-lateral surface slip of the 1999 Düzce earthquake was directly measured in the field where distinguishable surface markers such as roads, fences and tree lines are offset (Appendix 1). According to evaluation of the slip distribution, the rupture of the 1999 Düzce earthquake is dominantly pure dextral strike-slip (Fig. 26). The maximum dextral offset is about 500 cm according to the geodetic (Ayhan et al., 2001) and surface break data. In concordance with teleseismic and geodetic data surface rupture observations show that dextral slip distribution is symmetrical having the symmetry center at

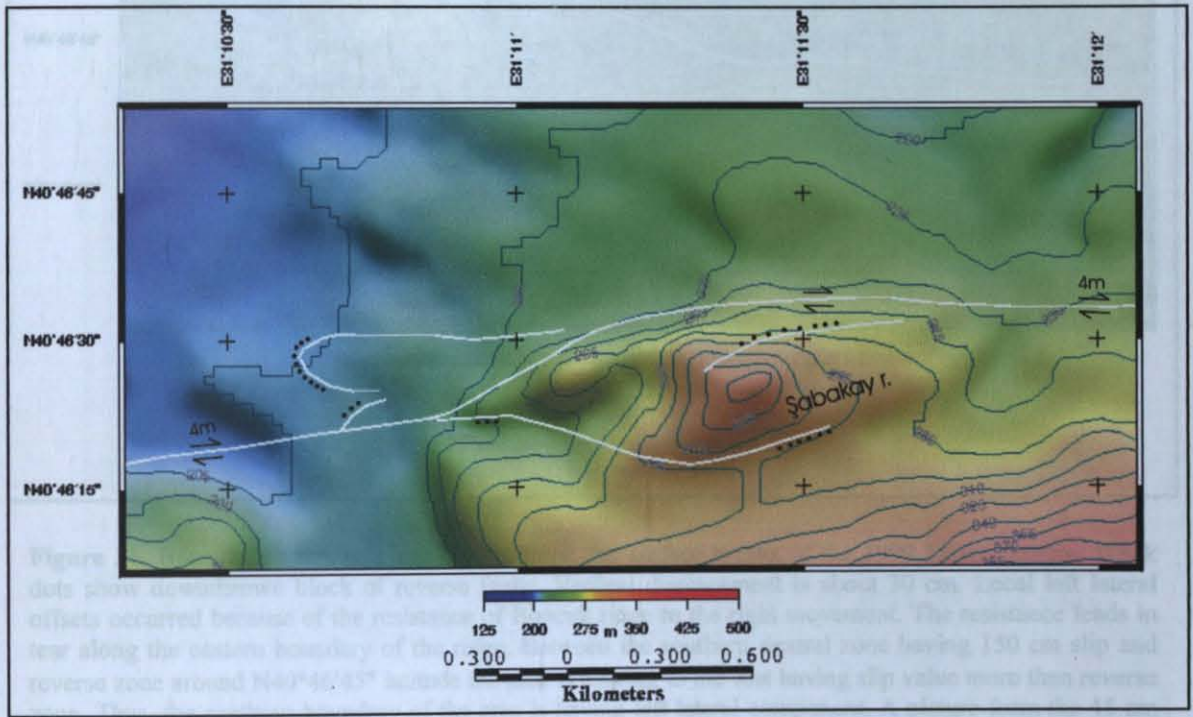


**Figure 30.** Şabakay left stepover area. White lines: the surface breaks of the 1999 Düzce rupture. Black dots show downthrown block of reverse faults. Vertical displacement is about 50 cm. The color scale shows altitude that is also shown by contours. Colored altitude layer is draped on the south shaded relief map. See figure 29 and 27 for the location of the Şabakay ridge and stepover.

the east of the Eflani segment, the Düzce fault has a typical dextral fault geomorphology (Section 1.1.3). On the other hand, Eflani segment has a typical north side down normal fault (Section 1.1.3). In the west of the westernmost left stepping, upside south normal slip component that occurred during the 1999 Düzce earthquake is substantial. Settlement results in an additional vertical separation in this region. Maximum vertical offset here is about 200 cm eliminating the soil settlement related observation points. This measurement is in concordance with the

paleoseismic data (Sugai et al., 2005). The right-lateral offset is diminishing from Değirmen stepover to the westernmost termini point of the rupture along the Efteni structural segment from about 350 to few centimeters (Fig. 27 and 26). Along the overlapping area which both 1999 surface ruptures occurred, the right-lateral offset of the 1999 Düzce surface rupture diminishes from 200 to few centimeters to the west (Fig. 26). The vertical offset is changing

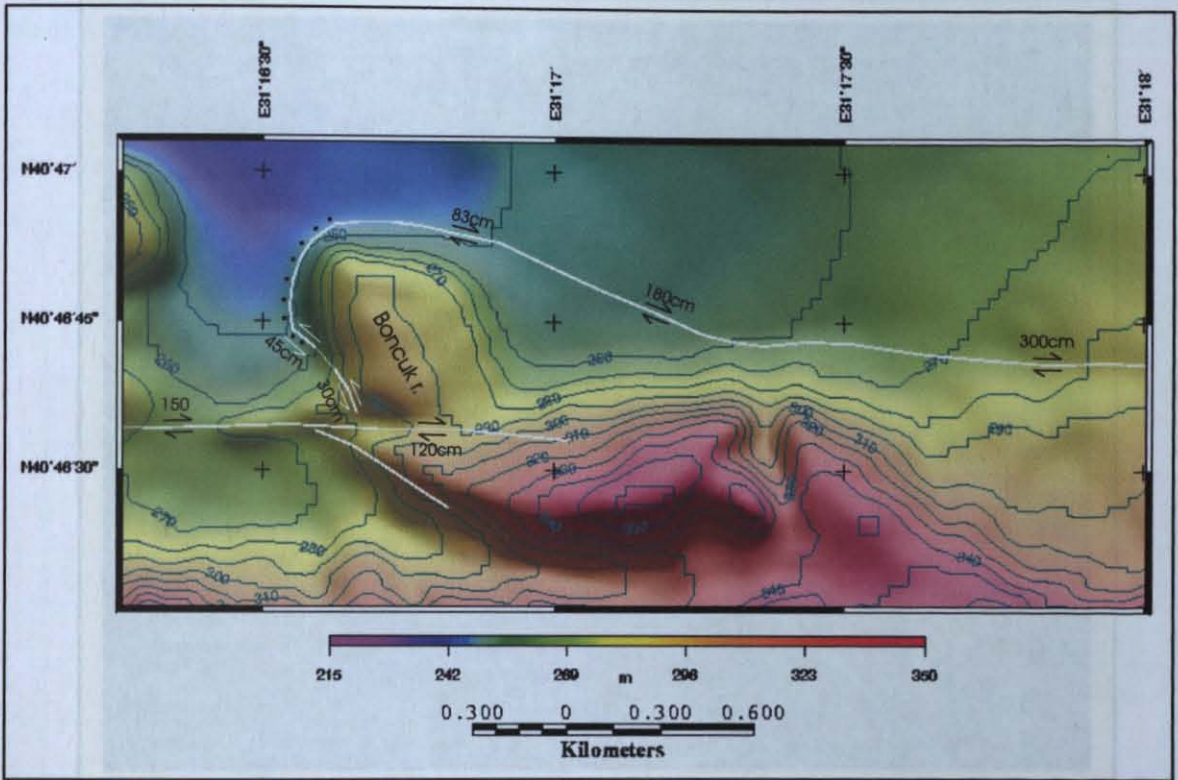


**Figure 31.** Boncuk left stepover area. White lines: the surface breaks of the 1999 Düzce rupture. Black dots show downthrown block of reverse faults. Vertical displacement is about 30 cm. Local left lateral offsets occurred because of the resistance of Boncuk ridge to the right movement. The resistance leads in tear along the eastern boundary of the ridge. Between the southern dextral zone having 150 cm slip and reverse zone around N40°46'45" latitude the area is moving to the east having slip value more than reverse zone. Thus, the northern boundary of the area is having left lateral component. A picture from the 45 cm left lateral offset rupture is shown in figure 32. The color scale shows altitude that is also shown by contours. Colored altitude layer is draped on south shaded relief map. See figures 29 and 27 for the location of the Şabakay ridge and stepover.

between few centimeters and 200 cm along this area and diminishing to the west (Fig. 25). In the east of the Efteni segment, the Düzce fault has a typical dextral fault geomorphology (Section 3.1.3). On the other hand, Efteni segment has a typical north side down normal fault morphology. The 1999 rupture follows this morphological anomaly. There are shutter ridges, deflected stream channels, sag ponds and so on along the fault that are representing its behavior during the Holocene (Section. 3.1.3). Three compressional areas at the left stepovers are some other geomorphologic indications forming probable seismic segment boundaries

within the Düzce rupture zone (Fig. 27). Compressional vertical deformations observed at the west sides of the Şabakay and Boncuk ridges which are located on the left stepover areas (See also Emre et al., 2000) (Fig. 30 and 31). The westernmost left stepping (Değirmen stepover) does not result in significant compressional features as vertical deformations on Şabakay and



**Figure 32.** Left lateral movement having reverse component along the southwestern boundary of the Boncuk ridge along the Düzce fault. Picture is clearly showing left offset along the fences (looking from south). See figure 31 for the location of the picture.

Boncuk stepovers. However, in this area, normal vertical component along the Efteni segment ends and pure dextral component starts towards the east all the way along the Aydınpinar, Mengencik and Kaynaşlı structural segments except stepover areas (Fig. 33 or 25). Slip has large normal vertical component along the Efteni segment because of a large right stepping at the western end of the Düzce rupture with Aksu fault (Fig. 25). Generally, the Düzce fault seems to have transpressional nature because the fault has just left stepovers and left bendings that are leading compression at these locations (Özden et al., 2000; Aydın and Kalafat, 2002). In addition, most of the vertical slip measurements along the two structural segments in the

middle including the middle part of the easternmost segment may also suggest systematic south-side down minor compressional component having N-dipping fault geometry (Fig. 26 and 27). The transpressional nature could be driven by the optimally-oriented Aksu fault tectonic boundary that is resulting to convert west directed general tectonic motion to SW direction over the Almacık block according to the Eurasian plate. This local conversion probably leads in the active counterclockwise rotation of the Almacık block on the contrary of clockwise rotation that was suggested by some scientists for the Almacık block (section 2.2).

where  $D$  is average displacement in meters and  $L$  is surface rupture length in kilometers.

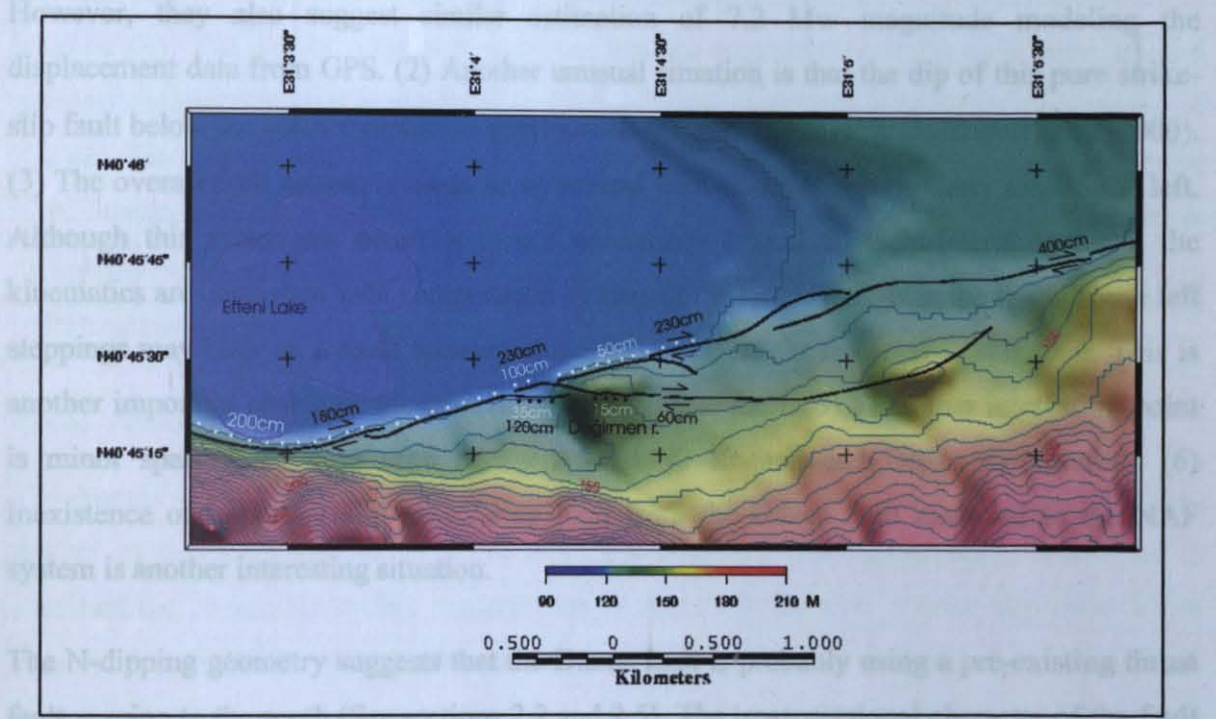


**Figure 33.** Değirmen left stepover area. Black lines: the surface breaks of the 1999 Düzce rupture. Black and white dots show downthrown block of reverse and normal faults, respectively. Vertical and dextral displacements are shown by white and black colored texts, respectively. The color scale shows altitude that is also shown by contours. Colored altitude layer is draped on south shaded relief map. See figures 29 and 27 for the location of the Şabakay ridge and stepover. The dextral offset difference is obvious between east and west of 31°5'30" longitude. Efteni segment that is mostly characterized by normal faulting ends between 31°4'30" and 31°5' longitudes. See figure 25 to locate the map area taking reference longitude 31°5'.

### 3.1.1.3. Discussions

The Düzce fault and its 1999 rupture exhibit interesting behaviors. (1) Based on the worldwide survey, end-to-end length of the rupture trace versus magnitude regression by Wells and Coppersmith (1994),  $M_w$  is estimated as 7.1. In addition, based on end-to-end length of the rupture trace versus magnitude ( $M_s$ ) regression for the eastern Marmara by

Ambraseys and Jackson (1998), same  $M$  is evident. The magnitude ( $M_w$ ) implied by regressions is about 7.1, and hence consistent with the seismic moment. Ayhan et al. (2001) identified that the Düzce earthquake had the highest slip-to-rupture-length ratio of any historical earthquake along the NAF (See also Arpat et al., 1999web) according to the relationship that

$$\log(D) = 1.43 + 0.88 \log(L)$$

where  $D$  is average displacement in meters and  $L$  is surface rupture length in kilometers. However, they also suggest similar estimation of 7.2  $M_w$  magnitude modeling the displacement data from GPS. (2) Another unusual situation is that the dip of this pure strike-slip fault below the surface rupture is approximately  $65^\circ$  to the N (E.g., Milkereit et al., 2000). (3) The overall fault system is made up of several fault traces that commonly step to the left. Although this systematic behavior is not necessarily typical of right-lateral systems, the kinematics are consistent with compression evident at the left steppings in the fault. These left steppings may infer an overall transpressional environment for the Düzce fault zone. This is another important characteristic behaviour of the Düzce fault. (5) The other interesting point is minor span of 87 days span between the 1999 Kocaeli and Düzce earthquakes. (6) Inexistence of important slip-transferring fault from the Düzce fault eastward to the NAF system is another interesting situation.

The N-dipping geometry suggests that the Düzce fault is probably using a pre-existing thrust fault verging to the south (See sections 2.2 and 2.5). The transpressional character of the fault could be related to counterclockwise rotation of the Almacık block (See section 2.2) that forces the location of the shear zone to shift towards the south relative to the Almacık block. Geomorphologically detected abandoned fault traces along the northern boundaries of the shutter ridges probably suggest southward shifting of the fault zone (See section 3.1.3). The active eastern slip-transferring mature fault may never be found because every shift of the shear zone to the south is resulting to form a new deformation zone that propagate to the east slowly. Delay of 87 days or smaller time span after the rupture of the Aksu fault may suggest time dependence of the 1999 Düzce fault failure to the 1999 Aksu fault failure (1999 Kocaeli rupture) (Aydın and Kalafat, 2002). On the other hand, this also results from the coincidence of the period of high stress along the Düzce fault with the 1999 Kocaeli rupture that occurred near the Düzce fault. 1999 Kocaeli earthquake probably results in stress transfer on the Düzce fault (Hubert-Ferrari et al., 2000). In this case, future or past failure of both the Aksu and

Düzce faults with single earthquake is possible. The reason of the south directed fault zone migration could be the southwest directed extrusion of the Almacık block (according to the Eurasian plate) along the Aksu fault because the northern block of the fault is forming a driving border that has NE-SW elongation. South-migrated new faults have been probably produced at the southwestern corner of the Düzce plain that has been formed between Aksu and Düzce faults as a pull-apart Efteni basin. New south boundary faults occur for every shift of the Almacık block to the south. Dextral motion along the northern border of the Almacık block uses the continuation of this new boundary faults as a shear zone. The high coseismic slip with respect to the rupture length is the function of recurrence interval of earthquakes and tectonic slip. The tectonic slip and recurrence interval deduced from GPS measurements and paleoseismological results respectively are in concordance with the co-seismic slip amount of 350 cm (See section 3.1.5 and also 4.4). Accordingly, it seems that some part of the fault have high resistance to accumulate this amount of slip. High slip of the Düzce rupture is compatible with the large recurrence interval of  $355 \pm 35$  year (% 70 probability) of surface rupturing earthquakes along the Düzce fault, which is mentioned in section 4.4.

### **3.1.2. AKSU FAULT**

The August 17, 1999 Kocaeli earthquake was felt strongly in Düzce town. The rupture is also known as the 1999 Gölcük or 1999 İzmit earthquake. Field investigations allow us to constrain the co-seismic surface rupture zone of about 150 km with a strike slip up to 4.5 m associated with the 1999 Mw 7.4 Kocaeli earthquake (Fig. 24) that occurred along the western seismic segments of the North Anatolian fault in the eastern Marmara region (Komut and Ikeda, 2000; Arpat et al., 2001). The rupture zone may be roughly divided into three at least two structural segments based on the tectonic landform features and displacement distributions that are obtained from the field observations (See also Komut and Ikeda, 2000). In addition, according to the teleseismic body wave analysis, Pınar et al. (2000) found stages of rupture separated in space and time. This result yields that different seismic segments are ruptured during the main shock and a separated stage of rupture is occurred at the eastern part of the source area along the Aksu segment (Pınar et al., 2000; see also Yılmaz and Demirtaş, 1999). These all indicate that the Aksu fault could be ruptured alone and is one of the smallest unit (seismic segment) of propagation on this part along the NAIS. For this reason, it could be distinguished as a probable seismic segment. The deformation characteristics of the surface ruptures and focal mechanism solutions reveal that the earthquake had a nearly pure right-lateral strike-slip mechanism. The rupture appears as a straight lineament trending east-west

along the alluviums of Adapazarı and İzmit basin. It slices through the Adapazarı basin in the east-west direction (Fig. 24). This part is named as Gölcük segment. On the other hand, the eastern and the western segments of the rupture are trending N70°E. The eastern segment was named as Aksu. In this section, the study is located along the Aksu segment of the Kocaeli rupture which has a close location to the Düzce basin (Fig. 24).

The Aksu fault is about 40 km including its eastern extension up to the Küçükmenen stream (Fig. 25) and it is considered as one of the major strike-slip faults along which strike-slip partitioning occurs in the east-west regional shortening and WSW extrusion of Almacık block according to the Eurasian plate in a long period of time. In concordance with this, Straub et al. (1997) suggested compressional deformation along the Aksu fault based on modeling of the GPS measurements. One other large earthquake ( $M = 7.2$ ) that occurred in the same year produced a 42.429-km-long surface rupture zone along the Düzce fault that located near the east of the Aksu fault (Section 3.1.1). The co-seismic rupture extends from the east of Akyazı in the Adapazarı plain and runs along the Karadere stream, passes the Kadifekale, runs along the Aksu valley and terminates in the southwestern part of the Düzce plain, is reaching up to 40 km in total length. The eastern part of the Aksu segment is located in the Aksu valley in a region of high mountains (with an average elevation 800 m). During the 1999 Kocaeli earthquake, some landslides have occurred along this valley (See also İleri and Gökten, 2002). The surface ruptures are distributed in a zone with width ranging from a few meters to 1.5 km, but generally from 1 to 5 m along the mountainous area. Wide deformations zone coincides to the easternmost extension of the fault where the fault enters to the Düzce plain. The distinct shear faults generally dextrally offset man-made structures. These co-seismic deformation characteristics of surface rupture markers reveal that the earthquake had mostly pure right-lateral strike-slip mechanism having probably up side north minor reverse component. The extensional cracks that are concentrated along the rupture zone generally show a left stepping en echelon pattern and are oblique to the general trend of the rupture zone, indicating a right-lateral shear as a part of mole track fabric. They vary from a few mm to 0.5-1 m in width and are greater than 0.5 m in depth in an individual crack. The measured dextral offsets are summarized in figure 24 (See also Emre et al., 2003). The evaluation of data about a detailed structural analysis of the surface rupture of this earthquake is in preparation. See Emre et al. (2003) for rather detailed information that is mostly compatible with my study about surface rupture of the 1999 Kocaeli earthquake. The displacements vary from several to few tens of centimeters at both ends of the Aksu segment. About 1.4-m-average and 2 m maximum right

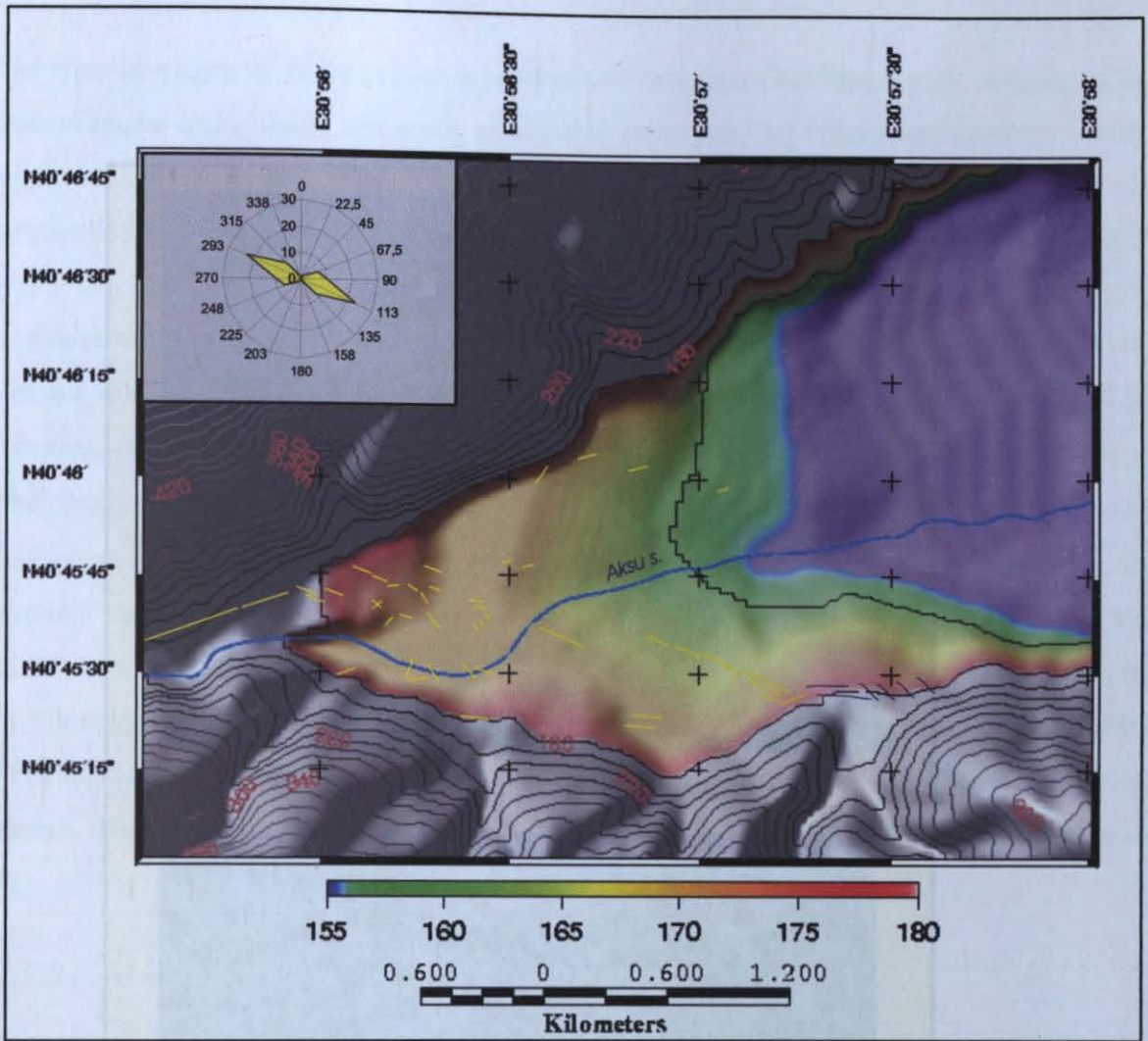


**Figure 34.** Splay of the 1999 Kocaeli rupture around western part of the Efteni Lake basin (Fig. 25) on the alluvial fan of the Aksu stream. Yellow short lines are showing exact locations of the cracks that have systematic strike. Yellow filled radar chart box upper left corner is showing general strike of the cracks. The strike is measured mostly (more than 20 cracks) about N113°E that is evident from the yellow filled radar. Average interval is at least one crack about every 100 m at the mouth of the Aksu valley. The color scale shows altitude between 155 and 180 meters in this figure. Contour interval is 20 m. The relief is shaded from northwest to show the details of the fan. Dark blue short lines are showing the location of cracks that mm to cm scale deformation occurred during both 1999 Kocaeli and Düzce earthquakes and western termini point of the 1999 Düzce rupture.

lateral offset are evident from the surface break measurements (See also Emre et al., 2003). The slip that was obtained by teleseismic body wave analysis (Pınar et al., 2000) shows the same distribution as the geological measurements at the surface. The rupture has about north side up systematic 30 cm vertical component (Emre et al., 2003). This could suggest transpressional character for the fault zone which has N70°E optimally-oriented geometry in the general tectonic movement, driving the Almacık block towards the S70°W direction and constructing a huge (about 20 km) left stepping in dextral system between the Gölcük and Düzce faults (Fig. 24).

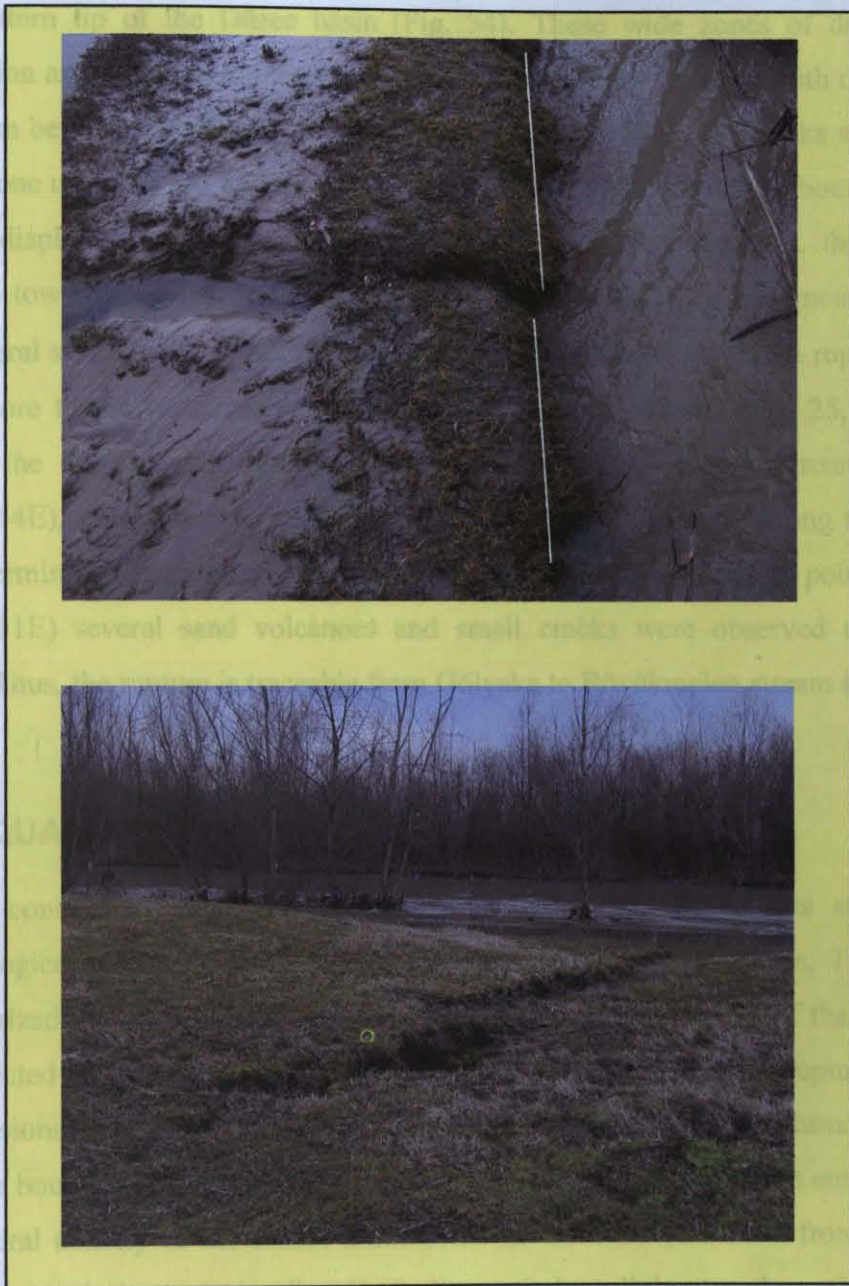


**Figure 35.** Right-lateral displacements of the 1999 Kocaeli rupture near Küçükmenen stream. See figure 25 for the location of the intersection point between the stream and rupture. Picture below and above were taken from southwest and north, respectively. The offset is a couple of centimeters in the location that is shown in the picture above. The offset that is deduced from en-echelon structures (see picture below) is more than 20 cm in the area.

The western extremity of the rupture at the southwestern tip of the Düzce plain consists of the discontinuous shear faults and many cracks that splay into an extensional horsetail at the southwestern tip of the Düzce basin (Fig. 34). These wide zones of deformation at the termination area appeared on the alluvial fan of Aksu stream at the mouth of the Aksu valley which can be recognized by detailed surveys in the field. Here, the cracks were distributed in a wide zone up to 1.5 km with an average interval of at least one crack about every 100 m. No distinct displacement can be observed along these cracks. However, they show NW-SE lineation towards the Düzce rupture (Fig. 34) and millimeter to centimeter scale openings. The general strike of the cracks is about N113°E. The easternmost of the rupture is continuing furthermore to the east, reaching up to the Küçükmenen stream (Fig. 25, appendix 1) and passing the Büyükmenen stream channel. Near the Büyükmenen stream (40:46:56.38N; 31:1:48.64E), several tens of centimeter right lateral offsets which belong to the eastern part of the termination area were measured (Fig. 35). At the easternmost point (40:47:19.85N; 31:3:40.11E) several sand volcanoes and small cracks were observed near Küçükmenen stream. Thus, the rupture is traceable from Gölyaka to Büyükmenen stream (see also appendix 1).

### **3.1.3. QUATERNARY OFFSET**

On the contrary of the Aksu segment, the Düzce fault represents strike-slip faulting morphological features that are serving measurable cumulative offsets. The Düzce fault is characterized by a pure dextral slip parallel to the southern boundary of the Düzce plain with the deflected stream channels (E.g., Fig. 36), left stepping en-echelon rupture array that have compressional component (E.g., Fig., 31), and shutter ridges. The Quaternary deposits along the basin boundary and the northern extremities of the slopes have been cut into slices by the right-lateral activity of the Düzce fault. Some of them are preserved from erosion. Shutter ridges are serving a typical strike-slip fault morphology lining up along the fault (E.g., Fig. 37). The northern edges of the mountain range are showing clear linearity having abrupt slope angle change (Fig. 29 and e.g., fig. 36). Some geomorphologic markers can be correlated between the southern and the northern blocks of the fault at some places (Fig. 36). According to the correlation and reconstruction of the shutter ridges with hills to the southern block and deflected stream channels along the Aydınpinar segment a total displacement of about 1 km was obtained (Fig. 36). The same kind of displacement is evident along the Mengencik segment on Girevlimengencik, Kahveci and Girevlimengencik shutter ridges (Fig. 29). These and the other shutter ridges along the Aydınpinar segment are made up with basement rocks

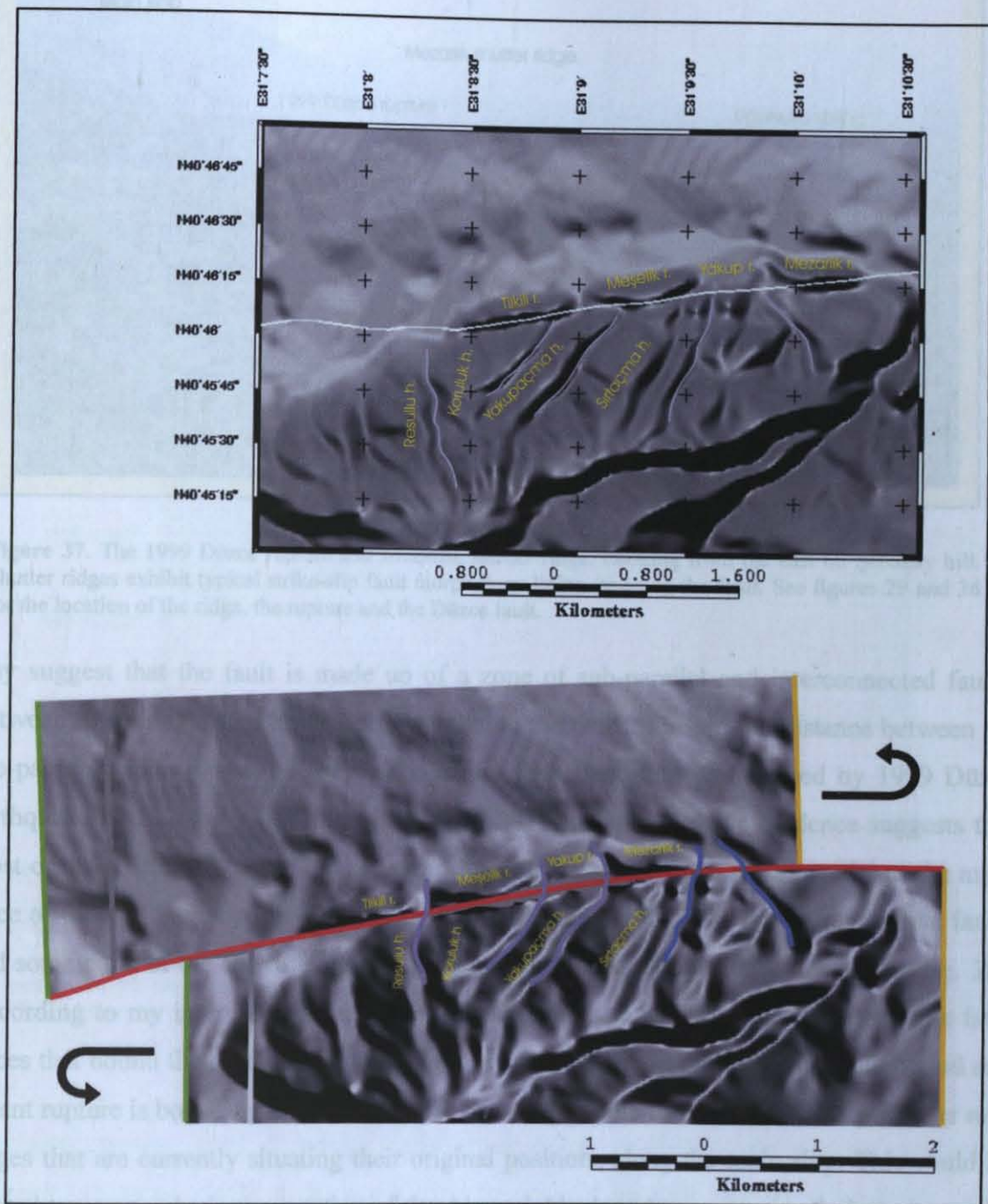


**Figure 36.** Reconstruction by left-lateral displacement of the shutter ridges to the probable original locations according to the morphological signs. The mach of the valleys suggest at this reconstruction is a possible one. The map above is current relief. White line is the surface breaks of the 1999 Düzce rupture on this map. See figure 29 to see the location of the series of the shutter ridges. The relief is shaded from south. The figure below shows left lateral reconstruction of northern block with respect to southern about 1 km along the Düzce fault (red line). Blue lines are stream valleys. Take ridge and hill names and stream valleys as references to notice the cumulated displacement.

Paleozoic and Palaeogene in age having massive and layered character. The same kind of basement material also exists along the northern slope of the Almacık Mountain (Herece and Akay, 2003). Interestingly, northern slopes of most of the shutter ridges are also showing linearities as the northern edge of the main slope parallel to the 1999 rupture (Fig. 38). This



**Figure 37.** The 1999 Düzce rupture and Mezarlık shutter ridge. Looking from the east on Şabakay hill. Shutter ridges exhibit typical strike-slip fault morphology lining up along the fault. See figures 29 and 36 for the location of the ridge, the rupture and the Düzce fault.

may suggest that the fault is made up of a zone of sub-parallel and interconnected faults. Between them long ridges are trending parallel to the faults. The similar distance between the sub-parallel faults is about  $1\frac{1}{2}$  km. The recent fault trace that was formed by 1999 Düzce earthquake bounds the south side of the ridges. This geomorphologic evidence suggests that most of the shutter ridges are cut by young faults from the northern sides parallel to the main trace of the fault zone to the south. Geomorphologic lineation of the northern in-active faults and some parts of the active faults can be connected by continuous fault lines (E.g., fig. 38). According to my interpretation, the rupture zone seems to move to the south because fault traces that bound the north side of the ridges seem to be idle in the active tectonic period and recent rupture is bounding main hill slope to the south. In the future, the fault may shutter new ridges that are currently situating their original positions along the main slop. This could be related to counterclockwise rotation of the Almacık block and transpressional character of the Düzce fault (See related discussion in section 3.1.1.2). In this case, measured cumulative offset using only the current rupture (E.g., fig. 36) is probably underestimated. There should be more Quaternary slip along the northern abandoned faults. In concordance with this, alluvial fan of the Uğursuyu stream shows furthermore cumulative offset up to 3 km. This is the maximum offset that is measured along the fault. Thus, the cumulative offset of the Düzce fault is minimum about 3 km. There could be more cummulative slip along the Düzce fault.

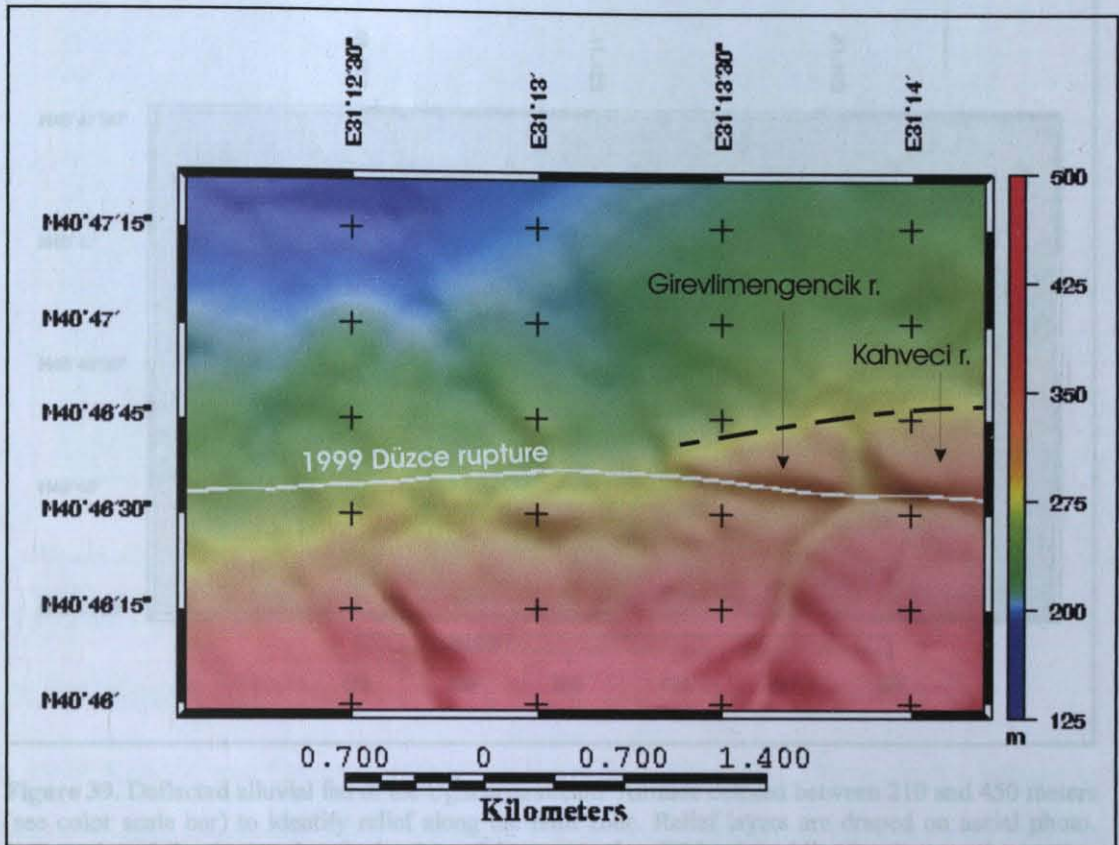


**Figure 38.** Linearity along the northern slope of the shutter ridges (dashed black line). This linearity suggests the existence of an abandoned rupture zone of the Düzce fault and probable southern migration of the fault zone because of the counterclockwise rotation of the Almacık block (See text in section 3.1.3). Topographic relief map is shaded from south. Color scale is showing altitude. See figure 29 for the location of the ridges and northern linearity. Same linearity also exists along the northern border of the Tilkili, Meşelik, Yakup and Mezarlık shutter ridge series (Fig. 36).

Uğursuyu stream valley is cutting sedimentary layers in Palaeogene age and granitoids (Herece and Akay, 2003) on the main slope flowing to the north. On the other hand, in the Düzce basin, the stream is flowing sub-parallel to the fault probably along the older fault trace of the Düzce fault to the west and reaches to the Efteni Lake instead of flowing along its direction to the north (Fig. 9, 39). This could be related to local basin (Efteni basin) formation to the west. It probably flew to the north and developed an alluvial fan during the initial stages of the Efteni basin. The Şabakay ridge just in the east of the stream channel along the border of the basin is made up with alluvial deposits that consist of granitoid and sedimentary gravels and blocks (Fig. 40). Remnant alluvial fan deposits were found in the east of the Uğursuyu

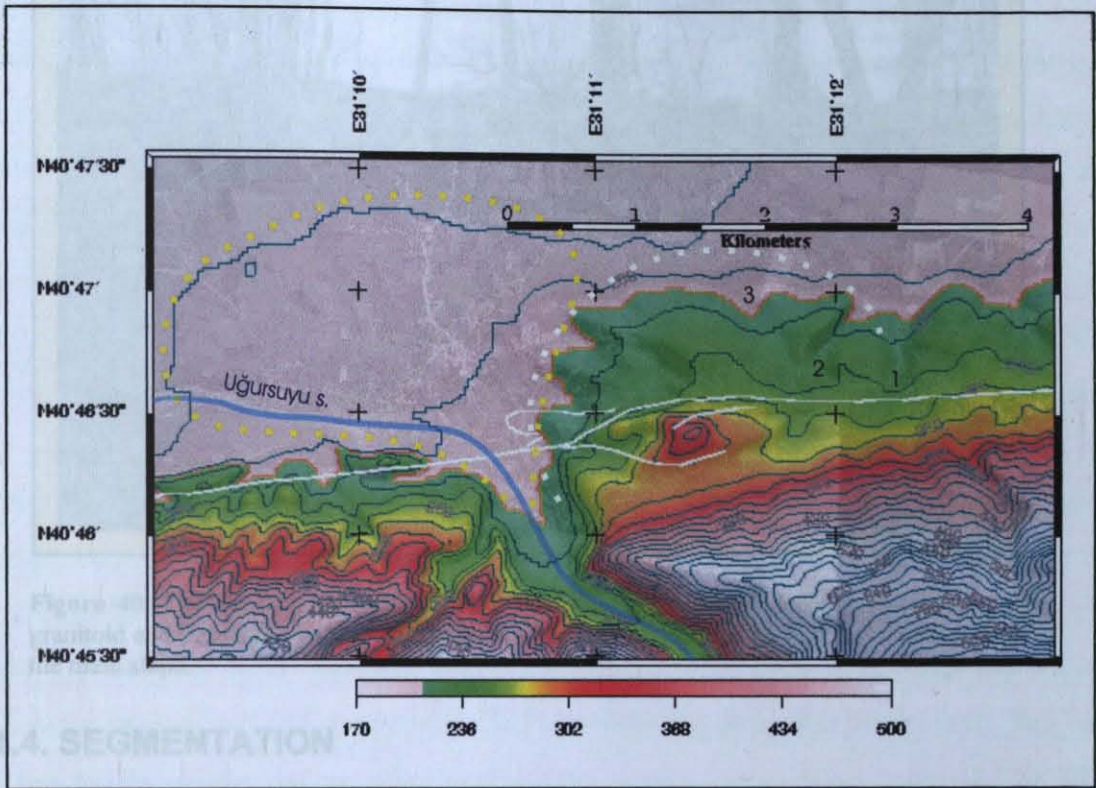


**Figure 39.** Deflected alluvial fan of the Uğursuyu stream. Altitude colored between 210 and 450 meters (see color scale bar) to identify relief along the fault zone. Relief layers are draped on aerial photo. Yellow dotted line is showing the borders of the current fan. White dotted line borders an observation area that includes deflected remnants of the older fan (Fig. 40). Numbered (1, 2 and 3) stream channels had been probably belonging to the Uğursuyu stream. According to the horizontal length scale, the channel 1 on the older fan has been dragged up to about 3 km to the east according to the main hill slope and Uğursuyu valley. The older fan area including Şabakay ridge on the left stepping area of the 1999 rupture (Fig. 30) made up with alluvial deposits.

valley mouth (Fig. 39). Its geomorphologic form is nearly identical to an alluvial fan. The remnant fan/s of the Uğursuyu stream was probably dragged to the east by the Düzce fault that is bounding it to the south. The right-lateral offset was estimated by measuring the offset between the axis of Uğursuyu remnant fans/channels and Uğursuyu stream. The throw is about 1 up to 3 km (Fig. 39).

Taking the maximum offset of 3 km and slip rate of 10 mm/yr (see section 3.1.5), the age of the cumulative offset is calculated about 0.03 Ma (upper Pleistocene). This result is concordant with the geological and geomorphological evidence about the age of the active tectonic phase (See section 2.5). The calculation of 3 km offset may be underestimated concerning the size of the Efteni basin (Fig. 25). However, further estimations will not probably change too much to the date of the active tectonic regime up to the Pliocene.

### 3.1.5. SLIP RATE



**Figure 40.** The Şabakay ridge (Fig. 39) is made up with alluvial deposits that consist of granitoid and sedimentary gravels and blocks which are transported by Uğursuyu stream from the main slope.

### 3.1.4. SEGMENTATION

The 1999 Kocaeli and Düzce earthquakes show that Aksu and Düzce faults belong to the different seismic segments. As it was described before in section 3.1.2, the Aksu fault seems to be a seismic segment that is ruptured with other segment/s to the west. According to field studies, the Aksu fault cannot be divided into segments in spite of a few hundred meters discontinuity along the 1999 Kocaeli surface rupture at the Kadifekale region. The discontinuity is probably related to a landslide around the Kadifekale region. On the other hand, the Düzce earthquake created a rupture with three probable structural segment boundaries along the Düzce fault. The fault is composed of the four segments that each has about 10.5-km length and separated with the left stepping structural discontinuities (stepovers) (Fig. 27). These segments are Efteni, Aydınpınar, Mengencik and Kaynaşlı (from west to east). The edges of the defined rupture segments are characterized by stepovers (Figs. 30, 31, 33) and sometimes minima in the displacement distribution (Fig. 26). The segments do not seem to be ruptured independently and they probably merged at depth along the Düzce fault zone (Section 3.1.1). According to independent paleoseismological results, the Düzce fault seems to be single seismic segment (Hitchcock et al., 2003; Emre et al., 2004 and Sugai et al., web). Trench excavation sites are situated at the different probable structural segments as mentioned. My paleoseismological study is also concordant with this result (See section 4).

### **3.1.5. SLIP RATE**

Slip rate is the rate of deformation characteristic of a fault and is representative of the average activity of the fault and therefore of its strain-energy release. The slip rate is calculated on the basis on the deformation produced by the fault during a particular interval of time. Although available knowledge is gathered from a few GPS stations (See section 2.4), according to the conclusion about tectonic regime in the study area, the Düzce fault appears to be the single principal structure accommodating strike-slip deformation that is measured by GPS in the north of the Almacık block (See section 2.5). On the other hand, the indirect information comes from the calculated slip using paleoseismological observations with average co-seismic slip of 1999 Düzce earthquake (See section 3.1.1.2) along the fault leaning on some assumptions (See section 4.4). If we compare the information that comes from the different sources, both GPS and geological data suggest a consistent slip rate of about 10 mm/yr along the Düzce fault of the Northern Almacık Strand (NAIS). GPS data are directly giving this value. On the other hand, statistical analysis of paleoseismological data suggest that average recurrence interval is  $9.5 \pm 1$  mm/yr with (% 70 probability) along the Düzce fault. See section 4.4. for details and discussions about probability analysis on recurrence interval. The  $355 \pm 35$  year (% 70 probability) interval was calculated from combined paleoseismological data from this study and from the study of Hitchcock et al. (2003). Sugai et al. (web) also suggested an average interval ranging from 400 to 500 years (See also Emre et al., 2004) and Hitchcock et al. (2003) 300 – 800 years. According to earthquake-geology studies on 1999 Düzce earthquake, average slip of the rupture is about 350-cm. Approximate slip rate of  $9.5 \pm 1$  mm/yr with % 70 probability is calculated dividing the average slip of the 1999 rupture by average recurrence interval of  $355 \pm 35$  year (% 70 probability).

### **3.2. SOUTHERN ALMACIK STRAND OF THE NAF**

The Southern Almacık Strand (SAIS) is inferred as constructing southernmost strand of the E-W-trending right-lateral strike-slip sub-parallel fault (NAF) network of a diffuse deformation zone (See section 3) in the easternmost Marmara region. In other words, the SAIS denotes the southern trace of the North Anatolian fault around Almacık Mountain. According to GPS measurements (Section 2.4) and geological considerations (Section 3.1.5), most of the motion has been taken up along the SAIS in the longitude range of the Almacık Mountain. A slip rate of 15 mm/yr was derived for this strand according to the GPS measurements. It extends for 110 km along the Dokurcun valley from the southwest of Bolu plain to the vicinity of

Sapanca, and describes a gently curving arc that is convex to the south (Fig. 4). To the northwest, the SAIS connected with the 1999 Kocaeli earthquake trace of the Gölcük structural segment of the North Anatolian fault (Fig. 24); to the northeast, strand appears to terminate within the Bolu fault zone that is the westernmost single trace of NAF (Fig. 4). This strand coincides spatially with the projected trace of pre-existing faults, and it is probably evolved by reactivation of older strands (See section 2.2). By this interpretation, the pre-existing fault is responsible for juxtaposing different lithological units in Dokurcun valley. On the other hand, the SAIS is only a relatively recent (Late Pliocene?) rupture developed within or close to the older faults (See section 2.5).

The SAIS zone was the site of three surface-rupturing earthquakes on 1 February 1944, 26 May 1957 and 22 July 1967. Starting from the east to the west, three earthquakes combined to produce a continuous rupture zone all the way along the SAIS. Three seismic segments that were ruptured in different combinations by these earthquakes along the SAIS are recognized. The distinction between the structural segments are based on contrast in the tectonic geomorphology and the geometry of surface ruptures that was obtained from the field observations (Öcal, 1959; Ambraseys and Zatopek, 1969; Ketin, 1969; Demirtaş, 1992). Extend of the ruptures, slip distribution of these earthquakes and segmentation will be described in the following paragraphs.

### **3.2.1. 1944 BOLU RUPTURE**

In 1944, 180 km rupture  $M_s=7.3$  (Ambraseys and Jackson, 1998) of the NAF occurred on February 1 crossing Bolu plain and having general direction of  $N75^\circ E$  (Taşman, 1944; Ketin, 1948 and see also Ketin, 1969) (Fig. 41). Another suggestion for the length is 160 km by Ambraseys and Jackson (1998). The rupture is also known as 1944 Gerede or 1944 Gerede-Bolu or 1944 Bolu-Gerede earthquake. Right lateral offset is 2-3, up to 3.5 meters measured by preliminary quality geological investigations (Ketin, 1969; see also Taşman, 1944). Near Gerede and Ilıca, the rupture has the south side up 40-100 cm vertical offset (Taşman, 1944 and Ketin, 1969). Some part of the western extremity of this rupture zone was probably re-ruptured by the 1957 Abant earthquake (See Öcal, 1959) and about 10-km part of the extremity was formed the southern sub-parallel break (about 700-m) to the 1957 Abant rupture. According to the paleoseismological study of Demirtaş (2000), the rupture has about 422 yr average interval and the interval probability is ranging between 200 – 779 yrs.

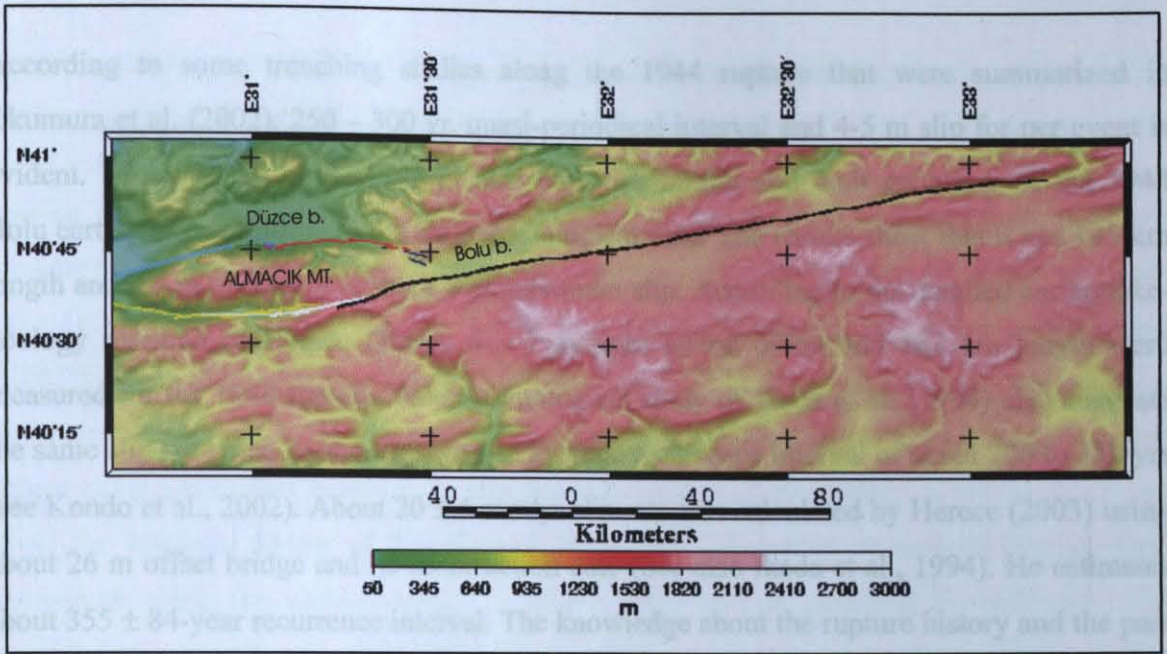


**Figure 41.** Surface rupture of the 1944 Bolu earthquake (After Ketin, 1969). Black line: the 1944 rupture.

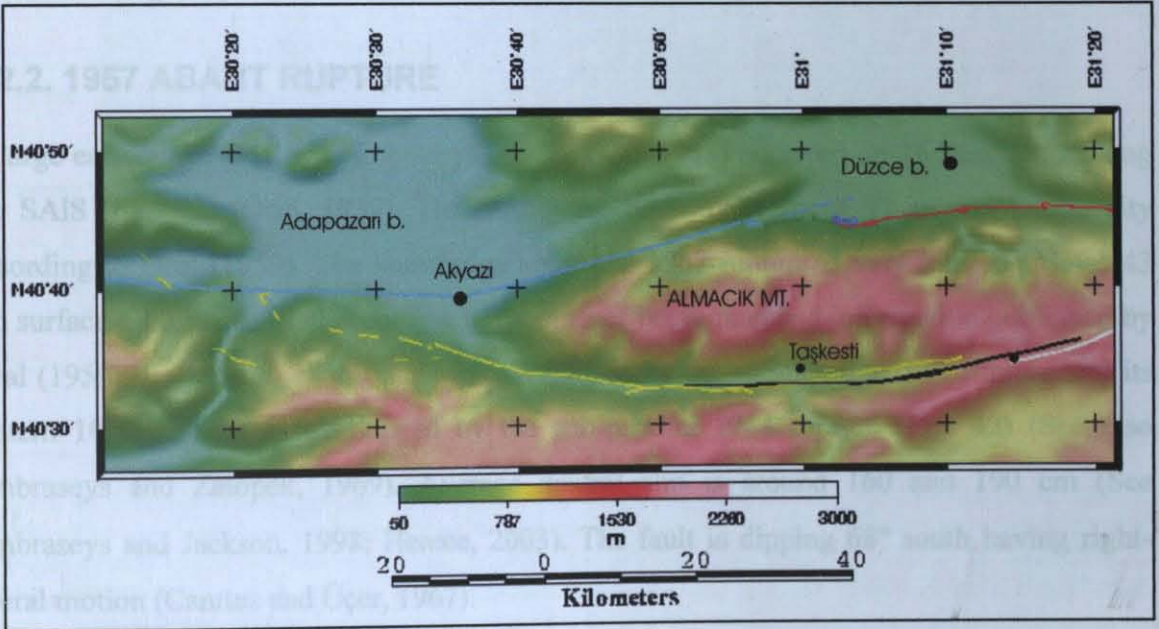


**Figure 42.** The surface rupture locations of 1957 Abant (black line, after Öcal, 1959) and 1967 Mudurnu (yellow line, after Ambraseys and Zatopek, 1969) earthquakes. Blue, red and white lines show the 1999 Kocaeli, Düzce and 1944 Bolu ruptures, respectively in the map area. Color scale shows altitude. Relief is shaded from south.

According to some trenching studies along the 1944 rupture that were summarized in Okumura et al. (2002), 250 – 300 yr. quasi-periodical interval and 4-5 m slip for per event is evident. Kondo et al. (2002) re-evaluated slip distribution and fault geometry of the 1944 Bolu earthquake according to the surface geological data. The results show that it has 185 km length and 3.5 m average and about 6 m maximum slip. According to the detailed earthquake-geology research of Herece (2003), 6 – 7 m right lateral offset and 183 km length were measured for the 1944 rupture. Paleoseismological study of Ikeda et al. (1994) also suggests the same slip per paleo-earthquake with an average recurrence interval of about 200 to 350 yrs (see Kondo et al., 2002). About  $20 \pm 4$  mm/yr slip rate was calculated by Herece (2003) using about 26 m offset bridge and its construction date (See also Ikeda et al., 1994). He estimates about  $355 \pm 84$ -year recurrence interval. The knowledge about the rupture history and the past slips is very limited. According to the review of the geological studies mentioned above, slip calculations are ranging between 7 and 33 mm/yr. However, considering the rupture representing the single strand part of the NAFZ and geodetically measured slip of about 25 mm/yr (McClusky et al., 2000), the slip on the rupture zone should be found 25 mm/yr paleoseismologically.

### **3.2.2. 1957 ABANT RUPTURE**

A large earthquake ( $M_s = 7$ , Ambraseys and Jackson, 1998) occurred on 26 May 1957 along the SAIS (Fig. 42) (Öcal, 1959). The earthquake intensity is about VI around Düzce city according to Öcal (1959). The knowledge about the 1957 rupture is very limited. About 43 km surface rupture occurred according to the surface break map and information published by Öcal (1959). Its western 28 km part was overlapped by the sub-parallel 1967 rupture and its eastern 10 km part was overlapped by the sub-parallel 1944 rupture (Fig. 42) (See also Ambraseys and Zatopek, 1969). Average dextral slip is around 160 and 190 cm (See Ambraseys and Jackson, 1998; Herece, 2003). The fault is dipping  $68^\circ$  south having right-lateral motion (Canitez and Üçer, 1967).

### **3.2.3. 1967 MUDURNU RUPTURE**

On 22 July 1967, an earthquake with a magnitude of  $M_s = 7.1$  (Ambraseys and Jackson, 1998) hit villages around Mudurnu valley and destroyed 10 % of the houses in the Düzce plain (Ambraseys and Zatopek, 1969). Ambraseys and Zatopek (1969) investigated the

surface ruptures and published detailed results about the distribution of the surface fault ruptures, seismicity and damage (See also Ambraseys et al., 1968).

Surface ruptures related to the Mudurnu earthquake, occurred along most of the southern boundary of the Almacik block and extended approximately 80 km, from 6 km east of Abant Lake (40:36:8,58N/31:11:1,36E) in the eastern end to Sapanca Lake at the western end (40:43:41,92N/30:13:43,95E) (Fig. 42). Right-lateral offset is up to 190 cm measured by Ambraseys and Zatopek (1969). Topographically, the Mudurnu surface rupture zone occurred almost along a boundary between the mountain ranges in a narrow valley. It is slightly curved along the southern border of the Almacik Mountain. The sense of vertical displacement component along the surface rupture is at the north side in generally downthrown. The vertical displacements vary from 20 to 50 cm at the eastern part where the surface was also

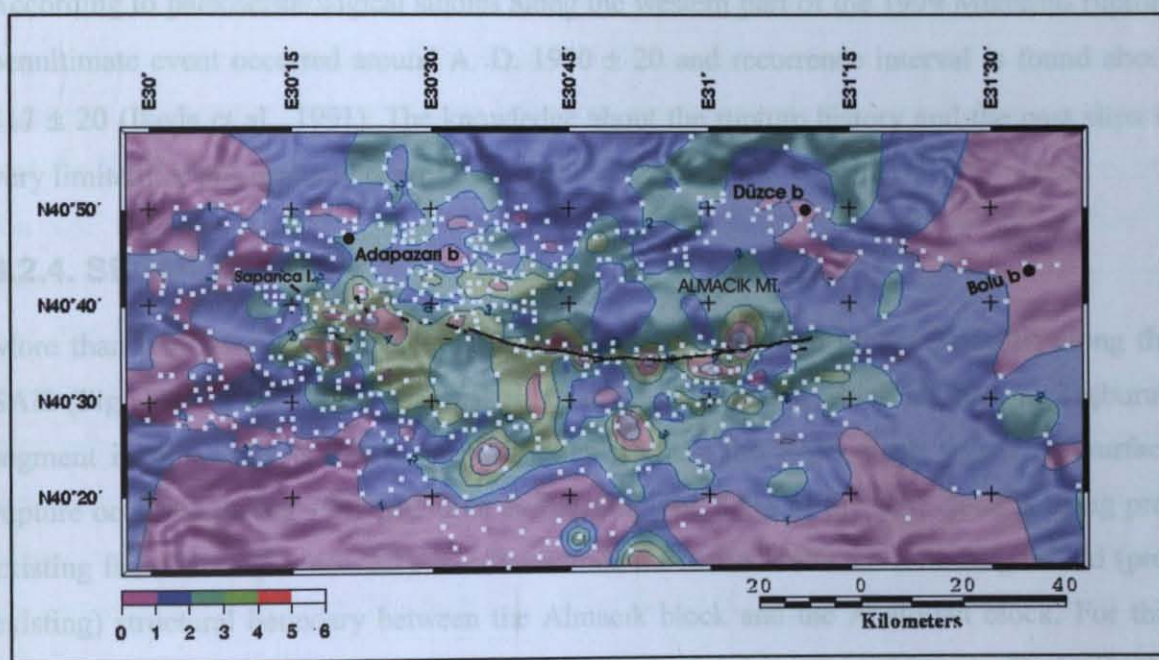


**Figure 43.** Damage distribution map. White dots: observation points. Black line: the 1967 Mudurnu rupture. Ratio of houses 'destroyed or damaged' to 'total number of houses' in villages based on Ambraseys and Zatopek (1969) grided and contoured. Color scale shows the ratio. 1: no damage; 2: 10%>; 3: 10%-25%; 4: 25% - 50%; 5: 50% - 75%; 6: 75% - 100%. The ratio is draped on topographic relief map that is shaded from south. Damage in the south of the rupture was pronounced more than north.

broken during 1957 Abant earthquake in the valley (Fig. 42). Damage distribution map of Ambraseys and Zatopek (1969) clearly shows that the damage was pronounced more at the southern side of the fault zone (Fig. 43). This may suggest that some parts of the fault have probably a dip to the south. Reuse of a pre-existing fault (See section 2.2) could result in this anomaly in damage distribution map and fault geometry. However, focal mechanism solution is unconcordant with this idea. It defines almost vertical plane (McKenzie, 1972). The surface

rupture generally forms a left stepping pattern about 15-25 km interval. Western WNW-ESE striking part of the rupture is about 50 km. On the other hand, 30-km-long eastern part has WSW-ENE general strike. This part was ruptured by both the 1967 and 1957 earthquakes for this reason it is described as an interim-segment. Western extremity of the western part of the 1967 rupture is forming tensional deformation zone with right stepping and again north facing fault scarps which have length of about 10 km. In concordance with this, a large aftershock (July 30, 1967) occurred in this area with a pure normal fault mechanism striking northwest southeast (Jackson and McKenzie, 1984). To the west, the fault connects with 1999 Kocaeli rupture system (Fig. 42). The western part could be a seismic segment that is forming the connection at the right stepping between the SAIS and the Gölcük segment that appeared during 1999 Kocaeli earthquake (Figs. 4 and 24).

According to paleoseismological studies along the western part of the 1999 Mudurnu rupture penultimate event occurred around A. D.  $1950 \pm 20$  and recurrence interval is found about  $317 \pm 20$  (Ikeda et al., 1991). The knowledge about the rupture history and the past slips is very limited for this ruptured part of the SAIS.

#### **3.2.4. SEGMENTATION**

More than one seismic segment exist in the east of the Taşkesti (about 31:0:0E) along the SAIS (Fig. 42). To the west of the Taşkesti, a structural segment which is called as Taşburun segment in this study is one of the major faults along the SAIS along which the surface rupture occurred during 1967 Mudurnu earthquake. The SAIS of the NAF zone is using pre-existing fault zones (Section 2.2). In other words, the active faults are following an old (pre-existing) structural boundary between the Almacık block and the Anatolian block. For this reason, the geometry of the strand has lateral irregularity along the NAF zone. Basically the reason of probable seismic segmentation is related to the geometry of the pre-existing fault zones and the strike of the segments of the strand is the same as the elements of the pre-existing fault fabric. The Taşburun segment is constructing a large right releasing bend between the SAIS and Gölcük segment to the west (Figs. 4 and 24). A series of northwest-striking short 1967 fault ruptures are mapped within the young alluvium. This pattern of faulting may represent complexities related to the intersection of the two segments. The rest of it, is relatively continuous and slightly curved and does not have significant left or right steppings along its trace until its eastern end around Taşkesti. The western end is bending to the right that has resulted in releasing around the vicinity of Akyazı in the western extremity

of the Almacık block. Along the releasing bend, it constitutes a wide and intense trans-tensional deformation zone (See also Neugebauer et al., 1997). The 1967 rupture of this structural segment has generally north-facing scarps that indicate extensional component of faulting. Extensional mechanism is consistent with recent geodetic results. The segment has generated significant amounts of space in front of the western part of the Almacık block considering 10 mm/yr slip along the Northern Almacık strand (NAIS) and much larger slip rate (15 mm/yr) along the Taşburun segment (See introductory paragraphs of the section 3). In addition, the extensional component is consistent with focal mechanism solutions of large aftershocks and the small earthquake composite focal mechanism solutions (Jackson and McKenzie, 1984; Neugebauer et al., 1997).

The eastern part of the SAIS is rather complex to the east of the Taşkesti. Along this part, the surface ruptures occurred during 1967 Mudurnu, 1957 Abant and 1944 Bolu earthquakes (Fig. 4 and 5). Surface expressions of the ruptures indicate that there are a couple of faults and segments. This part is forming a large left restraining bend area between Taşburun segment and the NAF to the east. The geometry and the location of the Almacık block are restraining the NAF here and releasing it to the west of the SAIS. In contrast to right-bending nature of Taşburun segment, this part is characterized by slight left bending fault geometry. The 1967 and 1957 ruptures of this part generally have the north-side-down scarps (Öcal, 1959; Ambraseys and Zatopek, 1969) which could indicate compressional component of faulting. As a general rule, reverse dip-slip fault segments are common within left-bending right-lateral strike-slip fault zones. Reverse nature that was interpreted from the systematic down slip behaviour in this vicinity would be compatible with the apparent left-bending geometry along the eastern part of the SAIS. The fault zone along the SAIS may adapt to a south-dipping pre-existing reverse fault (See previous section), but this speculation has not been confirmed. The geometry of this kind of pre-existing fault can be easily used by segments of along east of Taşkesti and this is ordinary. However, use of south-dipping pre-existing reverse fault by a right bended releasing strike-slip fault as Taşburun segment is uncommon in active tectonics frame. The ambiguous composite normal fault plane solution of Neugebauer et al. (1997) which has a problem with conjugate fault plane may be related to this uncommon kinematics in active tectonics frame representing abnormal fault zone of Taşburun segment. The other normal faulting composite solutions of microearthquakes in the study of Neugebauer et al. (1997) and the large aftershock of 1999 Mudurnu earthquake (Jackson and McKenzie, 1984) representing secondary faults are related to the local extensional gap in front of the releasing

bend. In this extensional area, the crust does not react rigidly but fill the gap by these normal faults which result in crustal thinning, basin formation and scattering of seismic waves (Neugebauer et al., 1997). Interseismic high-microearthquake activity that was mentioned by Neugebauer et al. (1997) is probably related to this diffuse and local basin formation procedure. The local extensional area occurred because of the right bending of the SAIS related to a pre-existing fault zone. It is suggested that this kinematic is not characterized stretching effect of the Aegean extensional region but local releasing kinematics that result from optimally-oriented pre-existing fault zone.

To the east, the regional strike of the SAIS turns gently towards the southeastern corner of the Bolu plain. Rest of the NAF zone is located along the southern border of the Bolu plain and parallel to the general strike of the NAF. The fault zone is marked by springs, bedrock scarps, and lineaments. The fault forms a visible gauge zone in the bedrocks along the southeastern border of the Bolu plain.

## **4. PALEOSEISMOLOGICAL INVESTIGATIONS: THE DÜZCE FAULT**

The knowledge of the Holocene earthquake history of the western NAF system is critical for evaluating seismic hazards and has implications for the long-term (late Quaternary) slip budget of various strands of the NAF system in Marmara region. My goal here is to decipher the ages of paleo-earthquakes on the Düzce fault. The contribution in this study is constraining the ages of as much earthquakes as and, as tightly them as possible along the Düzce fault by trenching. It is fact that this is an experimental study and not sufficient to solve the behavior of the Düzce fault at all. A paleoseismic history is hoped to develop in this study. Through the study of sedimentary archives, ages of the paleo-earthquakes have become increasingly apparent in further studies. Such information is invaluable in estimating the earthquake hazard of Düzce and finding the probability range of critical time period of a future large earthquake. Such data can be used for understanding the behavior of the Düzce fault and the NAF system in Marmara area better, and to address questions such as: 1) Does the Düzce fault typically fail in large 1999-type earthquakes (see section 3.1)? or can the structural segments of the Düzce fault fail independently of one another? 2) Does the NAIS typically fail in separate large earthquakes as in 1999 (Figs. 2 and 4) or can the Aksu and Düzce fault seismic segments fail dependently with a single earthquake? 3) Did the surface ruptures of the 967, 1509, 1719 earthquakes that were recorded in historical documents (see section 1.1) occur along the Düzce fault? The great 1509 historical earthquake ruptured the segment/s somewhere and damaged buildings between Marmara and Bolu (Ambraseys and Finkel, 1995). During the 1509 earthquake, Northern Almacık strand (NAIS) including the Düzce fault may have been ruptured. According to historical data that were presented by Ambraseys and Finkel (1995), except 1999 event, the destructive next and the last earthquake after the 1509 event struck Düzce area on 25 May 1719 (Konukçu, 1984; Ambraseys and Finkel, 1995). Using the review studies about historical data, the 1719 rupture is almost the same as the 1999 Kocaeli rupture.

There are no paleoseismic-standardized techniques to recognize unequivocally the evidence for the past earthquakes. Each site and each structure require a different method of study. First step in collecting primary paleoseismic evidence is to identify and map the deformation zone. The 1999 Düzce earthquake allows to locate surface deformation of the Düzce fault. The

benefit of using a recent rupture to compare serial ruptures lies in the fact that the location, magnitude, and slip vector of the most recent event are all well documented (section 3.1). The figure 3 shows the surface break left by the 1999 Düzce earthquake at the trench sites that were excavated across the Düzce fault in this study to establish a paleoseismic record for the fault.

The efforts are focused on the Mengencik and Aydınpinar structural segments (Fig. 27) and several potential sites that have been likely recorded and preserved paleoseismic data that would help me to get preliminary data to understand the behavior of the Düzce fault are found. A paleoseismic investigation has been conducted at four sites in three locations that are shown in figure 3 along ~42-km rupture of the 1999 Düzce earthquake. The paleoseismic data were collected from five trenches at the three sites along two segments (Appendix 2, Section 4.3.1). The trenches contain a variety of seismological fingerprints supporting the ages of six earthquakes, except 1999 event from about B.C. 1731. These fingerprints are stratigraphic and structural evidence representing the events that have been preserved in geological record. Seven <sup>14</sup>C accelerator mass spectrometry (AMS) dates related to the six events are combined with date data of single documented previous study of Hitchcock et al. (2003) on the Düzce fault to determine the recurrence intervals for large earthquakes (Table 2, section 4.4., appendix 3).

#### **4.1. SITE DESCRIPTION AND TRENCH LOCATION**

The search is focused on high potential paleoseismic sites along a portion of the Düzce fault in Beyköy and Kaynaşlı villages, with the objective of finding sites that would yield a record of the past several paleo-earthquakes. At least one site is selected for every possible seismic segments (Efteni, Aydınpinar, Mengencik and Kaynaşlı; see fig. 27) favorable for the paleoseismological trenching along the Düzce fault and two structural segments (Aydınpinar and Mengencik) where the potential results were higher (Fig. 3) (See section 3.1.4. for the identification of possible segments) are excavated. Three trenches are excavated across the Aydınpinar segment at a single site (Kaledibi) that is located near the eastern end of the segment (Fig. 3 and 44). Some radiocarbon age results are got in Kaledibi site which has two exploratory (Kaledibi-2) and one main trench (Kaledibi-1). Eight trenches were excavated along the Mengencik segment in three sites and all of them were located around its centre (Fig. 3 and 45). Three of the trenches are exploratory (Çayır-1, Çayır-2, Bend-2) and five

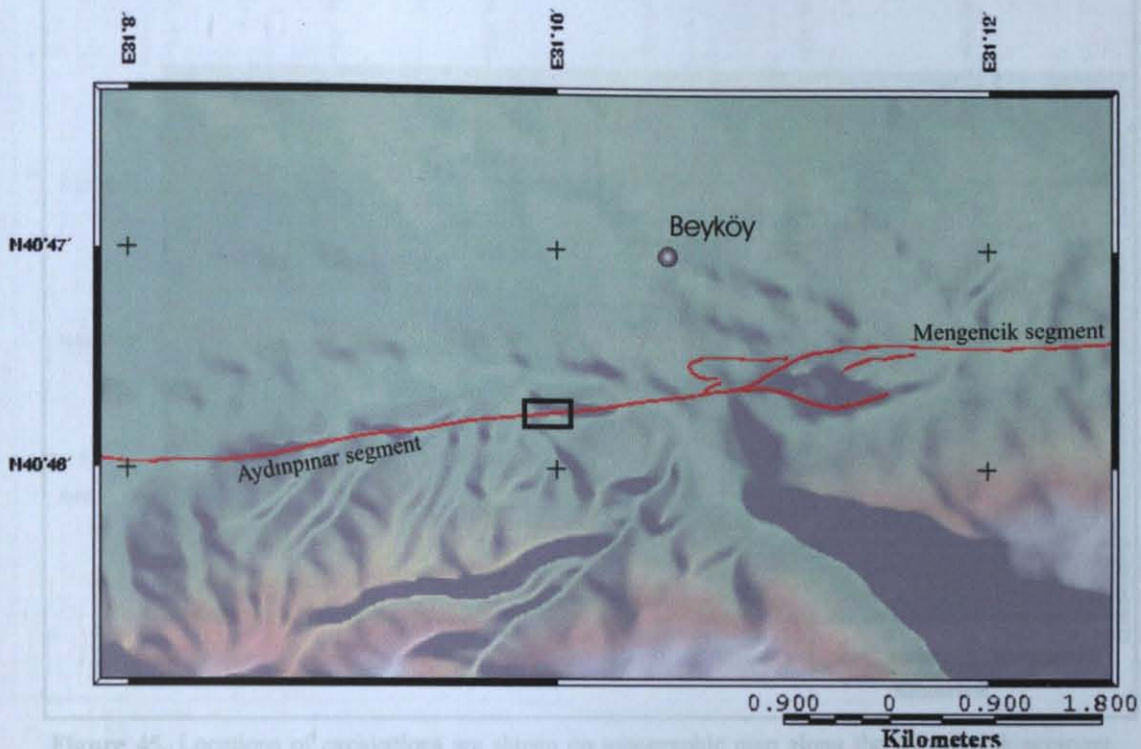


Figure 45. Location of excavations are shown on topographic map along the Mengencik segment and Aydınpınar segment. The rectangles on the left and right show the first and second excavations, respectively. See Figures 46 and 47 for large scale maps of the study area. Tick marks at the top and bottom of the map show the location of right rectangular excavations along the Mengencik segment. Yellow and gray rectangles are excavations and trenches, respectively.

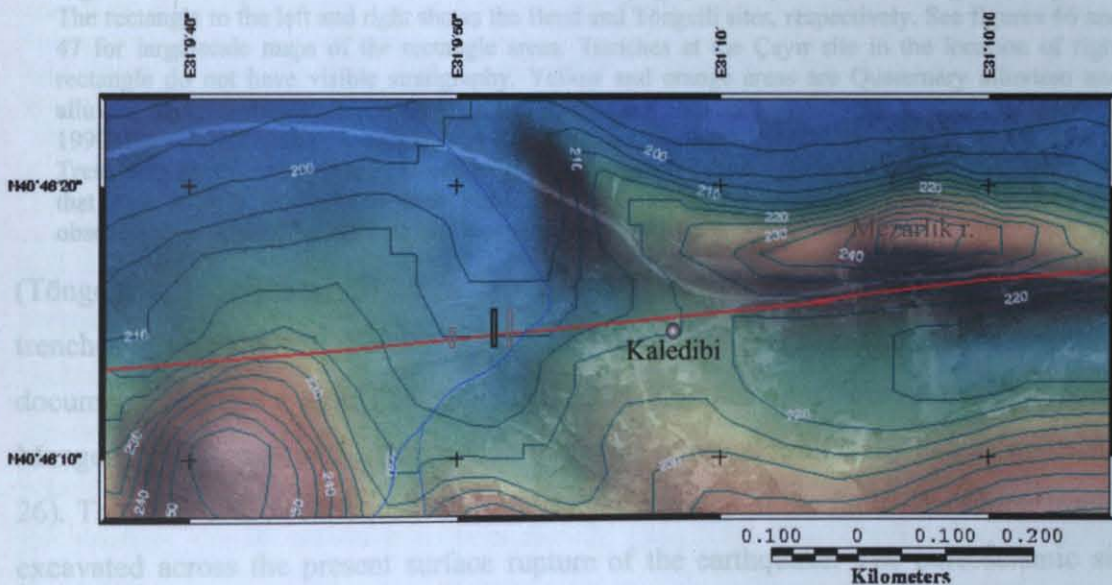
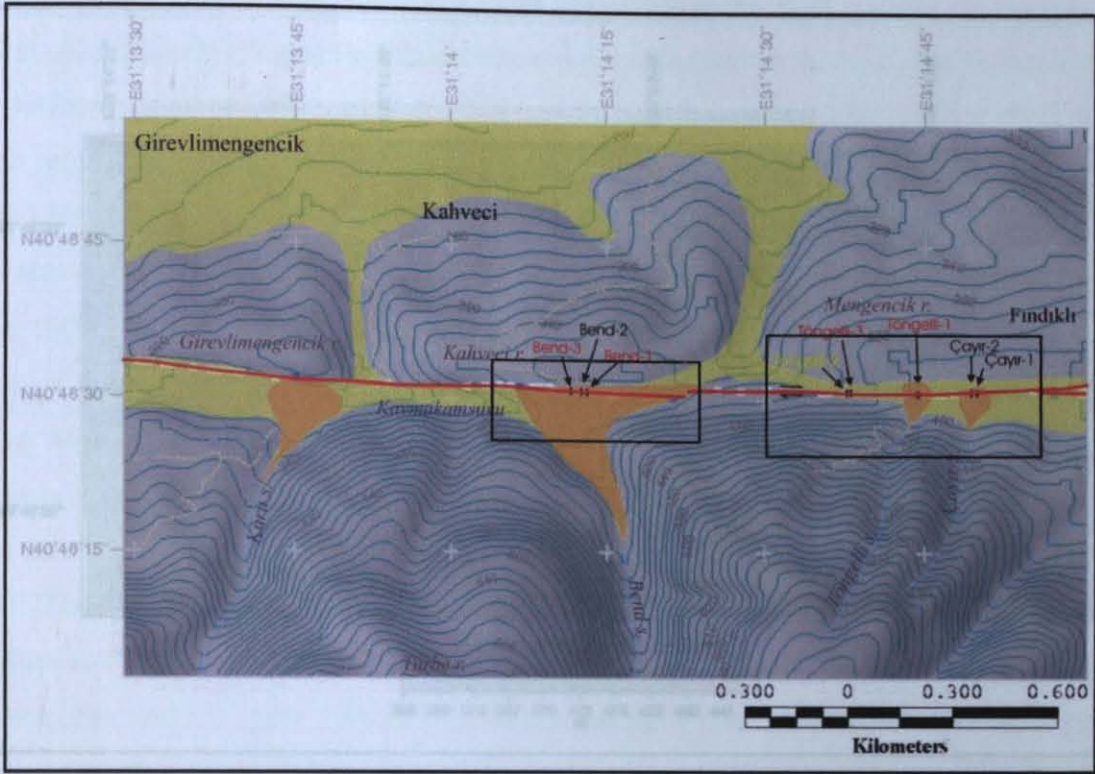


Figure 44. Location of the Kaledibi-1 trench in Kaledibi site. The location of the site map below is shown by a black box in the map above (See fig. 3 for the location of the map above). Black rectangle in the map below represents the trench. The other trenches that are shown with gray rectangles are exploratory. Air is photo draped on colored and contoured relief map shaded from south. Red line represents the 1999 Düzce rupture.

Four of the studied trenches along the Mengencik segment and related sites are close to each other. They are near to the border between Kılıncı and Fındıklı villages (Fig. 45). At the sites, the fault zone is located between similar ridges (Mengencik and Kılıncı) northwards.



**Figure 45.** Locations of excavations are shown on topographic map along the Mengencik segment. The rectangle to the left and right shows the Bend and Töngelli sites, respectively. See figures 46 and 47 for large-scale maps of the rectangle areas. Trenches at the Çayır site in the location of right rectangle do not have visible stratigraphy. Yellow and orange areas are Quaternary alluvium and alluvial cones of streams, respectively. Short black lines: excavations, red line: surface breaks of the 1999 Düzce earthquake. Trenches that their names are collared with red, contain dated events. Trenches that their names are colored with yellow contain events but do not have dating. Trenches that their names are colored with black do not have visible stratigraphy. White squares are observation points of the 1999 surface rupture.

(Töngelli-1, 2, 3; Bend-1, 3) are main trenches. Some radiocarbon age results are got for four trenches (Töngelli-1, 3; Bend-1, 3). In summary, five trenches have been examined and documented at three sites (Töngelli, Bend and Kaledibi sites) across the Aydınınar and Mengencik segments of the Düzce fault where the principal fault is defined as strike-slip (Fig. 26). The 1999 Düzce earthquake constrained the location of the fault. Therefore, trenches are excavated across the present surface rupture of the earthquake. The paleoseismic sites are located in the meadowy places mostly on alluvial fans. The trenches at the Çayır site do not have visible stratigraphy. Samples of events that were found in other trenches would be dated after finding financial support. The Düzce fault transverses many alluvial fans that have been built by the northward-flowing streams.

Four of the studied trenches along the Mengencik segment and related sites are close to each other. They are near to the border between Kahveci and Fındıklı villages (Fig. 45). At the sites, the fault zone is located between shutter ridges (Mengencik and Kahveci) northwards

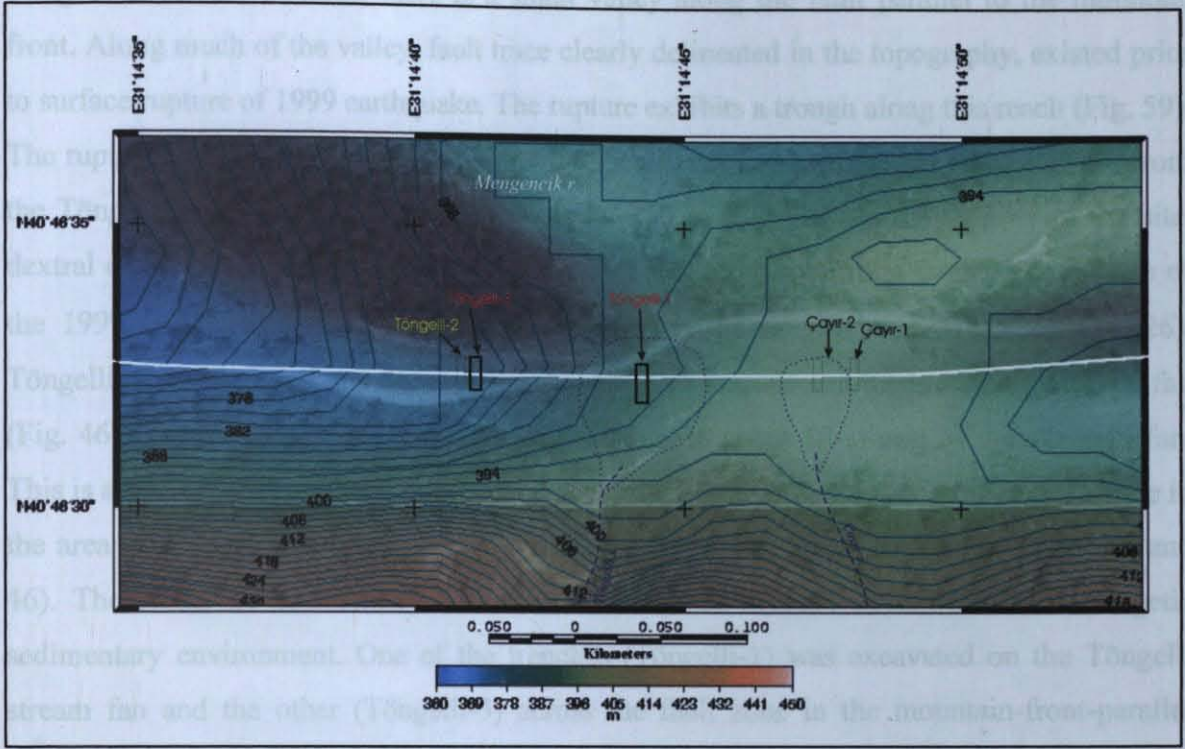


**Figure 46.** Töngelli and Çayır paleoseismological sites. The color scale shows altitude. Topographic data are draped on aerial photo. Relief is shaded from south. Contour interval is one m. Trenches that names are colored with red contain dated events. Trenches that names are colored with yellow contain events but do not have dating. Trenches that their names are colored with black do not have visible stratigraphy. Dotted lines are representing boundaries of the alluvial fans and dashed lines streams. See figure 45 for the location of the map area in small scale.

and a mountain front southwards. The surfacial expression of the Düzce fault here is a prominent set of this linear hills aligned up along the mountain front. The lithology of the shutter ridges are formed by terrestrial rocks that probably belong to the western hill slopes of the northern flank of Almacık Mountain (Section 3.1.3). The main fault along Mengencik segment usually bounds the southern site of the hills. Çayır, Töngelli and Bend streams are the primary young sediment sources for the sites (Fig. 45). The names of trenches are depending on names of streams (or sites) which their sediment was excavated. South of the hills, the previous fault ruptures are buried by late Holocene deposits of the streams. The Düzce fault transverses the alluvial fans built by these northward-flowing streams. Unstratified gravel deposits have been derived directly from the mountain front in flooding periods and massive clays interfingering with poorly sorted colluviums. Local mountain front in this site is composed of mainly sandstones. Therefore, the grains are sandstone in the site. Quaternary fans of the drainages are composed mostly of alluvium derived from the sandstone rocks of the mountain range that bounds the Düzce basin on the south. Between the fans of

Töngelli and Bend streams, there is a small valley along the fault parallel to the mountain front. Along much of the valley, fault trace clearly delineated in the topography, existed prior to surface rupture of 1999 earthquake. The rupture exhibits a trough along this reach (Fig. 59). The rupture has produced uphill-facing (south) scarp, with an average height of ~20 cm from the Töngelli-1 trench location to the east about 250 m (Fig. 57). In the vicinity of the site, dextral displacements ranging between about 300 and 400 cm forming the surface rupture of the 1999 Düzce earthquake were measured (around the longitude of 31°15' in Fig. 26). Töngelli stream is small and dry especially in summer seasons and feeds a small, alluvial fan (Fig. 46). There is a smaller valley that is extending to about 10-m-east of the Töngelli fan. This is a smaller stream (Çayır stream) and accordingly minor fan crossing the rupture zone in the area. Two exploratory trenches (Çayır-1 and -2) are excavated across here (Fig. 45 and 46). There was no sedimentary record in the trenches because of uniform low energetic sedimentary environment. One of the trenches (Töngelli-1) was excavated on the Töngelli stream fan and the other (Töngelli-3) across the fault zone in the mountain-front-parallel valley, which is the boundary between the Mengencik shutter ridge and mountain front, west of the Töngelli-1 trench (Fig. 46). Juxtaposition of locally higher topography (Kahveci shutter ridge) on the north side of the fault against Bend stream channel results in the blockage of the relatively large drainage (Bend stream) west of the Töngelli-3 trench site and trapped late Holocene alluvium within the lower topography along the fault zone (Fig. 45). The Bend stream is a blocked drainage within the fault zone. The stream is not dry in summer seasons. It is a deflected stream caused by slip along the Düzce fault. Late Holocene alluvium originating from the blocked drainage appears to form a westward-propagating alluvial fan. At the same time, the fan appears to be propagating back in to the valley filling it towards uphill direction (Fig. 45 and 47). Convex fan geometry on the topography does not exist here. This rather abnormal 3-D geometry is probably related to the erosion and faulting. Two trenches (Bend 1 and 3) were excavated on trapped alluvial fan of this stream and about 100 m away from the stream. Massive clay and flood deposits dominate in the exposures in this site.

At the trench site on Aydınpinar segment, there is a small stream near the west of Kaledibi village (Fig. 44). Along the fault, a scarp is clearly delineated in the topography, existed prior to 1999. The current height of the scarp varies from about 60 to 90 cm along its strike. Since this is up to 4 times higher than the scarp that was formed in 1999, it is reasonable to suspect that older scarp was formed because of several prior ruptures.

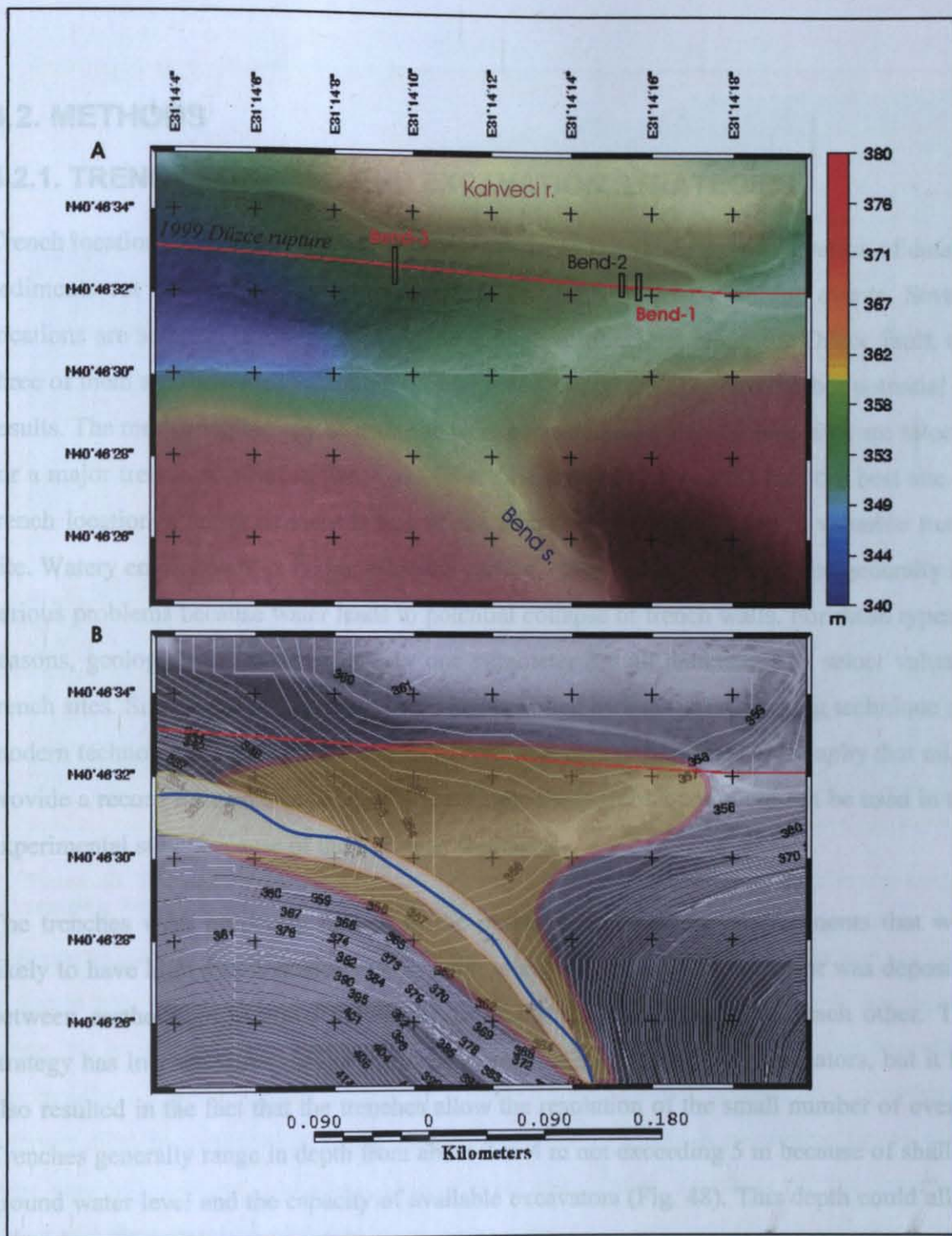


**Figure 47.** Locations of Bend 1, 2, 3 trenches in the alluvial cone of Bend stream. A: topographic relief map of the Bend site. Altitude is represented by color scale and relief is shaded from southwest. Rectangles are trench locations. No event was recognised in a trench that has black font trench name. Events were recognised and dated in the trenches that have red label. B is showing Quaternary development of Bend stream fan in the same area on contoured (1 m interval) topographic map. Both A and B have identical scale. Trapped alluvial cone of the Bend stream is shaded by dark yellow color drape on aerial photo. Light yellow is showing current bed of the stream. The fan had been propagated back in to the valley filling it towards uphill direction because it has been blocked from north by the Kahveci shutter ridge. See figure 45 for smaller scale topographic map of the area. Convex fan geometry on the topography does not exist here. This rather abnormal 3-D geometry is probably related to the erosion and faulting.

## **4.2. METHODS**

### **4.2.1. TRENCH LOCATING AND EXCAVATION STRATEGIES**

Trench locations should be carefully selected in order to maximize the preservation of datable sediments cut by the fault and the recognition of the past surface faulting events. Several locations are selected favorable for paleoseismological trenching along the Düzce fault, and three of them are excavated where permission was obtained and that have higher potential for results. The merit and potential of each site were evaluated, and then the best sites are selected for a major trenching effort in this study. There are many parameters to find the best site for trench location. Carbon richness is one of the important parameters to find valuable trench site. Watery environment provides sufficient carbon. However, this environment generally has serious problems because water leads to potential collapse of trench walls. For these types of reasons, geologists try to care not only one parameter but all parameters to select valuable trench sites. Site selection procedure could be supported by subsurface probing technique and modern technological devices that collect geophysical data to find fine stratigraphy that might provide a record for near-surface layers. Such supporting techniques could not be used in this experimental study because of the logistical shortages.

The trenches were purposely located in the places of sedimentary environments that were likely to have high sedimentation rate in order to ensure that enough sediment was deposited between earthquakes to allow individual earthquakes to be distinguished each other. This strategy has increased the visibility of stratigraphy for the paleoseismic indicators, but it has also resulted in the fact that the trenches allow the resolution of the small number of events. Trenches generally range in depth from about 2 to 4 m not exceeding 5 m because of shallow ground water level and the capacity of available excavators (Fig. 48). This depth could allow resolution of the limited number of events. Common strong erosional and flooding phases make it impossible to find more than about one or two events in 4-m-deep trenches. Thus, the sedimentation rate is not constant and the strong erosional and flooding phases make it impossible to distinguish different earthquake horizons in one specific trench. For this reason, abundant trench number can allow to expose complete paleoseismic history. In general, the fault area has very shallow ground water, near surface. Therefore, slow energy and continuous sedimentation environments that serve good stratigraphic resolution like a sag-pond couldn't be selected. Continuous stratigraphy but absence of visibility is highly possible at low energy



**Figure 48.** The picture of the Çayır trench site looking from north and the excavator that was used for trenching. See figure 46 for the location of the site.

domains as mentioned above (E.g., Çayır-1, see figs. 46 and 48). Thus, the trenches is chosen to locate near the mouths of small to medium size drainages (E.g., Töngelli-1, see fig. 45) where the grain size is predominantly sand and pebbles as opposed to the boulder deposits at the mouths of the drainages despite the fact that they are not optimal for paleoseismic interpretation. In particular, uncertainties are related to difficulty in correlating layers which were generally massive, containing large pebbles and cobbles, with lack of thin continuous layers and the possibility of depositional hiatus, strong erosional and flooding phases should be considered. Although the stratigraphy in the trenches is not as continuous as or as thinly bedded as at some other paleoseismic sites, sharp contrast that allows faulted and unfaulted units to be distinguished each other are present within most of the deposits. In many cases, fissure fills in massive clay provide upper and lower bounds on stratigraphic position of the earthquake horizon. That would appear to indicate poor stratigraphic resolution of position of earthquake horizons. However, because of high sedimentation rate, this uncertainty in the stratigraphic position of an earthquake horizon translates into an age uncertainty that is

smaller than the uncertainty due to the laboratory and calibration errors in the radiocarbon dates.

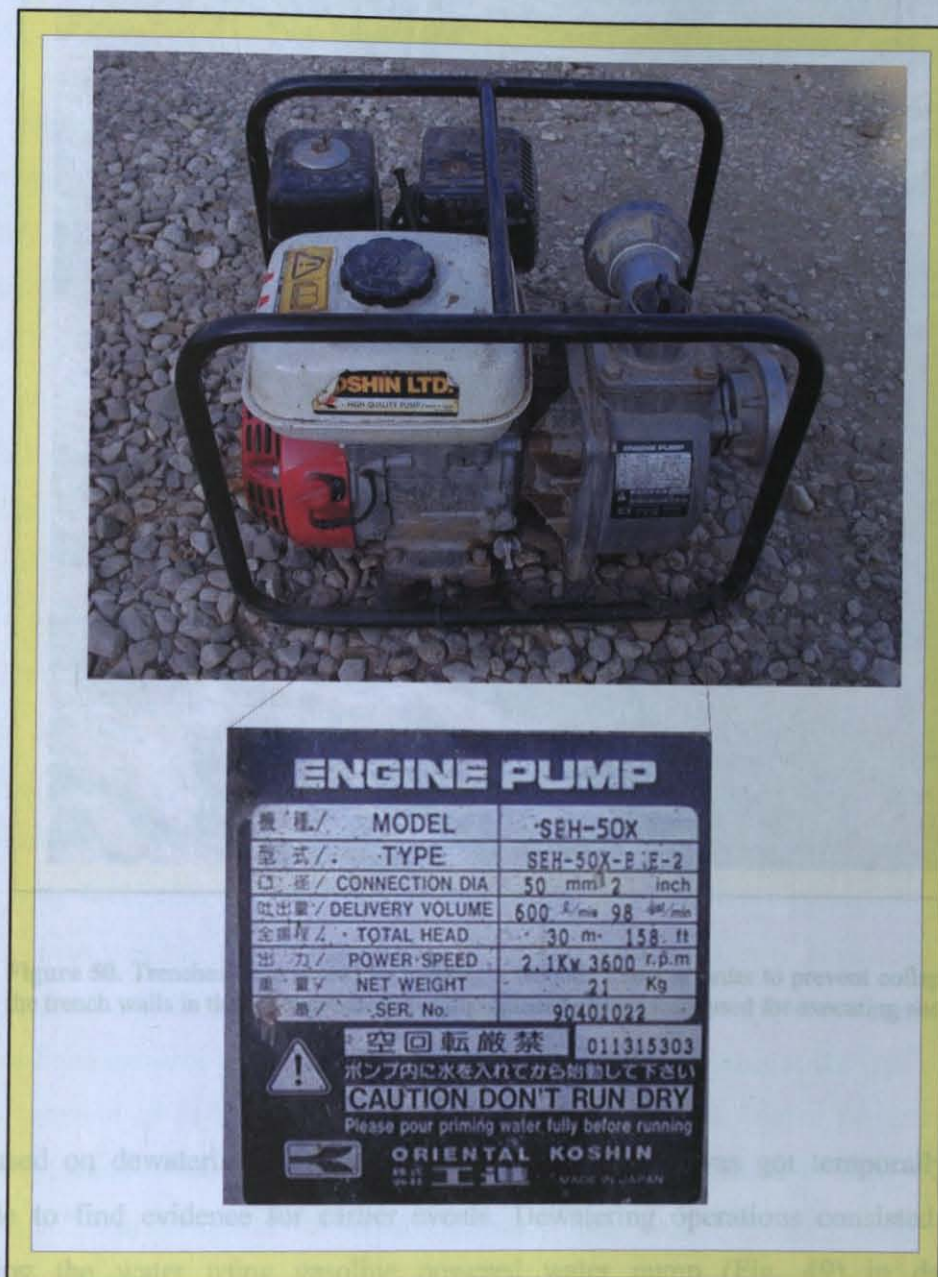
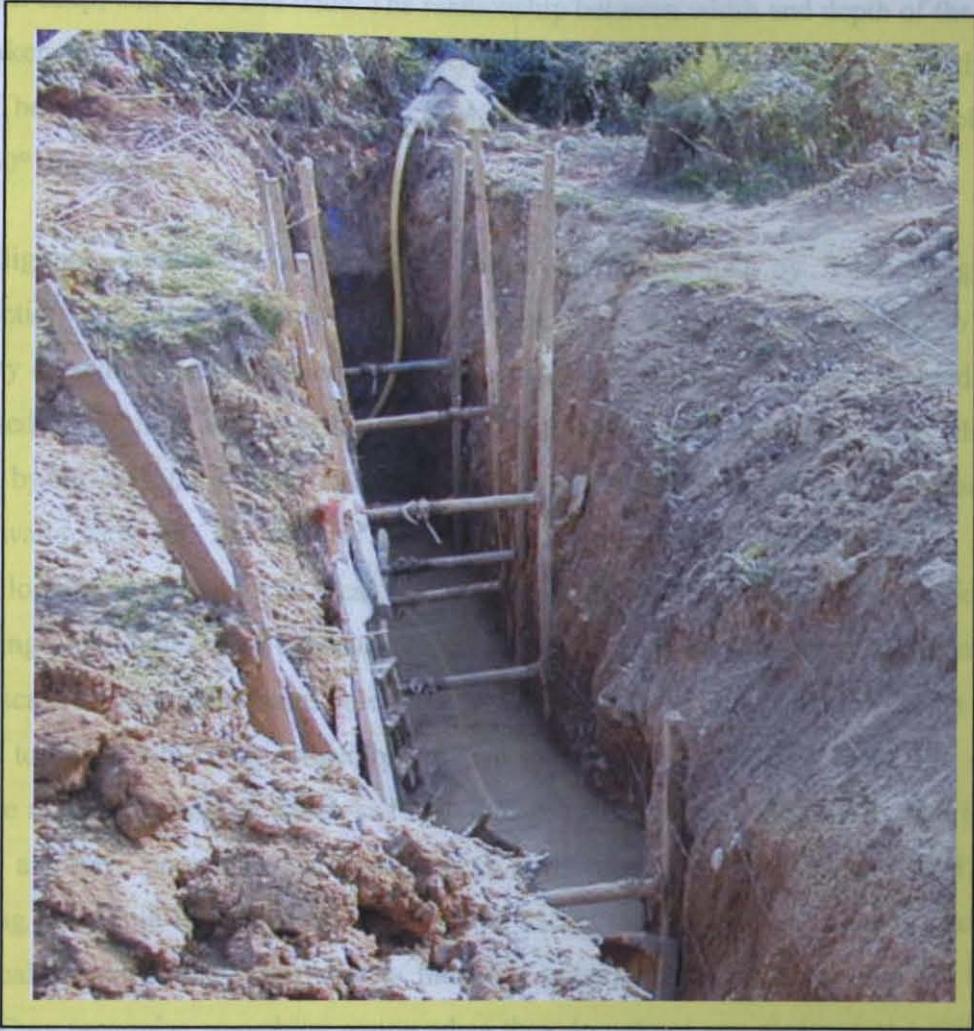


Figure 49. Gasoline powered water pump engine was used for dewatering operations.

Groundwater condition is an important parameter for locating trenches. It always leads to a technical problem because discharging is mostly very difficult. Dry seasons (fall) are chosen for excavating trenches to avoid shallow water table. However, for most of the field season it excavated to avoid trench collapse during the excavation. In general, trenches are 10-m long,



**Figure 50.** Trenches were shored by building a wooden frame in order to prevent collapse of the trench walls in the unconsolidated sediments. Screw jacks were used for executing shoring.

is focused on dewatering. In many cases, the water table was got temporarily as low as possible to find evidence for earlier events. Dewatering operations consisted of actively removing the water using gasoline powered water pump (Fig. 49) in daytime. The groundwater was successfully discharged out of the trench in daytime however, trench walls commonly collapsed at night because of the rewatering. Trenches were shored by building a wooden frame in order to prevent collapse of the trench walls in the unconsolidated sediments at the sites (Fig. 50). Screw jacks were used to execute shoring. After the first horizontal tire was excavated with a backhoe as possible as fast vertical wooden beams were located, then the first tire was widened and the second tire beneath the exposure of the first tier was excavated to avoid trench collapse during the excavation. In general, trenches are 10-m long,

3- to 4-m deep, and 1- to 2-m wide. The relationship between width and depth of the trenches were taken into account for trench stability and safety of the people examining the trench walls. The width is increased from deep to shallow to make trench walls more stable having about 60° dip angle.

After digging, smoothing of the trench walls was performed by hand using garden, construction and sculpture tools. The walls were made as planar as possible to increase visibility of sedimentary features and tectonic structures. Little color flags, pierced by nails were used to highlight important features. After that, horizontal and vertical grids which were formed by mostly 50-cm-wide squares by strings to serve as a reference frame for logging trench walls were set. The most of the expositions were documented by detailed drawings (trench logs) at a scale of 1:10. Scales are ranging 1:10 to 1:20. Log scale and grid size are depending on complexity of exposure. It sometimes depends on stability of the trench walls. Larger scale logging needs more time. Thus, small scales were used when the trench walls are seemed to be unstable (E.g., Kaledibi-1 trench in section 4.3.1.5). Just schematic drawings could be made for trenches which had high collapse risks (E.g., Töngelli-3 trench in section 4.3.1.2) and have poor logistical conditions (E.g., Bend-1 trench in section 4.3.1.3). All the trenching procedure was executed alone by me, except the first opening step by excavations. Periodical messages had been sent to the local governmental office during the trenching study. They recognize something wrong when they do not get any message at a critical time period. There was not any fatality during the study. All sedimentary structures and deposits exposed from trench walls were reported. The possible geological records of individual paleoearthquakes were highlighted, and at the same time the geometry, the type of movement, and the amount of deformation for each event were evaluated. Digital camera was used to take the pictures of the exposures. Pictures were rectified by applying “scale,” “screw,” and perspective” transformation in Adobe Photoshop until nails (control points) and grid net shown in the token overlapping picture sets matched their surveyed locations on detailed drawings to produce a realistic picture-mosaic. For some trenches, overlapping pictures of the exposures were rectified and merged using ER Mapper 6.1 software too. This software is more quantitative and automated however; it does not allow freehand transformations. Sometimes freehand transformations are essential. Especially pictures do not have enough quantitative control points to make valuable rectifications.

## 4.2.2. IDENTIFICATION OF EARTHQUAKE HORIZONS

The surface breaks are one of the hallmarks of large earthquakes. Buried surface breaks and their deformational features hold clues to the time of paleoearthquakes. The stratigraphic level that represents what the ground surface at the time of a paleoearthquake was is generally referred to an event horizon. Following the permanent coseismic surface deformation of actual or depositional layers or strata, local deformational or post-depositional processes take place trying to restore equilibrium in the existing sedimentation system. The critical issue is to make successful differentiation between the pre-paleoearthquake and post-paleoearthquake local sedimentary processes. The erosional features and sediments that are derived from post-paleoearthquake processes become the geologic records (seismit) of past surface faulting earthquakes. There are stratigraphic and structural (tectonic) evidence. (1) The most common features that indicate the formation of a fault scarp are colluvial wedges (debris slope, wash slope). Colluvial wedges are scarp-derived deposits that partially bury the scarp and they have been used to define event horizons as stratigraphic evidence. (2) Upper terminations of faults are tectonic evidence for individual events of displacement (E.g., event B in section 4.3.2.2 and event A in section 4.3.2.1). Upward termination of fault strands does not always provide us a reliable information on the stratigraphic position of the ground surface at the time of faulting event because for faults with historic ruptures, fault strands are not commonly visible all the way up to the ground surface (Bonilla and Lienkaemper, 1990). (3) Existence of fissure fills proves that at the time of the faulting event, the event horizon was deformed and a fissure was formed for a specific event as stratigraphic evidence (E.g., event D in section 4.3.2.4, event C in section 4.3.2.3 and event E in section 4.3.2.5). The evidence for paleoearthquake horizons consists of bracketing the upward termination of fissure fills between the fault strands. (4) Sometimes, the coseismic deformation is accompanied by a tilt of the sedimentary beds not only because of near-fault complexity but also because the fault scarp is accompanied by a flexure of the ground and sediments, rather than a sharp rupture. Related unconformity is a structural evidence and represents an event horizon (E.g., event F in section 4.3.2.6). (5) Faults continue to increase the amount of the deformation with increase in the age of sediments. This structural evidence can be particularly clear when there is a vertical component of slip. Note that no single feature taken alone can be used as an unequivocal evidence for an earthquake. In the following Analysis of Exposures section, seismit are described for each trench and event.

The final but critical step in a study of a trench is to date the event horizons in order to constrain the ages of the paleoearthquakes on the fault. In general, an age range for each event is constrained by the age of the sediments above and below the horizon of each particular event. Collecting correct samples in correct locations that is constraining the age of an event is depending on the accuracy of the interpretation of the event. As a general rule, collection of large amount of samples all over the trench could be valuable because the interpretations of exposures are made after closing the trenches in many times. However, in general, samples are not enough and sample allocation is not uniform at every trench sites. At this kind of trench sites, instant interpretations should be made carefully during the trenching operations to focus on event horizons for age sample collection. Shells, tufa, soil carbonate are generally unreliable for dating, because they do not form a closed system. In this study, age control for all events is based on the radiocarbon accelerator mass spectrometry (AMS) ages of peat samples. Several issues are applicable to all paleoseismic sites that rely on peat for age control. The depositional date of any sedimentary layer is likely to be younger than the dates of peat samples from that layer. This is because a lag time exists between the time that the interior of a branch on a bush stops exchanging carbon with the atmosphere and the time that the branch falls to the ground, and is transported and deposited (and perhaps re-transported and deposited again) in a sedimentary layer. Thus, all of the sample ages represent maximum estimates for the depositional ages of the layers. The magnitude of this discrepancy varies from a sample to another. It is also possible for peat samples to be younger than the sedimentary layers in which they were collected if the samples were emplaced into the layer through bioturbation. Peat samples were not collected from the obvious animal burrows; however, some samples were collected from massive, crudely bedded or thickly bedded deposits, in which burrows might be difficult to recognize. However, thinly bedded deposition parts of the trenches in which inexistence of the organic disruption would have been obvious. For each layer from samples which were dated, those that were least likely to be from bioturbated sediment for dating were selected.

In the text and figures, the event horizons are indicated by an alphanumerical code. Events are descending-sorted according to the alphanumerical order taking the youngest ruptured 1999 Düzce event as event G (E.g., event A0 indicates the oldest event). Ascending sorted numerical order is used for assigning events in the sequential rupture timing models (Section 4.4). Event G (1999 rupture) is constantly assigned to the 10<sup>th</sup> rupture in the models (e.g., 9<sup>th</sup> rupture is the penultimate and 8<sup>th</sup> is the pre-penultimate events).

### 4.2.3. RADIOCARBON DATING ISSUES

By far the most common and powerful method for dating in paleoseismology up to 52,000 years in age is the radiocarbon dating ( $^{14}\text{C}$  dating). Libby and co-workers at the University of Chicago first pursued the measurements of  $^{14}\text{C}$  in nature during the late 1940's (Arnold and Libby, 1949). They demonstrated the feasibility of using radiocarbon as a dating tool for ancient samples of known age: old tree wood dated by counting annual growth rings (dendrochronology) and artifacts dated by experts in ancient architecture and craftsmanship. Over the past forty years, radiocarbon has become the most commonly used dating tool for seismology. It is an isotopic method based on the radioactive decay of  $^{14}\text{C}$  (half-life 5,730 years) to  $^{14}\text{N}$ .

Carbon has three naturally occurring isotopes. The two most abundant isotopes are the stable isotopes,  $^{12}\text{C}$  (98.89 percent) and  $^{13}\text{C}$  (1.11 percent). On the other hand, the third isotope  $^{14}\text{C}$  ( $10^{-10}$  percent) is unstable and undergoes  $\beta$ -decay to  $^{14}\text{N}$ . This isotope is present on the atmosphere and troposphere. It is constantly produced by the interaction of cosmic rays with nitrogen, oxygen atoms in the atmosphere (Kamen, 1963). The carbon atom is oxidized within hours to  $^{14}\text{CO}$  which has an atmospheric lifetime of several months before it is in turn oxidized to  $^{14}\text{CO}_2$  to become well mixed throughout the troposphere.

The steady state  $^{14}\text{C}$  content of the atmosphere is determined by the exchange of carbon in  $^{14}\text{CO}_2$  with that in ocean and biosphere reservoirs by photosynthesis and hence throughout the food chain. Interaction and exchange with the atmosphere and oceans lead to all living tissue maintaining a fixed proportion of  $^{14}\text{C}$ . Thus, isotopic ratio of  $^{14}\text{C}$  to stable isotope  $^{12}\text{C}$  is kept constant during the lifetime of an organism as in atmosphere (in short period) by living system of that organism. Calculation of a radiocarbon age requires the assumption that the  $^{14}\text{C}$  of the carbon originally fixed in plant or animal tissues equated that of the atmospheric  $\text{CO}_2$  during pre-industrial times. After the death of an organism, the amount of  $^{14}\text{C}$  in the organic matter decreases with time due to its death  $^{14}\text{C}$  isotope of carbon in its tissues undergoes radioactive decay back to  $^{14}\text{N}$  (Fig. 51) because the exchange of carbon from atmosphere stops.  $^{14}\text{C}$  decay curve is prepared considering half-life of  $\beta$ -decaying of  $^{14}\text{C}$  to  $^{14}\text{N}$  is 5,730 years. If the tissue remains intact and isolated from exchange, the decrease in its  $^{14}\text{C}$  content form may be used to indicate the time since the death of the organism. This is the basis for radiocarbon dating.

The product of the radioactive decay,  $^{14}\text{N}$ , is not retained because it is gas and escapes as it forms. On the other hand, remaining amount of  $^{14}\text{C}$  is expressed as the ratio  $^{14}\text{C}$  to  $^{12}\text{C}$  (one of the stable isotopes of carbon) and gives the death date of tissue. To determine how much  $^{14}\text{C}$  is in a sample, radiation detectors count the number of  $\beta$  particles released by radioactivity of remaining  $^{14}\text{C}$ . The result is called as the ‘activity’ (disintegrations per minute per gram of carbon dpm/g). A sensitive detector can measure at most, nine half-lives (HL) from the emitted beta particles of  $^{14}\text{C}$  decay. For this reason, approximate maximum age in years that can be determined is about 52,000 years (Fig. 51). The radiocarbon age that is obtained from

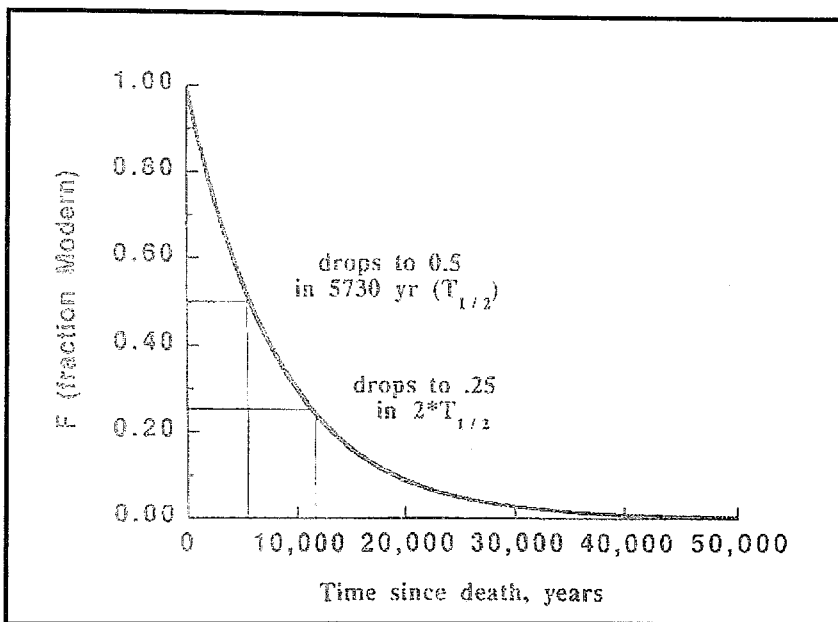


**Figure 51.**  $^{14}\text{C}$  decay curve. Decrease in radiocarbon with time according to radioactive decay (From Trumbore, 2000). Carbon content was expressed as the ratio of  $^{14}\text{C}$  to  $^{12}\text{C}$ . Half-life of  $\beta$ -decaying of  $^{14}\text{C}$  to  $^{14}\text{N}$  is 5730 years.

a radiocarbon measurement is a measure of how much radiocarbon is in the material. It is often referred to as the Conventional Radiocarbon Age (CRA) to distinguish it from the calendar, age. Dates are expressed as AD (CAL years or calendar years or absolute years), BC (also called BCE), BCE (before Common Era), and BP (before present). The accepted way to represent  $^{14}\text{C}$  ages is in terms of years BP. The BP is expressed as years before present where ‘‘present’’ means 1950, by convention. The year 1950 is the date that the calibration curves were established. It also predates the atmospheric testing of the atom bomb (thermonuclear weapons) which significantly upsets  $^{12}\text{C}/^{14}\text{C}$  ratios in the following years. This is a global isotopic spike for the carbon system. Atmospheric burden of  $^{14}\text{C}$  was approximately doubled

in few years preceding the implementation of the Nuclear Test Ban Treaty in 1967 (NNSA, 2003).

The production of  $^{14}\text{C}$  in atmosphere is not perfectly constant. This was recognized by Hans Suess and Walter Libby in the 1960's. The  $^{14}\text{C}$  content of the atmosphere has varied with time (from year to year), both because of the changes in the production rate of  $^{14}\text{C}$  (variations in incoming cosmic radiation and magnetic field variations) and because of the changes in the distribution of carbon among ocean, biosphere and atmospheric reservoirs. In recent years, the modern-day burning of fossil fuels (coal, oil and natural gas) has been diluting the relative amount of  $^{14}\text{C}$  in the atmosphere by releasing large amounts of  $^{12}\text{C}$  (Fig. 52). The variations,

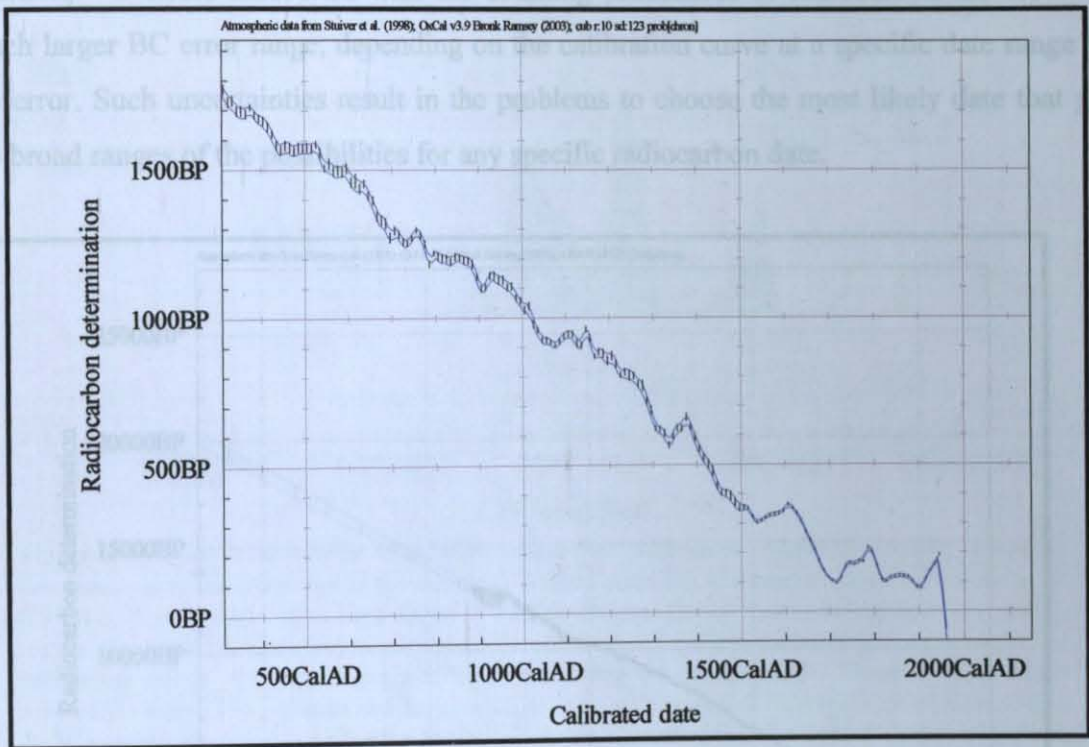


**Figure 52.** Radiocarbon calibration curve for recent years (Stuiver et al., 1998). Dilution of amount of  $^{14}\text{C}$  in the atmosphere by releasing large amounts of  $^{12}\text{C}$  after about 1950. Over 400 years correspond to a plateau in time range 1650-1950 A.D.

deduced from the  $^{14}\text{C}$  content of cellulose of known age taken from the annual growth rings of trees, are generally less than 10 percent over past 7000 years. Calibration curves that account for the fluctuation of  $^{14}\text{C}$  production in the atmosphere are widely used to correct ages to approximate calendar years (Stuiver et al., 1998). By using the findings of tree-ring research,

it is possible to "adjust" radiocarbon-determined dates to correct for variations in atmospheric  $^{14}\text{C}$  over time. To compensate for variations in  $^{14}\text{C}$ , scientists have developed calibration curves from the studies of tree-rings of the ancient trees (Fig. 53). Unless a correction curve is established, future age determinations for artifacts of our time will appear to be older than they should be because of the modern-day burning of fossil fuels. Through these studies (dendrochronology), calibration data that go back nearly 11,000 years have been developed. The tree-ring calibration curve is a non-monotonic. Sometimes a single radiocarbon date corresponds more than one corrected date (Fig. 54). In this case, a researcher should seek other information to verify the most likely date. On the other hand, researcher can use the distribution for each probability method that was described in this study (Section 4.4.1.4.1) if he/she has reasonable amount of data and a reasonable serial model (See section 4.4.1). In addition,  $^{14}\text{C}$  errors associated with the counting procedures of radiocarbon lab result in a much larger BC error range, depending on the calibration curve at a specific date range with lab error. Such uncertainties result in the problems to choose the most likely date that gives the broad ranges of the possibilities for any specific radiocarbon date.

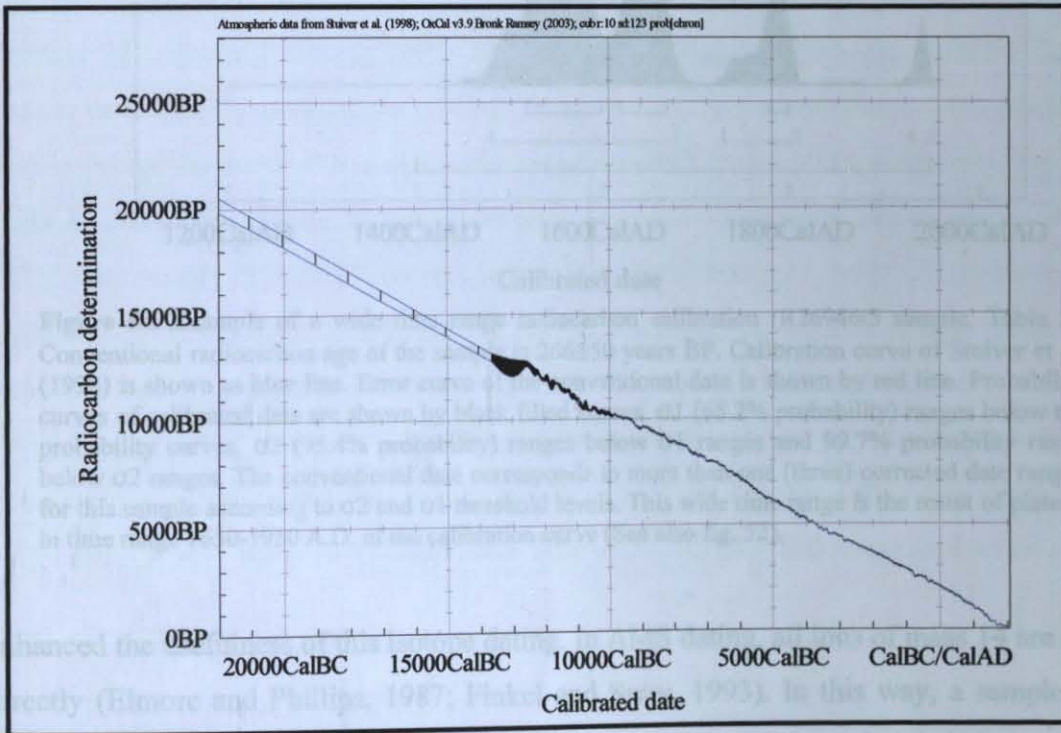


**Figure 53.** Radiocarbon calibration curve from studies of tree-rings of the ancient trees (Stuiver et al., 1998). It goes back nearly 11,000 years.

In conventional  $^{14}\text{C}$  dating, the sample size required for this method depends on the type of material, but is generally in the tens to hundreds of grams range. It may take several days to record enough radiation to provide a precision of  $\pm 80$  years. In the last two decades, improvements in the sensitivity of the radiocarbon measurement that have been achieved through the development of accelerator mass spectrometry (AMS) have considerably

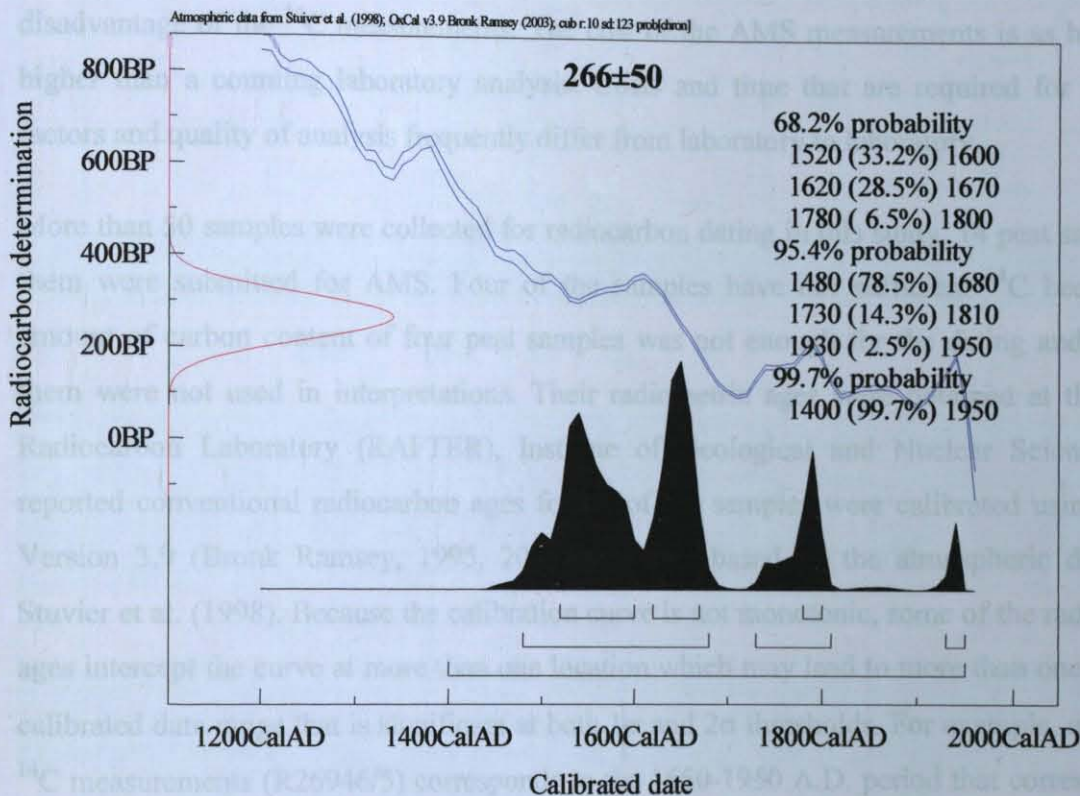


**Figure 54.** Example of a wide time range radiocarbon calibration (R26946/5 sample, Table 2). Conventional radiocarbon age of the sample is  $266\pm 50$  years BP. Calibration curve of Stuiver et al. (1998) is shown as blue line. Error curve of the conventional date is shown by red line. Probability curves of calibrated data are shown by black filled curves.  $\sigma_1$  (68.2% probability) ranges below the probability curves,  $\sigma_2$  (95.4% probability) ranges below  $\sigma_1$  ranges and 99.7% probability range below  $\sigma_2$  ranges. The conventional date corresponds to more than one (three) corrected date ranges for this sample according to  $\sigma_2$  and  $\sigma_1$  threshold levels. This wide time range is the result of plateau in time range 1650-1950 A.D. of the calibration curve (See also fig. 52).

enhanced the usefulness of this isotope dating. In AMS dating, all ions of mass 14 are counted directly (Elmore and Phillips, 1987; Finkel and Suter, 1993). In this way, a sample can be dated with a mass 1/1000-1/10000 that is necessary for the conventional dating, as low as 0.01 mg carbon. AMS measurement of  $^{14}\text{C}$  has greatly increased the potential use of  $^{14}\text{C}$  in this regard. By making it easier to find datable material, the use of AMS has greatly increased the application of carbon dating to paleoseismic studies. Thus, it has started a revolution in

the use of  $^{14}\text{C}$ . There are some disadvantages and limitations of radiocarbon measurements; 1) the limitation of radiocarbon to timescales of  $< 55,000$  years is an unavoidable feature of the half-life of radiocarbon. 2) It is nearly impossible to use  $^{14}\text{C}$  in time range 1650-1950 A.D. According to radiocarbon age vs. calendar age obtained from tree ring,  $^{14}\text{C}$  measurements over the past 400 years correspond to a plateau (Fig. 52). 3) High cost has always been a disadvantage of the  $^{14}\text{C}$  measurements. The cost of the AMS measurements is as high as or higher than a counting laboratory analysis. Costs and time that are required for analysis-factors and quality of analysis frequently differ from laboratory to laboratory.

More than 50 samples were collected for radiocarbon dating in this study. 14 peat samples of them were submitted for AMS. Four of the samples have not sufficient  $^{14}\text{C}$  because the amount of carbon content of four peat samples was not enough for the dating and three of them were not used in interpretations. Their radiometric ages were obtained at the Rafter Radiocarbon Laboratory (RAFTER), Institute of Geological and Nuclear Sciences. The reported conventional radiocarbon ages for all of the samples were calibrated using OxCal Version 3.9 (Bronk Ramsey, 1995, 2001 and web) based on the atmospheric data from Stuvier et al. (1998). Because the calibration curve is not monotonic, some of the radiocarbon ages intercept the curve at more than one location which may lead to more than one possible calibrated date range that is significant at both  $1\sigma$  and  $2\sigma$  thresholds. For example, one of the  $^{14}\text{C}$  measurements (R26946/5) corresponds to the 1650-1950 A.D. period that corresponds to a plateau in calibration curve (Fig. 54). For this reason, the calibrated age range for this sample is rather wide and it is nearly useless. The sample information and corresponding events are given in Table 2 (See also appendix 3). Three samples are from units above (maximum constraint) and four within and below (minimum constraint) the event horizon, with calendar ages between 1750 BC and 1950 AD ( $2\sigma$ ) (See following section or appendix 3).

### 4.3. ANALYSIS OF THE EXPOSURES

| Event | Reference | Laboratory Sample Number | <sup>14</sup> C age (Conventional, B.P.) | Calibrated Date in Terms of Confidence Intervals |      |           |                                      |      |                 | Constraints for Event | Sample Description |
|-------|-----------|--------------------------|--|--|------|-----------|--------------------------------------|------|-----------------|-----------------------|--------------------|
|       |           |                          |  | 2 Sigma Interval (%95.4 probability)             |      |           | 1 Sigma Interval (%68.2 probability) |      |                 |                       |                    |
|       |           |                          |  | min.   | max. | % of area | min.                                 | max. | % of area       |                       |                    |
| G     | •         |                          |  |  |      |           |                                      |      |                 |                       |                    |
| F     | •         | R26946/5                 | 266±50                                   | 1480   | 1680 | 78.5      | 1520                                 | 1600 | 33.2            | max. constraint       | Peat               |
|       |           |                          |  | 1730   | 1810 | 14.3      | 1620                                 | 1670 | 28.5            |                       |                    |
|       | 1930      | 1950                     | 2.5                                      | 1780   | 1800 | 6.5       |                                      |      |                 |                       |                    |
| •     | R26946/4  | 488±50                   | 1310                                     | 1360   | 9.8  | 1400      | 1460                                 | 68.2 | min. constraint | Peat                  |                    |
|       |           |                          | 1380                                     | 1500   | 85.6 |           |                                      |      |                 |                       |                    |
| E     | •         | R28325/10                | 757±40                                   | 1190   | 1300 | 95.4      | 1230                                 | 1290 | 68.2            | max. constraint       | Peat               |
| D     | •         | R28325/3                 | 1085±40                                  | 880  | 1030 | 96        | 890                                  | 930  | 22.9            | max. constraint       | Peat               |
|       |           |                          |  |  |      |           | 940                                  | 1000 | 45.3            |                       |                    |
| C     | ◊         | 69178                    | 1540±50                                  | 420  | 630  | 95.4      | 430                                  | 570  | 68.2            | max. constraint       | Charcoal           |
|       | •         | R28325/9                 | 1571±40                                  | 410  | 600  | 65.4      | 440                                  | 540  | 68.2            | min. constraint       | Peat               |
| B10   | ◊         | 69175                    | 1870±40                                  | 60   | 250  | 95.4      | 80                                   | 220  | 68.2            | max. constraint       | Charcoal           |
| B     | •         | R28325/8                 | 2272±40                                  | 400  | 340  | 38.7      | 400                                  | 350  | 33.7            | min. constraint       | Peat               |
|       |           |                          |  | 320  | 200  | 56.7      | 290                                  | 230  | 34.5            |                       |                    |
| A     | •         | R26946/1                 | 3367±45                                  | 1750   | 1520 | 95.4      | 1740                                 | 1710 | 11.5            | min. constraint       | Peat               |
|       |           |                          |  |  |      |           | 1700                                 | 1600 | 52.9            |                       |                    |
|       |           |                          |  |  |      |           | 1550                                 | 1530 | 3.8             |                       |                    |
| A10   | ◊         | 69179                    | 3700±40                                  | 2200   | 1950 | 95.4      | 2140                                 | 2030 | 68.2            | min. constraint       | Charcoal           |

Table 2. Radiocarbon dates from trenches across the November 12, 1999 Düzce rupture.

#### Notes

Calibrations according to atmospheric data from Stuiver et al (1998) (Fig. 53) using Calib 3.9 software (Ramsey, 1995, 2001 and web). Radiometric ages from this study were obtained at the Rafter Radiocarbon Laboratory (RAFTER), Institute of Geological and Nuclear Sciences. See appendix 3 for the spatial location of the samples and for the calibration curves. Sometimes maximum and sometimes minimum constraining dates of events are available in the trenches (See section 4.3.2)

Reference: • = this study; ◊ = from Hitchcock et al (2003); \* = the November 12, 1999 Düzce event.

Calibrated Date in Terms of Confidence Intervals: Bold font represents maximum and minimum limits of intervals for maximum and minimum constraining dates respectively.

## 4.3. ANALYSIS OF THE EXPOSURES

### 4.3.1. THE EXCAVATIONS

#### 4.3.1.1. Töngelli-1 (T1)

Alluvial cone of the Töngelli stream was excavated perpendicular to the surface rupture of the 1999 Düzce earthquake in August 2000 (Section 4.1, fig. 55). Upper 3 m of the sediment has been examined in most of this excavation. The exposure was mapped at the scale of 1:10 (Fig. 56 see also appendix 4). The trench exposed predominantly silty clay and gravelly strata that can be divided into two structural blocks separated by the fault zone. Just upper 2 m of the northern site (between 8<sup>th</sup> and 14<sup>th</sup> meters) can be examined because of high ground water-level and collapse of the trench walls. The western wall of the trench reveals two conspicuous faulting events that occurred before the 1999 Düzce earthquake. The first event (event A) was



**Figure 55.** The picture of the Töngelli-1 trench (looking from north). Alluvial cone of the Töngelli stream was excavated perpendicular to the surface rupture of the 1999 Düzce earthquake. See figure 46 for the location of the trench.

recognized as a normal faulting between 8<sup>th</sup> and 10<sup>th</sup> meters (See section 4.3.2.1). The second one (event F) was recognized as a compressional feature related to push up structure of the moletrack between 0<sup>th</sup> and 4<sup>th</sup> meters (Fig. 57). 4 samples were sent to the radiocarbon

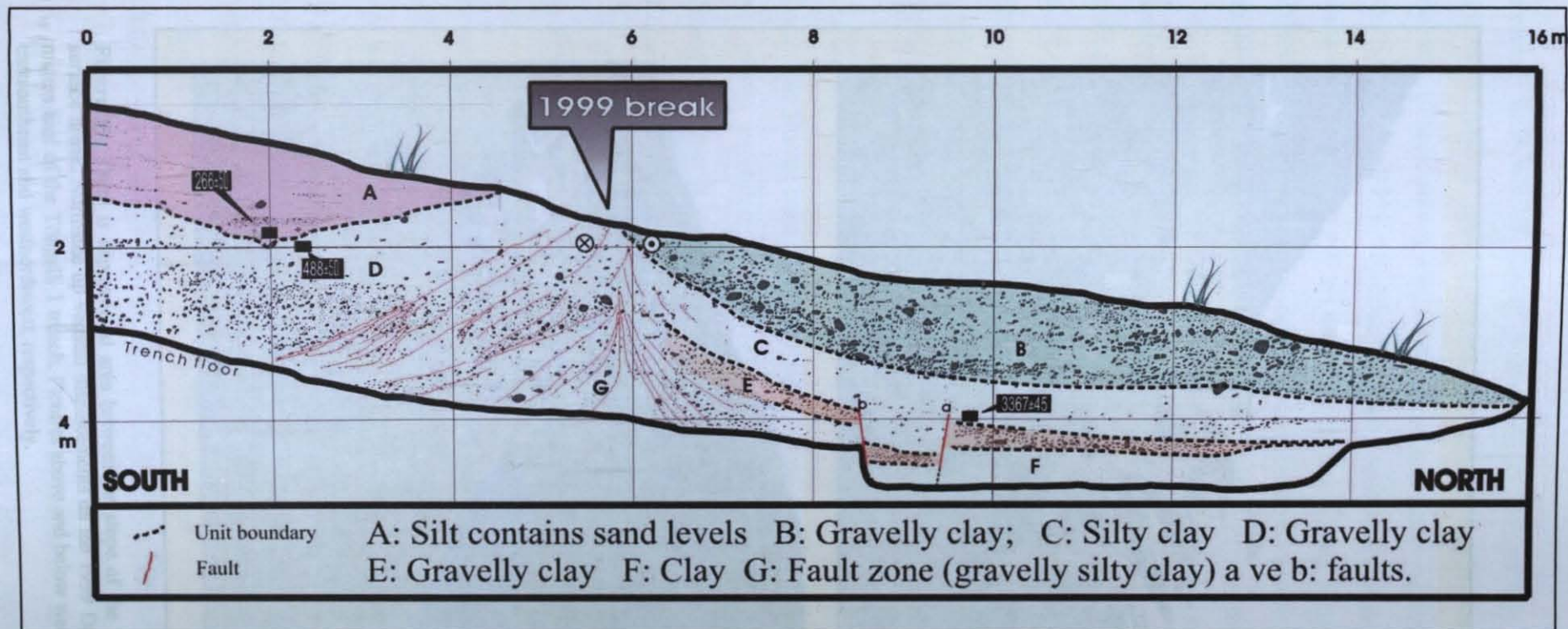


**Figure 56.** Log of the west wall of trench Töngelli-1. Carbon sample location is outlined in black rectangles.  $^{14}\text{C}$  ages is given in the rectangles. See figure 46 for the trench site. More detail drawing is available in appendix 4. There are two structural blocks left and right of the 6<sup>th</sup> meter (See the section 4.3.1.1). The 1999 rupture not visible in the exposure because of the chaotic nature of the fault material. The rupture clearly observed on the surface. The surface break location outlined in the figure. Event A was recognized as a normal faulting between 8<sup>th</sup> and 10<sup>th</sup> meters and event F as a compressional feature related to a push up. The local depression between 0<sup>th</sup> and 4<sup>th</sup> meters occurred between the push-up and slope of the fan. Unit A is the fill deposit in the depression.



**Figure 57.** There is a depression between the slope of the hill and the push-ups of the surface break. Northside up vertical displacements on the 1999 Düzce rupture, a couple of meters east of the Töngelli 1 trench. Pictures above and below were taken by looking from east-southeast and west-northwest, respectively.

laboratory for AMS  $^{14}\text{C}$  dating. 3 of them are successfully dated (Table 2). The section contained abundant peat of which we collected additional samples for future dating. According to radiocarbon dates, there is not any match of units across the fault zone (about sixth meter). The 1999 earthquake surface break study (Appendix 1) shows that the 1999 faulting occurred along this zone in the exposure having about 300 cm dextral offset. 1.5 m wide zone of the surface break is very clearly observed on the surface and its surface location precisely located on the maps and the log (Fig. 56) however, the 1999 faulting is not visible in the exposure because chaotic and fine grain nature of the fill material below the surface. Therefore, it couldn't be shown in the exposure and not drawn on the log. There is no significant scarp identified in the trench site on the topography because of the intense erosion. The 1999 surface rupture represents about 30cm north-side-down vertical offset just a few meter east of the trench (Fig. 57). Vertical component seems to be more pronounced towards the east in the area. Upper parts of the stratigraphic section of the northern site were not deformed (unit A) and topographic anomaly were eroded.

Strata are coded letters from A to G. Several thick gravel units (B, G, and E) in the section indicate that floods have buried the alluvium on occasion during the past 3500 years. Some brick pieces collected in the units G and B were probably transported by floods. Sedimentation rate is supposed to be very high during the flooding periods. For this reason, just one event exposed each side of the main fault in the trench. As it might be expected for the flooding periods, the thicknesses of the gravel deposits varies in the excavation unit to unit. They have not grade and poorly sorted. Several finer-grained gravely levels in unit B display flow structures. On the other hand, silty clay units represents low energetic environment between the flooding seasons (upper parts of D, C, A, F in fig. 56). Greenish C, F units and the upper parts of D unit, are massive and have invisible stratigraphy. Just unit A lets to see the sedimentation structures. The stratigraphy in this unit predominantly consists of well-bedded, sandy and silty sediments that are less than about 550 years old. These structures and the unit boundaries between massive silty clay and gravely deposits of other units are serving reference frames for recognizing the seismic deformation in the strata. The average rate of accumulation could not be estimated precisely because of the limited time control in the exposure and erosion at the top of the surface of unit B. According to dated sample (R26946/5) collected in the bottom part of the unit A (1500 mm depth), the sedimentation rate for this period is about 1 mm/yr for the local depression that unit A was deposited. This rate is probably underestimated here because of the recent erosion mentioned before. Other

sedimentary level that is dated by sample R26946/1 is at about 780 mm depth and rather older (about 3570 years). Calculated 0.2 mm/yr rate of sedimentation is totally rubbish for these sediments, because intense erosion is clear. All the units are bending towards the surface along the fault zone. This structural nature is undoubtedly related to push up deformation of the mole track. Sticky gray clay appeared in the bottom part of the trench in the fault zone (about 6<sup>th</sup> meter). More detailed information about the evidence related to the events (A and F) is given in section 4.3.2.

#### **4.3.1.2. Töngelli-3 (T3)**

The Töngelli-3 trench was exposed in October 2000 across an E-W trending small valley between the Mengencik shutter ridge and the northern slope of the Almacık Mountain and across the surface rupture of the 1999 Düzce earthquake that has about 300 cm dextral offset in this reach (Section 4.1., Fig. 46). Beside, the trench excavated in a dry season, the high level of the water table led important difficulty during the trenching period. The exposure was mapped at the scale of 1:20 (Fig. 58). Such a larger scale is used for this exposure because the trench had a high collapse risk. The surface break of the 1999 rupture is 6m away from the 6<sup>th</sup> meter of the trench and exhibits a trough geometry having about 50 cm depth (Fig. 59). The majority of the exposed deposits are laterally continuous and they can be traced along the trench. The stratigraphy exposed generally consists of silty clay and gravel. Silty clay is a massive undifferentiated package. The surface of the gravel unit in the bottom part of the trench is gently down to the north from the southern margin of the trench to the center of the valley. Two events are recognized in the trench. The evidences of these events are depressions that were formed by steep scarps of the fault zones like surface deformation of the 1999 rupture here. These depressions provide stratigraphic evidence for two earthquake ruptures within the trench exposure.

Descriptions of the stratigraphic units are provided in figure 46. The most prominent marker bed that exhibited sharp upper contact was unit B. Unit B is toughly faulted by two younger events. Upper levels of massive silty clay unit A are faulted by event E and its lower parts by another event to the north. The northern zone of faulting located between 4<sup>th</sup> and 6<sup>th</sup> meters was expressed in the massive older flood deposits. On the other hand, the southern fault zone (event E) that was exposed between 0<sup>th</sup> and 3<sup>rd</sup> meters appeared to represent a clear depression like the 1999 event. After the deposition of unit B, silty clay deposition was uniform about 1

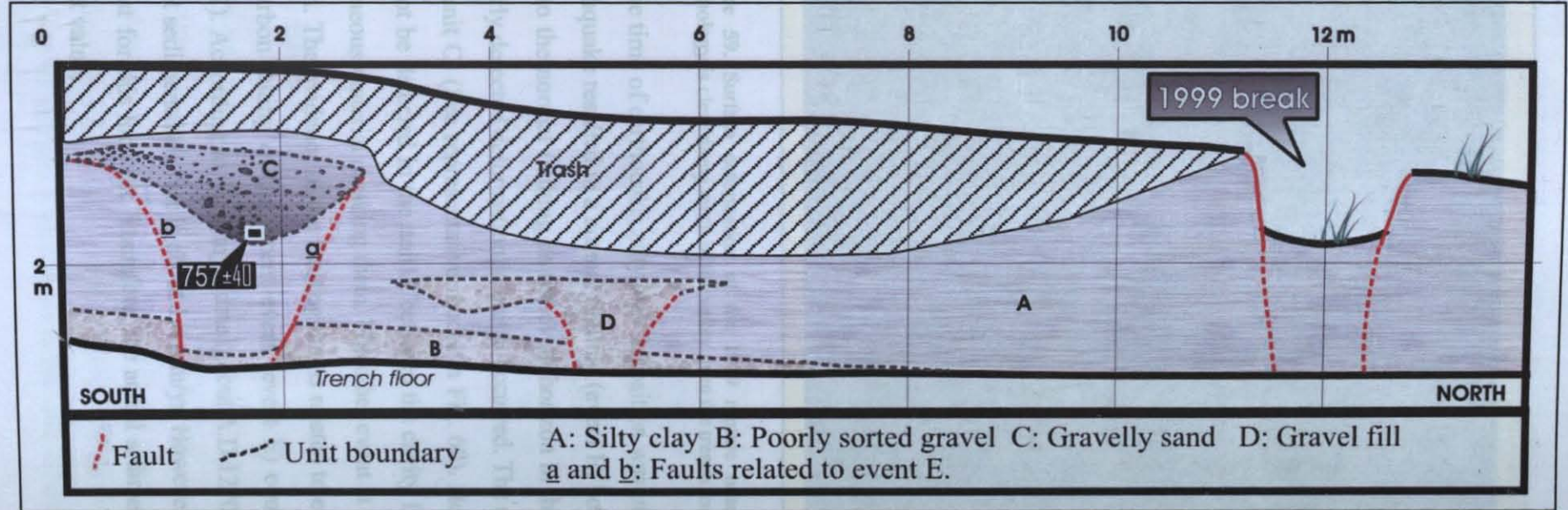


**Figure 58.** Log of the west wall of trench Töngelli-3. Carbon sample location is outlined in black square (R28325/10).  $^{14}\text{C}$  age is given in the rectangles. Shaded area in Unit A is a wedge fill that contains gravelly sand deposit (Unit C). Uniform deposition of the unit A around 2 m depth and around 2<sup>nd</sup> meter from south was probably interrupted (locally) by the deformation related to event E and unit C fill the fissure that was occurred on the event horizon like the fissure of the 1999 event. The other fissure fill (Unit D) represents another event. However it is not dated in this study. All of the events including the 1999 rupture have similar deformation as a normal faulting in the site. Both the sizes and shapes of the fissures are similar to each other. The typical trough morphology related to rupture clearly observed from the surface rupture of the 1999 earthquake in the site (See fig. 59). See figure 46 for the trench site. The part between 8<sup>th</sup> and 13<sup>th</sup> meters of the trench log is imported from the parallel trench (Töngelli-2).

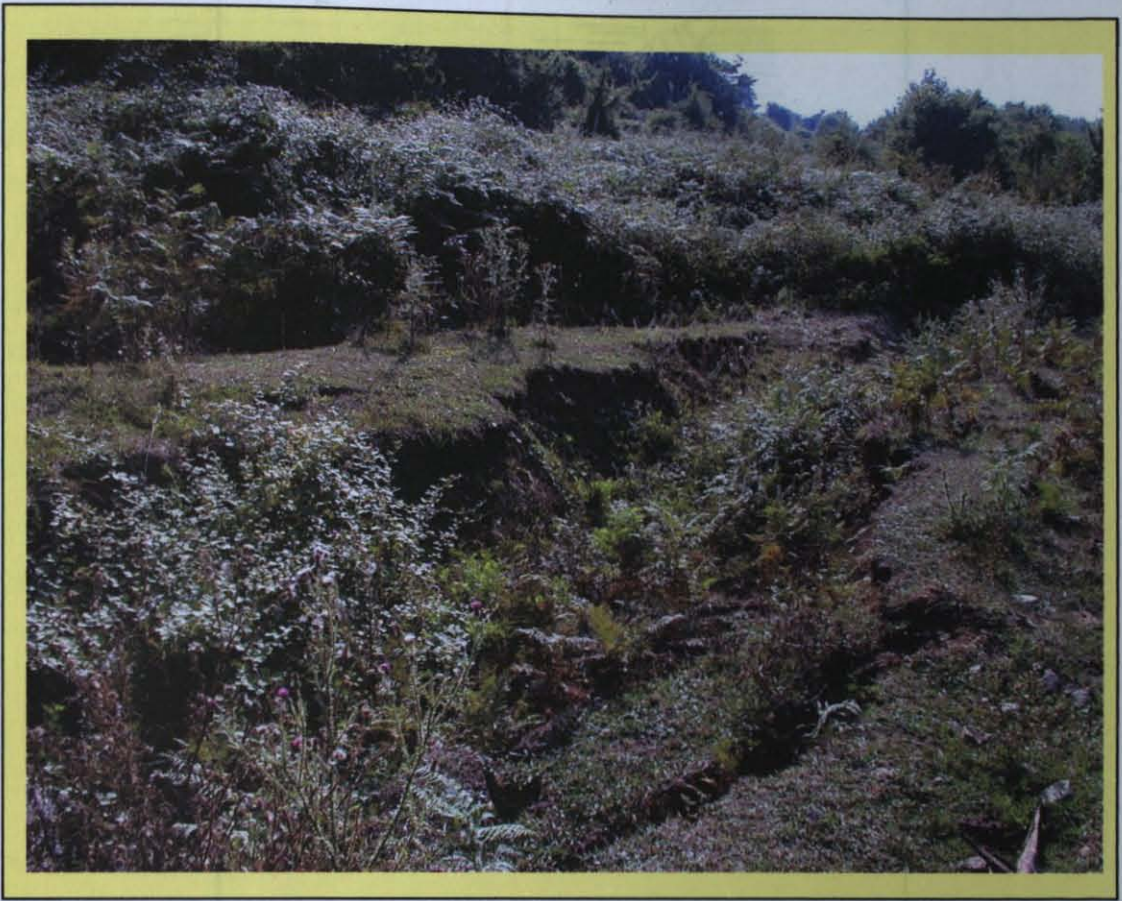


**Figure 59.** Surface deformation of the 1999 rupture near Töngelli-3 trench location. Trough morphology is clear along much of the valley from the trench location to the east (See fig. 46).

m. At the time of earthquake, silty clay deposition was interrupted locally. The deformation of the earthquake resulted in a normal faulting (event E) both in unit A and unit B. A depression related to the normal faulting on the event horizon in the silty clays of the unit A just above the clearly detected deformation in unit B occurred. The resultant cavity was filled by gravelly sands (unit C) (See representative model in Fig. 60). However, fractures related to the event could not be detected in the unit A between the cavity fill (unit C) and unit B because it has monotonous material masking them. The other event at the lower parts in the north could not be dated. The evidence of the faulting that is related to event E is given in the section 4.3.2.5. Radiocarbon dating of the recent event (event E) constrains its probable occurrence date (Table 2). According to the sample date (about A.D.1270 year) and the 180 cm deposition, the apparent sedimentation rate is about 1.4 mm/yr. However, there are probably erosional phases that exist for this location. Therefore, the actual sedimentation rate could be higher than the apparent value.

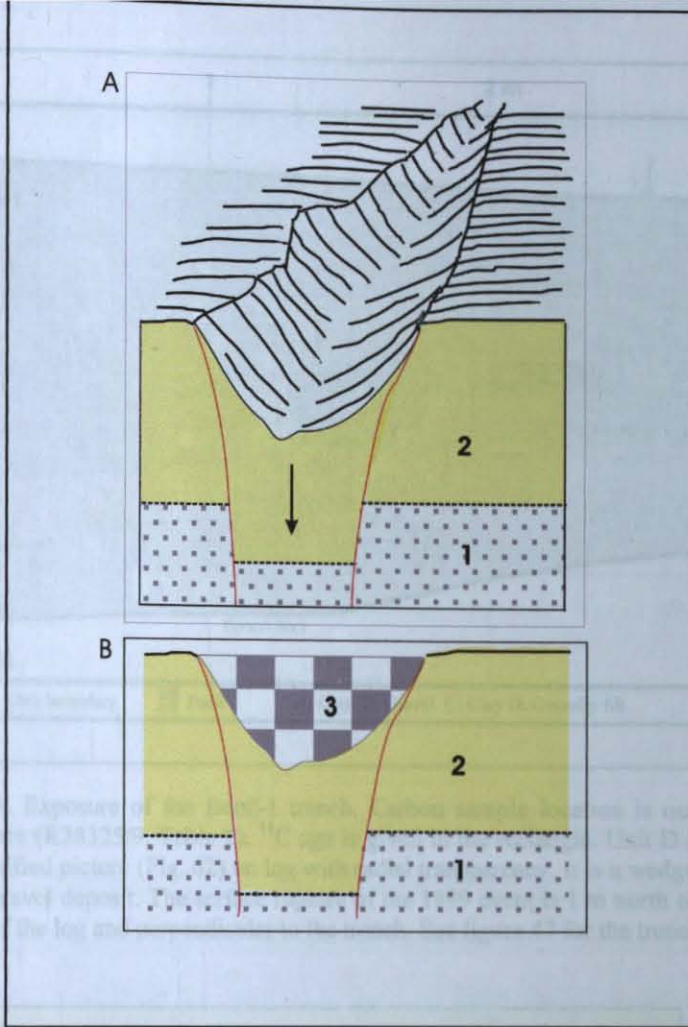


**Figure 60.** Normal faulting in clayey units (unit 2) cannot be seen because of their fine-grained nature. The faulting can be recognized by the existence of three evidence at the same time. One is offset of the unit boundaries (the boundary between units 1 and 2) below this kind of material. The other is existence of a cavity in the material. The cavity in the figure A related to occurrence of trough along the fault. The third, position of the cavity that has similar geometry to the normal faulting should be just on the normal faulting that is directly detectable along the boundary.

#### 4.3.1.3. Bend-1 (B1)

The paleoseismic site was excavated perpendicular and across to the recent surface (1999 rupture) break in August 2001 (Fig. 47). The 1999 rupture has about 300 cm dextral offset here. The sediments of the Bend-1 section are massive clays, silts, and gravels of fluvial origin (Section 4.1). Single event is recognized in the trench exposure besides the 1999 rupture (Fig. 61 and 62). Two strands of the fault are cutting gravelly unit B including unit C

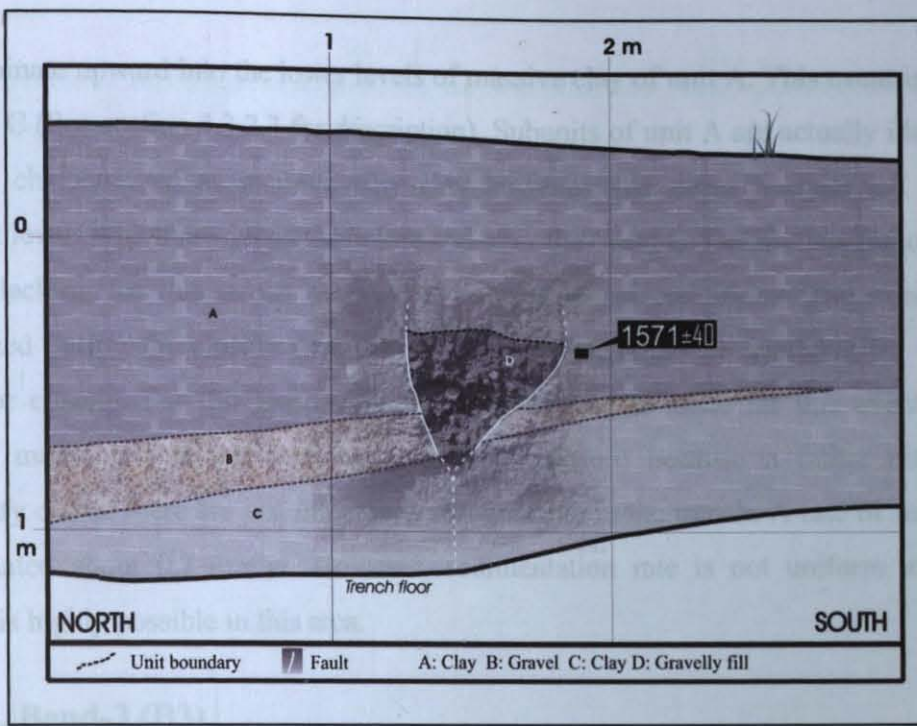


**Figure 61.** Exposure of the Bend-1 trench. Carbon sample location is outlined in black square (R28325/9, Table 2).  $^{14}\text{C}$  age is given in the rectangle. Unit D is shown with a rectified picture (Fig. 62) on log with radial transparency. It is a wedge fill that contains gravel deposit. The surface rupture of the 1999 event is 1 m north of the left boundary of the log and perpendicular to the trench. See figure 47 for the trench site.



**Figure 62.** The picture of the eastern wall of the Bend-1 trench. A wedge fill contains gravel deposit (See fig. 61).

and terminate upward into the lower levels of massive clay of unit A. This event is referred to as event C (See section 4.3.2.3 for description). Subunits of unit A are actually identical units that are characterized as massive silty clay however, the event horizon led to separate different levels which are deposited before and after the event C. Detail mapping of the trench wall is lacking for this trench because of poor logistical conditions. The event is totally recognized during the closing procedure. The excavator could be available for a couple of hours for closing. For this reason, a schematic drawing is made for this event. However, detailed mapping was not necessary for this exposure because a rather single simple stratigraphy exists; there are just three units recognizable in the trench. A rate of sedimentation is estimated about 0.7 mm/yr. However, sedimentation rate is not uniform and episodic erosion is highly possible in this area.

#### **4.3.1.4. Bend-3 (B3)**

This trench was excavated parallel to the Bend-1 trench to the east in August 2001 (Section 4.1, Fig. 47). Gravel and clay deposits are exposed in the trench (Fig. 63). Clay deposit is highly massive and representing low energy. It extends the entire length of the trench. The poorly sorted gravel deposit on the surface is derived from the local mountain front in recent flooding event by Bend stream. The 1999 earthquake event offsets (about 300 cm) the gravel deposits of the flood bed (unit A and B) laterally in the excavation. No evidence was found out about the faulting that was older than 1999 event in the southern half of the trench. Unit C is overlain by the sand and gravel layers of a flood that appears to drape the alluvium of unit C south of the 3<sup>rd</sup> meter. It thickens on the southern side of the excavation. Flood deposits can be separated into two units. Unit A is overlying a weakly consolidated fine-sand layer of unit B. Lack of the lateral continuity of unit A and B indicates lateral deformation along the fault zone formed during 1999 event. The northern extension of the unit A and B were laterally offset towards the east. This trenching area can be good candidate for finding the offsets of paleoseismic events. Unit C has massive (unstratified) clay that causes difficulty in distinguishing events. Even the fractures related to the 1999 rupture are invisible. A circumstantial evidence suggests a fault formation bounding a gravel fill in the northern half of the trench (Fig. 63). Some brick pieces were collected in this unit (Unit A). The unstratified gravel fill is representing the deformation evidence of an event in the northern part of the exposure. There are fractures in the fill unit. The oldest faulting event (event D) was dated in the lowest part of the fill (Section 4.3.2.4).

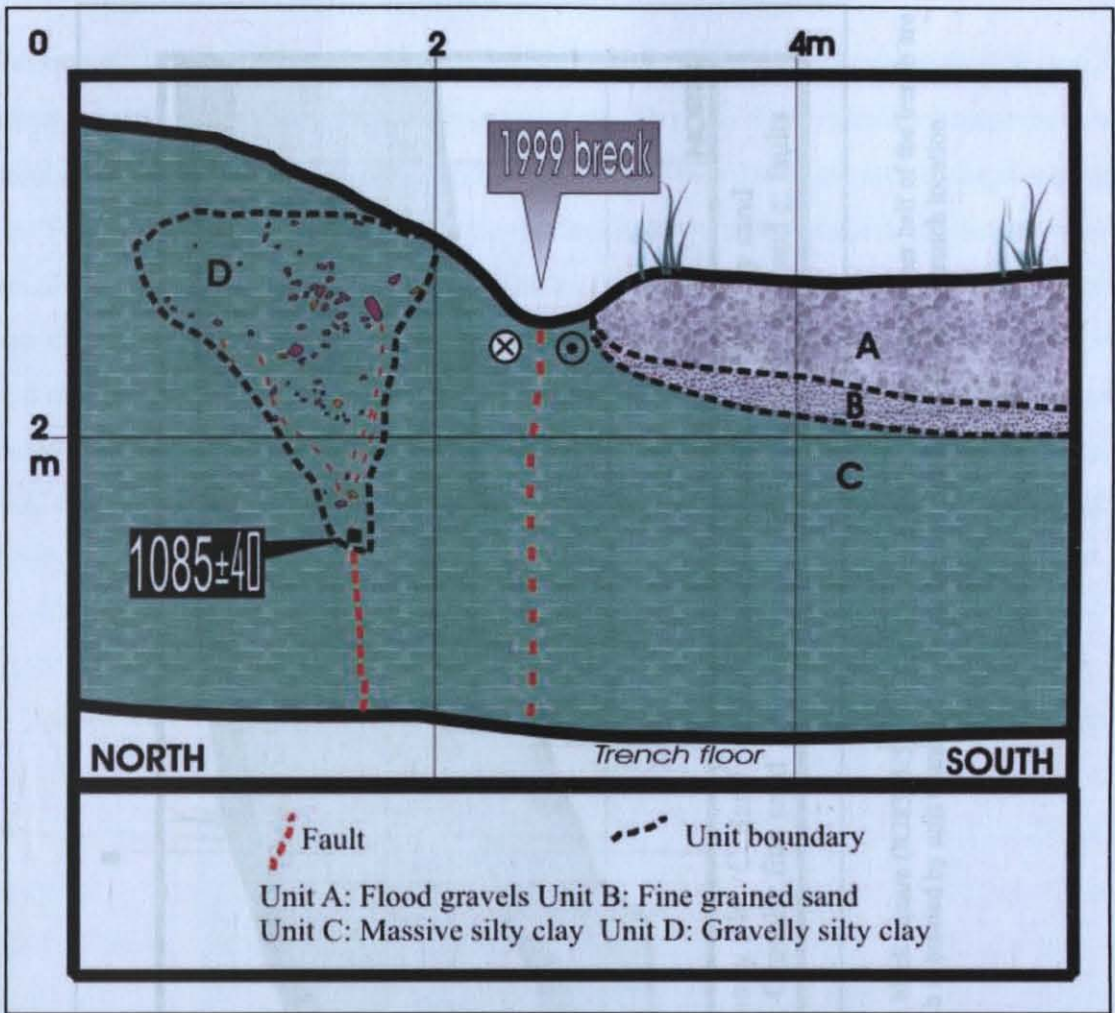


**Figure 63.** Log of the east wall of trench Bend-3. Location of the 1999 rupture not clearly detectable do to the fine nature of the material. Unit D is a wedge fill that contains gravelly silt deposit. Gravels are shaded by gray and brick pieces with orange in this unit. Carbon sample location is outlined in black square at 0.5 meter north of the station 2<sup>nd</sup> and at the bottom tip of the wedge (R28325/3). <sup>14</sup>C age is given in the rectangle. The saple represets the starting time of the deposition of the fill material just after the earthquake. Unit A and B: flood deposits. See figure 47 for the trench site.

According to dated sample (about 1050 year old) that was collected about 2 meter depth, sedimentation rate is about 1.9 mm/yr for this location. According to roughly calculated mean value of sedimentation rate (2 mm/yr), there is no absence of sedimentation or erosion here.

#### 4.3.1.5. Kaledibi-1 (K1)

13-m-long and 3-m-deep trench that extended from 8 m north to 5 m south of the surface break of 1999 rupture was excavated in August 2001 (Fig. 44). On the topography, significant south-facing scarp is identified in the trench site (Section 4.1). 1999 surface rupture represents about 15-cm southside-down vertical offset beside 350 cm right lateral offset. Upper 3 m of the sediment has been examined in most of this excavation (Fig. 64). The single event is dated

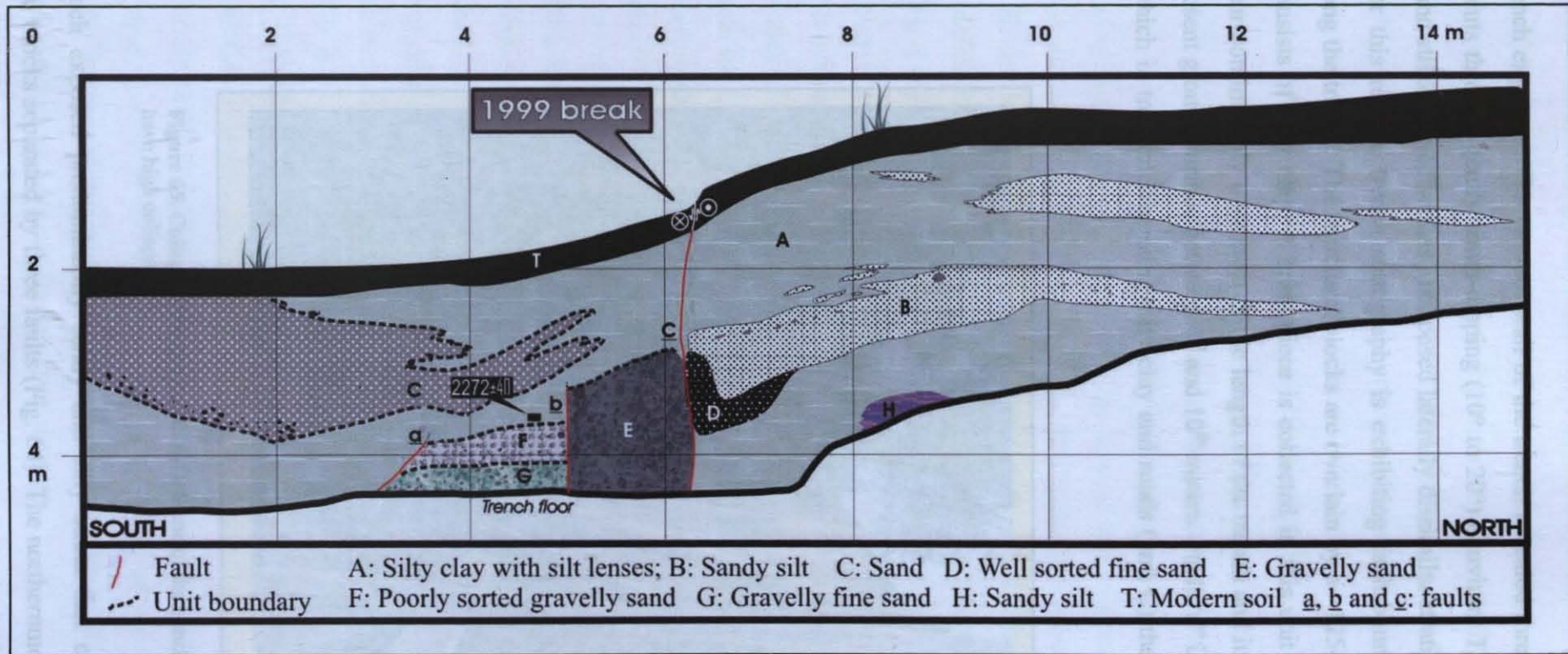


**Figure 64.** Kaledibi-1 trench exposure. Carbon sample location is outlined in black square (R28325/5).  $^{14}\text{C}$  age is given in the rectangle. The deeper half of the trench are divided into four structural blocks according to faults a, b and c. The faulting b is buried by unit C and dated by the sample. See figure 44 for the trench location.

in the trench exposure. The western wall of the trench revealed three clear fault zones. Each of them cuts through gently south-dipping ( $10^{\circ}$  to  $20^{\circ}$ ) alluvium. The fault zones are nearly vertical and strike-slip offset has juxtaposed laterally dissimilar stratigraphic sequences across them. For this reason, trench stratigraphy is exhibiting fault-bounded blocks between the faults along the trench. The structural blocks are overlain by a  $\sim 125$ -cm-thick shallowest unit which consists of silty clay. A brick piece is collected in this unit (unit A). Unit A can be traced near-continuously over most of the length of the trench and its planar base lies parallel to the present ground surface between 4<sup>th</sup> and 10<sup>th</sup> meters. Fault “a” is overlain by silty clay of unit A which in turn interfingering silty clay and sands (unit C) that are overlying fault “b” and “c”.

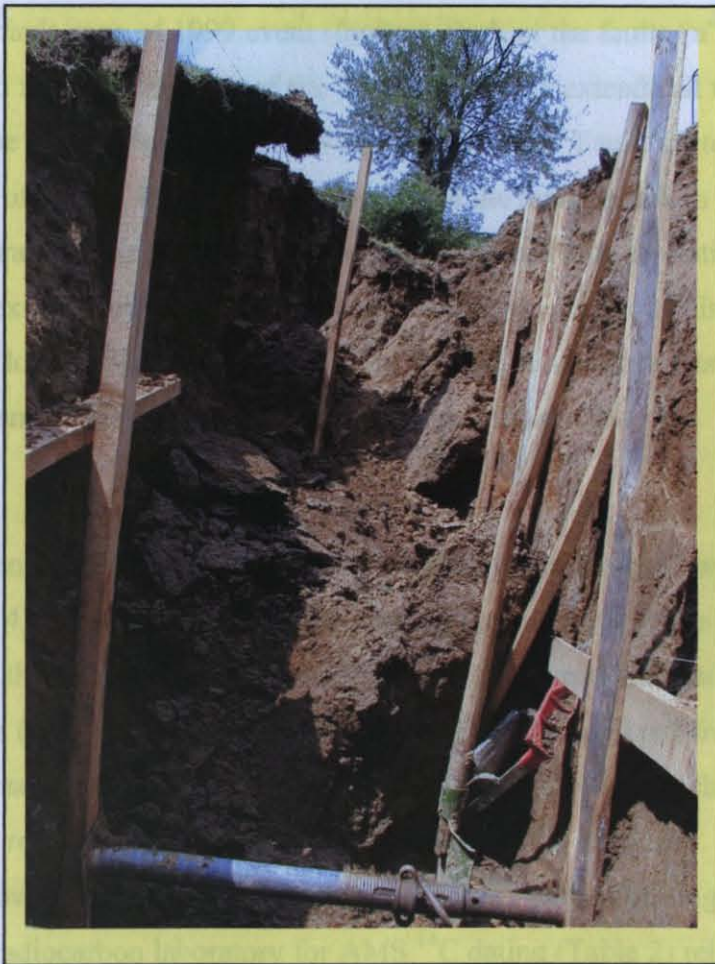


**Figure 65.** Collapsed trench (Kaledibi-1). Some of the trenches have high collapse risk.

The trench exposed predominantly sandy and silty strata that can be divided into four structural blocks separated by three faults (Fig. 64). The northernmost structural block (north of fault a) consists of 40-cm-thick weakly consolidated sands (unit B) overlain by the silty

clay bed (unit C). The lower deposit consists of massive silty clay. The other block is bounded by fault “a” to the north and fault “b” to the south. The stratigraphy in the upper 1-m of this block is similar to that of the northern block. The interfingering sands and silts overlie at least 1.5-m-thick gently south-dipping poorly sorted sandy gravels (unit E). The deeper part of the unit-E is beyond the base of the trench. The other structural block between the third and the fifth meters consists of the silty clay bed and interfingering sands and silts in the upper portion as the other blocks, overlain gravels (unit F). The poorly sorted unstratified sandy gravels of 40-cm-thick unit F grade downwards into well-sorted unstratified gravels (unit G). Units F and G appear to be similar, and differ only in sorting quality. The unit A and C interfingering sands, silts and clay overlie the upward terminations of the faults. Unit A is bioturbated around the second meter station. The Kaledibi trench revealed one clear fault (fault b) except fault zone of 1999 event (fault a). Both of the faults “a” and “b” have narrow and well-defined zones at the base of the trench. Fault “a” extends all the way to the ground surface that is the current horizon of 1999 earthquake event. Fault “b” terminates upward into the lower levels of unit A. It is possible that some of the fault strands in the fault zone are also ruptured at several event(s). However, no evidence is available to distinguish these between events if they exist. Fault “c” that is the southernmost structural discontinuity terminates upward into the lower levels of unit A as fault “b” and juxtaposes units F and G with unit A. It could represent a vertical faulting event or a faulting that has a significant vertical component.

The faulting event related to the fault “b” is referred to as Event B and related evidence is given in section 4.3.2.2. The exposure was mapped crudely at the scale of 1:20. Such a larger scale is used for this trench because its walls seemed to be unstable. It totally collapsed within a couple of days (Fig. 65). During the excavation, I greatly suffered from unstable nature of the trench because of the high ground water content, beside the trench excavated in the dry season. For this reason, deeper part of the trench cannot be examined. The unit A contained abundant peat however; carbon contents is poor in other units. The single sample (R28325/5) was sent to the radiocarbon laboratory for AMS  $^{14}\text{C}$  dating (Table 2) related to the event B. It is successfully dated. The average rate of accumulation could not be estimated because of the limited time control in the exposure. Rough estimate of the rate is about 2.5mm/yr considering the age of the sample (~732 years) and its depth from the surface (180 cm). Additional samples are collected for the future dating.

## 4.3.2. EVIDENCE FOR PALEOSEISMIC EVENTS

### 4.3.2.1. Event A

The vertical separation of unit E ascribable to a seismic event appears near the northern end of the Töngelli-1 trench (Section 4.3.1.1). This is the oldest event that is recognized in this study and is referred as event A. A set of two faults (fault “a” and “b”) terminate upward in the massive silty clay of unit C probably forming a depression. Apparent 30-cm of vertical offset occurred between these faults during event A (Fig. 56). These faults attributable to event A inferred to be normal and probably has dextral component. 100-cm part of 20-cm thick gravel unit E is displaced downward by these faults between the stations 8<sup>th</sup> and 10<sup>th</sup> meters. Its upper and lower surfaces displace the same faulting geometry and amount. The faulting occurred prior to gravel deposition of the flood unit B. After the deposition of the upper part of unit C, the scarps and the depression that were probably formed during the event A were completely undetectable on the current surface. Opened probable fissure or its fill in unit C could not be seen because it was probably eroded before filling process or probably filled by the same clays of unit C. Invisible upper edges of the faults in unit C should be overlain by the upper part of the unit relatively, because debris or remains of gravel unit E was not observed along the fault and the overhanging scarp did not collapse in the upper level of unit E. On the other hand, the event horizon could not be identified in unit C because faults could not be followed in massive clay of the unit. Thus, it is not clear whether the faults were formed just before the deposition of unit B or just after the deposition of unit E. However, it is clear that these faults have not been reactivated after the deposition of unit B. This is proved by the unbroken sediments of the unit B that blanked the fault (Fig. 56).

One sample of peat near the top of the unit E on the up-thrown side of the fault a (Fig. 56) indicates that a flood bed has been deposited around the middle of the millennium before the last millennium B.C. The sample about 1.6 m below the ground surface yielded an accelerator mass spectrometry (AMS) of a calibrated radiocarbon age ranges of B.C. 1740 -1530 ( $\sigma_1$ ), with the most probable date being B.C. 1700-1600 ( $\sigma_1$ ) (Table 2, sample R26946/1). The date of the faulting event that led to the formation of depression between the fault “a” and “b” is represented by this radiocarbon date. This date range provides a minimum limiting age for the faulting event and a maximum limiting age for unit E. This indicates a fact that the faulting was formed after B.C. 1740.

#### **4.3.2.2. Event B**

A fault (fault “b”) is exposed in the southern part and the lowest meter of the Kaledibi trench (Section 4.3.1.5). It exhibits apparent south-side-down normal separation (Fig. 64). Conspicuous faulting of Unit E, against the units F and G, juxtaposes dissimilar stratigraphic sequences, suggesting that it has probably experienced the significant strike-slip motion. Strata to the north of fault b are gently ( $25^\circ$ ) dipping southward whereas strata to the south are generally flat lying. Zone of the fault is narrow and well defined. Fault plane terminates at a horizon within 40 cm bottom part of unit A below the interfingering between clays and sands (Unit C). Unit C completely buried the fault deformation associated with the Event B. The event horizon could not be identified in unit A below the interfingering between clays and sands (Unit C) because faults could not be followed in its massive deposits.

The date of the faulting event that was juxtaposed different sequences is constrained by one radiocarbon date (Fig. 64). One sample of peat in the lowest part of the unit A yielded AMS calibrated radiocarbon age ranges of B.C. 400-230, with the most probable date ranges being B.C. 290-230 (Table 2 sample R28325/5). This date provides a minimum limiting age for the faulting event and antedates unit A. The date indicates that event B occurred after about B.C. 400.

#### **4.3.2.3. Event C**

The evidence for the occurrence of a faulting event (event C) between unit C and the upper parts of the unit A is indicated in one place in the exposure of Bend-1 trench (Section 4.3.1.3). The stratigraphic position of the gravel fill deposits (unit D) in the massive clay of unit A hampers the recognition of position of the possible event horizon and faults (Fig. 61). Two faults produced about 50-cm-deep depression in the lower parts of the unit A. The depression was left virtually intact and uneroded until it was preserved by unit D. The unit D and A completely buried the deformations associated with event C. That is, the current topography that represents the surface of unit A is a uniformly south-dipping plane that did not reflect an irregular topography produced by event C beneath the depression. The two faults are connected in the subsurface in unit C. This relationship is also apparent in the both walls of the trench. Faults attributable to event C inferred to be normal and probably has dextral component. There is no direct evidence of dextral offset available for this event. The unit B has probably no variation in thickness which would indicate a lateral slip across the fault

zone. If this fill is related to an event and not a stream channel, there could be two reasons for this; (1) the unit B has no variation in thickness in the site, (2) its surface has no east – west trending slope. A representative cross section of the faults is displayed in figure 61 in which one can see that the dip of the faults decreases progressively to a depth of about 10 cm, where the faults terminate in massive clay of the upper parts of unit C. Thus, the horizon probably lies along the upper boundary of the unit D (Fig. 62). However, it is ill defined because faults cannot be seen in the massive clays of unit A. The trench is not located in or near a stream channel but located near the surface faulting. There is an absence of any offset in unit B and unvisibility of the faulting in both units C and B. This feature can not be taken as a strong evidence for an event. For this reason, the event is not included to the periodic recurrence model that is introduced in section 4.4.

The minimum limiting age of the faulting event that led to the formation of fissure fill is constrained by a peat sample (Fig. 61). The sample just below the expected event horizon yielded an accelerator mass spectrometry (AMS) calibrated radiocarbon age of A.D. 440-540 (Table 2, sample R28325/9). This result indicates that event C occurred after about A.D. 440.

#### **4.3.2.4. Event D**

A gravely clay fissure fill appears to extend to the top of the unit C (the upper part of the excavation) a little less than a meter in the north of the fault of 1999 event in the Bend-3 trench (Section 4.3.1.4). The fissure fill package was deposited against the overhanging free faces of fault scarps that were formed during event D (Fig. 63). Overall the wall stratigraphy of the unit C is too poor that fault strands are present but not traceable. However, gravel fill precludes the existence of a fissure (Unit D in fig. 63). The gravel-filled fissure grades into the clay of unit C about 170 cm. No downward continuation of the fault zone is visible within the lowest massive clay (unit C) as the invisible fractures of the 1999 rupture in the trench. The possible occurrence of the faulting event/s younger than event D cannot be ruled out in the trench. The gravels were interpreted to have filling in the fault-bounded depression that was created during the event D. The fact that gravel fill was deposited in a manner consistent with the expected sedimentologic response to the surface deformation confirms that the fault did indeed rupture the ground surface during faulting. The gravely clay deformational (post-depositional) deposits that was filled in localized depressions were created by the surface rupture in silty clays of unit C during the event D and definitely postdate it.

The maximum limiting age of the faulting event that led to the formation of fissure fill is constrained by one radiocarbon date (Fig. 63). A sample (R 28325/3) from the bottom tip of the fill that represents the closest time to the event, yielded an accelerator mass spectrometry (AMS) calibrated radiocarbon age of A.D. 890-1000 (Table 2). This date range provides a minimum limiting age for the fill. Thus, the minimum limiting age of the sample is A.D. 890 antedates the fill and probable maximum age 1000 constrains the maximum limiting age of the event (event D).

#### **4.3.2.5. Event E**

Besides 1999 earthquake, the youngest event recognized in the Töngelli-3 trench is referred as event E (Section 4.3.1.2). The strongest evidence for this event is two normal faulting and subsidence in unit B between 0<sup>th</sup> and 3<sup>rd</sup> meters (Fig. 58). The fault in the south exhibits a south-side-up component of vertical slip and the fault in the north exhibits a north-side-up component of vertical slip in the dextral shear zone. After the deposition of unit B, silty clay deposition had been uniform about 1 m. During the earthquake, silty clay deposition was interrupted locally. The deformation of the earthquake resulted in normal faulting and subsidence both in unit A and unit B. Faulting of the oldest unit (unit B) also exhibits the same geometry as in unit A between the first and the second meter stations, providing evidence for event E. The normal faults exhibit about 50 cm of apparent vertical separation here. A depression related to the normal faulting on the event horizon in silty clays of the unit A just above the clearly detectable deformation in unit B occurred. The resultant trough or cavity was filled by gravelly sands (unit C). Similarly, the 1999 rupture has the same geometry and size as the trough in unit A having about 50 cm depth cavity in the site (See section 4.1). This deformational trough may be used as a channel in a short time temporarily. On the other hand, there is no stream around the site. The trough-like morphology of the site is related to the eastward movement of the shutter ridges along the fault zone (that is appeared by a surface rupture in 1999) with regard to the main slope of the hill. It is not related to a channel of a stream origin. The fractures of faulting are not visible and not expected to be visible in unit A because faulted units are unstratified as occurred in Bend-3 trench for 1999 event (Fig. 63). Gravel fill (unit C) is formed after the deposition of unit A. The fault tips at 0<sup>th</sup> and 3<sup>rd</sup> meter stations terminate at the same stratigraphic level, which lies between 40 and 50 cm below the ground surface.

A peat sample, R28325/10 from the base of unit C has been dated (Fig. 58). The sample's AMS  $^{14}\text{C}$  age ranges from A.D. 1230 to A.D. 1290 (Table 2). The peat sample from the deformational unit C immediately postdates the event E, with having a maximum possible age constraint of A.D. 1290. Therefore, the age of event E is constrained to some time before A.D. 1290.

#### **4.3.2.6. Event F**

Differentiation of the fault ruptures of event F from those of event 1999 is difficult in the Töngelli-1 trench (Fig. 56). There is no fault visible, which has occurred at the time of the event F. However, a push up attributable to event F occurs in the south of the main fault trace on the western trench wall (Fig. 66). The local compression is related to push up structure of the surface break of the event F. Evidence for deformation consists of a sagging that is formed between the push up to the north and slope of the hill to the south during event F (Fig. 57, section 4.3.1.1). The axis of the push up trending parallel to the slope of the hill is perpendicular to the axis of the alluvial fan and oblique to the main fault. Crest to trough amplitude range is about 40 cm similar to the size of push ups of the 1999 rupture. The trench like depressional shape of the paleosurface that appeared during the event remained virtually intact and uneroded until it was preserved by burial under unit A strata. Unit A seems to have deposited almost horizontally. Well-laminated silty sands with silty clays (unit A) fill the upper parts. Complete lack of disruption of overlying sand beds provides that faulting took place along this structure just after unit D had been laid down. The lowest part of the structure is choked with a couple of gravels, which are located at the bottom tip of the unit A (Fig. 56) and overlies the depositional (non-deformational, actual layers or strata) sediments (unit D). These materials probably fell into the domain shortly after its formation. A representative cross section of the structure is displayed on the left side of figure 56, in which one can see the depth of the northern flank of the structure increasing progressively to the surface where it terminates against the main fault. The gravel lineation in the unit D displays the same geometry, near the main fault. Similarly, unit B displays a symmetric geometry to the north of the main fault. At a glance, the structure appears to be a thrust fault. In actually, this is a push up geometry commonly happening in strike-slip shear zones. The deformation of the all deposits older than unit A by the same amount indicates that there was no older earthquake in the site. In addition, the fact that all deposits are horizontal and undisturbed in unit A indicates that there was no younger earthquake, which leads to the deformation at the time of deposition of unit A. Thus, the deformational (postdepositional) sedimentary record (Unit A)

at the southern site of the main fault in the exposure is allowing the recognizing of just one event.

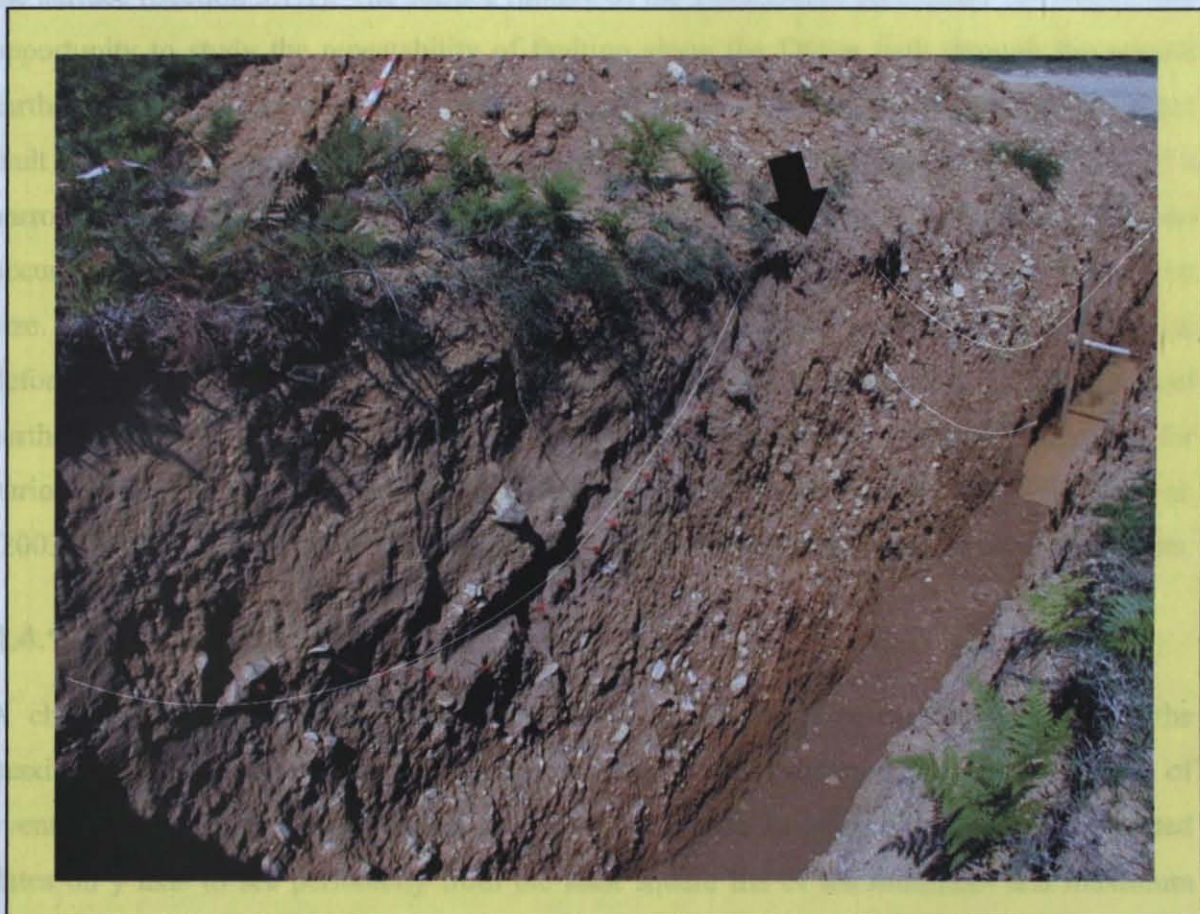


**Figure 66.** Western wall of the Töngelli-1 trench. All the units bend towards the surface along the fault zone related to compressional component. Black arrow represents the fault zone including the 1999 rupture. White lines indicate unit boundaries. See figure 56 for the complete log of this exposure.

The date of the event that led to the formation of the depression is constrained by two accelerator mass spectrometry (AMS) calibrated radiocarbon ages (see locations in fig. 56) which are listed in table 2. Based on the dating of two samples of peat, unit A is consistently younger than unit D confirming the stratigraphic order in the compressional exposure. The age of the gravels of unit A that are located at the bottom tip of the fill in the depression is in the range of A.D. 1520 and 1800 according to  $\sigma 1$  threshold level. The ages obtained indicates that the upper part of unit D was deposited between the age range of A.D. 1400 and 1460. This range represents younger part of the unit D that was deposited just before the event. The preferred age of event F is between A.D. 1400 and 1600. However, ages as old as 1310 and as young as 1950 are also possible but with lower probabilities (Samples R 26946/4, R 26946/5 in table 2).

## **4.4. TIMING THE EARTHQUAKES**

Düzce fault yield during the 1999 Düzce earthquake producing about 42-km-long rupture at the surface (Section 3.1.1). The surface rupture of the 1999 Düzce earthquake provides a rare opportunity to study the repeatability of faulting along the Düzce fault through the several earthquakes in the late Holocene history. Several trench sites were selected along the Düzce fault where fault trace is relatively simple (Section 4.1). In all trenches, the faults consist of a narrow fault zone. The excavations expose the evidence for seven earthquakes that had occurred since about 1740 B.C. Three exposures reveal three fill deposits. They are of similar size. Two reveal horizontal discontinuities, and one reveals a folding that is related to push up deformation (Section 4.3). Thus, all of these deformations and related events represent earthquakes of large magnitude. Using several radiocarbon ( $^{14}\text{C}$ ) age determinations for various faulted late Holocene layers including paleoseismological results of Hitchcock et al. (2003) from the eastern part of the fault, a recurrence interval is suggested between the events.

### **4.4.1. SEQUENTIAL MODEL**

A characteristic earthquake model is described considering the maximum values of the maximum limiting age ranges and minimum values of the minimum limiting age ranges of events. In this model, serial ruptures are located in sequential order on x axis and calibrated dates on y axis to see periodicity from the least square fits of the minimum and maximum constraints. Thus perfect fit suggests perfect periodicity. The November 12, 1999 event (1999,9) is set as intercept in regressions. Figure 68 is showing a good relationships for both minimum and maximum constraints. This suggests that the last seven earthquakes of serial-B are occurring nearly periodical according to the timing design of events and related constraints (see paragraphs below).

#### **4.4.1.1. Data-set Quality**

Paleoseismological trenching performed at five sites along the Düzce fault provides the first insights on its seismogenic behavior. The trenches only reveal a 2-D cross-section of the geologic record perpendicular to the fault and so it cannot fully assess the geologic effect of offset. Unfavorable trench stratigraphy and scarcity of datable material made the identification and characterization of individual paleoearthquakes quite difficult and sometimes impossible along the fault. In spite of the fact, six events were identified and dated besides the 1999 event. One of the events is constrained by maximum and minimum limiting

dates, two events are constrained by maximum limiting dates, and three events are constrained by minimum limiting dates by AMS radiocarbon technique. One of the maximum limiting date and related event (event C) are not used in the models because of its low level of reliability. However, a sample and its radiocarbon ( $^{14}\text{C}$ ) age determination from Hitchcock et al. (2003) are used for the event C. This sample is supplying a maximum limiting date for the event C.

#### **4.4.1.2. Serial-A Model**

Last four events seemed to be serial ruptures (Serial-A). The November 12, 1999 (1999,9) rupture is constantly assigned as 0<sup>th</sup> rupture in all models and as the event G. The radiocarbon age ranges are taken according to  $\sigma 1$  interval which has a probability of % 68.2. Rupture order is increasing from younger to older events. (1) The most recent event 0<sup>th</sup> rupture is the 1999 earthquake; (2) the penultimate one (1<sup>st</sup>) occurred between A.D. 1400 and 1600 (Event F); (3) the 2<sup>nd</sup> event occurred before about A.D. 1290 (Event E); (4) A.D. 1000 which is the maximum constraint of the event D, constrains the maximum limiting age of the 3<sup>rd</sup> rupture back (Table 2). Older two events (Event A and B) seem to be showing an irregularity and do not belong to the four serial ruptures (Serial-A) from 0<sup>th</sup> to 3<sup>rd</sup>. A hitherto unrecognized earthquake may eliminate this irregularity.

##### ***4.4.1.2.1. Event Identification and Model Design***

The event information comes from the different trenches, and some of the trenches are excavated along the different structural segments. Thus, the serial-A is not composed from a specific trench but from the different trenches and segments. This fact results in an important handicap in my sequential model. The trenches are exposed along the Aydınpinar and Mengencik segments of the four probable seismic segments defined in section 3.1.4 according to rupture parameters of 1999 event and geological and geomorphological indications along the Düzce fault. The event G (November 12, 1999 rupture) was clearly observed in all of the segments. Event F (A.D. 1520 and 1800) in Töngelli-1 trench, E (? - A.D. 1290) in Töngelli-3 trench, D (? - 1000) in Bend-3 trench and A (B.C. 1740 - ?) in Töngelli-1 trench were exposed along the Mengencik segment. On the other hand, event B (B.C. 400 - ?) is in Kaledibi-1 trench along the Aydınpinar segment. However, a reasonable relationship is observed between the events in a sequential model (See following paragraphs). The model is also concordant with the previous studies. Emre et al. (2002, 2004) and Sugai et al. (web)

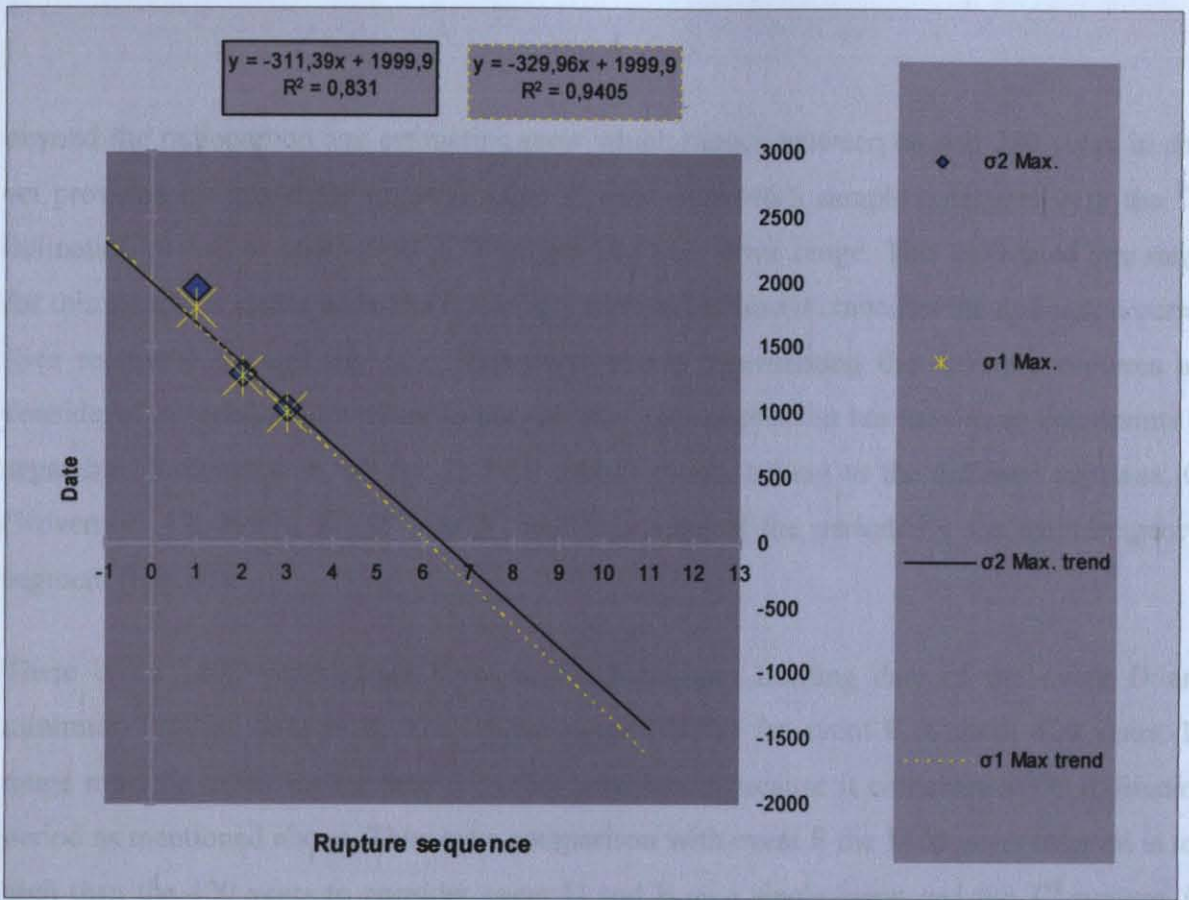


**Figure 67.** Serial-A least square fit of maximum limits of the maximum constraining event dates (See table 2). The November 12, 1999 (1999,9) event (0<sup>th</sup> rupture) is set as intercept in regressions. Equations of the trends are shown in boxes colored according to pattern and color of the trend lines. The four events including 1999 event in the serial are designed using data from this study. The serial seem to be sequential.

excavated trenches along the Aydınpinar and Efteni segments. According to their results, ranges of about A.D. 1650-1750 and 665-1050 are suggested for the penultimate (1<sup>st</sup>) and 3<sup>rd</sup> events, respectively (See introductory paragraphs of section 3.1). The mentioned ranges of Event F and Event D are consistent with these ranges.

First of all, it should be proved that observed events belong to whether the different or the same ruptures, in order to use them in a sequential model. The constraining samples are collected near the event horizons. Thus, they are limiting the events just before or after the exact time of the ruptures. In addition, the maximum and minimum time difference between the maximum limits of the separated events that follow each other in the serial-A (Event F, E and D) is about 510 and 290 years, respectively. Even the minimum value of 290 years is

beyond the radiocarbon age estimating error which ranges between 60 and 280 years in data set provided by this study given in table 2. Even R26946/5 sample coincides with the  $^{14}\text{C}$  dulationation period of 1650-1950 A.D having 280 year error range. This calibrated age range for this sample is rather wide and it is nearly useless because it coincides the dulationation period (See section 4.2.3 and fig. 52). Thus these events representing the different ruptures are considered in serial-A (described in the previous paragraph) that has maximum constraints as separable. In conclusion, all the G, F, E and D events belong to the different ruptures; 0<sup>th</sup> (November 12, 1999), 1<sup>st</sup>, 2<sup>nd</sup> and 3<sup>rd</sup> and they suggest the periodicity for the Mengencik segment (Fig. 67).

There is an 1400 years range between the maximum limiting date of the event D and minimum limiting date of B. The known range (limits) for event F is about 400 years. Its range must be much higher than the other time spans because it coincides a  $^{14}\text{C}$  dulationation period as mentioned above. Thus even comparison with event F the 1400 years interval is too high than the 400 years to consider event D and B as a single event and the 3<sup>rd</sup> rupture. In addition, the least square fit of maximum limits of maximum constraining dates are suggesting a maximum constraining date of about A.D. 750 for the 4<sup>th</sup> rupture (Fig. 67). Considering the event B as a separate event and the 4<sup>th</sup> rupture following back the event D, its date should be between A.D. 750 and B.C. 400. This 1150 years range is still too high considering the range of event F. For this reason, event B could not be located just after the 3<sup>rd</sup> rupture as the 4<sup>th</sup> rupture in the sequential model (Fig. 67). On the other hand, the oldest event (Event A) has B.C. 2140 minimum constraining limit. The interval of 1340 years between minimum limits of events A and B is about 3 times higher than the maximum value of interval between the maximum limits of serial-A. Thus, older two events (Event A and B) seem to be showing an irregularity and do not belong to the four serial ruptures (Serial-A) from 0<sup>th</sup> to 3<sup>rd</sup>. Consequently, these events are not used in serial-A model. Hitherto, unrecognized earthquakes may eliminate this irregularity between events B and A and events B and D.

In conclusion, there are four events in serial-A which is designed by using data from my trenching study. There are possibly four earthquakes including the 1999 event that had occurred since A.D. 1000 in the past 1000 years. According to least square regression of

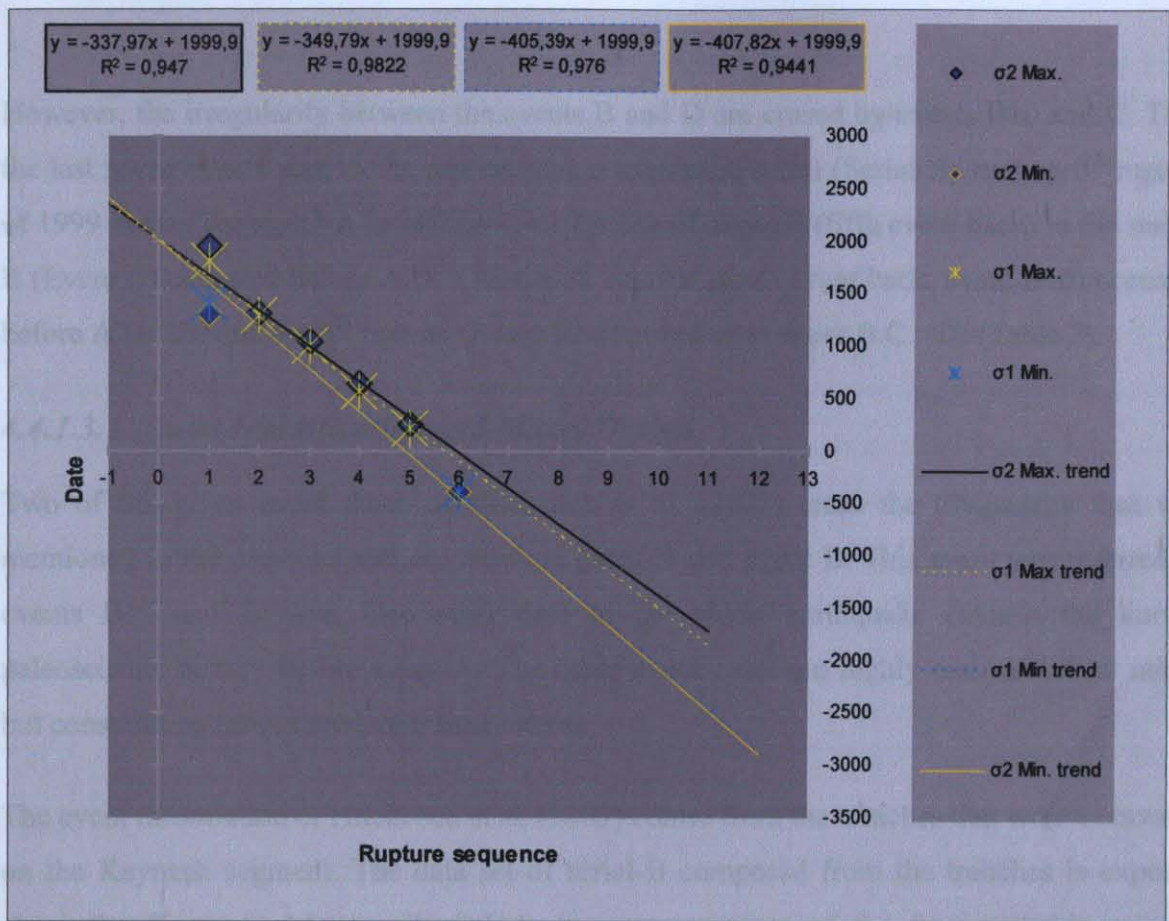


**Figure 68.** Serial-B least square fit of maximum and minimum limits of the maximum and minimum constraining event dates (See table 2). The November 12, 1999 (1999,9) event (0<sup>th</sup> rupture) is set as intercept in regressions. Equations of the trends are shown in boxes colored according to pattern and color of the trend lines. The earthquake recurrence interval value changes between 350 and 405 years according to  $\sigma 1$  interval. The last seven events including 1999 event in the serial are designed using data both from this study and from Hitchcock et al. (2003). The serial seem to be sequential. This serial is extended version of the serial-A including data from the previous study (Fig. 67). The data fills the gaps in my data and extends the serial back in time.

maximum limits (with % 68.2 probability) of events in serial-A, RMS values for the regressions are ranging between 0.83 and 0.94.

#### 4.4.1.3. Serial-B Model

Some paleoseismic events from the previous studies erase a part of the irregularity in the data mentioned before and help to constraint events that could be constraint just from minimum or maximum values. Concerning the previous study of Hitchcock et al. (2003), a new composition suggests that the last seven events seem to formed an event serial (Serial-B). Serial-B is just extended version of the serial-A by adding three events back in time (Fig. 68). In this case, two older events (event A and A10), continue to represent an irregularity.

However, the irregularity between the events B and D are erased by events B10 and C. Thus the last seven events seem to be representing a sequential serial (Serial-B) starting 0<sup>th</sup> rupture of 1999 event (See serial-A in section 4.4.1.2). The 4<sup>th</sup> rupture (fifth event back) in the serial-B (Event C) occurred before A.D. 570, the 5<sup>th</sup> rupture (sixth event back, event B10) occurred before A.D. 220 and the 6<sup>th</sup> rupture (Event B) occurred after about B.C. 400 (Table 2).

#### ***4.4.1.3.1. Event Identification and Model Design***

Two of the given event dates of Hitchcock et al. (2003) erase the irregularity that was mentioned in the previous section, between event D and event B. This event was referred as events B10 and B here. One other date of the oldest earthquake extends the known paleoseismic history before event A. The other event dates are highly comparable to mines but constraining ranges are larger than mines.

The event information of Hitchcock et al. (2003) comes from the trenches that were excavated on the Kaynaşlı segment. The data set of serial-B composed from the trenches is exposed along the Kaynaşlı, Mengencik and Aydınpınar segments of the four probable seismic segments. The event G (November 12, 1999 rupture) was clearly observed on all of the structural segments. According to serial-B model data set, event F (A.D. 1520 and 1800) in Töngelli-1 trench, E (A.D. ? - 1290) in Töngelli-3 trench, D (A.D. ? – 1000) in Bend-3 trench, A (B.C. 1740 - ?) in Töngelli-1 trench were exposed along the Mengencik segment. On the other hand maximum constraints of event C (A.D. ? – 570) was exposed along the Kaynaşlı segment. Event B10 (? - A.D. 220) and A10 (B.C. 2140 - ?) were exposed along the Kaynaşlı segment. On the other hand, event B (B.C. 400 - ?) were exposed in Kaledibi-1 trench along the Aydınpınar segment. Thus, the serial-B is not composed from a specific trench but from the different trenches and structural segments. However, a reasonable relation is also observed between the events in a sequential model (serial-B) as serial-A model (See following paragraphs). The concordance between serial-A and serial-B models including 1999 event strongly suggest the characteristic earthquake recurrence model along the Düzce fault. There is no paleoseismological data from the Efteni segment because the high groundwater level makes very difficult to dig trenches along its zone (See section 4.1). However, the 1999 event rupture that was considered in the serials occurred all the way along the Düzce fault including Efteni segment. This event is considered in the serial, as already mentioned.

The additional data were extracted from the logs of exposures that was published in the paper of Hitchcock et al. (2003). The constraining samples that represent these data were collected near the event horizons. Thus, they are limiting the events just before or after the exact time of the ruptures. The least square fit of maximum limits of maximum constraining dates in serial-A model suggests a maximum constraining date of about A.D. 750 for the 4<sup>th</sup> rupture that C event is assigned (Fig. 67). In this case, the A.D. 570 date is within the range that was suggested by the least square fit. In addition, the maximum and minimum time difference of the maximum limits between the separated events that are following each other in the serial A is 510 and 290 years, respectively. Considering the 69176 maximum constraining sample date maximum time limit difference between the D and C events is about 350 years. This is within the range of the difference of 510 – 290 years. Thus, the date of the 69176 sample is assigned as the maximum constraint of event C.

On the other hand, event B10 seems to be following event C that is represented as the 4<sup>th</sup> rupture in the model. The probability range of maximum constraining sample of 69175 (Table 2) has the maximum limit of A.D. 220 with % 68.2 probability. This date could not be maximum constraint of event B that has a minimum constraint of B.C. 400 because the range between its constraints becomes 620 years in this case. This range is too wide concerning with the range of 400 years of event F. As it was described above, event F has an abnormal range because of the problems in the calibration curves (See section 4.2.3). Thus, B and the B10 events are separated. The maximum and minimum time difference of the serial maximum limits between the separated events that are following each other in the serial A is 510 and 290 years, respectively. This range is same including event C in this model (serial B). The interval between the newly added maximum limit of event C and this maximum limit (event B10) is 350 years. Thus, this interval is within the range of 510 and 290. For this reason, event B10 is considered as the next rupture (the 5<sup>th</sup>) after event C back in time. On the other hand, event B has a just minimum constraint. The serial-B least square fit of maximum limits of maximum constraining dates is suggesting a maximum constraining date of about 0 for the 6<sup>th</sup> rupture. If one consider event B as the 6<sup>th</sup> rupture in the model following back the event D, its date should be between B.C. 400 and 0. A 400 year range for this event is similar to range of event F. On the other hand, considering the event B as the 7<sup>th</sup> rupture, the least square fit of the minimum limits of minimum constraints has worse RMS value than the fit that is modeled considering the event as the 6<sup>th</sup> rupture (Fig. 68). For these reasons, the event B is assigned to the 6<sup>th</sup> rupture (Fig. 69).

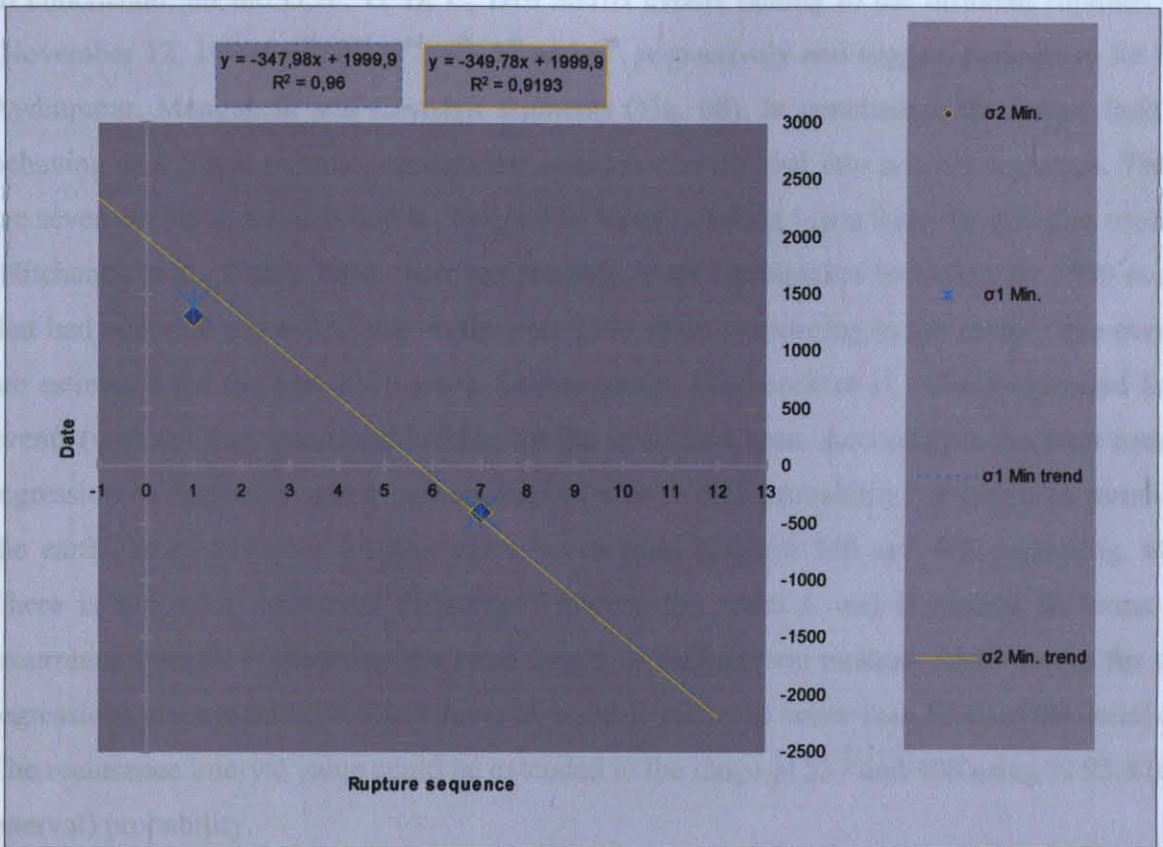


**Figure 69.** Least square fit of the minimum limits of the minimum constraining event dates assigning the event B to the 7<sup>th</sup> rupture (See table 2). RMS values related to this design worse values than the fit that modeled considering the event as the 6<sup>th</sup> rupture. The November 12, 1999 (1999,9) event (0<sup>th</sup> rupture) is set as intercept in regressions. Equations of the trends are shown in boxes colored according to pattern and color of the trend lines.

There is a 1340 years interval between the minimum limits of events B and A. This interval is too high (about three times) considering the 510 – 290 years interval between the maximum limits of the separated events that are following each other in the serial-A and B even considering the maximum interval of 510 years that was resulted in a large range of maximum limiting date of sample R26946/5 (See paragraph above). For this reason, this event can not be located just after the 6<sup>th</sup> rupture as the 7<sup>th</sup> rupture in the sequential model (Fig. 68). Older two events (Event A and A10) seem to be showing an irregularity and do not belong to the seven serial ruptures (Serial-B) from 0<sup>th</sup> to 6<sup>th</sup>. Thus, this events are not used in serial-B model. Hitherto unrecognized earthquakes may erase these irregularity between the events A and B. On the other hand, the oldest event (Event A10) has B.C. 2140 minimum constraining limit. The interval of 400 years between minimum limits of events A and B may suggest that A and A10 events are following each other. Because interval between the maximum limits ranging between 510 and 290 and least square fit of the minimum limits in serial-B and A are suggesting about 400 year interval. This relation is discussed in section 4.4.1.4.

In conclusion, all the G, F, E, D, C, B10 and B events belong to the different ruptures 0<sup>th</sup> (November 12, 1999), 1<sup>st</sup>, 2<sup>nd</sup>, 3<sup>rd</sup>, 4<sup>th</sup>, 5<sup>th</sup> and 6<sup>th</sup>, respectively and suggest periodicity for the Aydınpinar, Mengencik and Kaynaşlı segments (Fig. 68). In conclusion, the Düzce fault is behaving as a single seismic segment and could not be divided into seismic segments. There are seven events in serial-B that is designed by using combined data from the previous studies (Hitchcock et al., 2003). Thus, there are possibly seven earthquakes including the 1999 event that had occurred since B.C. 400 in the past 2400 years. According to the model, five events are estimated for the past 2100 years. Consequently, Hitchcock et al. (2003) estimated four events (with another, questionable fifth) for the same time span. According to the least square regression of maximum and minimum limits (with % 68.2 probability) of events in serial-B, the earthquake recurrence interval value is changing between 350 and 405 years (Fig. 68). There is not much important difference between the serial-A and B models in terms of recurrence interval considering the error ranges of radiocarbon method. RMS values for the regressions are around 0.98. RMS value of serial-B model is better than RMS of the serial-A. The recurrence interval value could be extended to the range of 337 and 408 using % 95.4 ( $\sigma$ 2 interval) probability.

#### **4.4.1.4. Final Serial Model**

##### ***4.4.1.4.1. Distribution for Each Probability***

In this case, each probability distribution of the maximum and minimum constraining dates of events are used in the serial-B instead of using maximum and minimum limits of the maximum and minimum constraining date ranges. Probability distribution of any target rupture event in the sequence is generated using a program code that was designed and written by Ersin KARABUDAK (Boğaziçi University, Department of Mathematics) based on Monte Carlo method. This program generates random samples from each event constraint distribution. According to method, denser random samples were generated from higher probability regions of the each event constraints. Then we applied LSQ to the 100.000 number of random serial. Probability distribution for the target rupture event (E.g., 0<sup>th</sup> rupture of event G or 7<sup>th</sup> unrecognized event) is displayed for the serial that was generated by LSQ estimation.

#### 4.4.1.4.2. Model

Final serial model has been designed by using the distribution for each probability that was mentioned above. First target is the 0<sup>th</sup> rupture that is constantly assigned to the November 12, 1999 event in the sequence. A serial is experimented including A and A10 events. Irregularity of these events in the serial model were removed by concerning two unrecognized events that

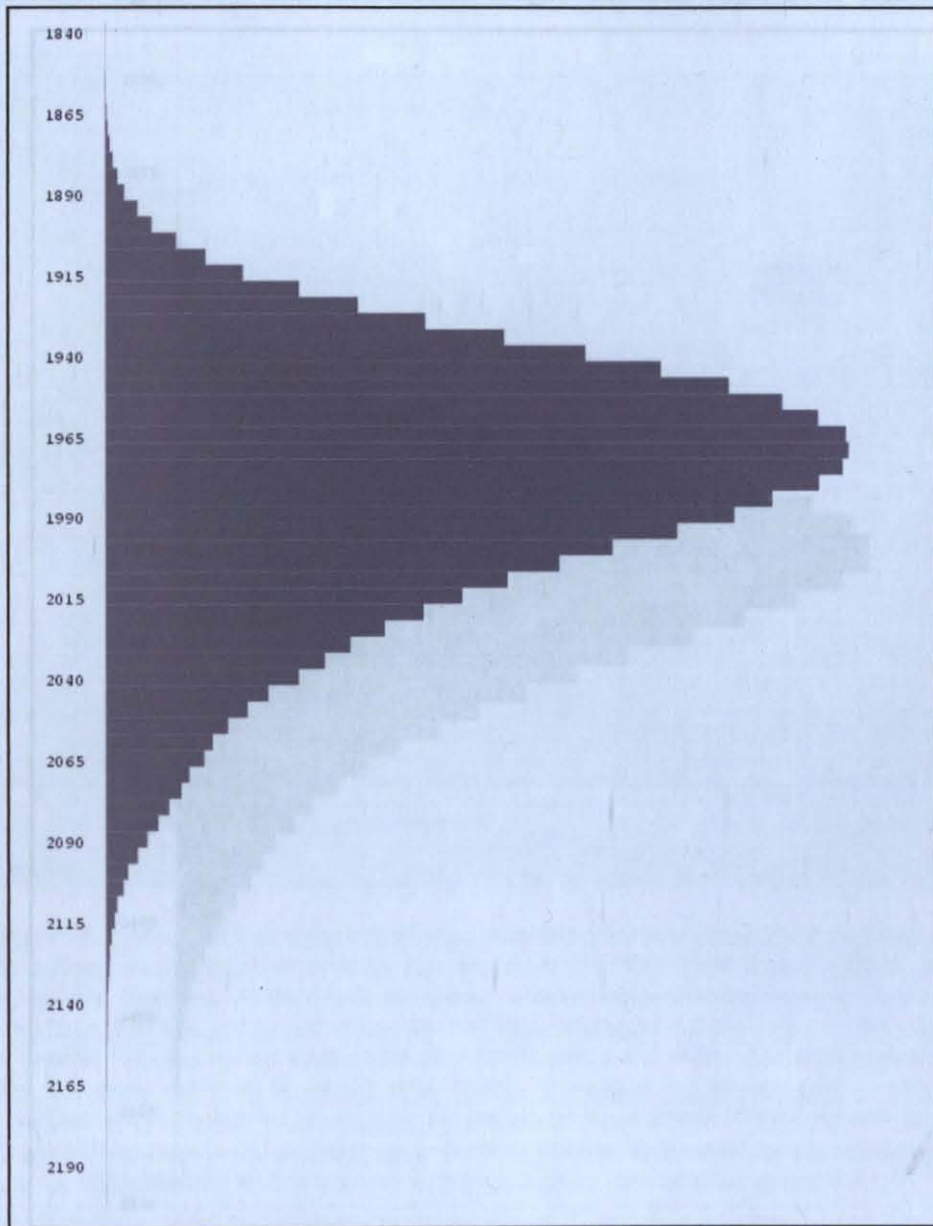


**Figure 70.** Probability distribution for the 1999 rupture (0<sup>th</sup> rupture) according to distribution for each probability of the constraints. This best estimation of the rupture is made by using the design of the final event serial that is shown in figure 72.

were assigned to the 7<sup>th</sup> and the 8<sup>th</sup> ruptures between the event B and event A and an unrecognized event between event A and A10. Thus, the event A and A10 were assigned to the 9<sup>th</sup> and 11<sup>th</sup> ruptures, respectively in the sequence. This design supplies the best estimation for the 1999 rupture. Thus, this is the final serial model. The resulting probability distribution is shown in figure 70. This distribution ranges between A.D. 1935 and 2005 with % 70

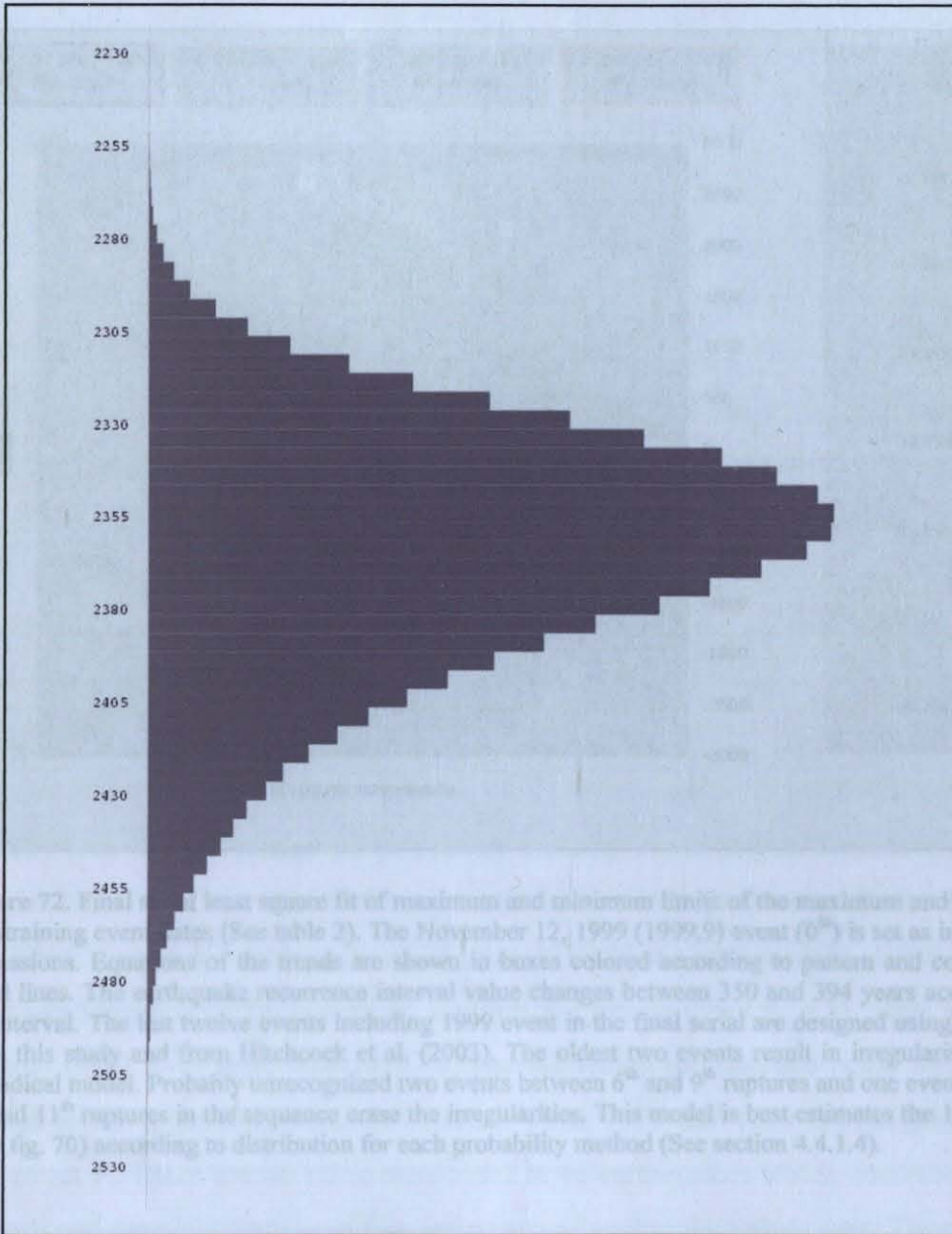


**Figure 71.** Probability distribution of the future rupture (-1<sup>st</sup>) according to distribution for each probability of the constraints. This distribution calculated using the model that best estimates the 1999 (0<sup>th</sup>) rupture (Fig. 70).

between A.D. 2295 and 2415 with % 90 probability. This event is also within the 60 ( $\pm 30$ ) probability. In other words, the predicted date for the 1999 event is about  $1970 \pm 35$  with % 70 probability. The suggested design seems to be successfully predicting the November 12, 1999 event, which is the 0<sup>th</sup> rupture in the serial. This event is also within the 60 ( $\pm 30$ ) year range that has % 62 probability. In the second step, considering this final model, the -1<sup>st</sup> rupture that is the future event in the sequence is taken as a target. The distribution for this event is shown

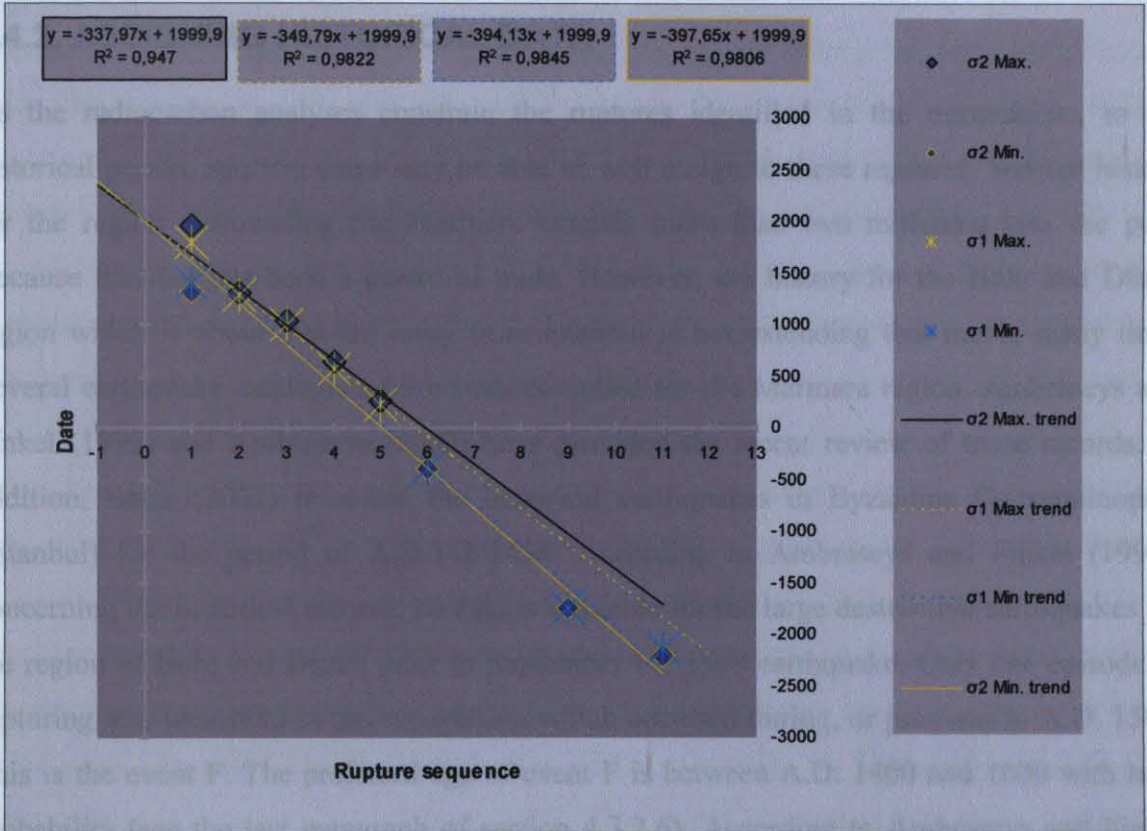


**Figure 72.** Final serial least square fit of maximum and minimum limits of the maximum and minimum constraining event dates (See table 2). The November 12, 1999 (1999,9) event (0<sup>th</sup>) is set as intercept in regressions. Equations of the trends are shown in boxes colored according to pattern and color of the trend lines. The earthquake recurrence interval value changes between 350 and 394 years according to  $\sigma 1$  interval. The last twelve events including 1999 event in the final serial are designed using data both from this study and from Hitchcock et al. (2003). The oldest two events result in irregularities in the periodical model. Probably unrecognized two events between 6<sup>th</sup> and 9<sup>th</sup> ruptures and one event between 9<sup>th</sup> and 11<sup>th</sup> ruptures in the sequence erase the irregularities. This model is best estimates the 1999 event (See fig. 70) according to distribution for each probability method (See section 4.4.1.4).

in figure 71. The probability distribution for this target rupture is ranging between A.D. 2320 and 2390 with % 70 probability. In other words, the predicted date for the first future earthquake is about  $2355 \pm 35$  with % 70 probability. In this case recurrence interval is about  $355 \pm 35$  year (% 70 probability) for the Düzce fault seismic segment. The anticipated range is

between A.D. 2295 and 2415 with % 90 probability. This event is also within the 60 ( $\pm 30$ ) year range that has % 66.5 probability. On the other hand, LSQ fits of the maximum and minimum limits of the maximum and minimum constraining date ranges, respectively suggest a range of 350-394 year for the final model of event rupture serial having about 0.98 and 0.99 RMS values, respectively (Fig. 72). The result is consistent with the range of probability (% 70) distribution of the future earthquake.

#### **4.4.2. ASSIGNING HISTORICAL DATA**

As the radiocarbon analyses constrain the ruptures identified in the excavations, to the historical period, specific dates may be able to well assign to these ruptures. Written history for the region surrounding the Marmara extends more than two millennia into the past. Because İstanbul has been a centre of trade. However, the history for the Bolu and Düzce region which is about 500-km away from İstanbul is not extending that much, many time. Several earthquake catalogues have been compiled for the Marmara region. Ambraseys and Finkel (1995) and Ambraseys (2002) have provided the recent review of these records. In addition, Bakır (2002) reviewed the historical earthquakes in Byzantine Constantinople (İstanbul) for the period of A.D.342-1454. According to Ambraseys and Finkel (1995), concerning the historical records, no data is available for the large destructive earthquakes for the region of Bolu and Düzce prior to September 10, 1509 earthquake. Only one episode of rupturing was identified in the excavations which occurred during, or previous to A.D. 1509. This is the event F. The preferred age of event F is between A.D. 1400 and 1600 with high probability (see the last paragraph of section 4.3.2.6). According to Ambraseys and Finkel (1995), in Düzce area, the destructive next and the last earthquake after the 1509 earthquake in the Düzce area is the earthquake of 25 May 1719 (See also Konukçu, 1984). This is also the first large event after the maximum limiting age for the event F, A.D. 1600 with the high probability (32.2 % of area, Appendix 3). The maximum limiting age could be extending to 1800 with lower probabilities (6.5 % of area). Thus, 1509 and 1719 are the good candidates for the event F. There are no other mentioned large earthquakes which occurred later in the eighteenth and the nineteenth centuries intimately related to the Düzce area. Thus, the episode of rupture can plausibly be associated with any of these two earthquakes (See section 1.1. for detailed information about these historical earthquakes). However, recurrence interval of about  $355\pm 35$  year (% 70 probability) for the Düzce fault segment is suggested by using the probability distributions of event constrains introduced in section 4.4.1.4.2. According to this

estimation penultimate event occurred around A.D. 1645±35. This range is consistent in some case with the 1650-1750 range that was suggested by Emre et al. (2002, 2004) and Sugai et al. (web). However, 1719 earthquake is out of limits of the estimated age in this study on the contrary of the range of 1650-1750. In this case, neither 1509 nor 1719 events can be assigned to any ruptures that occurred along the Düzce fault according to my results. A paleoseismological study conducted in Gölcük by Klinger et al. (2003) suggests that both magnitude and the sense of the dislocation during 1509 at their site were the same as in 1999. According to this suggestion with regarding the felt reports throughout the Mediterranean basin, the rupture of 1509 did not extend through the Düzce basin. However, vertical displacement along a large alluvial fan delta seems to be related to the settlement of unconsolidated loose delta material, related lateral spreading or reactivation of pre-existing secondary weakness zones (Arpat et al., 2001) but is not forming a stepover fault section of a fault rupture. In this case, the amount of displacement in this problematical area may not be a good data for the evaluation of the earthquake magnitude. Therefore, the study of Kiliner et al. (2003) cannot be credited to evaluate possibility that 1509 rupture extends through the Düzce basin. The 1999 Düzce earthquake occurred in the same year with about three months delay after the August, 17<sup>th</sup> 1999 Kocaeli earthquake. Radiocarbon dating will not be efficient to identify these two events as separates one. An extensive study with a large number of trenching critically located along the several structural segments would give a rather reliable magnitude data and therefore the number of the seismic segments involved during the same earthquake. The oldest historical earthquake that is related to the Düzce area is A.D. 967 earthquake in Byzantine period (Bakır, 2002). This earthquake was historically recorded for the region of Bolu. An episode of rupturing was identified in the Bend-3 trench (event D) that occurred before A.D. 1000. The preferred maximum limiting age for the event D is between A.D. 940 and A.D. 1000 with the highest probability (45.3 % of area for  $\sigma_1$  interval having % 68.2 probability) (Table 2). On the other hand, according to the 355±35-year (% 70 probability) interval estimation in section 4.4.1.4.2., the 3<sup>rd</sup> rupture back except November 12, 1999 event is occurred about 935±35 (% 70 probability). In this case the historical earthquake is within the probability range of 935. Thus, the 967 earthquake may be a good candidate for event D that constrains the earthquake about 1000. At this time, there was a small town in Düzce on the contrary, Bolu is an important city (personal communication with Nevra NECİPOĞLU from Boğaziçi University, Department of History and see also Konukçu, 1984). For this reason, it could be recorded just for damage of Bolu area but not for the region of

Düzce. However, it could be still a Bolu fault earthquake. For example Ambraseys and Jackson (1998) assumed to associate this historical event with Bolu fault according to Quaternary or the recent fault rupture. An extensive trenching study along the Düzce fault and the faults close to the Bolu and critical review of the paleoseismological studies along the 1944 Bolu rupture and along the SAIS would give more reliable information about this earthquake. There are controversial ideas about the recurrence interval of the 1944 rupture (Section 3.2.1).

## 5. SUMMARY AND DISCUSSION ON TECTONICS

In Düzce and the surrounding area, a young tectonic cycle (Phase-A) started with an initial stage of a peneplanation. Meandering pattern of stream channels and planar landscape in the peneplain area represented the phase-A. This cycle was followed by uplift (Phase-B) according to the Düzce basin. Some of these streams in uplifted areas that are surrounding the mountains of the Düzce plain have formed the deeply incised meandering water channels during the phase-B. Features such as abandoned terraces along rivers and remnant planar landscapes on the mountain areas are the indicators that are related to the tectonic uplift in the area. The date of the end of the peneplanation event phase (Phase-A) is the minimum limiting date that constrains the age of the Düzce basin. Thus, according to the geological data such as unconsolidated alluvial materials with geomorphological data such as uneroded planar surfaces and terraces along the valleys, the basin is young (Pliocene ?). In addition, the surrounding basins have similar age (See, Emre et al., 1998). Thus, the formation of the Düzce basin is probably related to a well known young tectonic feature of the NAF system that passes the basin. However, no active faulting excluding Düzce and Aksu faults, is detected along all the borders of the basin. On the other hand, all the borders of the basin and their extensions give a remarkable linearity impression that is possibly related to the faults. Some young faulting evidence are obtained along some of the geomorphological lineations. However, some other lineations are related to lithological contrasts and old faults. According to the previous studies, some slices of the basement were thrust in the area and rapid change in lithology is common along linear contacts.

Recent fault traces cross cut many linear boundaries of basins as in the case for the Marmara basins (Arpat and Şentürk, 2000; Le Pichon et al., 2001 and 2003). In addition, some inactive young fault zones are observed along the linearities that are the extensions of the basin boundaries. According to the field observations, no active fault morphology is detected as in the case for the Düzce and Bolu faults and so on along these linearities. On the other hand, based on the paleoseismological findings and rupture process of the 1999 Düzce earthquake, the Düzce fault takes up all the geodetically detected motion between Eurasian plate and the Almacık block. According to these lines of evidence most of the young faults that were responsible to the formation of the basin were probably inactivated in near past. The time of the probable inactivation points out the starting of another phase (active tectonic phase, phase-C) in the Düzce basin area. On the other hand, active pull-apart models were suggested for the

formation of the basins in the Marmara region (E.g., Barka and Kadinsky-Cade, 1988). These suggestions couldn't be accepted without having satisfactory data because of pull-apart and then continuing active formation of the Düzce basin hypothesis is not validated by rigorous data. In addition, several lines of evidence suggest that the active faults of the study area are not a part of a dextral pull-apart system that has been forming the Düzce plain. (1) The Düzce fault is not connecting an active normal fault system bounding the Düzce basin from the west but (2) connecting another dextral fault that is the part of 1999 Kocaeli rupture. (3) There is no significantly recognized connection between the Düzce fault and an active right-lateral fault system to the east to pull-apart the Düzce basin. (4) Furthermore, there is no basin bounding active normal faults along its eastern boundary and (5) no active dextral fault along its northern boundary. The basins in the Marmara region including the Düzce basin are young. However, (6) current tectonic regime across the plains is younger than the basin formation in the Marmara basins region because the east-west dextral shearing system is sometimes cross cutting the plains and their boundaries especially in Marmara sea.

It is probable that the Aegean extensional tectonic regime has played a major role in the motion of the Anatolian block (McKenzie, 1978). On the other hand, the continental collision in the eastern Turkey could have driven the Anatolian block (McKenzie, 1978). Thus, there are contraversary ideas related to driven force for the movement of Anatolian block and the kinematics of the Marmara region (McKenzie, 1978 and Taymaz et al., 1991). None of the models could be chosen in this study as a tectonic base because existing studies are not mature to explain tectonic nature. On the other hand, the reason of the recent inactivation of basin formation process and the inactivation of faults in the study area (change from phase-B to phase-C) must be associated with the recent change in the tectonic system that is considered as a driving force or associated with the evalutional history of the fault systems which is in a trend of obtaining more strait and vertical zones eliminating optimally-oriented zones. Considering the first case, only known recent dramatic change related to probable tectonic forces that drive the tectonics of the Marmara region occurred as continental collision (Pleistocene) in the South Aegean Subduction System (Piper and Perissoratis, 2003). If it is the case, following the collision, the deformation of the Marmara region was possibly restricted to a narrow zone rather than its diffuse and basin forming nature. The resulting narrow dextral zone in Marmara region is representing the NAFZ including its western part. The kinematics of this possiblity is a large matter of debate and should be studied in the future.

## 6. CONCLUSION

The right-lateral motion of the NAF seems to be shared by two active fault strands along the longitude range between the eastern and the western margins of the Almacık Mountain. These are the Northern Almacık Strand (NAIS) and the Southern Almacık strand (SAIS). The NAF along the southern border of the Bolu basin and these fault strands are forming the seismogenic sources that are identified in this study threatening the urbanization in the Düzce plain including the Düzce city. The dextral slip rate of the NAF is about 25 mm/yr. According to GPS measurements, the SAIS and NAIS are taking about 15 and 10 mm/yr of the 25 mm/yr motion, respectively. Consistently, the same  $9.5\pm 1$  mm/yr (% 70 probability) slip rate is calculated according to the paleoseismological findings in this study. The remaining 15 mm/yr movement is probably taken up by the SAIS. However, this suggestion should be verified by the paleoseismological studies along the SAIS.

Seismic surface deformation caused by the 1999 earthquakes along the NAIS are studied in details by using tectonic field observations. Tectonic field studies and the maps of surface deformations of other earthquakes that were occurred in the last 82 years along the SAIS and along the southern border of the Bolu basin are critically reviewed in this study. The NAIS consists of at least two seismic segments. One is the Aksu fault and the other is the Düzce fault. Probable seismic segmentation is configured considering the left stepovers along the Düzce fault (Fig. 27). However, aftershock distribution and some other lines of the evidence about rupture propagation suggest that the Düzce fault seems to be ruptured as a single structural segment. Sequential rupture model and uniform slip distribution that are proposed in this study are also suggesting the same conclusion and further suggesting a single seismic segment for the Düzce fault.

The transpressional character of the Düzce fault could be related to counterclockwise rotation of the Almacık block that forces the location of the shear zone to shift towards the south relative to the Almacık block. The eastern slip-transferring fault may never be found because every shift of the shear zone to the south has resulting in to form a new deformation zone that propagates slowly to the east. The reason of the south directed fault zone migration could be the southwest directed extrusion of the Almacık block (according to the Eurasian plate) along the Aksu fault, because the northern block of the Aksu fault is forming a driving border that has NE-SW elongation.

To the east of the Efteni Lake, the Düzce fault has a typical dextral fault geomorphology having systematic left steppings. Up to 3 km dextral cumulative offset is measured along the fault according to the remnants of Uğursuyu alluvial fan and its stream channels. Taking the maximum offset of 3 km and the slip rate of 10 mm/yr the age of cumulative offset was calculated about 0.03 Ma (upper Pleistocene). This result is concordant with the geological and geomorphological evidence about the age of the active tectonic phase. However, the calculation of 3 km offset may be underestimated concerning the size of the Efteni basin.

The 1999 Kocaeli earthquake rupture zone may be divided into three at least two seismic segments. The Aksu fault that is representing the easternmost segment of the 1999 Kocaeli rupture could be ruptured alone and a smallest unit of propagation on this part along the NAIS. It has 40 km length. About 1.4-m-average and 2-m-maximum right lateral offset are evident from the surface break measurements. On the other hand, the co-seismic deformation characteristics of the surface break markers reveal that the rupture probably has up side north minor reverse component. This could suggest a transpressional character for the fault zone which has N70°E optimally-oriented geometry in the general tectonic movement, driving the Almacık block towards the S70°W direction.

Starting from the east to the west, the three earthquakes in 1944, 1957, 1967 combined to produce a continuous rupture zone all the way along the SAIS. There are controversial ideas about the recurrence interval of the 1944 rupture and the slip distribution of 1944 and 1957 earthquakes. According to the paleoseismological studies along the 1944 rupture, slip calculations are ranging between 7 and 33 mm/yr. The knowledge about the rupture history and the past slips is very limited along the SAIS.

Evidence and reported dates for six large earthquakes in 3540 years before 1800 A.D are described in this study. These events were revealed in five excavations across the middle part of the Düzce fault at three sites along two structural (Mengencik and Aydınpinar) segments. Seven <sup>14</sup>C accelerator mass spectrometry (AMS) dates of the six events are combined with the date data of single documented previous study of Hitchcock et al. (2003) to determine the recurrence intervals for large earthquakes. Three of the given event dates of Hitchcock et al (2003) extend the event serial (Serial-A). A characteristic earthquake model is described considering the maximum values of the maximum limiting age ranges, minimum values of the minimum limiting age ranges of paleoseismic events and the 1999 Düzce event that ruptured

four of the probable seismic segments of Düzce fault. Two oldest events (event A and A10) represent an irregularity in the event serial. The model suggests that the last seven serial events (Serial-B) including the 1999 rupture occurred nearly periodical according to the timing design of events and related constraints. According to the sequential model, the Düzce fault behaves as a single seismic segment. Thus, it could not be divided into seismic segments. There are possibly seven sequential earthquakes including the 1999 event that had occurred since B.C. 400 in the past 2400 years. According to the least square regression of maximum and minimum limits (with % 68.2 probability) of last seven events in serial-B, the earthquake recurrence interval value is changing between 350 and 405 years. RMS values of the serial-B for the regressions are about 0.98. RMS values of the serial-B model that includes additional data from Hitchcock et al (2003) are better than the RMS values of the serial-A.

Each probability distribution of the maximum and minimum constraining dates of the events are also used for the serial-B instead of using maximum and minimum limits of the maximum and minimum constraining date ranges. To do that, Distribution for Each Probability method that bases on Monte Carlo technique is applied. Irregularity of the two oldest events in the serial-B model were removed by concerning two unrecognized events that were assigned to the 7<sup>th</sup> and the 8<sup>th</sup> ruptures between the event B and event A and an unrecognized event between event A and A10. This design supplies the best estimation for the 1999 rupture. Thus, the final serial model consists of the last twelve serial events including the 1999 event. The method and final model are tested taking the target of the November 12, 1999 Düzce event using the last eleven paleoseismic events. Resulting probability distribution ranges between A.D. 1935 and 2005 has % 70 probability. In other words, the predicted date for the 1999 event is about  $1970 \pm 35$  with % 70 probability. The suggested design seems to be successfully predicting the November 12, 1999 event. This event is also within the 30 year range but having % 62 probability. In the second step, considering this final model, the future event is taken as a target. The probability distribution for this target rupture is ranging between A.D. 2320 and 2390 with % 70 probability. In other words, the predicted date for the first future earthquake is about  $2355 \pm 35$  with % 70 probability. In this case, recurrence interval is about  $355 \pm 35$  year (% 70 probability) for the Düzce fault seismic segment. The range is between A.D. 2295 and 2415 with % 90 probability. On the other hand, LSQ fits of the maximum and minimum limits of the maximum and minimum constraining date ranges, respectively, suggest a range of 350-394 year for the final model of the event rupture serial

having about 0.98 and 0.99 RMS values, respectively. The result is consistent with the range of the probability distribution of the future earthquake.

The 1999 Düzce earthquake constrained the location of the fault. Therefore, trenches are excavated across the present surface rupture of the earthquake. The trenches were purposely located in the places of sedimentary environments that were likely to have high sedimentation rate in order to ensure that enough sediment was deposited between the earthquakes to allow individual earthquakes to be distinguished each other. However, this strategy allows the resolution of a small number of events. Common strong erosional and flooding phases make the sedimentation rate unconstant and the strong erosional and flooding phases make it impossible to distinguish different earthquake horizons in one specific trench.

The constraining samples are collected near the event horizons. Thus, they are limiting the events just before or after the exact time of the ruptures. The model is partly concordant with the previous studies. Emre et al (2002, 2004) and Sugai et al (web) excavated trenches along the Aydınpinar and Efteni segments. According to the results ranges of about A.D. 1650-1750 and 665-1050 are suggested for the penultimate (1<sup>st</sup>) and 3<sup>rd</sup> events, respectively. On the other hand, ranges of A.D. 1400-1800 and 1000-? are suggested for the 1<sup>st</sup> and the 3<sup>rd</sup> events, respectively. According to my probability estimation, penultimate event occurred around A.D.  $1645 \pm 35$ . This range is consistent in some case with the 1650-1750 range that was suggested by Emre et al. (2002, 2004) and Sugai et al. (web). However, 1719 historical earthquake is out of limits of the estimated age in this study on the contrary of the range of 1650-1750. In this case, neither 1509 nor 1719 historical events cannot be assigned to any ruptures that occurred along the Düzce fault according to my results. On the other hand, according to the  $355 \pm 35$ -year (% 70 probability) interval estimation, the 3<sup>rd</sup> rupture occurred about  $935 \pm 35$  with % 70 probability. In this case, the A.D. 967 historical earthquake is within the probability range of 935 event. Thus, the 967 earthquake may be a good candidate for event D. However, it could be still a Bolu fault earthquake. Hitchcock et al (2003) described and reported the dates for at least four and possibly five events (including 1999) that occurred in the past 2100 years along the Kaynaşlı segment. Similar result is found in this paleoseismic study. Five events that occurred in the past 1560 years are described. Hitchcock et al (2003) could underestimate one event in the earthquake number since 2100 according to my models because of a possibility of an unrecognized earthquake. The minor span of 87 days between the 1999 Kocaeli and Düzce earthquakes is an interesting point. The delay of 87 days time span between the 1999 events

may suggest the time dependence between the Düzce and Aksu segments. On the other hand, the small delay also results from the coincidence of the period of high stress along the Düzce fault as in the case for the 1999 Düzce event (10<sup>th</sup> rupture) according to my sequential model, with the 1999 Kocaeli rupture that occurred near the Düzce fault. 1999 Kocaeli earthquake probably results in stress transfer on the Düzce fault (Hubert-Ferrari et al., 2000). In this case, the future or the past failure of both the Aksu and Düzce faults with single earthquake is possible.

A reasonable relationship is observed between the events in a sequential model. However, it is fact that this is an experimental study and not sufficient to solve the behavior of the Düzce fault at all. Paleoseismological trenching performed at three sites along the Düzce fault provides the first insights on its seismogenic behavior. The trenches only reveal a 2-D cross-section of the geologic record perpendicular to the fault and so it cannot fully assess the geologic effect of offset. Unfavorable trench material in the stratigraphy and scarcity of datable material made the identification and characterization of individual paleoearthquakes quite difficult and sometimes impossible along the fault. The apparent hiatus in activity before event B argues that periodicity does not hold for this period. Present study with a few paleoseismic trenching along the ~40-km-long Düzce fault does not answer all of the current questions about the nature of serial rupture of the Düzce fault. For example, one of the ages either maximum or minimum is not known for most of the events. In addition, the lengths of ruptures of these paleoearthquakes are not known. The event information comes from the different trenches and some of the trenches are excavated along the different structural segments. Thus, the sequential models is not composed from the specific trench sites but from the different trenches and structural segments. This fact results in an important handicap in my sequential model. There is no paleoseismological data from the Efteni segment because of high watertable level along its zone. However, the 1999 event rupture that was considered in the serials occurred all the way along the Düzce fault including Efteni segment. Only this event was considered for the Efteni segment in the serials as mentioned.

## ACKNOWLEDGEMENTS

This thesis was mostly supported with the project of 01T201D by Boğaziçi University Research Fund, including AMS radiocarbon dating and was partially funded by Boğaziçi University Kandilli Observatory and Earthquake Research Institute. I would like to express my appreciation to the administration of Kandilli Observatory and Earthquake Research Institute and Department of Geophysics of it. I began the thesis with Prof. Dr. Balamir Üçer, as the advisor and continued with Prof. Dr. Cemil Gürbüz. Prof. Cemil Gürbüz read this thesis critically and offered numerous valuable suggestions. I sincerely thank them because of their supports for encouraging me to start and complete the thesis, and their genuine advices for the whole content of my thesis. The subject and the scope of the thesis were designed by the help of Esen Arpat in every steps of this study. I am grateful to Esen Arpat for suggesting the problems that I concerned, inspiring guidance from the initial field work to the completion of the thesis and critically reviewing the manuscript. I thank Prof. Dr. Aykut Barka for his help, support and advices in the initial stages of this design. I wish to thank Prof. Y. Ikeda for guiding this study from the initial field work. I thank Mustafa Aktar for his helpful advices and suggestions.

I thank to Profs. Hadi Özbal, Caroline Finkel and Mehmet Özdoğan for inspiring guidance concerning historical earthquakes. I am grateful to Prof. Dr. Nevra Necipoğlu, Dr. Aslı Özyar and Mevlüde Bakır, for valuable information about historical earthquakes. I am indebted to Prof. Dr. Alp Eden and Ersin Karabudak for providing prior to programming and the application of statistical methods.

I thank my family, especially my wife, who checked every lines of the thesis in a critical short time, because of persuading me to start the thesis and their moral support. I thank Dr. Tolga Bekler, who supply special effort about pressing the documents, Dr. Bülent Tank, Birsen Can and Ethem Görgün, for their review and suggestions.

I wish to thank Recai Akyel, the governor of Gölyaka village, for giving me the full backing of his office during my field study. I thank the commandership of gendarme, the governorship of Gölyaka and Düzce, and the headman of Kadifekale for accomodation. I thank Fevzi Çelebi and his father for giving valuable information and discussing about the historical earthquakes in the region. I am thankful to Hasırcılar company, the fire brigade and the governorship of Düzce, the municipalities and mayors of Beykoz, Kaynaşlı and Gölyaka because of providing the equipment, excavator and transport. The success of the field program was due in part to the generous hospitality extended to me by Süavi Şakar, Sema Şakar, Aslı and Çağla Tütüncüoğlu of Düzce. I am grateful to the people in the region, especially to f. Kazım for accommodation, for their generous help during the site inspections, for their hospitality and for giving the knowledge about Efteni thermal spring.

## REFERENCES

- Abdüsselamoğlu, M. Ş., 1959. Almacıkdağı ile Mudurnu ve Göyçük Civarının Jeolojisi., İstanbul Üniv. Fen Fak. Monografileri (Tabii İlimler Kısmı), 14, 94p.
- Akartuna, M. 1968. The Geology of Armutlu Peninsula, İstanbul Üniversitesi Bülteni. 20:1-105.
- Akyüz, H. S., Barka, A., Altunel, E., Hartleb, R. and Sunal, G., 2000. Field Observations and Slip Distribution of the November 12, 1999 Duzce Earthquake (M=7.1), Bolu - Turkey., The 1999 İzmit and Düzce Earthquakes: Preliminary Results., 63-70.
- Akyüz, H. S., Hartleb, R., Barka, A., Altunel, E., Sunal, G., Meyer, B. and Armijo, R., 2002. Surface Rupture and Slip Distribution of the 12 November 1999 Düzce Earthquake (M 7.1), North Anatolian Fault, Bolu, Turkey, Bull. Seism. Soc. Am., 92, 1, 61-66.
- Ambraseys, N., 2002. The Seismic Activity of the Marmara Sea Region over the Last 2000 Years, Bull. Seism. Soc. Am., 92, 1, 1-18.
- Ambraseys, N. N. and Finkel, C. F., 1995. The Seismicity of Turkey and Adjacent Areas: A Historical Review, 1500-1800. Eren, 240p.
- Ambraseys, N. N. and Jackson, J. A., 1998. Faulting associated with historical and recent earthquakes in the Eastern Mediterranean region. Geophys. J. Int., 133, 390-406.
- Ambraseys, N. N. and Jackson, J. A., 2000. Seismicity of the Sea of Marmara (Turkey) since 1500., Geophys. J. Int., 141, 3, F1.
- Ambraseys, N. N., Zatopek, A., Taşdemiroğlu, M. and Aytun, A., 1968. The Mudurnu valley, West Anatolia earthquake of 22 July 1967, UNESCO Publ. 22, 135pp.
- Ambraseys, N. N., and Zatopek, A., 1969. The Mudurnu Valley, West Anatolia, Turkey, Earthquake of 22 July 1967. Bull. Seism. Soc. Am., 59, 521-589.
- Ardel, A., 1964. Batı Karadeniz bölgesi'nde Morfolojik Müşahadeler. İst. Üniv. Coğr. Enst. Der. VII, 14, 62-75.
- Argus, D. F., Gordon, R. G., DeMets, C. and Stein, S., 1989. Closure of the Africa - Eurasia - North America Plate Circuit and Tectonics of the Gloria Fault., J. Geophys. Res., 94, 5585-5602.
- Arnold, J. R. and Libby, W. F., 1949. Age Determinations by Radiocarbon Content: checks with samples of Known Age. Science, December, 23, 110.
- Arpat, E. and Bingöl, E., 1969. Ege Bölgesi Graben Sisteminin Gelişimi Üzerine Düşünceler., M.T.A. Derg., 73, 1-9.
- Arpat, F., Herece E., Komut, T. and Özgül, N., 1999web. 12 Kasım 1999 Düzce Depremi İlk Üç Günlük Jeolojik Saha Verilerinin Ön Değerlendirmesi. <http://www.koeri.boun.edu.tr/>

jeofizik/duzce1.html, first appeared on 20<sup>th</sup> Novebber 1999 and last seen on 26<sup>th</sup> February 2003.

Arpat, E., Herece, E., Komut, T. and Şentürk, K., 2001. 1999 Kocaeli ve Düzce Depremlerine neden olan fayların Marmara Bölgesinin sismotektonik yapısı içindeki yeri. 54<sup>th</sup> Geological Congress of Turkey, May 7-10, 2001, Ankara, Proceeding no: 54-29.

Arpat, E. and Şentürk, K., 2000. Marmara Denizi nin Gelişimi., Marmara Denizi 2000 Sempozyumu (11-12 Kasım 2000, İstanbul), 231-237.

Aydın, A. and Kalafat, D., 2002. 17 August and 12 November 1999 İzmit and Düzce Earthquakes in Northwestern Anatolia, Turkey: Their Tectonic and Kinematic Significance and the Associated Damage., Bull. Seism. Soc. Am., 92, 1.

Ayhan, M. A., Demir, C., Kiliçoğlu, A., Sanlı, I. and Nakiboglu, S. M., 1999. Crustal motion around the Western Segment of the North Anatolian Fault Zone: Geodetic Measurements and Geophysical Interpretation. International Union of Geodesy and Geophysics (IUGG 99), 18-30 July, Birmingham, United Kingdom, 1999.

Ayhan, M. E., Bürgmann, R., McClusky, S., Lenk, O., Aktug, B., Herece, E. and Reilinger, R. E., 2001. Kinematics of the Mw = 7.2, 12 November 1999, Düzce, Turkey Earthquake. Geoph. Res. Let., 28, 2, 367-370.

Bakır, M., 2002. Impact and Consequences of Earthquakes in Byzantine Constantinople and its Vicinity, A.D.342-1454., Ms. Thesis, Boğaziçi Univesity, 214p.

Barka, A. A., 1992. The North Anatolian Fault., *Annales Tectonicae*, 6, 164-195.

Barka, A. A., 1996. Slip Distribution Along the North Anatolian Fault Associated with the Large Earthquakes of the Period 1939 - 1967., Bull. Seism. Soc. Am., 86, 1238-1254.

Barka, A. A. and Kadinsky-Cade, K., 1988. Strike-slip Fault Geometry in Turkey and its influence on Earthquake Activity. *Tectonics*, 7, 3, 663-684.

Bingöl, E., Akyürek, B. and Korkmazer, B., 1973. Geology of the Biga peninsula and some characteristics of the Karakaya formation. Papers Congress of Earth Sciences on the Occasion of the Fifth Anniversary of the Tukiş Republic, Ankara, MTA (Ed.: S. Doyuran). 71-77

Bingöl, E. and Şengün, M., 1988. Geological Evolution of Anatolia from Paleozoic to Paleogen. A Plate Tectonic Interpretation. MTA, Ankara, (unpublished repord) p5.

Birgören, G., Sekiguchi, H. and Irikura, K., 2004. Rupture Model of the 1999 Düzce, Turkey, Earthquake Deduced from High and Low Frequency Strong Motion Data., *Geophys. Res. Letts.*, 31, 5, L05610.

Blumenthal, M., 1941. Eskipazar Transversal Dağlarının Jeolojisi ve Madensuyu Menbaları. MTA Bulletin, 4, 25, 550-593.

Bock, G., Tibi, R., Baumbach, M., Grosser, H., Milkereit, C., Kind, R. and Zschau, J., 2000. Rupture Processes of the August 17 İzmit and November 12, 1999 Düzce (Turkey) Earthquake., *The 1999 İzmit and Düzce Earthquakes: Preliminary Results.*, 106-108.

- Bonilla, M. G., and Lienkaemper, J. J., 1990. Visibility of Fault Strands in Exploratory Trenches and Timing of Rupture Events. *Geology*, 18, 153-156.
- Bouchon, M., Bouin, M-P., Karabulut, H., Toksöz, M. N., Dietrich, M. and Rosakis, A. J., 2001. How Fast is Rupture during an Earthquake? New Insights from the 1999 Turkey Earthquakes., *Geophys. Res. Letts.*, 28, 14.
- Bronk Ramsey, C. 1995 Radiocarbon Calibration and Analysis of Stratigraphy: The OxCal Program *Radiocarbon* 37(2) 425-430
- Bronk Ramsey, C., 2001, Development of the Radiocarbon Program OxCal, *Radiocarbon*, 43 (2A) 355-363.
- Bronk Ramsey, C., web. Online version of the OxCal program, Ver. 3.9, Oxford Radiocarbon Accelerator Unit, <http://www.rlaha.ox.ac.uk/orau/index.html> (first accessed on August 11, 2004)
- Bürgmann, R., Ayhan, M. E., Fielding, E. J., Wright, T. J., McClusky, S., Aktug, B., Demir, C., Lenk, O. and Türkezer, A., 2002. Deformation during the 12 November 1999 Düzce, Turkey, Earthquake, from GPS and InSAR Data. *Bull. Seis. Soc. Am.*, 92, 1, 161-171.
- Canitez, N. and Üçer, B., 1967. A Catalogue of Focal Mechanism Diagrams for Turkey and Adjoining Areas, İ. T. Ü. Maden Fak. Yay.
- Chase, C. G., 1978. Plate Kinematics: the Americas, East Africa, and the Rest of the World., *Earth Planet. Sci. L*, 37, 355-368.
- Cianetti, S., Gasperini, P., Boccaletti, M. and Giunchi, C., 1997. Reproducing the Velocity and Stress Field in the Aegean Region., *Geophys. Res. Letts.*, 24, 16, 2087-2090.
- Çakır, Z., Barka, A. A., De Chabaliere, J-B., Armijo, R. and Meyer, B., 2003. Kinematics of the November 12, 1999 (Mw=7.2) Düzce Earthquake Deduced from SAR Interferometry., *Tr. J. of Earth Sciences TÜBİTAK*, 12, 105-118.
- DeMets, C., Gordon, R. G., Argus, D. F. and Stein, S., 1990. Current Plate Motions, *Geophys. J. Int.*, 101, 425-478.
- DeMets, C., Gordon, R. G., Argus, D. F. and Stein, S., 1994. Effects of Recent Revisions to the Geomagnetic Reversal Time Scale on Estimates of Current Plate Motions., *Geophys. Res. Letts.*, 21, 2191-2194.
- Demirtaş, 1992. İğneciler (Bolu)-Dokurcun (Adapazarı) Arasında Kuzey Anadolu Fay Zonunun Neotektoniği ve Depremselliği. Ms. Thesis, Ankara University, Turkey.
- Demirtaş, 2000. Kuzey Anadolu Fay Zonu'nun Abant-Gerede Arasında Kalan Bölümünün Neotektonik Özellikleri ve Paleosismisitesi. PhD Thesis, Ankara University, Turkey.
- Demirtaş, R., Gökten, E. and Özaksoy, V., 1997. Kuzey Anadolu Fayı Gerede Segmenti Batı Kesiminde Aktif Tektonik Çalışmaları; 1997 Abant Trenchi (hendek) Ön Sonuçları., *Aktif*

Tektonik Araştırma Grubu, I. Toplantısı, Makaleler, 9-9.

DePaolo, C. M., Clarck, D. G., Slemmons, D. B., and Ramelli, A. R., 1991. Historical Surface Faulting in the Basin and Range Province, Western North America: Implications for Fault Segmentation. *Journal of Structural Geology*, 13, 123-136.

Doğan, B., 2001. İzmit Körfezi Çevresinin Kuvaterner Stratigrafisi ve Tektonik Modeli., 54. Türkiye Jeoloji Kurultayı.

Elmore, D. and Phillips, F. M., 1987. Accelerator mass spectrometry for measurement of long-lived radioisotopes. *Science*, 236, 543-550.

Emre, Ö., Erkal, T., Tchapylyga, A., Kazancı, N., Keçer, M. and Ünay, E., 1998. Doğu Marmara'nın Neojen ve Kuvaterner'deki Evrimi. MTA bulletin, 120.

Emre, Ö., et al., 1999. 17 Ağustos 1999 Depremi Sonrası Düzce (Bolu) İlçesi Alternatif Yerleşim Alanlarının Jeolojik İncelemesi. MTA and Ankara Üniversitesi Ortak Araştırma Projesi, unpublished project report, Ankara, TÜBİTAK, 59p.

Emre, Ö., Duman, T. Y., Doğan, A., Özalp, S. and Çörekçioğlu, E., 2000. 12th November 1999 Düzce Earthquake on the North Anatolian Fault Zone, Turkey., *Active Fault Research for the New Millennium, Hokudan International Symposium and School on Active Faulting (17-26 January 2000)*, 75-79.

Emre, Ö., Duman, T. Y., Toda, S., Okuno, M., Dogan, A., Özalp, S., Tsutsumi, H., Tokay, F., Haraguchi, T., Kondo, H., Sugito, N. and Nakamura, T., 2002. Paleoseismicity of Düzce Fault in the Last Millennium, North Anatolian Fault Zone (NAFZ), Turkey., *1st International Symposium of the Faculty of Mines (İTÜ) on Earth Sciences and Engineering 16-18 May 2002, İstanbul, Turkey*, 59-59.

Emre, Ö., Awata, Y. and Duman, T. Y., 2003. Surface Rupture Associated with the August 17, 1999 İzmit Earthquake. *Special Publication Series – 1, MTA Ankara*, 280p.

Emre, O., Toda, S., Doğan, A., Awata, Y., Tokay, F. and Ozalp, S., 2004. Paleoseismic Behaviour of the Karadere Fault Between İzmit and Düzce Ruptures in 1999, North Anatolian Fault, Turkey. *32nd IGC, Florence 2004 - Abstracts*.

Erendil, M., Kuşçu, I. and Kato, H., 1988. Tectonics of Armutlu Peninsula (Turkey): Aspects of the western North Anatolian Fault Zone. *Report of International Research and Development Cooperation ITIT-Project, no: 8513, Research on Quaternary Crustal Movement and Earthquake Prediction. MTA, Turkey*.

Ergintav, S., Bürgmann, R., McClusky, S., Çakmak, R., Reilinger, R. E., Lenk, O., Barka, A. and Özener, H., 2002. Postseismic Deformation near the İzmit Earthquake (17 August 1999, M7.5) Rupture Zone., *Bull. Seism. Soc. Am.*, 92, 1, 194-207.

Erinç, S., Bilgin, T. and Bener, M., 1961. Melen boğazı. *İst. Üniv. Coğr. Enst. Der.*, 12, 161-165.

Finkel, R. and Suter, M., 1993. AMS in the Earth Sciences: Technique and applications. *Advances in Analytical Geochemistry*, 1, 1-114.

Gaiser, A., 1991. Geologie und Tektonik der Abant-Silsilesi SE des Abant-Sees (Türkei). Diplomarbeit, Universität Tübingen.

Gökten, E., 2004. Present Stress Distribution and the Earthquake Risk of the Bolu pull-apart basin in the North Anatolian Fault Zone, west Turkey. 32<sup>nd</sup> IGC Conference, 2004, August, Floreçe.

Gökten, E., Çemen, I., Özaksoy, V. and Erkmen, C., 1999. The Mechanism of the 17 August 1999 İzmit-Adapazarı Earthquake, NW Turkey. *International Conference on Earthquake Hazard and Risk in the Mediterranean Region. EHRMR'99 Abstracts*, Near East University. 18-22 October 1999 Nicosia, North Cyprus, 19-19.

Gözübol, A. M., 1978. Mudurnu – Dokurcun – Abant Yöresinin Jeolojisi ve Kuzey Anadolu Yarılıminin Yapısal Özellikleri. PhD Thesis, İstanbul University.

Herece, E., 2003. Marmara Denizi Doğusundaki Kuzey Anadolu Fayı (KAF)'nın Batı Bölümünün Depremselliği. *Marmara Denizi ve Doğu Marmara'nın depremselliği Konferansları- 2 kitabı, JMO 30. yıl Etkinlikleri*, 18 August, 2003 İzmit, 11-28.

Herece and Akay, 2003. Atlas of North Anatolian Fault (NAF) Scale: 1/100 000. MTA Special Publication Series, Ankara.

Herford, M., 1991. Stratigraphie und Tektonik der Abant Silsilesi in Nordanatolied, NW-Türkei. Diplomarbeit, Universität Tübingen.

Hitchcock, C., Altunel, E., Barka, A., Bachhuber, J., Lettis, W., Kozacı, Ö., Helms, J. and Lindvall, S., 2003. Timing of Late Holocene Earthquakes on the Eastern Düzce Fault and Implications for Slip Transfer between the Southern and Northern Strands of the North Anatolian Fault System, Bolu, Turkey., *Tr. J. of Eath Sciences TÜBİTAK*, 12, 119-136.

Hubert-Ferrari, A., Barka, A., Nalbant, S. S., Jacques, E., Meyer, B., Armijo, R., Tapponnier, P. and King, G. C. P., 2000. 17 Ağustos 1999 İzmit Depremi Sonrasında Marmara da Deprem Riski., *Bilim ve Teknik*, Nisan, 54-58.

Huss, A.R., 1992. Eine Spannungskonzentration an der Nordanatolischen Störung zwischen Bolu und Adapazarı/Nordwest-Türkei – ein Finite-Element-Modell. University of Tübingen, PhD, Dissertation, 185 p.

Iio, Y., Horiuchi, Ş., Barış, Ş., Çelik, C., Kyomen, J., Üçer, B., Honkura, Y. and Işıkara, A. M., 2002. Aftershock Distribution in the Eastern Part of the Aftershock Region of the 1999 İzmit, Turkey, Earthquake. *Bull. Seism. Soc. Am.*, 92, 1, 411-417.

Ikeda, Y., 1983. Thrust-front Migration and its Mechanisms-evolution of Interplate Thrust Fault Systems. *Dept. Geography, University of Tokyo Bulletin*, 15, 125-159.

Ikeda, Y., Suzuki, Y., Herece, E., Şaroğlu, F., Işıkara, A. M. and Honkura, Y., 1991. Geological Evidence for the Last Two Faulting Events on the North Anatolian Fault Zone in

the Mudurnu Valley, Western Turkey., *Tectonophysics*, 193, 335-345.

Ikeda, Y., Herece, E., Suzuki, Y., Tatar, Y., 1994. Late Holocene Activity of the North Anatolian Fault from Gerece to İsmetpaşa, Western Turkey: Preliminary Results., *Multidisciplinary Research on Fault Activity in the Western Part of the North Anatolian Fault Zone (5)* (Eds: A. M. Işıkara and Y. Honkura), Tokyo, 5-14.

Ikeda, Y. and Komut, T., 1999. Surface Ruptures Associated with the Kocaeli, Northwestern Turkey, Earthquake of August 17, 1999, Programme and Abstracts, The Seismological Society of Japan, 1999 Fall Meeting, A64 (in Japanese), 1999.

Irmak, T. S., 2000. 12 Kasım 1999 Düzce Depremi Kaynak - Yırtılma Mekanizması., *Aktif tektonik Araştırma Grubu*, 4. Toplantısı, Bildiri Özetleri, 21-21.

İleri, N. and Gökten, E., 2002. Kuzey Anadolu Fayı Sapanca-Gölyaka segmentinin Aksu deresi kesimindeki yapısal kontrollü kütle hareketleri. *Aktif Tektonik Araştırma Grubu Toplantısı – 6 (ATAG-6)*, Ankara, Abst. 75.

Jackson, J. A., 1992. Partitioning of Strike-slip and Convergent Motion between Eurasia and Arabia in Eastern Turkey and the Caucasus. *Jour. Geophys. Res.*, 97, 12471-12479.

Jackson, J. and McKenzie, D. P., 1984. Active Tectonics of the Alpine Himalayan Belt Between Western Turkey and Pakistan., *Geophys. J. R. Astron. Soc.*, 77, 185-246.

Jackson, J. A., Haines, J. and Holt, W., 1994. A Comparison of Satellite Laser Ranging and Seismicity Data in the Aegean Region, *Geophys. Res. Letts.*, 21, 25, 2849-2852.

Kahle, H-G., Cocard, M., Peter, Y., Geiger, A., Reilinger, R., Barka, A. and Veis, G., 2000. GPS-derived Strain Rate Field within the Boundary Zones of the Eurasian, African, and Arabian Plates. *Jour. Geophys. Res.*, 105, B10, 23353-23370.

Kamen, M. D., 1963. Early history of carbon-14. *Science* 140, 584–90.

Ketin, İ., 1948. Son on yılda Türkiye’de vukua gelen büyük depremlerin tektonik ve mekanik nicelikleri hakkında. *T.J.K. Bült.*, 2, 1, 1-13.

Ketin, İ., 1969. Kuzey Anadolu Fayı Hakkında., *M.T.A. Bulletin of Turkey*, 72, Nisan, 1-27.

King, G and Nabelek, J. L., 1985. Role of Fault Bends in the Initiation and Termination of Earthquake Rupture, *Science*, 228, 984-987.

Klinger, Y., Sieh, K., Altunel, E., Akoglu, A., Barka, A., Dawson, T., Gonzalez, T., Meltzner, A. and Rockwell, T., 2003. Paleoseismic Evidence of Characteristic Slip on the Western Segment of the North Anatolian Fault, Turkey., *Bull. Seism. Soc. Am.*, 93, 6, 2317-2332.

Komut, T., 1998. A Review of the Tectonics of the Tectonics of the Aegean Region. Ms. Thesis, Boğaziçi University, 254p.

Komut, T. and Ikeda, Y., 2000. 17/08/1999 Kocaeli Depremi Yüzey Kırığı’nın Arazi İncelemesi., *Aktif Tektonik Araştırma Grubu*, 3. Toplantısı, 44-50.

- Kondo, H., Awata, Y., Omer, E., Dogan, A., Ozalp, S., Tokay, F., Yildirim, C., 2002. Re-evaluation of Fault Geometry and Slip Distribution of the 1944 Bolu-Gerede Earthquake Rupture, North Anatolian Fault System, Turkey., *Eos. Trans. AGU*, 83(47), Fall Meet. Suppl., Abstract, S11B-1154 0830h POSTER.
- Konukçu, E., 1984. Düzce Tarihi (İlk Devirlerden Cumhuriyete), *Türkiye İmar Turizm ve Sanayi Mecmuası*, 212-133, 18, 12-23.
- Le Pichon, X. and Angelier, J., 1979. The Hellenic Arc and Trench System: A Key to the Neotectonic Evolution of the Eastern Mediterranean Area, *Tectonophysics*, 60, 1-42.
- Le Pichon, X., Chamot-Rooke, N., Lallemand, S., Noomen, R. and Veis, G., 1995. Geodetic Determination of the Kinematics of Central Greece With Respect Europe: Implications for Eastern Mediterranean Tectonics., *J. Geophys. Res.*, 100, B7, 12,675-12,690.
- Le Pichon, X., Chamot-Rooke, N., Rangin, C. and Şengör, A. M. C., 2003. The North Anatolian Fault in the Sea of Marmara. *J. Geophys. Res.* 108, B4, 2179.
- Le Pichon, X., Şengör, A. M. C., Demirbağ, E., Rangin, C., İmren, C., et al., 2001. The Active Main Marmara Fault. *Earth Planet. Sci. Lett.*, 192, 595-616.
- Lyberis, N., 1984. Tectonic Evolution of the North Aegean Trough. *Geological Evolution of the Eastern Mediterranean*.
- Maiwald, U., 1991. Geologische Kartierung des Mudurnutales im Bereich der Nordanatolischen Störungzone bei Yongalik, NW Türkei. Zur Abhängigkeit des Radongehaltes in Quellwassern vom Urangehalt der Grundwasserleiter – Hydrochemische und Grammaspektroskopische Untersuchungen. Diplomarbeit, Universität Kiel.
- McCalpin, J. P., 1996. *Paleoseismology*. Academic Press, 588p.
- McClusky, S., Balassanian, S., Barka, A., Demir, C., Ergintav, S., Georgiev, I., Gurkan, O., King, R., Kotsev, V., Lenk, O., Mahmoud, S., Mishin, A., Nadariya, M., Ouzounis, A., Paradissis, D., Peter, Y., Prilepin, M., Reilinger, R., Sanli, I., Seger, H., Tealeb, A., Toksöz, M. N. and Veis, G., 2000. Global Positioning System constraints on plate kinematics and dynamics in the eastern Mediterranean and Caucasus. *J. Geophys. Res.*, 105, 5695-5720.
- McKenzie, D. P., 1972. Active Tectonics of the Mediterranean Region., *Geophys. J. R. Astron. Soc.*, 30, 109-.
- McKenzie, D. P., 1978. Active Tectonics of the Alpine-Himalayan Belt: the Aegean Sea and Surrounding Regions (Tectonics of Aegean Region), *Geophys. J. R. Astron. Soc.*, 55, 217-254.
- Meade, B. J., Hager, B. H., McClusky, S. C., Reilinger, R. E., Ergintav, S., Lenk, O., Barka, A. and Özener, H., 2002. Estimates of Seismic Potential in the Marmara Sea Region from Block Models of Secular Deformation Constrained by Global Positioning System Measurements., *Bull. Seism. Soc. Am.*, 92, 1, 208-215.

Meghraoui, M., Pantosti, D., Akyüz, H.S., Leroy, S., Mai M., Atakan, K. 2004, The RELIEF Project : Large earthquake faulting and implications for the seismic hazard assessment in Europe, the 1999 İzmit-Düzce earthquake sequence (Mw 7.3 - 7.1, Turkey). 32nd IGC, Florence 2004 - Abstracts, p. p. 123.

Michel, G. W., 1990. Ein Plosspannungspfad an der North-Anatolischen Störung vorn Alttertiar bis heute (Dokurcun, Türkei). TSK 3, 138.

Michel, G. W., 1994. Neo-Kinematics along the North-Anatolian Fault (Turkey). University of Tübingen, PhD, 248p.

Milkereit, C., Zünbül, S., Karakisa, S., Irvul, Y., Zschau, J. (SABO grup), Baumbach, M., Grosser, H., Günther, E., Umutlu, N., Kuru, T., Erkul, E., Klinge, K., Ibs von Scht, M., Karahan, A. and Task Force, 2000. Preliminary Aftershock Analysis of the Mw=7.4 Izmit and Mw=7.1 Düzce Earthquake in Western Turkey., The 1999 İzmit and Düzce Earthquakes: Preliminary Results., 179-187.

MTA, 2000. Geology Map of Turkey (1:100.000). The Institute of General Directorate of Mineral Research and Exploration (MTA), Ankara.

Mueller, S., Kahle, H.-G. and Barka, A., 1997. Plate Tectonic Situation in the Anatolian-Aegean Region., ATNAMPP, 13-28.

Neugebauer, J., Löffler, M., Berckhemer, H. and Yatman, A., 1997. Seismic Observations at an Overstep of the Western North Anatolian Fault (Abant - Sapanca Region, Turkey)., Geol Rundsch, 86, 93-102.

NNSA, 2003. Nuclear Explosion Monitoring: Building the Knowledge Base, 25<sup>th</sup> Seismic Resaearch Review, Tuscon, Arizona, September 23-25, 2003 (<https://www.nemre.nnsa.doe.gov>, accessed on May 28, 2005).

Noomen, R., Ambrosius, B. A. C. and Wakker, K. F., 1993. Crustal Motions in the Mediterranean Region Determined from Laser Ranging to LAGEOS., Contributions of Space Geodesy to Geodynamics: Crustal Dynamics, Geodyn. Ser. (Eds: D. E. Smith and D. L. Turcotte), 23, 331-346.

Nowack, E., 1932. Kreide-Entwicklung und Gross-Tektonik in North Anatolien, Centralblatt. Min., etc., B., 286-299.

Nurlu, M., Görmüş, S. and Özmen, B., 1999. New Approach: Potantial Earthquake Risk and Hazard Model by using Geographical Information System. International Conference on Earthquake Hazard and Risk in the Mediterranean Region. EHRMR'99 Abstracts, Near East University. 18-22 October 1999 Nicosia, North Cyprus, 144-144.

Okumura, K., Awata, Y., Duman, T. Y., Tokay, F., Kuscu, I. and Kondo, H., 2002. Rupture History of the 1944 Bolu-Gerede Segment of the North Anatolian Fault: Gerede-Ardicli Trench Re-excavated., Eos. Trans. AGU, 83(47), Fall Meet. Suppl., Abstract, S11B-1155 0830h POSTER.

- Oral, M. B., 1994. Global Positioning System (GPS) Measurements in Turkey (1988-1992): Kinematics of the Africa-Arabia-Eurasia Plate Collision Zone, Ph.D. Thesis., Mass. Inst. of Tech., Cambridge, 344.
- Oral, M. B., Reilinger, R. E. and Toksöz, M. N., 1993. Preliminary Results of 1988 and 1990 GPS Measurements in Western Turkey and their Tectonic Implications., Contributions of Space Geodesy to Geodynamics: Crustal Dynamics, Geodyn. Ser., 23, 407-416.
- Oral, M. B., Reilinger, R. E., Toksöz, M. N., King, R. W., Barka, A. A. and Kınık, I., 1995. Coherent Plate Motions in the Eastern Mediterranean Continental Collision Zone, Eos, Trans. AGU, 76, 2, 9-11.
- Orkan, İ.N., Aktimur, H.T., Sungur, G. and Işıklar, İ.S., 1977. Ankara-İstanbul otoyol güzergahı Boludağı geçişi ve Hendek dolaylı jeoloji incelemesi. MTA rapor, 5847.
- Öcal, N., 1959. 26 Mayıs 1957 Abant Zelzelesi., Maarif Vekaleti, İstanbul Kandilli Rasathanesi, Sismoloji Yayınları, 4.
- Örgülü, G. and Aktar, M., 2001. Regional Moment Tensor Inversion for Strong Aftershocks of the August 17, 1999 Izmit Earthquake (Mw=7.4)., Geophys. Res. Letts., 28, 2, 371-.
- Özalaybey, S., Aktar, M., Ergin, M., Karabulut, H., Bouchon, M., Tapırdamaz, C. and Yoruk, A., 2000. Aftershock Studies Following Recent Earthquakes in Turkey. XXVII General Assembly of the European Seismological Commission (ESC), Lisbon University, Lisbon, Portugal, September 10-15, p. 31.
- Özalaybey, S., Ergin, M., Aktar, M., Tapırdamaz, C., Biçmen, F. and Yörük, A., 2002. The 1999 Earthquake Sequence in Turkey: Seismological and Tectonic Aspects. Bull. Seis. Soc. Am., 92, 1, 376-386.
- Özden, S., Tutkun, S. Z., Tatar, O., Mesci, B. L., Koçbulut, F., Doğan, B. and Tüvar, O., 2000. 12 Kasım 1999 Düzce Depreminin Yüzey Kırığı, Atım Dağılımları ve Bölgesel Tektonik Anlamı., Aktif tektonik Araştırma Grubu, 4. Toplantısı, Bildiri Özetleri, 19-19.
- Paluska, A. and Sipahioğlu, S., 1985. Bericht über Geologische Untersuchungen in der Mudurnu-Sapanca Region. DFG, Bonn-Bad Godesberg. Projektbegleitendes Vorhaben zum Vorhaben der Deutschen Forschungsgemeinschaft: "Geodatisch Geophysikalische Untersuchungen im seismoaktiven Bereich der Nord-Anatolischen Verwerfungs-Zone".
- Pantosti, D., Pucci, S., Palyvos, N., Zabei, C., DeMartini, P. M., Uçarkus, G., Dikbas, A., Meghraoui, M., Akyuz, S. and Collins, P., 2004., Paleoearthquakes Along the Duzce Fault Segment of the North Anatolian Fault Zone (Turkey). 32nd IGC, Florence 2004 – Abstracts.
- Pekcan, N., 2000. Düzce – Akçakoca Bölgesinin Jeomorfolojisi. Filiz Kitabevi, 122p.
- Pınar, A., Kalafat, D., Horasan, G., Özel, N., Yılmaz, M., Işıkar, A. M. and Gülen, L., 2000. Rupture Process of the August 17, 1999 İzmit (Kocaeli) Earthquake., The 1999 İzmit and Düzce Earthquakes: Preliminary Results., 71-78.

- Pickett, E. A., Robertson, A. H. F. and Dixon, J. E., 1992. The Karakaya Complex, NW Turkey: Paleotethyan Accretionary Complex? ISGB International Symposium on the Geology of the Black Sea Region, Ankara Turkey, Abstracts, MTA. p.30.
- Piper, D. J. W. and Perissoratis, C., 2003. Quaternary Neotectonics of the South Aegean Arc. *Marine Geology*, 198, 3, 259-288.
- Reilinger, R. E., McClusky, S. C., Oral, M. B., King, R. W., Toksöz, M. N., Barka, A. A., Kınık, I., Lenk, O. and Şanlı, I., 1997. Global Positioning System Measurements of Present-day Crustal Movements in the Arabia-Africa-Eurasia Plate Collision Zone., *J. Geophys. Res.*, 102, B5, 9983-9999.
- Royden, L. H., 1993a. Evolution of Retreating Subduction Boundaries Formed During Continental Collision., *Tectonics*, 12, 3, 629-638.
- Royden, L. H., 1993b. The Tectonic Expression Slab Pull at Continental Convergent Boundaries., *Tectonics*, 12, 2, 303-325.
- Sakin, O., 2002. Tarihsel Kayıtlarıyla İstanbul Depremleri. Kitabevi, 170p. ISBN: 975-7321-66-4.
- Saner, S., 1977. Geyve – Osmaneli – Taraklı Alanının Jeolojisi, Eski Çökelme Ortamları ve Çökelmenin Evrimi. PhD Thesis, İstanbul University, 312p.
- Saraç, A. N., 1995. Seismo - Tectonic Characteristics of the North Anatolian Fault Zone between Akyazı and Düzce (Bolu), Turkey., Second International Turkish Geology Workshop (September 6-8, 1995, Cumhuriyet University, Sivas - Turkey)., 95-95.
- Sarıbudak, M., Sanver, M., Şengör, A. M. C. and Görür, N., 1990. Paleomagnetic evidence for substantial rotation of the Almacık flake within the North Anatolian Fault zone, NW Turkey. *Geophys. J. Int.*, 102, 563-568.
- Scholz, C. H., 1990. *The Mechanics of Earthquakes and Faulting*. Cambridge University Press, 439p.
- Schwartz, D. P. and Coppersmith, K. J., 1984. Fault Behaviour and Characteristic Earthquakes: Examples from the Wasatch and San Andreas Faults. *J. Geophys. Res.*, 89, 5681-5698.
- Sipahioğlu, S., 1984. Geological and Tectonic Development of the Mudurnu River Valley. Internal Report of the İstanbul University, İstanbul Üniversitesi, Müh. Fak., Jeofizik Mühendisliği Bölümü.
- Söhlmann, R., 1989. Geologie, Tektonik und Geochemie des westlichen Abant Silsilesi südlich der Nordanatolischen Störungszone bei Mudurnu, Türkei. Diplomarbeit, Universität Tübingen.
- Stablein, H., 1991. Die Jura-Kreide Abfolge des westlichen Abant Silsilesi südlich der Nordanatolischen Transformstörung bei MudurnuTürkei. Diplomarbeit, Universität Tübingen.

- Straub, C. and Kahle, H.-G., 1994. Global Positioning System (GPS) Estimates of Crustal Deformation in the Marmara Sea Region, Northwestern Anatolia., *Earth Planet. Sci. L*, 121, 495-502.
- Straub, C. and Kahle, H.-G., 1995. Active Crustal Deformation in the Marmara Sea Region, NW Anatolia, Inferred from GPS Measurements., *Geophys. Res. Letts.*, 22, 18, 2533-2536.
- Straub, C., Kahle, H.-G. and Schindler, C., 1997. GPS and Geologic Estimates of the Tectonic Activity in the Marmara Sea Region, NW Anatolia., *J. Geophys. Res.*, 102, B12, 27587-27601.
- Straub, C. and Kahle, H.-G., 1997. Recent Crustal deformation and Strain Accumulation in the Marmara Sea Region, NW Anatolia, Inferred from Repeated GPS Measurements., *Active Tectonics of Northwestern Anatolia-The Marmara Poly-Project* (Ed: C.Schindler, M. Pfister), 417-447.
- Stuvier, M., Reimer, P. J., Bard, E., Beck, J. W., Burr, G. S., Hughen, K. A., Kromer, B., McCormac, F. G., v.d. Plicht, J. and Spurk, M., 1998. *Radiocarbon* 40, 3, 1041-1083.
- Sugai, T., Awata, Y., Toda, S., Emre, O., Dogan, A., Ozalp, S., Haraguchi, T., Kinoshita, H., Takada, K. and Yamaguchi, M., web. Paleoseismic investigations of the 1999 Duzce earthquake fault at Lake Efteni, North Anatolian fault system, Turkey. <http://unit.aist.go.jp/actfault/english/reports/h12seika/turkey.html>, first visited on 18th May 2005 and last on 19<sup>th</sup> May 2005 at 10:36 GMT.
- Şaroğlu, F., 1988. Age and Offset of the North Anatolian Fault. *Metu J. of Pure and Applied Sci.*, 21, 6569.
- Şaroğlu, F., Emre, Ö. and Kuşçu, İ., 1992. Türkiye Diri Fay Haritası., M.T.A. Genel Müdürlüğü.
- Şengör, A. M. C. and Yılmaz, Y., 1981. Tethian Evolution of Turkey: a Plate Tectonic Approach., *Tectonophysics*, 75, 181-242.
- Şengör, A. M. C., Büyükaşıkoglu, S. and Canitez, N., 1983. Neotectonics of the Pontides: Implications for Incompatible Structures Along the North Anatolian Fault., *J. Structural Geology*, 5, 2, 211-216.
- Şengör, A. M. C., Görür, N. and Şaroğlu, F., 1985. Strike slip faulting and related basin formation in zones of tectonic escape: Turkey as a case study. Strike slip deformation, basin formation and sedimentation, *Society of Economic Paleontologists and Mineralogists*, Tulsa, 37, 227-264.
- Şimşek, O. and Dalgiç, S., 1997. Düzce Ovası Killerinin Konsolidasyon Özellikleri ve Jeolojik Evrim ile İlişkisi., *Türkiye Jeoloji Bülteni*, 40, 2, 29-38.
- Taşman, C. E., 1944. Gerede - Bolu depremi., *M.T.A. Mecm.*, 1, 31.

Tatar, V., Polat, E. and Işıkkara, A. M., 1995. Armutlu Yarımadası ve Almacık Dağı'ndaki Volkanik Kayaların Paleomanyetizması. *Jeofizik*, 9, 10, 219-228.

Tibi, R., Bock, G., Xia, Y., Baumbach, M., Grosser, H., Milkereit, C., Karakisa, S., Zünbül, S., Kind, R. and Zschau, J., 2001. Rupture Processes of the 1999 August 17 Izmit and November 12 Düzce (Turkey) Earthquakes., *Geophys. J. Int.*, 144, 2, F1.

Trumbore, S. E., 2000. Radiocarbon Geochronology. In *Quaternary Geochronology Methods and Applications*, edited by J. S. Noller, J. M. Sowers, and W. R. Lettis, pp. 41-60. AGU Reference Shelf 4, American Geophysical Union, Washington, D.C.

Umutlu, N., Koketzu, K. and Milkereit, C., 2004. The rupture process during the 1999 Düzce, Turkey, earthquake from joint inversion of teleseismic and strong-motion data., *Tectonophysics*, 391, 315-324.

Vogelmann, M., 1989. Tektonische und Geochemische Untersuchungen im Bereich der Abant Silsilesi Westtürkei. – Diplomarbeit, Universität Tübingen.

Wells, D. L. and Coppersmith, K. J., 1994. New Empirical Relationships among Magnitude, Rupture Length, Rupture Area, and Surface Displacement. *Seismological Society of America Bulletin* 84:974-1002.

Woith, H., Zschau, J., Yılmaz, R., Karakisa, S., Zünbül, S., Baumbach, M., Grosser, H., Milkereit, C., Lang, D. H., Raschke, M., Schwartz, J., Welle, W., Michel, G. W., Xia, Y., Kaufmann, C., Reigber, C., Ünlü, F., Pekdeger, A., 2000. Multidisciplinary Investigation of the German Task Force for Earthquakes Related to the Izmit Earthquake of August 17, 1999 and the Düzce Earthquake of November 12, 1999., *The 1999 İzmit and Düzce Earthquakes: Preliminary Results.*, 233-245.

Yagi, Y. and Kikuchi, M., web. Preliminary Results of Rupture Process for The November 12, 1999 Turkey Earthquake. <http://www.eri.u-tokyo.ac.jp/yuji/trk2/Turkeyafter.html>. (visited on 28th June 2001 at 17:11:38).

Yeats, R. S., Sieh, K. and Allen, C. R., 1997. *The Geology of Earthquakes*. Oxford University Press, 568p.

Yılmaz, R. and Demirtaş, R., 1999. The August 17 1999 İzmit Bay Earthquake NW Turkey. *International Conference on Earthquake Hazard and Risk in the Mediterranean Region. EHRMR'99 Abstracts*, Near East University. 18-22 October 1999 Nicosia, North Cyprus, 7-7.

Yılmaz, Y., Gözübol, O. and Tüysüz, O., 1982. Geology of an area in and around the North Anatolian transform fault zone between Bolu and Akyazı. *Multidisciplinary Approach to Earthquake Prediction* (Eds.: A.M. Işıkkara and A. Vogel), 45-66.

Zünbül, S., Karakisa, S., Üretürk, N., Atın, N. and Türkoğlu, M., 2001. 12 Kasım 1999 Düzce Depremi (Mw=7.2) SABONET Artçıdeprem Çalışmaları., *Jeofizik*, Ocak, 82-85.

Zünbül, S., Karakisa, S. and Milkereit, C., 2003. SABONET, 17 Ağustos 1999, İzmit Depremi ve 12 Kasım 1999, Düzce Depremi Artçıdeprem Çalışmaları: Günümüze Kadar

Olan Etkinlik Durumu (Mart 2003)., Kocaeli 2003 Deprem Sempozyumu, 12-14 Mart 2003, Tam Metin Kitabı, 62-69.

**APPENDIX 1**

The 1999 Surface Rupture of the Düzce Fault. Included in CD media.

**APPENDIX 2**

Site locations, trench sites, exposures and dating probability curves. Included in CD media.

**APPENDIX 3**

Radiocarbon ages from trenches across the November 12, 1999 Düzce rupture. Included in CD media.

**APPENDIX 4**

Exposure of the Töngelli-1 trench. Included in CD media.

*Curriculum Vitae*

1970

*Born in İstanbul, Turkey on 24th of December 1970. My first encounter with natural sciences in geography lessons at primary school. I try to make an erosion model to understand the role of trees against erosion when I was a 10-year-old child.*

1986

*I try to understand the most important thing for the human mind in high school. The founded answer is realistic thought.*

1987

*I began to study geology in İstanbul Technical University. After the 1st year, I try to find the answer of a question following four years. The question is what is the *●real●*?*

1992

*I found the answer for the *●real●*. The *●real●* is the true knowledge about causes and results. Many scientists, whose enthusiasm for geology caused my addiction to this subject matter. I was especially inspired by the scientists that explain and prove causes and reasons about geological processes in the field studies.*

1994

*The contents my bachelor thesis, supervised by Prof. Dr. A. Aykut BARKA (Inshallah he is resting in peace), includes Quaternary geology and active tectonic investigations in the area between İstanbul city walls and Küçükçekmece. During this study, I applied some city geology techniques in highly urbanized areas. He introduced me to use data and techniques from various disciplines including geology to find more realistic causes about resultant geological phenomenon.*

1996

*In 1996 I introduced Boğaziçi University. Since 1997, I have been working in the Boğaziçi University, Kandilli Observatory and Earthquake Research Institute, Department of Geophysics. I am involved in earthquake prediction research and made my master thesis on the review of the tectonics of the Aegean region. During the thesis, my effort focused on critically reviewing all the geo-scientific information about problems of Aegean region that has well known important unsolved tectonic problems. The most important thing that I learned during the thesis is the importance of knowing reliability of data to perform realistic evaluations. I greatly thanks to Esen ARPAT who shows me how to perform critical review on data and related evaluation.*

1999

*Just after the occurrence of 1999 Kocaeli earthquake on 17th of August I and Yasutaka IKEDA (Tokyo University) made one-week study of surface rupture of the earthquake starting from the eastern end of the rupture. During the fist day of the field trip, Yasutaka IKEDA showed the very young lateral deformational geomorphic features of the Düzce fault. I decided to study Düzce fault, which its last rupture is not known, and forming single un-ruptured part except Marmara sea region along the North Anatolian Fault during the last century. However, it was ruptured just one week after my seminar about Kocaeli and Düzce faults in Sivas (ATAG-3 meeting in Cumhuriyet University) and during the shopping for trenching equipment in İstanbul. Since the preliminary field trip on 1999 Kocaeli rupture I have been studying on Düzce area. My PhD thesis includes this study about basic geological data on seismogenic sources in and around Düzce city.*